Experimental Studies on Cryogenically Conditioned Nanoencapsulated PCM-embedded Cement Mortar for Cooling Applications in Buildings

THESIS

Submitted in partial fulfillment
of the requirements for the degree of

DOCTOR OF PHILOSOPHY

by

NAVEEN KUMAR G

ID. No. 2015PHXF0515H

Under the Supervision of

Prof. R. PARAMESHWARAN

&

Prof. V. VINAYAKA RAM

BIRLA INSTITUTE OF TECHNOLOGY AND SCIENCE, PILANI

2024

BIRLA INSTITUTE OF TECHNOLOGY AND SCIENCE, PILANI

CERTIFICATE

This is to certify that the thesis titled **"Experimental Studies on Cryogenically Conditioned Nanoencapsulated PCM-embedded Cement Mortar for Cooling Applications in Buildings"** is submitted by **Naveen Kumar. G, ID No. 2015PHXF0515H** for the award of Ph.D. Degree of the Institute embodies original work done by him under my supervision.

Signature of the Supervisor :

Name in capital letters : Prof. R. PARAMESHWARAN

Designation : Associate Professor, Department of Mechanical Engineering

Date : 21/05/2024

Signature of the Co-supervisor:

Name in capital letters : Prof. V. VINAYAKA RAM

Designation : Professor, Department of Civil Engineering

Date 21/05/2024 :

DECLARATION

I, **Naveen Kumar G**, hereby declare that the thesis entitled "**Experimental Studies on Cryogenically Conditioned Nanoencapsulated PCM-embedded Cement Mortar for Cooling Applications in Buildings**" submitted for the degree of Doctor of Philosophy at **BITS Pilani Hyderabad Campus**, is my original work and has not been submitted for any other degree or professional qualification. This thesis has been carried out under the supervision of **Prof. R. Parameshwaran**, Department of Mechanical Engineering and **Prof. V. Vinayaka Ram** Department of Civil Engineering, BITS Pilani Hyderabad Campus.

I affirm that all sources and materials used in the preparation of this thesis have been duly acknowledged in the reference section. The work contained in this thesis has not been previously published or written by another person, except where due reference is made in the text of the thesis.

I also certify that all information derived from the private work of others (published and unpublished) has been fully recognized and discussed in the text and noted in the bibliography. This thesis has not been submitted to any other educational institution for the award of any academic degree or diploma.

I understand the University's regulations concerning plagiarism and I acknowledge that the University reserves the right to take legal action against anyone who engages in plagiarism. I certify that this thesis meets the ethical standards pertaining to academic honesty and integrity.

Signature: 

Date: 15/05/2024

Place: Hyderabad

ACKNOWLEDGEMENTS

Firstly, I praise and thank God, the 'Almighty,' for blessing me with the opportunity to undertake this research and granting me the strength and confidence to proceed successfully. I would like to express my sincere thanks to my advisors, **Prof. R. Parameshwaran** and **Prof. V. Vinayaka Ram**, for their support and guidance throughout my Ph.D. program. Their constant encouragement and timely guidance helped me to sustain and write this thesis. This journey could not have been imagined without my supervisors. Their profound knowledge and experience have inspired me in my academic research and everyday life. As supervisors, they consistently guided me well in this program. Particularly, I am very thankful to **Prof. R. Parameshwaran** for his patience, kindness, and continuous supervision, and for helping me out several times not just in my research but also in a variety of other personal problems. I deeply appreciate the constant motivation received from his end, which always helped me develop myself professionally and personally. I thank him for giving me a chance to work with him and for encouraging my research efforts in the course of my Ph.D. on Thermal Energy Storage in Building Applications.

I am grateful to my doctoral advisory committee members, **Prof. N. Jalaiah** and **Prof. Murari R. R. Varma,** for their valuable advice during semester reviews. I want to express my gratitude to the Doctoral Research Committee (DRC) members for providing valuable support during this research work.

My deep sense of regard goes to **Prof. N. Suresh Kumar Reddy,** current head, **Prof. Amit Kumar Gupta**, and **Prof. Y. V. Daseswara Rao**, former heads, Department of

Mechanical Engineering, BITS-Pilani, Hyderabad campus, for providing an amiable ambiance leading to the successful completion of my research.

My sincere gratitude to **Prof. Soumyo Mukherji,** Director, BITS-Pilani, Hyderabad Campus, for providing me all the resources and state-of-the-art facilities at the campus to carry out my research. I thank **Prof. Venkata Vamsi Krishna Venuganti**, Dean, BITS-Pilani, for his support throughout the research work. I extend my heartfelt gratitude to all the Faculty Members, Department of Mechanical Engineering, BITS-Pilani, Hyderabad Campus, for their support and encouragement to carry out my research work. I would like to acknowledge the assistance provided by lab technicians from the Mechanical Engineering Department, Structural Engineering laboratory from the Civil Engineering Department, and Central Analytical laboratory, without which my work could not have been carried out smoothly.

Special thanks to the Management and Administration of **CVR College of Engineering**, Ibrahimpatnam, who constantly supported me in providing the study leave for performing the experimentations and interactions with my supervisor and co-supervisor. My sincere gratitude to **Prof. M. Venkata Ramana**, Head of Mechanical Engineering Department (CVRCE), for his advice and support. I thank all my colleagues of the Mechanical Engineering Department (CVRCE), who supported me a lot by adjusting my workload during my study leave.

I am very thankful to **Mr. G. V. N. Trivedi, Dr. R. Naresh**, and **Ms. L. Swetha** (Ph.D. Scholars from the Mechanical Engineering Department) for their support during my Ph.D.

I am very grateful to **Dr. B. Sreedhar,** Senior Principal Scientist, CSIR-IICT, Hyderabad, who helped me with materials characterization. Further, I extend my sincere thanks to

Mr. Kamalakannan, Ragha Labs, Chennai for fabricating and delivering the experimental prototype in a short time.

Last but not least, I would like to pay high regards to my family members **(Gouroju Narsimha Chary, G. Krishna Kumari, G. Vasavi,** and **G. Vihaan)** for their unconditional love, encouragement, and support throughout my tenure of my Ph.D. Besides this, I thank every individual who directly or indirectly helped me to complete my thesis.

ABSTRACT

The global average temperature is steadily on the rise, with a particularly pronounced impact in tropical countries. An alarming consequence of this trend is the ever-increasing demand for space cooling. Approximately 2 billion air conditioning units are operational across the globe, making space cooling a primary contributor to the escalating electricity demand in buildings and necessitating capacity additions to cater to peak power requirements. Looking ahead to the next three decades, the use of air conditioners is projected to surge, becoming one of the top drivers of global electricity demand. Considering the substantial implications of energy consumption on both a country's economy and the environment, there is a need to develop energy-efficient building materials capable of effectively mitigating heat into the rooms resulting in significant energy savings.

Among various energy efficient technologies, Latent Thermal Energy Storage (LTES) technology is recognized as a vital advancement wherein Phase Change Material (PCM) plays a crucial role in absorbing a huge amount of latent heat, it also stores and redistributes the absorbed latent heat, and the process takes place over a range of temperature. PCM used in building applications can effectively reduce heat gain within a room, thus delaying the peak temperatures.

Among various techniques available for integrating PCM in the building fabrics, direct impregnation is the simplest method of incorporating the PCM in the cementitious materials. However, direct impregnation has led to leakage issues from the building fabrics, which in turn reduces energy storage capability, loss of material integrity. Moreover, when PCM comes directly into contact with cementitious material, there is a significant drop in compressive strength. Encapsulation technique can overcome the negative effects of direct

impregnation, wherein the PCM is coated with shell material. The shell material protects the PCM from interaction with surrounding cementitious material.

Nevertheless, the use of encapsulated PCM embedded in the cement mortar for external plastering has been associated with only a marginal temperature difference between indoor and outdoor environments, which falls short of being satisfactory. Despite a significant demand for energy-efficient materials, both pure PCM and encapsulated PCM have struggled to gain a foothold in the commercial market due to the aforementioned limitation, restricting their availability. Given these challenges, there is an imperative to develop a new materials and strategies for implementing PCM in building fabrics to achieve substantial benefits, including reduced heat gain, minimized temperature differentials between indoor and outdoor spaces, and delayed peak temperatures. These improvements, in turn, can lead to reduced air conditioner capacity requirements and result in energy savings.

The current research work aims to develop a novel encapsulated PCM with increased energy utilization efficiency, which are compatible with cementitious materials, can result in sustainable energy savings in the buildings for hot climatic conditions. Despite the various types of PCM available, organic PCM has the advantages of congruent phase transformation, non-corrosiveness, non-toxic, good thermal and chemical stability. Keeping in view the advantages of organic based PCMs, 1-Dodecanol and n-Octadecane PCM were selected for the current research work.

Initially, the work commenced with the synthesis of Cu-TiO_2 hybrid nanocomposites (HN), with the intent to enhance thermo-physical properties of 1-Dodecanol PCM and n-Octadecane PCM. The HN composites were dispersed in the PCM with varying proportions ranging from 0.02% to 0.1% with the increment of 0.02% by wt. of PCM. The HN inclusions

in the 1-Dodecanol PCM (HDP) enhanced thermal conductivity to the maximum value of 0.1926 W/m K at 0.08% by wt. of the PCM, which is equivalent to 5.53% improvement. The highest dispersion of HN at 0.1% led to significant enhancement of 33.6% and 14.28% in freezing and melting times. The pure n-Octadecane PCM thermal conductivity is 0.195 W/m K, the HN inclusions in the n-Octadecane PCM (HOP) enhanced the thermal conductivity by 124.10% than the pure PCM. Due to HN inclusions in the n-Octadecane PCM, the enhancement in the freezing and melting times was 39.4% and 21.7% respectively. The HOP exhibited an upward trend enhancing the onset decomposition temperature increased by 55 °C compared to that of the pure n-Octadecane PCM. The enhancement in the thermal properties due to HN inclusions in the n-Octadecane PCM was more effective than 1-Dodecanol PCM.

To establish energy storage in the building fabrics, direct impregnation technique was used to incorporate HDP and HOP in the cement mortar. During the curing process it was noticed that the PCM is leaking out.

To overcome the negative effect of direct impregnation, PCM encapsulation is carried out. Predominantly used organic shell materials are Melamine Formaldehyde (MF), polymethyl methacrylate, and polystyrene. Especially, melamine formaldehyde attracted more attention as the shell material for encapsulating the PCM. Melamine has very good mechanical strength, which makes it suitable to use as a shell material and thereby ensures that the PCM is not leaked.

In-situ polymerization technique was used to encapsulate both the PCMs. The synthesis process yields Microencapsulated 1-Dodecanol PCM (MDP) capsules ranging from 60 nm to 980 nm. The core 1-Dodecanol PCM inside the capsule exhibited dual stage freezing process namely α (rotator phase) and β (triclinic phase) which commenced from 20.78 °C and 14.21

°C, respectively. Whereas the melting process took place in single stage which commenced at 19.68 °C with the encapsulation ratio (R) of 40.9%. The thermal conductivity of the pure PCM and the MDP were measured 0.186 W/m K and 0.172 W/m K, respectively. The drop in the thermal conductivity was mainly due to polymer-based melamine formaldehyde shell material. Since, the present research work aims to develop enhanced PCM based plastering material intended for internal plastering for an air-conditioned room. When the MDP based cement mortar is incorporated as internal plastering for an air-conditioned room, it becomes evident that the crystallization temperature of the MDP deviates from the designated operating conditions of 22 °C to 26 °C. In an effort to tackle this concern, an attempt was made to encapsulate the PCM at nano size.

Fine tuning the synthesis process of nanoencapsulated 1-Dodecanol PCM (NDP) resulted in the size reduction of the capsules, with the average size of 132 nm. The phase change behaviour of NDP was similar to that of MDP, the core PCM inside the shell material initiated its freezing at a specific temperature of 19.78 °C, indicative of the α phase, whereas the onset of the β phase occurred at 13.44 °C with an encapsulation ratio of 51.9%. However, it's important to note that the phase change temperatures of both MDP and NDP falls beyond the operational parameters of end applications, which ranges from 22 °C to 26 °C. Given this context, the adoption of n-Octadecane PCM was deemed necessary to achieve the desired objectives.

The pure n-Octadecane PCM commences its freezing and melting process in a single step at a temperature of 23.17 °C and 24.90 °C thereby absorbing and releasing the latent heat of 204.91 J/g and 203.18 J/g respectively. The synthesis process of the nanoencapsulated n-Octadecane PCM (NP) yields the capsules size ranging from 50 nm to 450 nm. The NP exhibited good phase change characteristics, the core n-Octadecane PCM inside the capsules freezes and melts at 25.06 °C and 26.12 °C, their latent heats are 159.73 J/g and 156.89 J/g

respectively. Encapsulating the PCM using MF shell material has enhanced thermal stability by 19 °C than the pure n-Octadecane PCM. The n-octadecane PCM encapsulated using polymer-based MF shell material (NP) tends to reduce thermal conductivity**.** The percentage drop in thermal conductivity of NP was 37.94% compared with pure n-Octadecane PCM. The developed NP capsules incorporated in the cement mortar may reduce the thermal conductivity furthermore. To overcome this issue, the HN which played a vital role in enhancing thermal conductivity, was adsorbed on the NP capsules to enhance thermal properties.

The adsorption of HN on nanoencapsulated PCM (HNNP) has greatly enhanced thermal conductivity of 47.17% and 137.19% compared with the pure n-Octadecane PCM and NP respectively. HNNP exhibited good thermal characteristics in terms of phase change characteristics, thermal stability, and thermal conductivity. The novel HNNP exhibited good thermal reliability. Based on the above finding the HNNP exhibited better over NP in terms of phase change temperature, thermal stability, thermal conductivity and thermal reliability. Further, the NP before HN adsorption and the novel HNNP were incorporated in the cement mortar, with varying proportions ranging from 3% to 15% with the increment of 3% by weight of cement.

As the compressive strength gain of the cement mortar is closely connected with the curing period; the investigations were carried out after curing the cube specimens for 7 days and 28 days respectively. The thermal conductivity of Nanoencapsulated PCM embedded cement mortar (NPeCM) cube specimens was reduced in comparison with reference cement mortar; this is mainly due to polymer-based shell material. Contrarily, the thermal conductivity of HNNP embedded cement mortar (HNNPeCM) cube specimens were increased. The thermal conductivity enhancement of HNNPeCM-10 (15% of HNNP) over reference cement mortar and NPeCM-10 (15% by wt. of NP) were 13.14% and 51.50%

respectively. The average compressive strength of NPeCM-10 and HNNPeCM-10 cube specimens (15%) are 27.36 MPa and 24.66 MPa respectively. The maximum dispersion of NP and HNNP incorporated in the cement mortar resulted in compressive strength reduction, however, the compressive strength achieved is acceptable for plastering material.

Cryogenic temperatures are acknowledged as one of the most extreme environments for utilizing concrete, exerting a substantial influence on various aspects of concrete performance, including its mechanical properties, freeze-thaw resistance, and overall durability. Cement-based materials exhibit markedly distinct characteristics at cryogenic temperatures compared to ambient conditions. Keeping in view, an attempt was made treating the reference cement mortar and HNNPeCM-10 at cryogenic temperatures using Liquid Nitrogen (LN). Considering the curing process with respect to the time, investigations were carried out to study the impact of cryogenic conditioning of the reference cement mortar cube specimens and HNNPeCM cube specimens with different curing periods such as 6 hours, 12 hours, and 24 hours.

The FESEM results infer that the microstructure of cryogenically conditioned HNNPeCM-10 samples exhibited increased porous structure. It was noticed from the FESEM images that there were absence of cracks and increased air void sizes observed for the Cryo-conditioned HNNPeCM-10 samples. The compressive strength of cryogenically conditioned reference cement mortar and the HNNPeCM-10 were reduced, this could be due to increased porous structure. Despite the drop in the compressive strength of the cryo-conditioning of HNNPeCM-10 cube specimens, the resulted values for 24 hours cryo-conditioned HNNPeCM-10 are on higher side than the desired compressive strength which makes suitable for internal plastering.

Despite satisfactory compressive strength of HNNPeCM-10 samples cryogenically conditioned for 24 hours which suits for internal plastering in buildings, challenges in Cryo-conditioning and application persist. The compressive strength needs further improvement to surpass the values achieved with the 28 days curing period, making it recommendable for specialized applications.

Heat transfer analysis was carried out to evaluate the behaviour of reference mortar and an HNNP-based mortar. The investigation conforms to ASTM C1363 standards, using an "Insulated Test Chamber" where the hot chamber is held constant at 42°C and the cold chamber at 22°C. The results suggest that the peak temperatures of the HNNPeCM-10 slab during heating process were delayed by 52 minutes relative to the reference cement mortar slab, indicating enhanced thermal resistance. Moreover, when the reference slab reached 42°C, the HNNPeCM-10 slab maintained a significantly lower temperature, exhibiting a notable difference of 3.12°C. This significant differential underscores the effectiveness of the HNNPeCM-10 material in maintaining cool internal conditions compared to traditional cement mortar. This clearly indicates the potential of HNNPeCM-10 plaster in improving indoor thermal comfort.

Based on the above findings and facts, the Novel HNNP capsules exhibit the remarkable capability to undergo freezing and melting within the range of human thermal comfort zone. This distinctive feature renders them exceptionally well-suited for integration into the internal plastering materials for buildings, addressing the cooling requirements in hot climatic conditions. Moreover, HNNP proves to be highly compatible for incorporation into cement mortar, seamlessly enhancing cooling applications within structures without compromising structural stability. This not only makes it an optimal choice but also contributes to increased energy utilization efficiency in buildings.

TABLE OF CONTENTS

Title	Page No.
Title Page……..	i
Certificate……..	ii
Declaration……	iii
Acknowledgements……...	iv
Abstract…….	vii
Table of Contents…….…….	xiv
List of Tables……...	xxi
List of Figures……	xxiii
Abbreviations……..	xxviii
CHAPTER - 1	
INTRODUCTION…….	1
1.1. Energy scenario……..	1
1.2. Motivation of the research…….	6
1.3. Energy efficient technologies……	6
1.4. Thermal energy storage…….	7
1.4.1. Sensible heat storage system……...	8
1.4.2. Latent Thermal Energy Storage System (LTES)…….	9
1.4.3. Thermo-chemical energy storage system……...	9
1.5. Summary……	10
1.6. Organization of the thesis……..	11
CHAPTER - 2	
LITERATURE REVIEW…….	12
2.1. Classification of PCM's……..	13

2.2. Establishing the LTES system in buildings…… 14

2.2.1. Active system……... 14

2.2.2. Passive system…… 15

2.3. PCM incorporation in buildings…… 16

2.4. Need of Research on PCM…… 17

2.5. Direct impregnation of pure PCM in the building materials…… 20

2.6. Encapsulation of PCM……..... 21

2.7. Encapsulated PCM in the cement mortar (Thermo-structural investigation…….. 30

2.8. Encapsulated PCM in the cement mortar…….……. 33

2.9. Enhancing the thermal properties of PCM using nanoparticles……..….. 37

2.10. Thermal enhancement of encapsulated PCM…….. 41

2.11. Summary of the literature survey…… 42

2.12. Research gaps…… 43

2.13. Problem definition……... 45

2.14. Reasons behind selecting the PCM and hybrid nanocomposites for the current study…… 45

2.14.1. Comparison with other nanoparticles…… 47

2.14.2. Other synthesis methods…….. 48

2.14.3. Efficiency and cost comparison……. 48

2.14.4. Comparison with other techniques…… 49

2.15. Objectives of the study…… 50

2.16. The limitations of the study were outlined in the thesis following the stated 50

objectives.....

CHAPTER – 3

RESEARCH METHODOLOGY…… 52

3.1 Methodology…….…….. 52

3.2. Plan of action……..….... 53

3.3. Overview of various samples prepared……. 55

3.4. Details of instruments for materials characterization…… 56

CHAPTER - 4

MATERIALS AND METHODS…… 62

4.1. Materials……. 62

4.2. Synthesis of Cu-TiO_2 hybrid nanocomposites (HN)……. 64

4.3. Preparation of Cu-TiO_2 hybrid nanocomposites based 1-Dodecanol PCM (HDP)…… 65

4.4 Preparation of Cu-TiO2 hybrid nanocomposites based 1-Dodecanol PCM embedded cement mortar (HDPC)…… 66

4.5. Synthesis of Microencapsulated 1-Dodecanol PCM (MDP)……. 68

4.6. Synthesis of nanoencapsulated 1-Dodecanol PCM……..... 70

4.7. Synthesis of Cu-TiO_2 hybrid nanocomposite-based n-Octadecane PCM (HOP)……..... 71

4.8. Preparation of Cu-TiO_2 HN based n-Octadecane PCM embedded cement mortar cube specimens (HOPC)……. 72

4.9. Synthesis of nanoencapsulated n-Octadecane PCM (NP)……. 73

4.10. Synthesis of Cu-TiO_2 hybrid nanocomposites adsorbed nanoencapsulated n-Octadecane PCM (HNNP)……... 74

4.11. Challenges encountered during synthesis…… 76

4.12. Preparation of pure PCM, NP and HNNP embedded

cement mortar cube specimens……. 76

4.12.1. Mix design for cube specimen preparations…….. 76

4.13. Cryogenic treatment……. 77

4.13.1. Need for cryogenic conditioning of cement mortar……. 78

4.13.2. Cryogenic conditioning of reference cement mortar and

HNNPeCM…… 78

CHAPTER - 5

RESULTS AND DISCUSSIONS…… 80

5.1. Results of HN and HDP……. 80

5.1.1. Morphology of hybrid nanocomposite (HN)…….. 80

5.1.2. Crystal structure and chemical stability of the HDP……... 81

5.1.3. Phase change characteristics of pure PCM and HDP……. 83

5.1.4 Heat storage and release properties……. 85

5.1.5. Thermogravimetric analysis……..... 88

5.1.6. Thermal conductivity of pure PCM and HDP samples…….. 89

5.1.7. Compressive strength of HDPC…….. 90

5.1.8. Summary…… 92

5.2. Microencapsulated 1-Dodecanol PCM (MDP)…….. 93

5.2.1. Morphology of the MDP……. 93

5.2.2. Particle size distribution of the MDP…….. 94

5.2.3. Crystal structure of the MDP…….. 95

5.2.4. FTIR analysis of MDP…… 96

5.2.5. Phase change and latent heat properties of the MDP…….. 98

5.2.6. Thermal stability of the MDP……. 103

5.2.7 Thermal conductivity of the MDP…… 105

5.2.8. Thermal cycling test of the MDP…… 106

5.2.9 Summary from the synthesis of MDP…….. 109

5.3 Results and discussions of Nanoencapsulated

1-Dodecanol PCM (NDP)…… 110

5.3.1. Surface morphology of Nanoencapsulated

1-Dodecanol PCM (NDP)……. 110

5.3.2. Phase change characteristics of nanoencapsulated

1-Dodecanol PCM (NDP)……. 110

5.3.3. Summary from the synthesis of NDP……. 113

5.4. Cu-TiO_2 hybrid nanocomposites-based n-Octadecane PCM embedded

cement mortar (HOPC)…… 113

5.4.1. Chemical stability…… 113

5.4.2. Phase change characteristics of pure PCM and HOP……. 114

5.4.3. Heat storage and release characteristics of n-Octadecane

pure PCM and HOP…….. 116

5.4.4 Thermogravimetric analysis…… 119

5.4.5. Thermal conductivity of pure PCM and HOPC samples……... 120

5.4.6. Thermal conductivity of HOPC cube specimens……..... 121

5.4.7. Compressive strength of HOPC cube specimens……..... 122

5.4.8. Summary……. 123

5.5. Nanoencapsulated n-Octadecane PCM (NP) and Cu-TiO_2 HN adsorbed

nanoencapsulated PCM (HNNP)…….. 124

5.5.1. Surface morphology of HN, NP and HNNP……... 124

5.5.2. Crystallinity of the HNNP…….. 127

5.5.3. Particle size analysis…… 128

5.5.4. Chemical structure and chemical stability…….. 130

5.5.5. Phase change characteristics of pure PCM, NP and HNNP…… 132

5.5.6. Thermal stability of pure PCM, NP and HNNP……. 136

5.5.7. Thermal conductivity of pure PCM, NP and HNNP…….. 138

5.5.8. Thermal reliability of HNNP…….. 140

5.5.9. Distribution of capsules in the cement mortar…… 141

5.5.10. Density of the cube specimen……... 142

5.5.11. Thermal conductivity of NPeCM and HNNPeCM cube specimens…… 143

5.5.12. Compressive strength of NPeCM and HNNPeCM…… 146

5.5.13. Summary……... 149

5.6. Cryogenic conditioning…….. 150

5.6.1. Micro-structural behaviour of cryogenic conditioning of cube samples…. 151

5.6.2. Compressive strength of cryo-conditioned cube specimens……... 152

CHAPTER – 6

THERMAL ANALYSIS OF HNNP BASED CEMENT MORTAR…… 162

6.1. Experimental setup details ……..…… 162

6.2. Slab preparation…… 164

6.3. Test procedure……. 165

6.4. Observation from the experimentation…… 166

6.4.1. Heating process…….. 166

6.4.2. Cooling process……. 167

CHAPTER-7

CONCLUSIONS AND RECOMMENDATIONS…… 170

7.1. Conclusions……..... 171

7.2. Specific contributions…… 175

7.3. Potential commercialization paths for HNNP in building applications……. 176

7.4. Practical challenges of implementing cryogenically conditioned plastering materials in real-time building applications…… 178

7.5. Future scope of work…….…….. 179

REFERENCES…… 181

APPENDIX-1

PRELIMINARY TESTS ON CEMENT AND SAND…… 203

APPENDIX-2

ERROR ANALYSIS…….…….. 208

BRIEF BIOGRAPHY OF STUDENT…….. 212

BRIEF BIOGRAPHY OF SUPERVISOR…….. 213

BRIEF BIOGRAPHY OF CO-SUPERVISOR…… 214

LIST OF PUBLICATIONS……... 216

LIST OF TABLES

Table No.	Name of the Table	Page No.
Table 1	List of organic PCMs used for building applications……	20
Table 2	Shell material types for PCM encapsulation……	23
Table 3	PCM encapsulation……	24
Table 4	Encapsulated PCM used in internal plastering applications……..	37
Table 5	Summary of synthesis carried out for the current work……..	55
Table 6	Equipment details with specifications……	57
Table 7	Overview of materials preparation and characterization……	59
Table 8	Strategy for cryogenically conditioning of reference cement mortar and HNNPeCM specimens……...	61
Table 9	Details of the materials…….……	62
Table 10	Heat storage and release characteristics of pure PCM and HDP……	88
Table 11	Summary of FTIR results of pure PCM, Melamine and MDP……..	97
Table 12	Thermal properties of PCM and MDP……..……	99
Table 13	Thermal energy storage capability of pure PCM and MDP……...	102
Table 14	Thermal properties of PCM (Literature)……	103
Table 15	Thermal energy storage capability of pure PCM, and MDP……..	108
Table 16	Thermal properties of pure 1-Dodecanol PCM and NDP…….….	112
Table 17	Thermal energy storage capability of pure 1-Dodecanol PCM and	

nanoencapsulated PCM……. 112

Table 18 Thermal properties of pure n-Octadecane PCM and HOP 116

Table 19 Heat storage and release characteristics of pure PCM and HOP……. 117

Table 20 Thermal decomposition of pure n-Octadecane PCM and HOPC……. 119

Table 21 Literature on particle size of nanoencapsulated PCM…….. 129

Table 22 Summary of FTIR results of pure PCM, melamine, NP and HNNP……. 131

Table 23 Thermal properties of pure PCM, NP and HNNP…..... 135

Table 24 Thermal energy storage capability of pure PCM, NP, and HNNP…… 136

Table 25 Thermal stability of pure PCM, NP and HNNP…… 137

Table 26 Comparison of thermal conductivity of encapsulated PCM using melamine/urea formaldehyde shell material with literature…… 139

Table 27 Thermal conductivity of NPeCM and HNNPeCM specimens cured for 28 days……. 144

Table 28 Compressive strength of NPeCM and HNNPeCM specimens cured for 7 days and 28 days……. 148

Table 29 Compressive strength of cryogenic conditioning of reference cement mortar and HNNPeCM-10 specimens……. 154

Table 30 Results summary…… 155

Table 31 Comparison between MDP, NDP, NP, and HNNP……. 157

LIST OF FIGURES

Figure No.	Figure Title	Page No.
Figure 1	Energy consumption sector wise……..	2
Figure 2	GHG emissions from different sectors…….	3
Figure 3	Electricity consumption by various sectors from 1980-2019…….	3
Figure 4	End user application of energy at residential buildings……	4
Figure 5	Global air conditioner stock from 1990-2050……..	5
Figure 6	Principle of phase change materials……	9
Figure 7	Desirable properties of ideal PCM……...	13
Figure 8	Classification of phase change materials……	14
Figure 9	Cement mortar and concrete ingredients……..	17
Figure 10	PCM encapsulated in a spherical shell material……	22
Figure 11	PCM Encapsulation techniques……	22
Figure 12	Challenges with PCM……..	38
Figure 13	Characterization techniques to test the PCM……	38
Figure 14	Workflow chart……	54
Figure 15	Synthesis of HN……	65
Figure 16	Pure 1-Dodecanol PCM and HDP samples……..	66
Figure 17	Schematic representation for preparation of HDPC ……	66

Figure 18	HDPC preparation and curing process…….	68
Figure 19	Graphical representation of MDP synthesis procedure……	70
Figure 20	Synthesis procedure of NDP ……..……	71
Figure 21	Cu-TiO_2 Hybrid nanocomposite based n-Octadecane PCM (HOP)…….	72
Figure 22	Cu-TiO_2 HN based n-Octadecane PCM embedded cement mortar cube specimens…….	72
Figure 23	Synthesis procedure of NP……...	74
Figure 24	Graphical representation of NP and HNNP synthesis procedure…….	75
Figure 25	Graphical representation of Cu-TiO_2 hybrid nanocomposites adsorbed nanoencapsulated n-Octadecane PCM (HNNP)……	75
Figure 26	NPeCM and HNNPeCM cube specimen preparation……	77
Figure 27	Cryogenic conditioning of cement mortar cube specimens…….	79
Figure 28	Cryo-conditioned cement mortar cube specimens…….	79
Figure 29	FESEM and EDX of HN……..	81
Figure 30	XRD pattern of HN……..	82
Figure 31	FTIR spectra of the pure PCM and HDP……	83
Figure 32	DSC graphs of pure PCM and HDP……	84
Figure 33	Thermal energy storage setup……	86
Figure 34	HDP samples & testing the samples using TES setup…….	87

Figure 35	Freezing and melting curves of pure PCM and HDP samples…….	87
Figure 36	TGA curves of pure PCM and HDP…….	89
Figure 37	Thermal conductivity of pure PCM and HDP……..	90
Figure 38	28-day compressive strength of HDPC specimens……..	91
Figure 39	Pictures showing the cube specimens during preparation, curing and post testing stages…….	91
Figure 40	FESEM images of MDP……...	94
Figure 41	Particle size distribution of the MDP……...	95
Figure 42	XRD pattern of the MDP……..	96
Figure 43	FTIR spectra of the PCM, MF shell and the MDP……...	97
Figure 44	DSC graphs of pure PCM and MDP……	99
Figure 45	TGA graphs of PCM and the MDP …….	105
Figure 46	DSC graph of MDP after thermal cycling……	107
Figure 47	FTIR spectra of MDP before and after thermal cycling……...	109
Figure 48	FESEM Images of NDP……...	110
Figure 49	Phase change characteristics of pure 1-Dodecanol PCM and NDP……	111
Figure 50	FTIR spectra of the pure PCM and HOP…….	114
Figure 51	Phase change characteristics of pure PCM and HOP……...	115
Figure 52	Pure PCM and HOP samples……	116

Figure 53	Freezing and melting process of pure PCM and HOP samples……	117
Figure 54	TGA curves of pure PCM and HOP……..	120
Figure 55	Thermal conductivity of pure PCM and HOP samples…..……...	121
Figure 56	Thermal conductivity of HOPC cube specimens…….	122
Figure 57	28-day compressive strength of HOPC specimens……..	123
Figure 58	FESEM of HN and EDAX results of HN…….	125
Figure 59	FESEM results and EDAX Results of NP……	126
Figure 60	FESEM results of HNNP…….	126
Figure 61	EDAX results of HNNP……..	127
Figure 62	XRD pattern of HN, NP and HNNP…….	128
Figure 63	Particle size distribution of HN, NP and HNNP and average particle size ……	129
Figure 64	FTIR spectra of pure PCM, Melamine, HN and HNNP……..	130
Figure 65	Phase change characteristics of pure PCM, and NP…….	134
Figure 66	Phase change characteristics of HNNP and thermal cycling of HNNP……..	135
Figure 67	Thermal decomposition of pure PCM, NP, HNNP before and after thermal cycling…….	138
Figure 68	Thermal conductivity of pure PCM, NP and HNNP……	139
Figure 69	FESEM results of NPeCM-10 sample (28 days curing period)……	141

Figure 70	FESEM results of HNNPeCM-10 sample (28 days curing period)…….	142
Figure 71	Density of NPeCM and HNNPeCM 28 days cured specimens……	143
Figure 72	Thermal conductivity of reference cement mortar (CM-2), NPeCM and HNNPeCM samples cured for 28 days……...	145
Figure 73	Thermal conductivity of CM-2, NPeCM-10 and HNNPeCM-10 specimens cured for 28 days……..	145
Figure 74	Compressive strength of reference cement mortar, NPeCM and HNNPeCM specimens 7 days and 28 days curing period……	147
Figure 75	24 hrs cryogenic conditioning of cube specimens of HNNPeCM-10 ……	152
Figure 76	Schematic of Insulated Test Chamber……	163
Figure 77	Insulated Test Chamber and slab positioned between hot and cold chamber……..	163
Figure 78	Reference and HNNPeCM slab……	165
Figure 79	Heating process of reference cement mortar and HNNPeCM-10 slab specimen…….	167
Figure 80	Cooling process of reference cement mortar and HNNPeCM-10 slab specimen…….	169

LIST OF ABBREVIATIONS

Abbreviation	Description
CTS-co-PMAA	Chitosan-co-poly(methacrylic acid)
DSC	Differential Scanning Calorimeter
DDW	Double Distilled water
EDX	Energy Dispersive X-Ray Analysis
FESEM	Field Emission Scanning Electron Microscopy
FTIR	Fourier Transform Infrared Spectroscopy
GHG	Greenhouse gas
HN	Cu-TiO_2 Hybrid Nanocomposites
HDP	Cu-TiO_2 Hybrid Nanocomposites based 1-Dodecanol PCM
HDPC	Cu-TiO_2 Hybrid Nanocomposites based 1-Dodecanol PCM embedded Cement Mortar
HOP	Cu-TiO_2 Hybrid Nanocomposites based n-Octadecane PCM
HOPC	Cu-TiO_2 Hybrid Nanocomposites based n-Octadecane PCM embedded Cement Mortar
HNNP	Cu-TiO_2 Hybrid Nanocomposites adsorbed Nanoencapsulated n-Octadecane PCM
HNNPeCM	Cu-TiO_2 Hybrid Nanocomposites adsorbed Nanoencapsulated n-Octadecane PCM embedded Cement Mortar
HVAC	Heating Ventilation and Air-conditioning
IEA	International Energy Agency
JCPDS	Joint Committee on Powder Diffraction Standards
LTES	Latent Thermal Energy Storage

MDP	Microencapsulated 1-Dodecanol PCM
NDP	Nanoencapsulated 1-Dodecanol PCM
NP	Nanoencapsulated n-Octadecane PCM
NPeCM	Nanoencapsulated n-Octadecane PCM embedded Cement Mortar
PCM	Phase Change Materials
PSA	Particle Size Analyzer
PVP	Polyvinylpyrrolidone
TES	Thermal Energy Storage
TCA	Thermal Conductivity Analyzer
TGA	Thermogravimetric Analyzer
Wt.	Weight

CHAPTER - 1

INTRODUCTION

This chapter emphasizes the worldwide energy demand and supply by the various sectors, as well as information about energy end user by residential buildings. This chapter highlights the need for Thermal Energy Storage (TES) in buildings, which is a crucial part of energy-efficient technologies. This chapter discusses and explains the working principle of Phase Change Materials (PCM), their classification, advantages, disadvantages, and their wide range of applications in building materials.

1.1. Energy Scenario

One of the most crucial challenges confronting modern civilization is the escalating demand for energy, driven by factors like the rapid expansion of metropolitan areas and the continuous improvement of living standards. The growing consumption of energy from nonrenewable sources has emerged as a major cause for concern. Additionally, the World Meteorological Organization (WMO) has issued alarming reports, indicating a rapid increase in the global mean temperature over the past eight years.

In recent decades, a global debate has ensued concerning the mitigation of climate change through the reduction of energy usage. According to data from the International Energy Agency (IEA), energy consumption is distributed across various sectors. Approximately 30% of the energy is consumed by the transport sector, 27% by residential buildings, 29% by the industrial sector, commercial and other sectors consume 9% and 5%, respectively. The proportions related to energy consumption are shown in Fig. 1 **[1-4]**.

Furthermore, buildings play a significant role in Greenhouse Gas (GHG) emissions, with reports indicating that they contribute substantially to environmental impact. Specifically, GHG emissions amount to around 31% from the transport sector, while emissions from

residential and non-residential sources (both direct and indirect) contribute 17% and 11%, respectively. The construction industry is responsible for an additional 11% of GHG emissions, while other industries and miscellaneous sources account for 31% and 11%, respectively. Notably, building-related GHG emissions alone make up almost one-third of the total emissions, as depicted in Fig. 2 **[1, 2]**. Given that excessive emission of greenhouse gases (GHG) is widely recognized as a significant contributor to climate change and global warming, numerous nations are diligently striving to reduce their GHG output in the coming years **[1]**. Multiple studies have consistently identified the construction sector as the primary source of greenhouse gas emissions. However, direct policies targeting GHG mitigations in building practices are seldom put into practice, despite many nations proposing and implementing various measures to curb GHG emissions from buildings.

Numerous policies actively promote the advancement of green buildings or building energy efficiency, with a primary emphasis on reducing operational energy usage and the associated Greenhouse gas (GHG) emissions during the building's operational phase. This includes measures to address energy consumption from air conditioning, lighting, heating, and other relevant aspects **[5, 6]**.

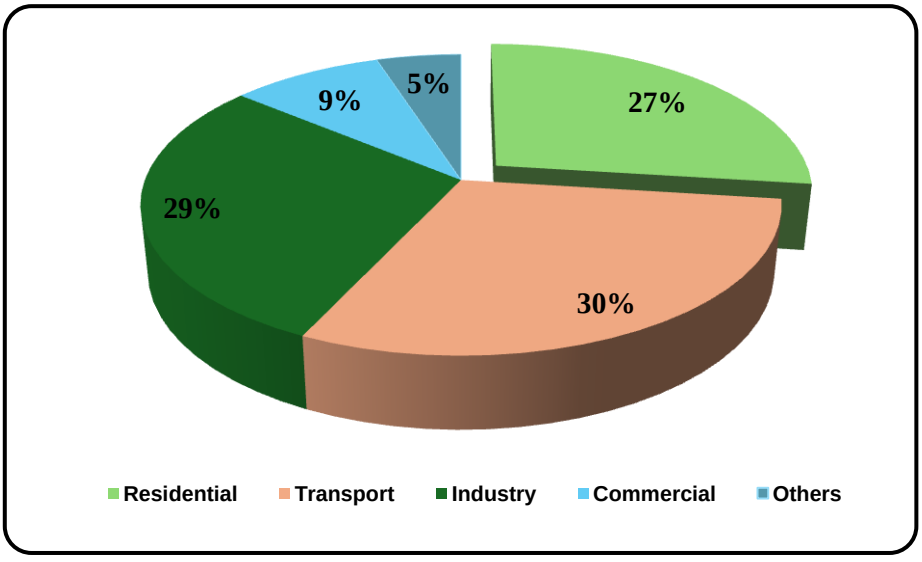

Fig. 1. Energy consumption sector wise [**1**].

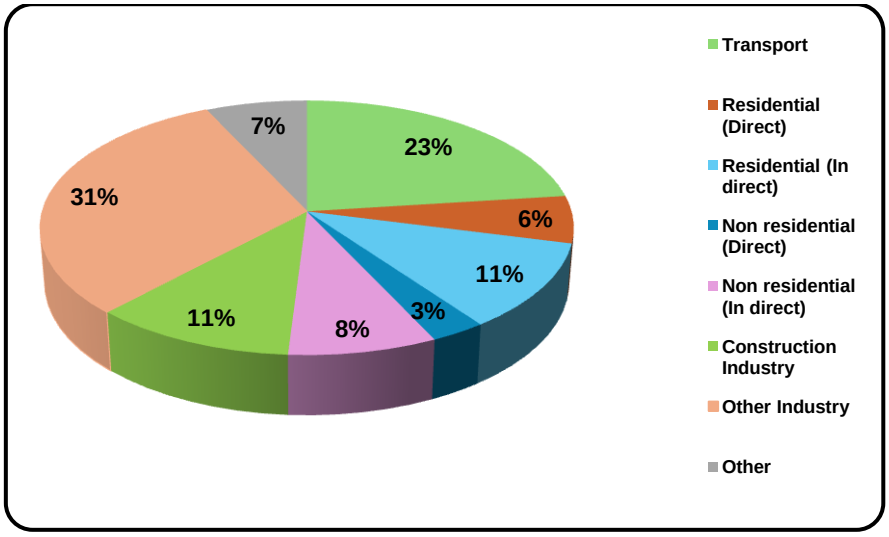

Fig. 2. GHG emissions from different sectors [**1**].

Fig. 3 displays information concerning global electricity consumption categorized by sectors. The data was sourced from the International Energy Agency and covers the years 1980 to 2019 **[1, 2]**. Among the various sectors, industries emerge as the primary consumers of electricity, followed by buildings. Notably, there is a consistent upward trend in electricity consumption within the building sector each year. This pattern raises concerns, signaling an alarming situation that calls for immediate action to promote energy efficiency in buildings and achieve significant energy savings.

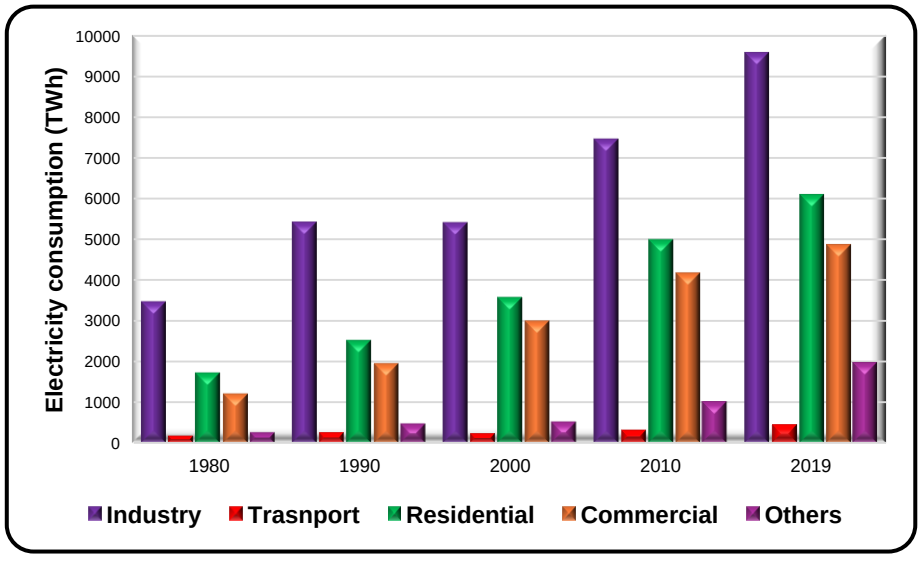

Fig. 3. Electricity consumption by various sectors from 1980-2019 **[1]**.

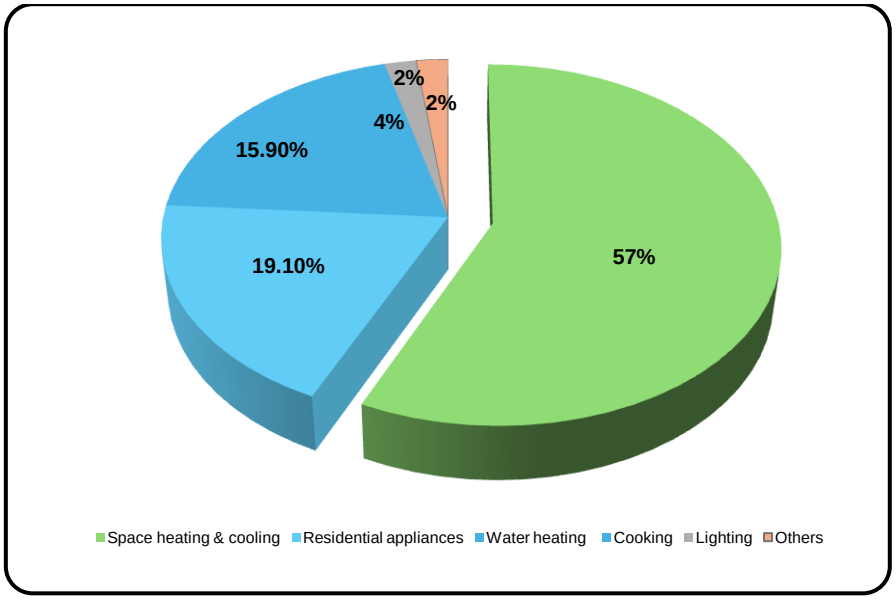

Fig. 4. End user application of energy at residential buildings **[1]**.

Fig. 4 illustrates the breakdown of energy consumption in residential buildings based on end-user applications. Remarkably, approximately 57% of the energy is allocated to space heating or cooling, emphasizing its significance in maintaining comfortable living conditions. Water heating follows at 15.90%, while residential appliances account for 19.10%. A smaller portion of energy, about 4%, is utilized for cooking, with an additional 2% dedicated to lighting and 2% for other household appliances **[1, 4, 7]**. Clearly, the substantial share of energy in residential buildings is dedicated to regulating indoor temperatures using air conditioners or room heaters.

The global usage of air conditioners is experiencing a significant and rapid increase, leading to an increase in electricity demand. Projections suggest that the usage of air conditioners is set to nearly triple by 2050 as shown in the Fig. 5. Notably, air conditioners currently account for approximately 20% of the total electricity consumed worldwide, as they are indispensable in maintaining comfortable indoor temperatures for human habitation in buildings **[1, 2, 8]**. Consequently, the escalating demand for space cooling is placing an additional load on electricity resources in numerous countries**.**

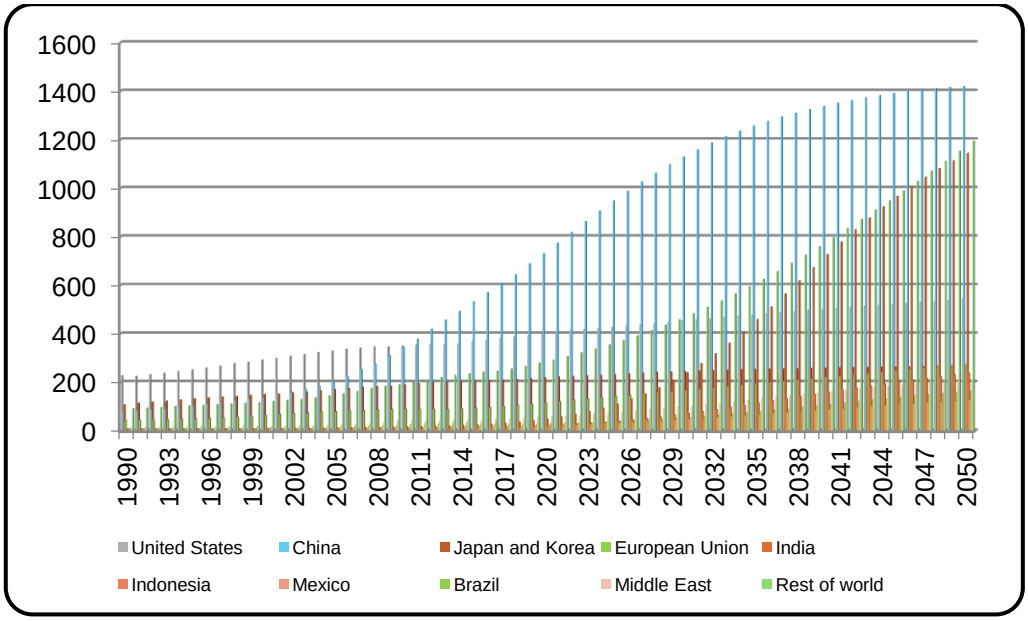

Fig. 5. Global air conditioner stock from 1990-2050 [**1**].

It is evident that the global demand for space cooling and the associated energy requirements will continue to escalate, particularly in tropical regions where the necessity for space cooling is more pronounced. Therefore, there is a need to prioritize energy efficiency and seek innovative solutions to reduce energy consumption and operational costs in buildings through the adoption of energy-efficient materials.

Many building energy efficiency standards commonly exclude historic buildings, places of worship, and other special-purpose structures of significant aesthetic and historical importance. This exemption is often granted due to the intricate challenge of incorporating energy-efficient practices without undermining the cherished architectural and intrinsic values intended for conservation. Nevertheless, a positive shift has emerged in certain countries in recent times, where the recognition of the significance of energy-efficient technologies is growing.

1.2. Motivation of the Research

Clearly discernible from the IEA data 2022, there is a notable and rapid escalation in the global utilization of air conditioners, leading to a substantial increase in the demand for electricity **[1]**. Projections suggest that by the year 2050, the usage of air conditioners is anticipated to witness an almost threefold increase. Notably, air conditioning systems presently account for roughly 20% of the total global electricity consumption, primarily attributed to the imperative of maintaining comfortable indoor temperatures within structures. This escalating need for space cooling is undeniably contributing to increased electricity consumption in numerous countries. Undoubtedly, the worldwide desire for space cooling is on an upward trajectory, ensuring that the energy required for maintaining optimal building temperatures will continue to expand. The increased energy demand for space cooling in buildings leads to the development of energy efficiency technologies.

1.3. Energy efficient technologies

"A way of managing and regulating the growth in energy consumption" is energy efficiency. Therefore, a structure is considered energy efficient, if it provides the same level of services while using less energy. Due to the viability of end-use products that use less energy throughout the course of their lifetime, energy efficiency holds paramount importance across all sectors of engineering and technology **[9]**. Over the past few years, there has been a noticeable surge in the significance placed on energy efficiency, especially within the realm of building services engineering. This trend can be traced from the initial stages of building design and extends throughout the entirety of the construction phase. There is no doubt that Energy Efficiency and Energy Conservation are connected to one another and are designed to reduce the amount of energy that is consumed, primarily in the form of heat gain or heat loss within the structure thereby expecting sustainable energy, besides ensuring minimum GHG, so that the global emissions do not lead to irreversible damage to the earth system. In recent

years, a wide range of energy-efficient technologies has emerged. Notably, thermal energy storage has gained significant prominence, offering valuable benefits to end users by facilitating energy absorption and redistribution.

1.4. Thermal Energy Storage

Energy in the form of cold or heat is stored in the material and can be made available when demands for later usage. The principles encompassing the storage of thermal energy through sensible heat, latent heat, and reversible thermo-chemical reactions have been effectively implemented over the years to accomplish the redistribution of energy and enhance energy efficiency, both in the short term, such as on a diurnal cycle, and over the long term **[4]**.

The amount of energy needed to offset the essential load demand is frequently stored within the thermal energy storage during the charging phase, usually taking place under part load conditions. Subsequently, during the discharge process, the stored thermal energy from the TES is retrieved and supplied to the intended end-use utility for its designated purpose [**10, 11**].

It is possible to effectively achieve energy redistribution in the form of load shifting from on-peak to off-peak conditions if TES is integrated with standard thermal interface systems. This, in turn, makes it possible for the cooling/heating plant or utility to function at its base capacity or nominal capacity, which contributes to improved energy efficiency as well as operational performance of the thermal system. The capacity to store and release thermal energy hinges predominantly on the characteristics of the storage medium, specifically the material employed for storage, as well as the temperature interactions that occur between the storage medium and the energy source **[4, 12].** In addition to that, the advantages of implementing TES in buildings are listed below.

1. Extensive usage of conventional fuel energy sources can be reduced.
2. Decreasing the percentage of GHG emission.
3. Bridges the gap between energy supply and demand.
4. Energy savings.
5. Reducing the peak loads on cooling or heating system during On-Peak demand.

According to the way the heat is stored, thermal energy storage can be divided into 3 types.

i. Sensible heat storage system.
ii. Latent heat storage system.
iii. Thermo-chemical storage system.

1.4.1 Sensible heat storage system

The materials used for a sensible heat storage system absorb, store, and redistribute the heat energy wherein the material changes its temperature. The sensible materials can be in the form of solid or liquid, however, there are no phase transformations observed during the sensible heating or cooling process [**4**].

Amount of heat stored can be evaluated using eq. (1).

$$Q = m \cdot C_p \cdot (T_2 - T_1) \text{ ------ } (1)$$

Where m is the mass of the storage material, C_p is the specific heat at constant pressure, T_1 and T_2 are the initial temperature and final temperature of the material.

In comparison to latent heat or thermo-chemical storage systems, sensible heat storage systems are simple. Nonetheless, they do have the drawback of being bulkier and incapable of maintaining consistent energy storage at constant temperature. Compatibility with its containment, a crucial factor for both the heat storage material and the confinement, stands as a paramount determinant of the overall cost of the storage system. The storage material properties largely determine the sensible heat storage solution's final cost. Commonly

employed storage mediums include cost-effective materials such as water, rocks, pebbles, and sand [**4, 12**].

1.4.2. Latent Thermal Energy Storage system (LTES)

Latent thermal energy storage system is more popular, wherein PCM plays a key role in absorbing the energy at off-peak demand, it stores the energy and redistributes during On-peak demand **[4]**. The phase change materials have a capability of high energy storage density and the fact that it can store heat at a constant temperature close to the phase transition temperature. The material absorbs latent heat during phase transformation from liquid to solid and redistributes the same when transforming from solid to liquid at constant temperature as shown in Fig. 6.

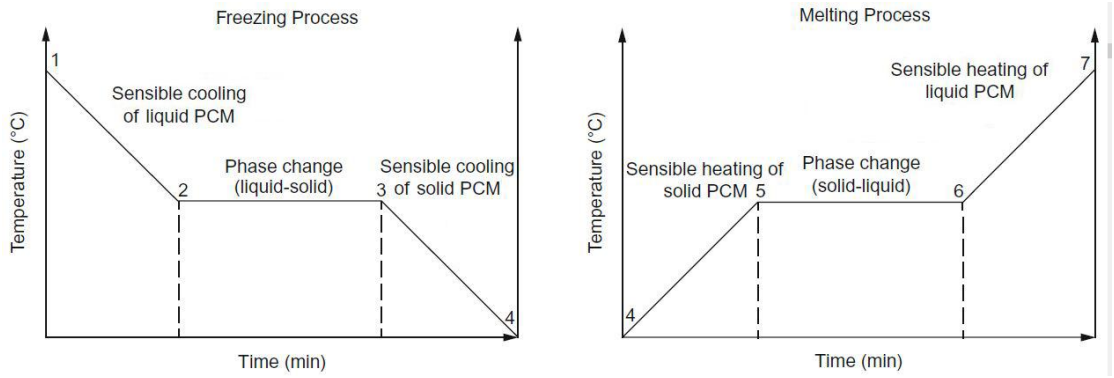

Fig. 6. Principle of Phase Change Materials **[4]**.

1.4.3. Thermo-chemical Energy Storage System

Thermo-chemical Energy Storage System (TCES) uses the chemical potential of some materials to absorb, store and release thermal energy. When it comes to the storage and retrieval of thermal energy in the TCES, the reversible chemical interactions which take place between the reactive elements of materials or chemical species are absolutely essential [**13**]. In fact, the endothermic reaction of chemical components can be stimulated by the application of heat energy, which subsequently makes it possible for chemical materials to undergo storage and release processes.

1.5. Summary

In summary, the reports from IEA suggest that the energy usage by residential sector is increasing every year, there is also an increased percentage of global air conditioner stock as reported by IEA. Energy-efficient materials are designed to minimize heat transfer, which can significantly reduce the amount of energy required to heat or cool a building. LTES system is more prominent in which PCM which has a capability of absorbing and releasing the energy can address the challenges and reduce the cooling load demand for the buildings.

The driving force behind the research on PCM embedded cement mortar is the essential requirement to develop energy-efficient and environmentally responsible building materials. Such materials have the potential to revolutionize the construction industry, positively impacting energy consumption, and contributing to a more sustainable and eco-friendly future. The aforementioned data alarms the need of developing energy efficient materials which can reduce heat gain in the room and facilitate to store energy during off-peak demand and redistribute it during on-peak demand, which enables the air conditioner to operate at minimum capacity, this results in energy saving consequently reducing GHG emissions.

1.6. Organization of the thesis

The thesis is structured into six chapters, and a succinct overview of the contents of each chapter is outlined below.

Chapter-1: In this chapter, an exploration of the global energy within buildings is undertaken, encompassing a comprehensive analysis of energy consumption in the building sector. Special attention is given to the energy demands imposed by air conditioning systems for space cooling in buildings. The chapter also delves into an examination of the global air conditioner stock, alongside an investigation of thermal energy storage techniques, and an elucidation of both active and passive cooling methodologies.

Chapter-2: This chapter provides a comprehensive review on the synthesis and thermal characterization of encapsulated PCM. Furthermore, a review was performed on the thermo-structural properties of pure PCM, and encapsulated PCM embedded in cement mortar. This chapter reviews the articles concerning energy savings and temperature fluctuations resulting from the incorporation of PCM-based cement mortar used for internal and external plastering applications. Research gap, problem statement, and research objectives were presented.

Chapter-3: This chapter presents the research methodology and plan of action to achieve the proposed objectives.

Chapter-4: This chapter emphasizes the material details, and synthesis procedure. It also highlights the procedure adopted for the direct impregnation of pure PCM and the prepared encapsulated PCM embedded in the cement mortar for cube specimen preparations.

Chapter-5: The test results encompassed a wide range of critical aspects, including the surface morphology, crystal structure, chemical stability, phase transition, thermal energy storage capacity, thermal stability, and thermal conductivity of the pure and encapsulated forms of 1-Dodecanol PCM, and n-Octadecane PCM. This chapter presents the study involved in comprehensive thermal and structural investigations of reference cement mortar and PCM based cement mortar samples.

Chapter-6: This chapter presents the overview of the results and key conclusions derived from the current research endeavor.

Chapter-7: This chapter addresses the future avenues for this research, providing insights into potential areas of exploration and development.

CHAPTER - 2

LITERATURE REVIEW

This chapter provides a comprehensive review on the synthesis and thermal characterization of encapsulated PCM. A critical review has been done on the thermo-structural properties of pure PCM, and encapsulated PCM embedded in cement mortar. This chapter reviews articles concerning energy savings and temperature fluctuations resulting from the incorporation of PCM-based cement mortar used for internal and external plastering applications. This chapter presents the research carried out to enhance the thermal properties of pure PCM and the shell of the encapsulated PCM using nanoparticles. Based on the extensive literature review, research gaps was identified, which plays a crucial role in defining the problem statement, and formulating research objectives.

Among various types of storage systems discussed in the aforementioned chapter, the LTES system is gaining importance. The fundamental working of PCM makes it a viable candidate for more attention in building applications. Based on the above considerations, there has been a rise in interest in finding ways to store and distribute heat/cool energy, with many studies focusing on thermal energy storage systems that make use of efficient latent heat storage materials. The inclusion of LTES systems in buildings is heavily reliant on the phase change properties of the heat storage material under consideration. However, practically phase transformation of PCM does not take place at constant temperature rather, it takes place over a small range of temperature **[10]**. Proper utilization of PCM can effectively minimize peak heating and cooling loads, while also possessing the capacity to maintain indoor temperatures within the comfort range by mitigating smaller temperature fluctuations. As a result, this approach can lead to a reduction in the dimensions and energy consumption of the TES system **[14, 15].** One of the primary merits associated with PCM employment is

its ability to amplify thermal storage potential, all the while requiring only minimal alterations to the current building design.

The choice of PCM primarily hinges on freezing and melting temperatures, with latent heat emerging as a crucial factor. Additionally, Fig. 7 illustrates the desirable properties that make a PCM desirable.

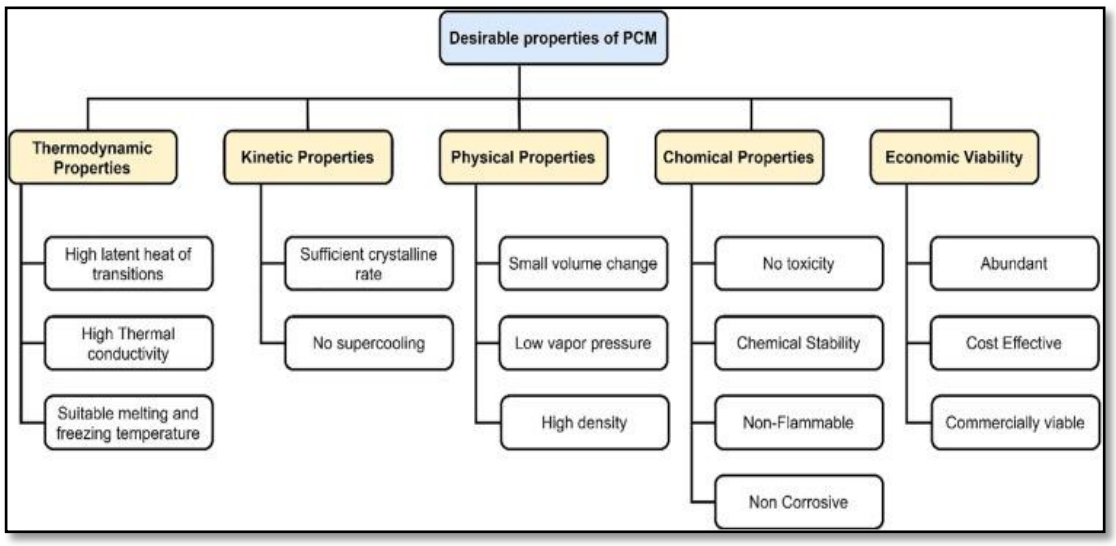

Fig. 7. Desirable properties of ideal PCM [**4**].

2.1. Classification of PCM

An ideal Phase Change Material (PCM) should exhibit the aforementioned properties; however, it's important to acknowledge that in practice, finding a PCM that encompasses all these traits is quite challenging. The market offers a wide range of PCMs, each characterized by distinct phase change temperatures. Each type will have its own advantages. The selection of PCM for a particular application depends mainly on the phase change temperatures, besides latent heat and thermal conductivity, and other thermo-physical properties also play a vital role. Furthermore, latent heat, thermal conductivity, and other thermo-physical attributes also hold a significant way in the selection process.

A comprehensive categorization of phase change materials has been depicted in Fig. 8. Among various PCMs available in the market, organic PCMs possess distinct benefits such as congruent phase transformations, non-corrosive properties, non-toxicity, and good thermal as well as chemical stability **[16]**. Despite these advantages, organic PCMs are beset by challenges including the super cooling phenomenon, low thermal conductivity, high volume changes, and susceptibility to flammability **[17, 18, 19, 20]**. Especially, thermal conductivity is considered very crucial for the PCM, poor thermal conductivity results in a lower number of phase change cycles per day **[21]**.

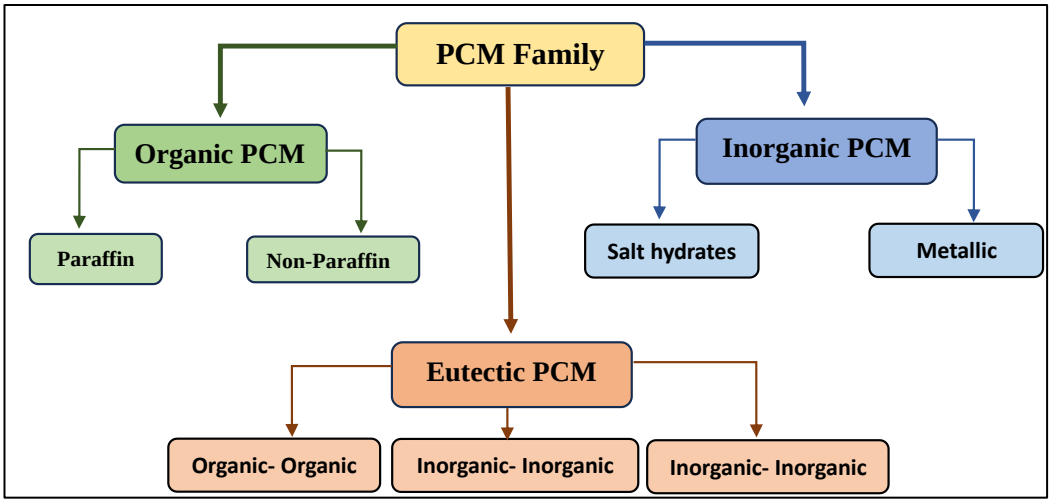

Fig. 8. Classification of phase change materials.

2.2. Establishing the LTES system in buildings

Establishing the LTES system using phase change materials in building can be done in two ways.

2.2.1. Active system

An active storage system is one that comprises a mechanical assisted component support to enable the thermal energy exchange between the system and the heat source. This type of system is also known as an active thermal energy storage system [**4, 11**].

2.2.2. Passive system

Without the intervention of any additional mechanisms, natural convection or buoyant forces (owing to a density gradient) are the means by which thermal energy interactions take place in a passive storage system and are responsible for the heat transfer between the system and the source [**4, 11**].

By considering the peak load demand in buildings, it becomes possible to establish the allocation of cooling/heating energy between the thermal energy storage system and the building's overall energy system. Both systems are equally important in establishing TES system in buildings. The application of system depends upon the following factors such as

1. Location
2. Atmospheric conditions
3. Heating /cooling load profile of the building.

PCMs can indeed mitigate the energy requirements of cooling systems and the indoor temperature fluctuations. Nevertheless, the effective implementation of PCMs for passive cooling within the building envelope necessitates careful consideration of several selection criteria. From a physical standpoint, it is imperative that the melting point of the PCM falls within the range of 10 °C to 30 °C to ensure optimal thermal comfort for occupants. This temperature range should be chosen in accordance with the average day and night temperatures, as well as other climatic conditions prevailing at the building site.

In recent years, there has been a significant surge of interest in passive design for both heating and cooling, especially in the last decade. This trend is a crucial element of the sustainable architecture movement. Environmentally friendly, passive building energy efficiency strategies offer pragmatic solutions to tackle the issues stemming from the energy crisis and environmental pollution.

2.3. PCM incorporation in Buildings

Various ways researchers have tried to establish the TES system by incorporating PCM in buildings such as ceiling, floor, walls, claddings, and as a plastering material **[15, 22-24]**. The energy saving potential of the PCM when incorporated in the building envelope depends on the type of the PCM and the environment of the building. In general, the PCM is incorporated either with the building material or with the HVAC system. The overall effect of the PCM on the use of energy on space cooling and heating varies from place to place and condition to condition. Incorporation of PCM in building fabrics is more prominent. The building envelope, which serves as the boundary between indoor and outdoor environments, plays a crucial role in influencing indoor quality and maintaining indoor conditions regardless of external fluctuations. Comprising a range of components including walls, roofs, windows, and foundations, the building envelope offers opportunities for incorporating PCM across its various elements. However, PCM integration is most commonly found in walls, roofs, ceilings, floors, and windows due to their ease of installation and their ability to facilitate more efficient heat transfer. To establish thermal energy storage in buildings, PCM is mixed with cementitious materials.

Cement, regarded as one of the most vital building materials, serves as a binding agent that undergoes a process of setting and hardening to adhere firmly to various building elements, including bricks, tiles, stones, tiles, and more. Generally, cement refers to an exceedingly fine powder primarily composed of limestone (calcium), sand or clay (silicon), bauxite (aluminum), and iron ore, with the potential inclusion of materials like marl, clay, chalk, shells, shale, blast furnace slag. When mixed with water, cement initiates an exothermic chemical reaction, resulting in the formation of a paste that sets and hardens, securely bonding individual structural components of building materials. Cement plays a pivotal role in the construction industry, as it is employed not only in the creation of concrete but also in

mortar, ensuring the integrity of infrastructure by firmly uniting building blocks. Concrete, a composite material, comprises cement, water, and sand, mixed in varying proportions, while mortar consists of cement, water, and fine aggregate as shown in the Fig. 9. Both cement mortar and concrete compounds are essential for binding rocks, stones, bricks, and various building units, as well as for filling gaps and crafting decorative designs. PCM, either in its own form or other forms such as encapsulated PCM, can be mixed with cement mortar or concrete. The integration of PCM into the cementitious material should not compromise its structural strength. The potential benefits of PCM in building fabrics are indeed substantial and encompass various aspects of energy efficiency and sustainability.

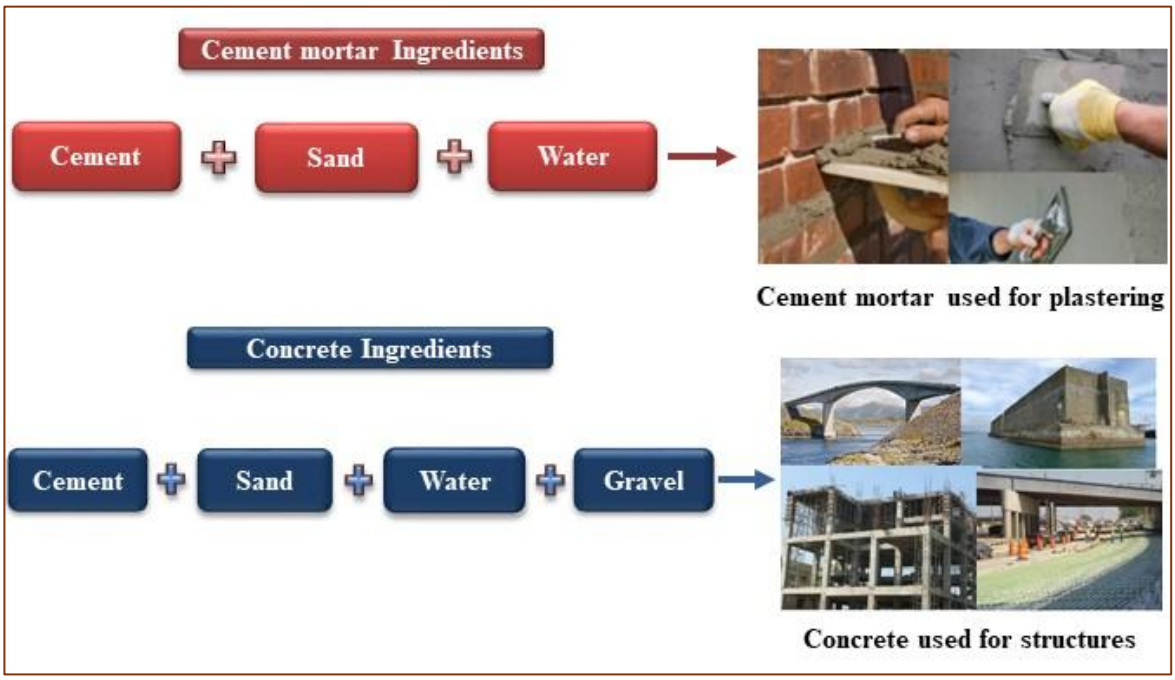

Fig. 9. Cement mortar and concrete ingredients.

2.4. Need of Research on PCM

As the demand for energy-efficient building solutions intensifies, the need for research on Phase Change Materials (PCMs) becomes increasingly significant. Here are some key technical aspects that underscore the importance of PCM research:

1. **Enhancement of Thermal Properties**: Research is needed to develop PCMs with higher latent heat capacities, improved thermal conductivity, and optimal phase change temperatures tailored to different climatic conditions. Improving these properties can significantly enhance the energy efficiency of buildings.

2. **Development of Advanced Encapsulation Techniques**: Innovative encapsulation methods are essential to prevent PCM leakage and degradation, especially under repetitive thermal cycles. Research into durable, efficient, and cost-effective encapsulation technologies will help overcome major barriers to PCM use in construction.

3. **Hybrid PCM Systems**: Exploring hybrid systems that combine PCMs with other energy-saving technologies like solar panels and HVAC systems can lead to more comprehensive solutions that maximize energy savings and sustainability in buildings.

4. **Lifecycle and Sustainability Analysis**: Investigating the full lifecycle impacts of PCMs, including production, usage, and disposal, is critical. Research should focus on developing environmentally friendly PCMs and recycling methods to reduce the overall carbon footprint.

5. **Compatibility and Integration**: Research must address the compatibility of PCMs with common building materials to ensure that PCM-enhanced materials can be easily integrated into existing building practices without compromising structural integrity or aesthetic qualities.

6. **Cost Reduction Strategies**: High costs associated with PCM production and implementation are a significant barrier. Research aimed at reducing the cost through innovative manufacturing processes and material sourcing is crucial for wider adoption.

7. **Regulatory and Standardization Efforts**: Establishing standardized testing and performance criteria will help integrate PCMs into building codes and regulations more effectively. Research should also explore the regulatory aspects to ensure safety, efficacy, and quality control in PCM applications.

8. **Smart PCM Systems**: Integrating PCMs with IoT devices and smart building technologies could revolutionize building energy management. Research into smart PCM systems would involve developing materials that can dynamically adjust their properties based on real-time environmental and occupancy data.

Each of these research areas holds the potential to significantly advance the application of PCMs in building technologies, paving the way for more sustainable, energy-efficient, and comfortable living environments.

Several research works have been dedicated in establishing Latent Thermal Energy Storage (LTES) systems in building fabrics. Despite the diverse range of PCM availability in the market, organic PCMs have gained significant popularity in building applications as presented in Table 1. These organic PCMs offer several advantages, including low super cooling effect, absence of phase segregation, thermal stability, chemical stability, and provide non-corrosive and non-toxic option for practical use **[25, 20].** Table 1 presents the list of PCM used for cooling applications in buildings. Two prominent approaches for integrating PCM in building fabrics are direct impregnation and encapsulation, as reported in works **[3, 26, 27]**. These findings and approaches offer valuable insights for the development and implementation of advanced PCM-based systems in building applications, aiming to optimize thermal performance and energy efficiency. A detailed literature review has been carried out regarding direct impregnation of organic based PCM in the cement mortar.

Table 1. List of organic PCMs used for building applications

S. No.	PCM	Melting Temp. (°C)
1	1-Dodecanol PCM	21
2	n-Octadecane PCM	26
3	Methyl Palmitate	29
4	n-Nonadecane PCM	19
5	Paraffin wax	32

2.5. Direct Impregnation of pure PCM in the building materials

Direct impregnation of PCM in building fabrics is simple and very economical. In this technique, the selected PCM or nano based PCM is directly embedded in the cementitious materials to establish a thermal energy storage system. Below are a few studies that reported the impact on thermo-structural properties of cement mortar due to PCM direct impregnation.

Cunha et al. [**28**] directly impregnated paraffin based PCM in the cementitious material, it is reported that due to the presence of PCM, there was a reduction in the water absorption besides, higher content of PCM in the cement mortar led to a higher drop in the compressive strength and flexural strength. Kheradmand et al. [**29**] carried out the thermo-structural investigation of PCM based cement mortar, the test results revealed that due to the direct impregnation of PCM into the cement mortar, the PCM is leaking from the cube specimens during curing, besides the density of cube specimens was reduced, which resulted in reduction in the compressive strength and flexural strength. The compressive strength was 32 MPa and 20 MPa with the inclusion of 10% and 20% grated PCM in the cement mortar respectively. Besides, thermal conductivity was also reduced by 20% and 40% due to the presence of 10% and 20% PCM embedded in the cement mortar respectively.

Cunha et al. **[30]** directly impregnated paraffin based PCM in the cement mortar. The mass proportions of PCM embedded in the cement mortar in the study were 0%, 2.5%, 5%, and 7.5% of fine aggregate. The author reported that the water added to the admixture decreased with the increased percentage of PCM content. Due to direct impregnation, there was no change in the compressive strength until the incorporation of 2.5% PCM in the cement mortar, beyond 2.5% there was a drastic drop in the compressive strength.

Kong et al. **[31]** prepared PCM based cement mortar, and reported a drastic drop in the density which was due to the porous structure which resulted in a reduction in the flexural strength and compressive strength, this was due to direct impregnation of PCM in the cementitious material.

The literature review suggests that the direct impregnation of PCM in building fabrics has some significant drawbacks, including leakage issues, reduced energy storage capability, loss of material integrity, and volumetric changes during phase transformation. Additionally, direct contact between PCM and cementitious materials results in a substantial drop in compressive strength. To overcome these challenges, researchers have focused on developing PCM in a compatible form using encapsulation techniques.

2.6. Encapsulation of PCM

The schematic of PCM encapsulation is depicted in Fig. 10, where the core PCM is protected within a shell. This encapsulation enables the PCM to undergo phase transformation, efficiently absorbing and releasing energy from the surroundings. The encapsulated PCM typically takes a spherical shape due to surface tension, with sizes ranging from nanometers to millimeters. Researchers have developed various techniques for encapsulating PCM as shown in Fig. 11, each offering its own advantages and limitations.

The choice of encapsulation technique depends on factors such as the nature of the PCM, the shell material used, capsule size, and surface morphology **[32].**

The selection of the shell material is crucial in encapsulating PCM, and it depends on the compatibility between the PCM and the shell material, considering interfacial properties and intermolecular forces between them. Table 2 presents different types of shell materials used for encapsulating PCM. The shell material should possess good mechanical strength to prevent leakage, as well as exhibit good thermal conductivity and thermal stability to maintain effective energy storage capabilities. These considerations are essential for successful PCM encapsulation, offering a promising solution to overcome the limitations of direct impregnation in building fabrics.

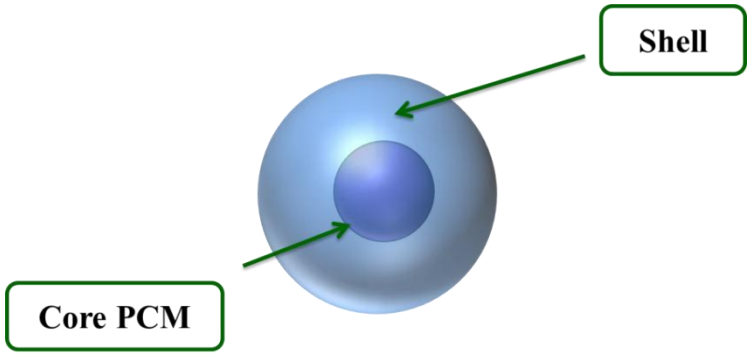

Fig. 10. PCM encapsulated in a spherical shell material.

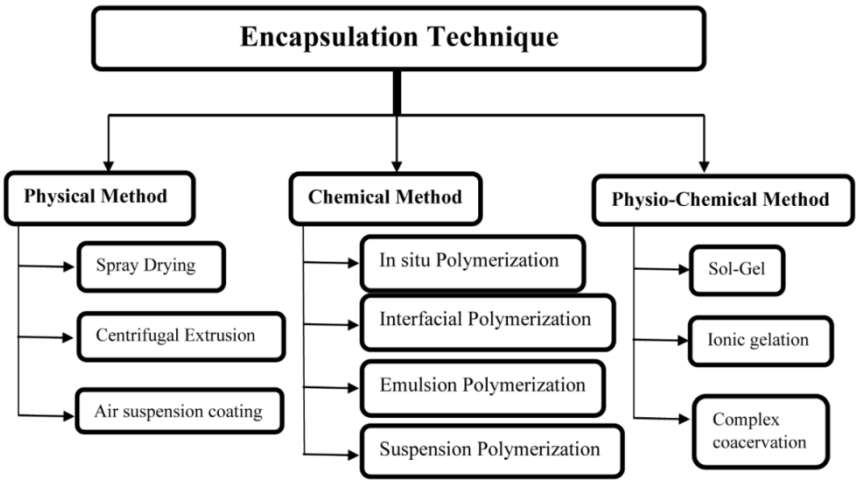

Fig. 11. PCM Encapsulation techniques.

Among various types of shell materials available for encapsulation, organic type shell materials are mostly preferred due to their distinct advantages. Based on the size of the encapsulated PCM it is further classified as mentioned below.

1. Macro encapsulated PCM
2. Microencapsulated PCM
3. Nano encapsulated PCM

The size of the capsules plays a vital role in achieving the properties. Smaller size capsules exhibit a great increase in surface-to-volume ratio, it is predicted that the 1 mm size of encapsulated PCM increases the surface area by 300 m^2/m^3 compared with bulk PCM **[33]**. The thermal properties will greatly enhance if the encapsulated PCM can be fabricated at a nano level. Wide varieties of shell materials are available for encapsulating the PCM, the shell materials are of organic material, Inorganic material type **[34].** A detailed literature review has been carried out regarding encapsulating a variety of PCM with different types of organic shell materials and presented in Table 3.

Table 2. Shell material types for PCM encapsulation

Shell material	
Organic shell	Inorganic shell
Melamine formaldehyde	Silica
Urea formaldehyde	Alumina
Acrylic	Titania
Polyurea	Calcium carbonate
Poly (urea-urethane)	Zinc oxide

Table 3. PCM encapsulation

S. No.	PCM	Shell	Size	Method	Onset Melting Temp. (°C)	Encapsulation ratio	Remarks	References
1	n-Octadecane	Methyl–methacrylate	300-500 nm	Phase inversion emulsification and suspension polymerization	23.2	67.4	Thermal stability increased with increased shell thickness.	**[35]**
2	n-nonadecane	Poly (styrene-co-methacrylic acid) P(St-co-MAA)	Average size 212 nm	Mini-emulsion polymerization	32.16	54	Dual peaks evolved during Freezing and Melting process	**[36]**
3	n-Octadecane	Polystyrene	100-123 nm	Mini emulsion In-situ polymerization	25.5	53.5	The nano capsules exhibited good thermal stability	**[37]**
4	n-tetradecane	Polystyrene	Average 132 nm	Mini emulsion In-situ polymerization	4.04	44.74	The capsules were stable even after 40 times freezing thaw cycles	**[38]**
5	n-nonadecane	Poly(methyl methacrylate)	Mean diameter of 8.18 µm	Emulsion polymerization	31.23	60.3	The capsules are clustered, and the surface is rough in	**[39]**

S. No.	PCM	Shell	Size	Method	Onset Melting Temp. (°C)	Encapsulation ratio	Remarks	References
							nature	
6	n-eicosane	Poly(methyl methacrylate)	Average size 135 nm	Mini emulsion	34.66	61.6	Due to nanoencapsulation, there was drop in super cooling effect.	**[40]**
7	Paraffin	Methyl methacrylate	200-400 nm	Interfacial Polymerization	21.42	52.95	The capsules exhibited very good thermal stability.	**[41]**
8	Butyl palmitate	Polystyrene-co-methyl methacrylate	Average size 210 nm	Suspension polymerization	21	60	Thermovision test was varied out to study energy storage capability of NPCM/gypsum.	**[42]**
9	Paraffin	Melamine-urea-formaldehyde	Average size 350 nm	In-situ polymerization	9.53	36.7	Nanocapsules were prepared using high intensity ultrasound assisted emulsification process	**[43]**
10	n-Octadecane	PNDA modified melamine formaldehyde	80-140 nm	In-situ polymerization	26	58.6	Phosphorous nitrogen containing diamine modified MF shell exhibited good	**[44]**

S. No.	PCM	Shell	Size	Method	Onset Melting Temp. (°C)	Encapsulation ratio	Remarks	References
							flame-retardant characteristics	
11	Polyethylene glycol	Urea formaldehyde	Average size 141 nm	In situ polymerization	41.9	10	The capsules exhibited good thermal stability.	**[45]**
12	Hexadecane	Urea formaldehyde	Mean particle size is 270 nm.	Mini-emulsion polymerization	16.15	68.9	Leakage test was carried out, no traces of PCM after being heated upto 100 °C for 12 hrs.	**[46]**
13	Hexadecanol	Polystyrene	Average size 120 nm	One-pot emulsion polymerization	45	48.7	One-pot emulsion polymerization doesn't require high shear homogenization.	**[47]**
14	n-Octadecane	Melamine formaldehyde	Average size 636 nm	In situ polymerization	26.76	63	The capsules exhibited stable phase change characteristics even after 300 thermal cycles.	**[48]**
15	Eicosane+ Hexadecane (1:10)	CTS-co-PMAA	Average size 438 nm	Emulsion formation through coacervation	9	66	No much variation in the phase change characteristics when the capsules are	**[49]**

S. No.	PCM	Shell	Size	Method	Onset Melting Temp. (°C)	Encapsulation ratio	Remarks	References
							subjected to 20 and 100 thermal cycles	
16	n-Octadecane	Methyl methacrylate-co-octadecyl methacrylate copolymer	Average 368 nm	Mini-emulsion polymerization	23.4	46	The copolymer shell effectively suppressed supercooling effect	**[50]**
17	Heneicosane	Poly (methyl methacrylate)	Average size 25.2 µm	Emulsion polymerization	30.14	43	The capsules exhibited good thermal stability and chemical stability	**[51]**
18	Octacosane	Poly (methyl methacrylate)	Average size 37.1 µm	Emulsion polymerization	57.60	56.7	The capsules exhibited good thermal stability and chemical stability	
19	n-Octadecane	Styrene-Methyl methacrylate	Average size 152 nm	In situ polymerization	28.4	45	Even after 350 thermal cycles, the capsules are stable in terms of chemical and thermal stability	**[52]**

S. No.	PCM	Shell	Size	Method	Onset Melting Temp. (°C)	Encapsulation ratio	Remarks	References
20	RT-80	Styrene-butyl acrylate copolymer	52-112 nm	Mini emulsion polymerization	82.8	78	The nano capsules exhibited good thermal stability even after 200 thermal cycles	**[53]**
21	n-Octadecane	n–Octadecyl methacrylate–methacrylic acid co–polymer	1.6-1.7 µm	Suspension polymerization	26.5	21%	The micro capsules exhibit good potential for energy storage by using monomer as side chain long alkyl group in the preparation of shell material	**[54]**
22	n-Octadecane	Poly (butyl methacrylate), Poly (butyl acrylate)	2-75 µm	Suspension polymerization	29.1	55.6%	There were minor changes in the phase change temperatures and latent heat after the capsule subjected to 1000 thermal cycles	**[55]**
23	n-heptadecane	Polystyrene	1-20 µm	Emulsion	21.5	63.3%	Approximately 22.7% drop in	**[56]**

S. No.	PCM	Shell	Size	Method	Onset Melting Temp. (°C)	Encapsulation ratio	Remarks	References
				polymerization			the thermal conductivity of encapsulated PCM compared with pure PCM	
24	n-nonadecane	Polystyrene	0.1-35 µm	Emulsion polymerization	31.2	60.3%	The thermal conductivity of micro/nano encapsulated PCM and pure PCM are 22 W/m K and 18 W/m K respectively	**[33]**
25	n-dotriacontane	Polystyrene	Average size 168.2 nm	Ultrasonically initiated Mini-emulsion polymerization	70.9	61%	The PCM inside the capsule freezes and melts in a single stage with no solid-to-solid phase transformations	**[57]**

The studies have explored PCM encapsulation extensively, achieving particle sizes ranging from micro to nano scale. Nonetheless, it remains crucial to investigate the microstructural, thermal, and structural changes resulting from the incorporation of encapsulated PCM into cement mortar. Below is the literature that explores the thermo-structural behavior of encapsulated PCM embedded within cement mortar.

2.7. Encapsulated PCM in the Cement Mortar (Thermo-structural investigations)

Researchers tried impregnating the encapsulated PCM in building fabrics and performed various studies such as the condition of capsules in the cement mortar, leakage test, energy storage and release capability of capsules impregnated in building fabrics, compressive strength, and thermal conductivity. Below is the literature about the study on the thermo-structural behaviour of cement mortar due to encapsulated PCM impregnation.

Joulin et al. **[58]** studied the thermal behaviour of microencapsulated PCM embedded cement mortar. The authors have reported a drop in the thermal conductivity from 0.65 W/m K to 0.37 W/m K due to microencapsulated PCM inclusion in the cement mortar, the drop was approximately 43%. The capsules embedded in the cement mortar exhibited good phase change characteristics which commence its freezing at 26 °C. besides, the PCM based cement mortar has the capability of absorbing and releasing energy which is approximately 41% more than the plain cement mortar. Djamai et al. **[59]** examined the behaviour of cement mortar by adding the encapsulated PCM in the proportions of 5%, 10%, and 15%. The author stated that the decrease in the degree of hydration and increased porosity could be the reason for the drop in the compressive strength of encapsulated PCM embedded cement mortar compared with the reference cement mortar. However, the drop in the compressive strength due to the inclusion of encapsulated PCM in the cement mortar is low compared with PCM direct impregnation. Jayalath et al **[60]**. carried out a thermo-structural investigation by embedding paraffin based microencapsulated PCM embedded in the cement mortar. The sand

was replaced with encapsulated PCM in the percentage of 5%, 10%, 20%, 35%, and 55% which resulted in reduced compressive strength of 38%, 14%, 27%, 43%, and 50% respectively. As the thermal conductivity of fine aggregate is more than the encapsulated PCM, there was a reduction in the thermal conductivity of the PCM based cement mortar. The author reported that the optimum level of replacement is 20%.

Cunha et al. **[61]** embedded paraffin based microencapsulated PCM in the cement mortar. Melamine formaldehyde shell was used to encapsulate the PCM. The author reported a drop in the flexural strength and compressive strength by 28% and 60% respectively. It was stated that the drop in strength could be due to formation of pores in the cement mortar due to encapsulated PCM dispersion. Kontoleon et al. **[62]** carried out a thermo-structural investigation by incorporating paraffin coated PCM capsules in the proportion of 10%, and 20% in the cement mortar. The fine aggregate was replaced with encapsulated PCM in the cement mortar. The PCM capsules embedded in the cement mortar with the proportion of 10%, and 20% resulted in the porosity of 6.39% and 9.86% respectively. Due to the porous structure of PCM based cement mortar, the compressive strength was reduced by 30%, and 33% compared with reference cement mortar. Illampas et al. **[63]** prepared PCM based cement mortar by incorporating the microencapsulated paraffin PCM in the proportion of 5%, 10%, and 20% by the weight of mortar. The author reported porosity formation due to micro PCM capsule inclusions in the cement mortar. The accessible porosity for the reference cement mortar reported was 9.3%, on the other side, with the increased percentage of microencapsulated PCM of 5%, 10%, and 20%, the accessible porosity resulted was 9.9%, 12.7%, and 15.7% respectively. Due to increased accessible porosity, the compressive strength was reduced proportionately. Besides, thermal conductivity was reduced by 36.19%, 49.97%, and 64.63% due to microcapsule inclusion of 5%, 10%, and 20% respectively.

10% and 20% microencapsulated PCM capsules were embedded by Haurie et al. **[64]** in the cement mortar. The prepared samples were cured for 7 days, 28 days and 90 days. The density of cement mortar embedded with 10% and 20% microencapsulated PCM were reduced by 8.95% and 22.39% respectively compared with the reference mortar. The compressive strength was reduced by 43.81% due to inclusion of 20% microcapsules in the cement mortar, and it was reported that porosity could be the principle reason for the drop. Yoo et al. **[65]** developed laboratory size test cell that resembles the actual construction. A novel energy storage aggregate (TESA) was developed to resolve the issue of zeolite impregnated with paraffin wax and coated with epoxy resins silica fume hand silicon carbide. Thermal shock cycling test carried out for TESA yields long term thermal reliability. TESA used as plastering mortar for external walls reduce the maximum temperature by 7 °C and fluctuations in temperature range compared with the reference cement motor. Amin Al-Absi et al. **[66]** developed PCM-based composite material which is used as external plastering to reduce the heat gain. The microencapsulated PCM inclusion in the cement mortar has reduced thermal conductivity and compressive strength by 52.6% and 53% respectively compared with the reference cement mortar.

The encapsulated PCM incorporated in the cement mortar has really favoured overcoming the barrier of leakage issues and the shell material of the capsules avoided the PCM interacting with cementitious material, however on other side the encapsulated PCM embedded in the cement mortar tends to reduce compressive strength and thermal conductivity. Nevertheless, the reduction is less compared with PCM direct impregnation technique. The study pertaining to the thermal behaviour of encapsulated PCM embedded in building fabrics in terms of heat gain into the room, peak temperature delay, and energy savings bare crucial. Keeping in view, a detailed literature study has been presented below.

2.8. Encapsulated PCM in the cement mortar

Sa et al. **[67]** developed a new composite material that contains paraffin PCM capsules embedded in the cement mortar. The developed composite construction material used as internal plastering has the capability of absorbing 25 kJ/kg while melting in the range of 23 °C and 25 °C. The author reported the maximum indoor temperature for the reference test cell and the PCM based test cell are 26.3 °C and 23.7 °C respectively. Besides, the differences in the minimum indoor temperature were 13.5 °C. The peak temperature inside the PCM based test cell was delayed by 3.5 hours compared with the reference test cell.

The experimental investigation was carried out by Kuznik et al. **[68]** by embedding PCM material in the building wall and subjected to controlled thermal and radiative effects was carried out in the summer and winter seasons. The temperature of the air is lowered and kept under control in the PCM room. The decrement factor was measured to be approximately 0.7 across all seasons when comparing the PCM room to the non-PCM room. The PCM wall significantly decreased the overheating effect, which stores energy and then distributes it throughout space when the temperature is at its lowest point.

Sun et al. **[69]** conducted a comprehensive parametric study to investigate the thermal response of a building wall incorporating a PCM layer for passive space cooling. Numerical models were developed, and rigorously validated against experimental data. The findings revealed the existence of an optimal range for the placement of the PCM layer within the wall cavity, resulting in heat flux reductions exceeding 50% for various outdoor-indoor air temperature differences. Furthermore, the authors reported that as the thermal resistance of the wall insulation increased, the optimal location of the PCM layer slightly was shifted towards the exterior of the wall. Additionally, increasing the thickness of the PCM layer led to an initial increase in peak heat flux reductions, followed by a subsequent decline in performance.

Meng et al. **[70]** performed experimental and numerical investigations by incorporating composite PCM (two PCM with different melting temperatures) in the walls of the test room. Thermal load leveling, Indoor air temperature, heat absorbed/released by the wall, and walls inner surface temperature were studied, and a comparison was done between composite PCM test room and the reference room. It was reported that compared with the reference room the composite PCM room can drop the temperature about 4.28 ~ 7.7 °C and 11.21 ~ 14.12 °C in the daytime of summer and winter respectively. It was also stated that choosing the appropriate PCM for the test room can substantially increase the heat absorbed from the room and decrease the heat released to the room during the summer. In the winter, it can increase the heat discharged into the room and decrease the heat absorbed by the room.

Frozzica et al. **[71]** developed a composite material by embedding two varieties of commercial encapsulated PCM which melts at a temperature of 23 °C and 26 °C. The author reported that the developed PCM based cement mortar used as plastering material helps in minimizing the fluctuations in the temperature and the peak temperatures were delayed.

The thermal performance of microencapsulated PCM-based cement render and foamed concrete for exterior wall finishing was experimentally examined by Al-Absi et al. **[72]**. To investigate the efficacy of PCM in lowering both indoor and surface temperatures, the experiment was carried out using test cells with a volume of 300 cm^3 under controlled conditions. According to the findings, the peak internal surface temperature was reduced by up to 3.95 °C, and the heat flux was decreased by 26 watts per square meter. As a result, the indoor temperature of the cell that was put through the test was 3.05 °C lower than the temperature of a reference cell.

A numerical investigation of RT-28 PCM enhanced building wall was carried out by Salihi et al. **[73]** Annual average ATFR of 1.91 °C. Besides, a study was also carried out with double and triple layered PCM which suggests more efficient than single layer PCM with the

energy consumption reduction from 30% to 21%. Tripled layered PCM comprising Paraffin RT 21, RT 25, and RT 28 facilitates energy performance for cooling in summer and heating in winter resulting in annual energy savings of 324 kWh and 102 kWh respectively.

Kheradmand et al. **[74]** subjected realistic daily temperature profiles to a prototype test cell (with hybrid PCM plastering mortar) and compared its performance with a similar prototype test cell (without PCM) to determine the hybrid mortar's thermal performance. To verify the capability of simulating temperature evolved within the prototype with hybrid PCM and to comprehend the contribution of hybrid PCM to energy efficiency, a numerical simulation model was applied (using ANSYS-FLUENT). It was reported that plastering mortars that include hybrid PCM have been found to have the potential to reduce heating/cooling temperature demands for maintaining the interior temperature within comfort levels, in comparison to both traditional mortars (without PCM) and mortars comprising a single type of PCM.

During the hot season in China, Su et al. **[75]** studied the thermal performance of a binary micro-encapsulated PCM drywall system (two distinct phases change temperature) in a model room during the hot season in China. The investigation was carried out by increasing the thickness from 1 mm to 5 mm, it was reported that the peak air temperature decreased by approximately 6.7 °C, and the comfort temperature in the indoor air was increased by approximately 12 °C, compared to other drywalls.

Saffari et al. **[76]** carried out a simulation-based optimization to determine the ideal melting temperature of PCM to improve the overall energy efficiency of cooling and heating a residential structure in a variety of climates. It was reported that the optimal melting temperature of PCM to reduce annual energy usage in a climate with cold temperatures is between 24 °C to 28 °C. However, in warm climates, the PCM that has melting temperatures ranging from 18 °C to 22 °C is the most appropriate.

The thermal behavior of the wall was investigated in several orientations during the summer, and Lee et al. **[77]** presented a plug-and-play wall structure integrated with an air-conditioning system. The author reported that the peak heat flow was postponed by around 2–3 hours, and the peak heat transfer rate of the wall is seen to be greatly reduced.

Numerical analysis was carried out by Barrientos et al. **[78]** by incorporating the PCM into the external walls. Large differences in the heat gain resulted during the summer season, due to higher solar radiation fluxes. However, not much reduction in the heat was observed during the winter season despite the wall's orientation.

Upon reviewing the literature, it is evident that integrating encapsulated PCM into building fabrics has significantly reduced heat gain within rooms and delayed peak temperatures. However, further improvements are necessary to maximize energy savings, which depend on various factors. One crucial aspect lies in enhancing the inherent thermo-physical properties of the base PCM.

Despite the diverse range of PCM availability in the market, organic PCMs have gained significant popularity in building applications as evident from the above literature. Inspite of several advantages of organic PCM, they are flammable and suffer from poor thermal conductivity, leading to extended freezing and melting times and, consequently, a reduction in the number of phase change cycles per day **[79].** PCM encapsulation has overcome few issues such as material congeniality, leakage issues, nevertheless thermal behaviour and the thermal conductivity are considered crucial as discussed to remove the barriers for its end applications.

Researchers tried incorporating the encapsulated PCM in the cement mortar used as internal plastering material to achieve peak temperature delay and energy savings. Table 4 depicts the literature related to the encapsulated PCM used in the internal plastering.

Table 4. Encapsulated PCM used in internal plastering applications

Author	Encapsulated PCM	Outcomes
Ana et al. [80]	25% of Microencapsulated PCM capsules (Industry manufactured) were used.	There was differences in peak temperature by 2.6 °C compared with reference cement mortar.
Yasiri et al. [81]	Petroleum-based paraffin wax was employed as a PCM in this study, the melting temperature range of paraffin lies within the daily temperature range of the location considered for the study.	The outcomes exhibited PCM effectiveness to stabilise the indoor temperature, showing an AITR of 2 °C during the day. The PCM amount should vary in walls considering their orientation and peak outdoor conditions.
Rathore and Shukla [82]	Paraffin based encapsulated PCM melts at 23 °C with enthalpy of 96 kJ/kg	The results indicated peak temperature reduction by 40.67 % - 59.79 %, time lag extension by 60–120 min and electrical energy saving by 0.40 US $/day

Several works were carried out by the researchers towards enhancing the properties such as thermal stability, thermal reliability, especially thermal conductivity which plays a crucial role in reducing freezing and melting times. A detailed review regarding enhancing the properties of the various PCM using metallic and non-metallic nanoparticles has been presented below.

2.9. Enhancing the thermal properties of PCM using nanoparticles

PCMs exhibit a diverse range of phase change temperatures, but only a limited number of them are suitable for building applications. In addition, PCMs, regardless of their applications, encounter common challenges, as illustrated in Fig. 12. To overcome these challenges, the thermal properties of the PCM can be significantly improved through the dispersion of nanoparticles. Fig. 13 provides an overview of the instruments used for testing the thermal and physical properties of the PCM and their respective purposes.

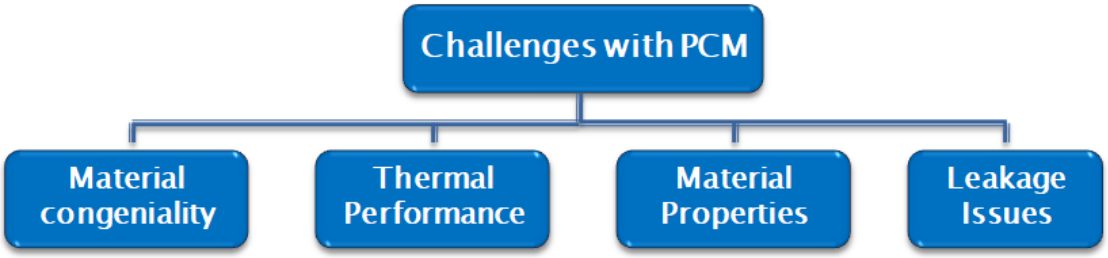

Fig. 12. Challenges with PCM.

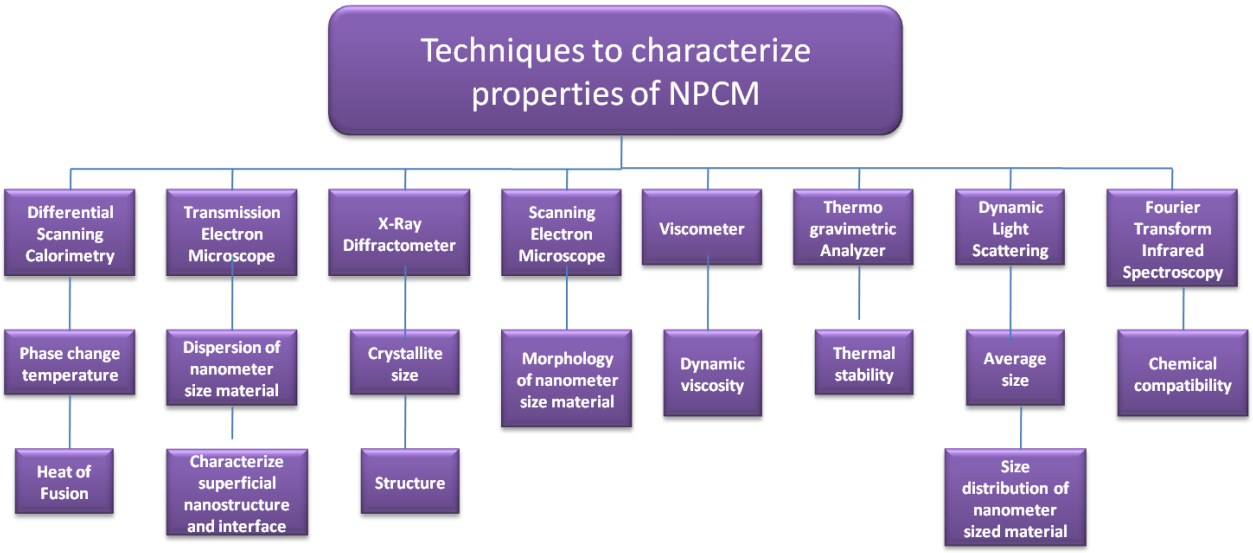

Fig. 13. Characterization techniques to test the PCM.

Wu et al. **[83]** enhanced the thermal conductivity of paraffin PCM by dispersing copper nanoparticles. 2% by wt. of Cu nano inclusions in the PCM enhanced thermal conductivity by 14.2% and 18.1% in liquid and solid state respectively. The enhanced thermal conductivity resulted in reduced melting and freezing times by 33.3% and 31.6%, respectively. Samiyammal et al. **[84]** fabricated MgO nanoparticles, the prepared nanoparticles were dispersed in the paraffin PCM. 1.0% by wt. of MgO nano inclusions in the PCM enhanced thermal conductivity by 55.5%, besides thermal stability was also enhanced with nano inclusions. Kalaiselvam et al. **[85]** conducted an experimental and analytical study to develop a Latent Thermal Energy Storage (LTES) system for building applications. The

researchers dispersed nanoparticles in the PCM to enhance its heat transfer capabilities. Six different types of PCMs were analyzed in their pure form, and then aluminium and alumina nanoparticles were dispersed in them. The findings revealed that by dispersing alumina and aluminium in a mixture of 60% n-tetradecane and 40% n-hexadecane PCM, the solidification time was reduced by 4.97% and 12.97%, respectively. This indicated an improvement in heat transfer efficiency during the melting and freezing processes. The enhanced heat transfer was attributed to the micro convection effects generated within the PCM mixture without compromising energy efficiency. These results demonstrate the potential of using nanoparticles to enhance PCM performance in LTES systems for building applications.

Ma et al. **[86]** prepared Cu-based RT-24 PCM, which favoured approximately 8.3% and 25.1% more heat charged and discharged respectively, compared with pure PCM. Khan and ahmad khan **[87]** dispersed various nanoparticles aluminium nitride, aluminium oxide and graphene nanoplatelets in the paraffin PCM, which resulted in an increase in the charging rate by 36.47%, 28.01%, and 44.57%, and the discharging rate by 39.45%, 14.63%, and 41%, respectively. Zeng et al. **[88]** improved the thermal conductivity of 1-tetradecanol PCM from 0.32 W/m K to 1.46 W/m K, with the dispersion of 11.8% by vol. of silver nanoparticles. It is reported that the composition exhibited reasonable energy storage of 76.5 kJ/kg.

Alumina nanoparticles with a weight proportion of 5% and 10% were dispersed in the n-Octadecane PCM. Ho et al. **[89]** reported that with the increased mass percentage of nanoparticles in the PCM, there was a non-linear increase in the thermal conductivity compared with pure PCM. Soni et al. **[90]** enhanced the thermal conductivity of Erythritol PCM using various nanoparticles such as titania (TiO_2), copper (Cu), alumina (Al), and silicon oxide (SiO_2). There was an enhancement in the PCM, however, the thermal enhancement of the PCM was 8% greater due to the dispersion of Al and Cu nanoparticles in the PCM compared with TiO_2 and SiO_2. The time taken for melting the expanded graphite-

based stearic acid was lowered by 63% compared to pure PCM, during the investigation that was carried out by Li et al. **[91].** Elbahjaoul et al. **[92]** enhanced the heat transfer characteristic and solidification process by preparing copper nano-based n-Octadecane PCM.

Parameshwaran et al. **[93]** prepared Ag-TiO_2 hybrid nano-based dimethyl adipate PCM (HiNPCM), the maximum dispersion of nanoparticles in the PCM enhanced thermal conductivity by 58.4% than pure PCM. Besides, the HiNPCM reduces the freezing and melting times by 29.9% and 9.17% respectively. Ag nano/organic ester PCM prepared by Parameshwaran et al. **[94]** exhibited good thermal properties. Thermal conductivity was increased from 0.284 W/m K to 0.765 W/m K, which reduced the freezing and melting times by 30.8% and 11.3%, respectively. The thermal conductivity of Palmitic acid PCM was enhanced by Wang et al. **[95]** by dispersing multi-walled carbon nanotubes. It was reported that with the dispersion of 0.01 mass fraction of CNT, thermal conductivity was enhanced by 46% and 38% at a temperature of 25 °C and 65 °C, respectively. Interestingly, the thermal conductivity of the CNT/PCM composite in a solid state near its melting point increases suddenly, and the value drops when the composite is in a liquid state. Harikrishnan et al. [**96]** enhanced thermal conductivity of oleic acid by dispersing copper-oxide nanoparticles. The enhanced thermal conductivity resulted in reducing the freezing and melting times by 27.67% and 28.57%, respectively. Besides, the CuO nano-based PCM exhibited good thermal reliability even after 150 thermal cycles.

From the literature discussed above, it is clear that the dispersion of metallic and non-metallic nanoparticles in PCM has proven to be highly effective in enhancing its thermal properties, particularly thermal conductivity. This improvement is crucial in reducing the freezing and melting times, and in some cases, it also contributed in enhancing thermal stability.

From the literature studies of PCM encapsulation, it is noticed that the organic-based polymer shell materials have gained prominence due to their optimal combination of strength and flexibility. In contrast, inorganic shell materials, such as silica, offer excellent thermal conductivity but are prone to brittleness and frequent fracturing, which can disrupt their fundamental function of safeguarding the PCM within the shell **[19]**. The review focused on organic-based shell materials in PCM encapsulation sheds light on strategies to enhance the thermal properties of encapsulated PCM. This progress has paved the way for applying encapsulated PCM and advanced encapsulation technologies in construction for efficient thermal energy storage (TES) systems. Below is the literature pertaining to the enhancement of encapsulated PCM.

2.10. Thermal enhancement of Encapsulated PCM

Researchers have tried various strategies to enhance the thermal properties especially the thermal conductivity of organic Based shell material.

Trivedi et al. **[97]** encapsulated dimethyl adipate PCM using melamine-formaldehyde shell material. Further cryogenic conditioning of microencapsulated PCM was carried out to enhance the thermo-physical properties. Graphene-oxide-modified poly (melamine formaldehyde) micro encapsulated n-Dodecanol PCM was developed by Zhongguao et al. **[98]**. Cui et al. **[99]** modified a polyurea shell of micro encapsulated PCM using graphite. The graphite-modified microcapsules with size ranging from 150 to 350 μm was dispersed in the cement motor resulting in a drop in the compressive strength, despite the reduction still the value stands higher at 32.9 MPa.

The Thermal conductivity of melamine formaldehyde shell-based microcapsules was enhanced by Zhang et al. **[100]**. The shell of microcapsules was modified using hydrophobic silicon carbide. Modified capsules with 2% H-SiC enhanced thermal conductivity by 55.82% and latent heat of melting was 93.21 J/g, H-SiC modified microcapsules exhibited good

thermal stability than unmodified capsules. Song et al. **[101]** coated silver nanoparticles on the bromo-hexadecane based micro encapsulated PCM. The nanoparticles coated on the aminoplast shell of microcapsules enhanced thermal stability and toughness. Cui et al. **[102]** developed modified carbon nanotubes reinforced melamine formaldehyde resin used as the shell for encapsulating an Octagon PCM. The modified CNT-reinforced melamine formaldehyde-based microcapsules enhanced thermal conductivity by 24% compared with unmodified micro encapsulated PCM.

Non- Pickering emulsion polymerization technique was used by Parvate et al. **[103]** to develop TIO_2 nanoparticles quoted micro encapsulated extradition PCM. Poly (4-methyl styrene co-dvinyl benzene) copolymer shell was used to encapsulate the PCM. TIO_2 nanoparticles coated capsules exhibited good thermal stability. The author reported that the developed capsules use in the field of residential building, biomedical, and industries as thermal energy storage. Wang et al. **[104]** encapsulated n-tetradecane PCM using melamine-formaldehyde shell material, further TIO_2 nanoparticles were adsorbed on the capsules to enhance the thermo-physical properties.

2.11. Summary of the Literature Survey

From the extensive literature review, it is clear that the direct impregnation of PCM in cementitious materials has been associated with leakage issues and a significant drop in compressive strength. However, PCM encapsulation has effectively addressed these difficulties. Encapsulating PCM has proven to overcome leakage problems, with the core PCM inside the shell demonstrating good phase change characteristics during freezing and melting processes. The concept of PCM encapsulation has also been shown to improve thermal stability and reliability. When incorporating encapsulated PCM in cement mortar, a marginal drop in compressive strength was observed, but it was less compared to PCM direct impregnation. Despite the advantages of using organic-based shell materials for

encapsulation, their thermal conductivity is low, which can leads to reduce the overall thermal conductivity of the cement mortar due to incorporation of organic shell based PCM capsules.

Overall, the research demonstrates the effectiveness of PCM encapsulation in addressing the limitations of direct impregnation and highlights the potential benefits of incorporating encapsulated PCM in building materials for improved thermal performance and energy efficiency. It also enlightens the necessity of metallic and non-metallic nanoparticles to enhance the thermal properties of organic PCM.

2.12. Research Gaps

The literature review carried on the utilization of encapsulated PCM in cement mortar for external plastering; the findings suggest that it can effectively reduce heat gain within a room, thus delaying the peak temperatures. Nevertheless, the use of encapsulated PCM-based cement mortar for external plastering has been associated with only a marginal temperature difference between indoor and outdoor environments, which falls short of being satisfactory. Besides, research on encapsulated phase change materials (PCMs) for indoor applications addressing heating challenges are limited. Typically, these capsules are sourced from industrial suppliers. This underscores the need to develop encapsulated PCM capsules that can freeze and melt within the range of human comfort temperatures. The literature reveals that the capsules used for indoor applications exhibit low thermal conductivity, leading to reduced phase change cycles per day. The encapsulated PCM capsules used for internal plastering applications did not yield significant temperature differences. Despite a significant demand for energy-efficient materials, both pure PCM and encapsulated PCM have struggled to gain a foothold in the commercial market due to the aforementioned limitations, limiting their availability. Given these challenges, there is an imperative to develop new materials and strategies for implementing PCM in building fabrics to achieve substantial benefits, including

reduced heat gain, minimized temperature differentials between indoor and outdoor spaces, and delayed peak temperatures. These improvements, in turn, can lead to reduced air conditioner capacity requirements and result in energy savings.

The existing literature indicates a conspicuous scarcity of studies addressing the development of encapsulated PCM-incorporated cement mortar for internal plastering, specifically for cooling applications in buildings. Furthermore, there is a notable dearth of research concerning the micro-structural, thermal, and structural alterations associated with this application. In contrast to encapsulated PCM-based cement mortar for external plastering, the variant intended for internal plastering necessitates a robust thermal conductivity. This is imperative for rooms equipped with air conditioners, as internal plastering utilizing encapsulated PCM-based cement mortar requires high thermal conductivity to effectively absorb and release energy during peak and off-peak periods, respectively. Optimal thermal conductivity facilitates rapid phase change in encapsulated PCM, allowing for an increased number of phase change cycles per day and consequently enhancing energy utilization efficiency. This improvement in thermal conductivity can be achieved by controlling the size of the capsules, scaling them down from micro to nano, as demonstrated in prior research. Additionally, the incorporation of nanoparticles onto the PCM capsules has the potential to augment thermal conductivity, although there is a paucity of studies addressing this concept. The addition of metallic and non-metallic nanoparticles has shown promise in improving the thermal properties of PCM, but further exploration is needed to optimize these enhancements for practical applications. There is a clear gap existing on the optimal types and concentrations of nanoparticles that maximize energy efficiency and thermal stability while minimizing adverse effects on the material's structural properties.

Most research articles have focused on the behavior of cement mortar containing encapsulated PCM inclusions over 7 and 28 days curing period. From the literature it is evident that there is a scarcity of studies pertaining to the cryogenic treatment of cement mortar, and to date, no research has been reported on the cryogenic treatment of encapsulated PCM-embedded cement mortar with varying curing rates.

2.13. Problem Definition

Considering the identified research gaps and the potential advantages associated with the mentioned material, there exists a substantial opportunity for enhancing the thermal properties of encapsulated PCM-incorporated cement mortar designed for internal plastering. Moreover, it is imperative to elevate the thermo-structural characteristics of cement mortar. Specifically, the encapsulated PCM integrated into cementitious materials intended for internal plastering should possess the capability to efficiently absorb and release energy within the temperature range of 22 °C to 26 °C, aligning with typical indoor comfort temperatures. This capability would ensure effective cooling and precise temperature control within enclosed spaces. Continued research and development efforts in this domain hold the promise of delivering innovative solutions that can significantly contribute to sustainable and energy-efficient building practices. Based on the existing research gap, the following objectives were formulated for the current work.

2.14. Reasons behind selecting the PCM and Hybrid nanocomposites for the current study.

The availability of Phase Change Materials (PCMs) that phase transition at temperatures within the human comfort range is notably limited. Within this limited selection, 1-Dodecanol and n-Octadecane emerge as notable organic PCMs capable of undergoing phase change precisely within this temperature spectrum. Additionally, the latent heat of fusion

values for 1-Dodecanol and n-Octadecane PCMs stand at 194.43 J/g and 203.18 J/g, respectively.

As an organic compounds, 1-dodecanol and n-Octadecane are generally considered safer and less toxic compared to inorganic PCMs like salts, which can be corrosive or have other hazardous properties. This safety aspect is essential for indoor applications where health considerations are critical.

While organic PCMs like 1-dodecanol might not always be the cheapest option, their benefits in terms of energy savings and environmental impact can make them cost-effective solutions in the long term.

Keeping In view the phase change temperatures and latent heat storage, the above two PCMs were selected for the current study which enables them to absorb and release a significant amount of thermal energy during the phase change process, enhancing thermal inertia and reducing temperature fluctuations.

The primary advantages of using Copper-Titania (Cu-TiO_2) Hybrid Nanocomposites in phase change materials (PCMs) are their enhanced thermal properties and stability:

1. **Enhanced Thermal Conductivity**: Copper significantly boosts the heat transfer rate within the PCM, crucial for the efficient freezing and melting processes due to its high thermal conductivity.
2. **Increased Thermal Stability**: Titanium dioxide (titania) enhances the PCM's structural integrity and chemical stability under repeated thermal cycling, mitigating degradation.

3. **Synergistic Effects**: The combination of copper and titania leverages the high thermal properties of copper and the stability of titania, improving the PCM's freezing and melting behavior.

4. **Dispersion Stability**: Titania facilitates better dispersion of copper nanoparticles, reducing agglomeration and promoting uniform distribution, critical for consistent thermal performance throughout the PCM.

2.14.1. Comparison with Other Nanoparticles

1. Metals like Silver and Aluminum: While silver offers higher thermal conductivity, it is more expensive. Aluminum is cheaper but less effective than copper.

2. **Carbon-Based Materials (Graphene, Carbon Nanotubes)**: These offer very high thermal conductivities but are costly and challenging to integrate effectively due to dispersion issues.

Synthesis Process - Sol-Gel Chemical Process:

- **Advantages**:
    - **Low Temperature Synthesis**: Allows control over nanoparticle properties with reduced energy costs.
    - **Homogeneous Mixing**: Ensures uniform distribution of copper and titania at the molecular level.
    - **Versatility and Control**: Enables fine-tuning of nanoparticles' size, distribution, and morphology by adjusting synthesis parameters.
    - **Cost-Effectiveness**: Generally less expensive in terms of equipment and operational costs compared to other methods.

2.14.2. Other Synthesis Methods

1. Chemical Vapor Deposition (CVD) and **Physical Vapor Deposition (PVD)**: While offering high purity and controlled compositions, these methods involve higher costs and energy.

2. Hydrothermal Synthesis: Effective for growing oxide crystals but involves high pressure and temperature, which adds to the complexity and cost.

2.14.3. Efficiency and Cost Comparison

The sol-gel process stands out for its efficiency in producing well-mixed Cu-TiO2 composites and its cost-effectiveness compared to other nanoparticle synthesis methods like CVD, PVD, and hydrothermal synthesis. The use of relatively low-cost materials like copper and titania further enhances the economic viability of Cu-TiO2 hybrid nanocomposites for PCM applications.

In-situ polymerization technique is used for encapsulating the selected PCM with melamine formaldehyde. The technique has the following advantages mentioned below.

1. Control and Uniformity: In-situ polymerization typically results in better control over shell morphology compared to interfacial polymerization. While interfacial polymerization can sometimes produce uneven shell thickness due to the complex dynamics at the interface, in-situ polymerization allows for a more uniform and consistent shell because the polymerization reaction occurs uniformly around the PCM.

2. Chemical and Thermal Integrity: In-situ polymerization ensures that the shell material is chemically bonded to the PCM, enhancing the integrity and stability of the encapsulation. Interfacial polymerization may result in weaker bonding at the interface, which can be susceptible to delamination under thermal cycling or mechanical stress.

2.14.4. Comparison with other techniques

In-situ Polymerization vs. Spray Drying:

1. Shell Integrity: Spray drying typically involves the rapid drying of a carrier solution containing the PCM and shell material, which can lead to less control over the microstructure and potential defects like porosity or weak spots. In contrast, in-situ polymerization creates a more robust and impermeable shell by forming the polymer directly around the PCM.

2. Material Efficiency: Spray drying can lead to significant losses of material during the process, especially if the PCM or polymer is sensitive to the conditions used (e.g., high temperatures or shear forces). In-situ polymerization occurs at milder conditions and encapsulates the PCM more efficiently, reducing material wastage.

In-situ Polymerization vs. Physical Methods (e.g., Fluidized Bed Coating):

1. Seamless Encapsulation: Physical methods like fluidized bed coating might not achieve as seamless a coating as in-situ polymerization, which can form a more integral and contiguous shell. This is crucial for preventing leakage of the PCM, especially under conditions where the capsule might be subject to compressive or tensile forces.

2. Thermal and Chemical Resistance: The chemical cross-linking possible in in-situ polymerization provides superior resistance to thermal and chemical degradation compared to physical coatings, which may degrade or melt at lower temperatures or under solvent exposure.

Process Benefits:

Scalability and Environmental Impact: In-situ polymerization can be scaled up with relatively lower environmental impact compared to techniques like spray drying, which require significant energy input for heating and maintaining the drying environment. In-

situ polymerization reactions are generally conducted at ambient or slightly elevated temperatures, saving energy and reducing carbon footprint.

2.15. Objectives of the study

1. To develop new cryogenically conditioned nanoencapsulated PCM-embedded cement mortar for sustainable cooling in buildings.
2. Synthesis and characterization of the cryogenically conditioned nanoencapsulated PCM-embedded cement mortar through different sequence of operations pertaining to the mix preparation.
3. To evaluate and compare the thermal behaviour of reference cement mortar and nanoencapsulated PCM-based cement mortar subjected to identical heating and cooling conditions in an insulated test chamber, aiming to assess the shift in peak temperatures and thermal regulation.

Taking into account the previously outlined problem statement and the identified research gap, two specific types of organic PCMs namely 1-Dodecanol PCM and n-Octadecane PCM were selected, in order to address the objectives. Notably, the freezing and melting temperatures of both PCMs fall within the human comfort range (22 °C to 26 °C), which served as a pivotal criterion for their inclusion in the current research endeavor.

2.16. The limitations of the study were outlined in the thesis following the stated objectives

1. The complex procedures involved in synthesizing the nanoencapsulated PCM-embedded mortar might lead to variations in the final product depending on slight changes in the synthesis process.

2. The performance of PCM-embedded mortars is highly dependent on environmental conditions. Different climates might yield different results, limiting the general applicability of findings.
3. Any modeling or simulation work to predict performance can have limitations in terms of assumptions made, which may not fully capture real-world complexities.

CHAPTER - 3

RESEARCH METHODOLOGY

3.1. Methodology

Based on the thorough literature review on the proposed research topic, the following investigations pertaining to the proposed CNPCs are planned:

1. Cryogenic conditioning of the nanoencapsulated PCM-embedded cement mortar is one of the novel ideas of the proposed research work.
2. Systematic preparation of hybrid nanocomposites based PCM and nanoencapsulated PCM will be performed.
3. The as-prepared hybrid nanocomposite based PCM and nanoencapsulated PCM were experimentally analyzed using the physical and structural characterization techniques including micro-structural (FESEM), crystallization nature (XRD), surface structure (FTIR), phase change temperatures and latent heat capacities (DSC), thermal stability (TGA), thermal conductivity and thermal reliability.
4. The nanoencapsulated PCM with varying proportions are embedded in the cement mortar, and the cube specimens were cured in the water and also conditioned at cryogenic temperatures.
5. Thermo-structural studies of cryogenic conditioned nanoencapsulated PCM-embedded cement mortar samples are carried out.
6. Thermal behaviour of reference cement mortar and nanoencapsulated PCM-based cement mortar are carried out subjected to identical heating and cooling using Insulated Test Chamber.

3.2. Plan of action

The proposed objectives have been successfully realized, as illustrated in the Fig. 14 depicting the action plan. The entire project was divided into three distinct stages. Initially, the work commenced with 1-Dodecanol PCM, aimed at enhancing thermo-physical properties through the dispersion of Cu-TiO_2 hybrid nanocomposites. Subsequently, direct impregnation of pure PCM and HN based PCM into the cement mortar was carried out for further investigations. To address potential leakage issues in the cube specimens, 1-Dodecanol PCM was encapsulated at both micro and nano size.

The same synthesis and investigative procedures were replicated in stage 2, but with n-Octadecane PCM. After thorough analysis of phase change characteristics, thermal conductivity, and the cement mortar's behaviour with encapsulated PCM inclusions, the election of PCM (1-Dodecanol and n-Octadecane PCM) and the optimal proportions suitable or practical applications were finalized.

Stage 3 was dedicated to preparing cement mortar cube specimens with the chosen encapsulated PCM and the ideal proportions for cryogenic treatment. Various curing rates were considered to evaluate the compressive strength gain of PCM-based cement mortar when subjected to cryogenic liquid treatment.

Finally the developed PCM based cement mortar slab were tested to study the behaviour when subjected to temperature of 42 °C and 22 °C on either side of the slab. Due to temperature difference heat transfer take place through the slab, and the temperatures were recorded using J type thermocouples. The same experimentation was carried using reference cement mortar slab for comparative study. The detailed information regarding the experimentation and the observations were presented in the Chapter-6.

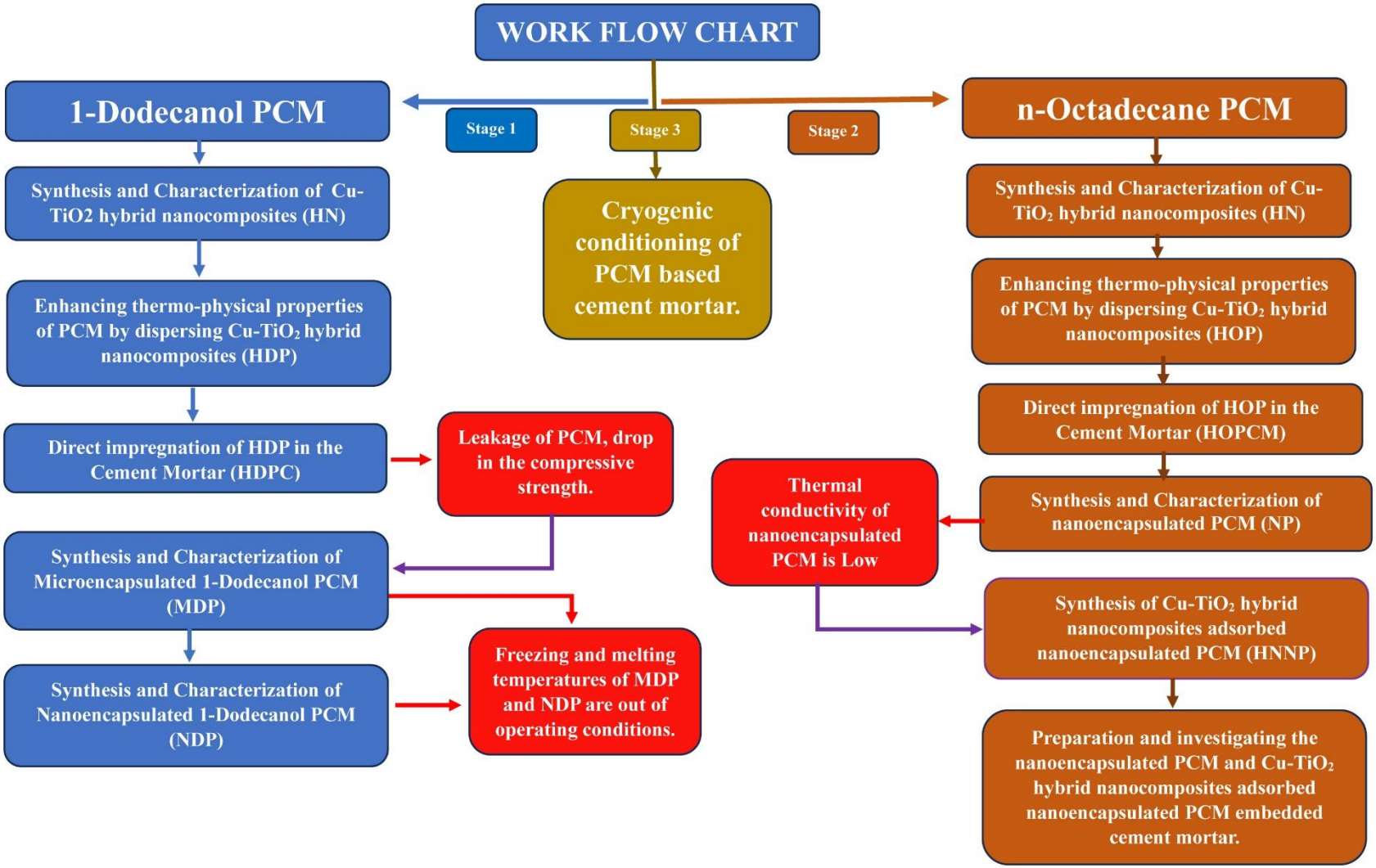

Fig. 14. Workflow chart

3.3. Overview of various samples prepared

Table 15 presents the details regarding the synthesis of HN, MDP, NDP, NP, HNNP, the table also exhibits the information related to the preparation of HN based PCM and the encapsulated PCM embedded cement mortar samples.

Table 5. Summary of synthesis carried out for the current work.

S. No.	Preparation	Technique	Details
1	Cu-TiO_2 hybrid nanocomposites (HN)	Sol-gel chemical process	Copper nanoparticles are adsorbed on the titania nanoparticles
2	Cu-TiO_2 hybrid nanocomposites based 1-Dodecanol PCM (HDP)	Sonication was used for dispersion of HN	The HN nanocomposites were dispersed in the 1-Dodecanol PCM
3	Cu-TiO_2 hybrid nanocomposites based 1-Dodecanol PCM embedded cement mortar cube specimens (HDPC)	Direct impregnation	The prepared HDP sample was dispersed in the cement mortar
4	Microencapsulated 1-Dodecanol PCM (MDP)	Insitu polymerization	Melamine formaldehyde shell materials was used for encapsulating the PCM
5	Nanoencapsulated 1-Dodecanol PCM (NDP)	Insitu polymerization	Melamine formaldehyde shell materials was used for encapsulating the PCM at nano level
6	Nanoencapsulated n-Octadecane PCM (NP)	Insitu polymerization	Melamine formaldehyde shell material was used for encapsulating the PCM at nano level
7	Cu-TiO2 hybrid nanocomposites adsorbed nanoencapsulated PCM (HNNP)	Insitu polymerization	Cu-TiO2 hybrid nanocomposites were adsorbed on the nanocapsules
8	Cu-TiO_2 hybrid nanocomposites based n-Octadecane PCM	Direct impregnation	Pure PCM direct impregnation in the cement mortar

S. No.	Preparation	Technique	Details
	embedded cement mortar cube specimens		
9	Nanoencapsulated n-Octadecane PCM embedded in the cement mortar cube specimens (NPeCM)	Encapsulated PCM impregnation	The NP capsules in the proportion of 3 to 15% by wt. of cement with the increment of 3% were dispersed in the cement mortar
10	Cu-TiO2 hybrid nanocomposites adsorbed nanoencapsulated PCM (HNNP) embedded in the cement mortar cube specimens	Encapsulated PCM impregnation	The HNNP capsules in the proportion of 3 to 15% by wt. of cement with the increment of 3% were dispersed in the cement mortar
11	Cryogenic treatment of optimized proportion of HNNP (15%) embedded in the cement mortar cube specimens	Cryogenic treatment	Cryogenic treatment of HNNPeCM cube specimens. Optimized proportion of HNNP samples embedded in the cement mortar cube specimens were treated

3.4. Details of instruments for materials characterization

The prepared samples were characterized using the below mentioned instruments. The specifications of the equipment being used for all the characterization tests are summarized in Table 16. The summary of the tests carried out on the prepared materials was presented in Table 17. The cryogenic conditioning of the reference cement mortar and PCM based cement mortar are crucial in the study, Table 18 exhibits a strategic plan carrying out the experiment using liquid nitrogen. The samples were cured with liquid nitrogen for 6 hrs, 12 hrs and 24 hrs, another case study is hybrid approach treating the samples with liquid nitrogen followed by water curing.

Table 6. Equipment details with specifications

Instrument type	Model & Make	Specifications	Test sample type
Field emission scanning electron microscope (FESEM) with energy dispersive X-ray spectrometry (EDAX)	APERO S, FEI,	200 V – 300 kV (STEM) Detector: ETD	Powder sample
X-ray diffractometer (XRD)	ULTIMA IV, RIGAKU	Intensity: 40 kV, 30 mA Step size: 0.0001° Cu Kα (λ=1.54060 A°)	Powder / Liquid (Attachment required)
Fourier Transform Infrared (FTIR) spectroscopy	FT/IR – 4200, JASCO	Max resolution: 0.5 cm^{-1} Infrared wavelength: 400 to 4000 cm^{-1} Max resolution: 0.5 cm^{-1} S/N ratio: 30,000:1 Display wave number range: 15,000 to 0 cm^{-1} (standard)	Powder/Liquid
Differential scanning calorimeter	DSC TA – 250 SHIMADZU	Heat flow ± 40 µW; Temperature range -150 °C to 600 °C; Cooling time 6 min from 600 °C to 40 °C with LN_2	Solid/Liquid
Thermo gravimetric analyser (TGA)	DTG-60, SHIMADZU	Room temperature to 1100 °C Readability: 0.001 mg Measurable range: ± 500 mg Measurable range: ± 1000 µV Sample quantity: 1 g max, in gross weight	Solid/Liquid

Instrument type	Model & Make	Specifications	Test sample type
Thermal conductivity analyser	TPS 500S, HOT DISK	Thermal conductivity: 0.03 to 200 W/m K; Accuracy: ±2% Measuring Range: -35 °C to 200 °C. Accuracy: Better than 5%, Reproducibility: 2% (thermal Conductivity) Reproducibility: 10% (thermal diffusivity)	Solid /Liquid /Powder/
Compression testing machine	402 model	Supply input: 220 to 240 V AC, 50 Hz, capacity: 2000 kN, horizontal clearance: 475 mm, load resolution: 0.1 kN up to 1000 kN, displacement control: 0.001 mm, Max. displacement: 50 mm, load control: 0.1 kN/sec. to 50 kN/sec	Solid
PCR thermal cycler	Master cycler pro S & Eppendorf India Pvt. Ltd	Temp. Control Range 4° to 99°C Gradient Range 1° to 24° C Control Accuracy±0.2°C Heating Rate: 6 °C/sec Heating Rate: 4.5 °C/sec Power Supply: 950W	Solid

Table 7. Overview of materials preparation and characterization

PCM	Preparation	PSA	FESEM	FTIR	DSC	Thermal conductivity	TGA	Thermal cycling	Freezing and Melting time	Compression Testing
1-Dodecanol PCM	Cu-TiO_2 hybrid nanocomposites (HN)	**Yes**	**Yes**	**Yes**	**NA**	**Yes**	**NA**	**NA**	**NA**	**NA**
	Cu-TiO_2 hybrid nanocomposites based 1-Dodecanol PCM (HDP)	**NA**	**NA**	**Yes**	**Yes**	**Yes**	**Yes**	**Yes**	**Yes**	**NA**
	Cu-TiO_2 hybrid nanocomposites based 1-Dodecanol PCM embedded Cement Mortar (HDPC)	**NA**	**NA**	**Yes**	**NA**	**Yes**	**NA**	**NA**	**NA**	**Yes**
	Microencapsulated 1-Dodecanol PCM (MDP)	**Yes**	**Yes**	**Yes**	**Yes**	**Yes**	**Yes**	**Yes**	**NA**	**NA**
	Nanoencapsulated 1-Dodecanol PCM (NDP)	**Yes**	**Yes**	**Yes**	**Yes**	**Yes**	**Yes**	**Yes**	**NA**	**NA**
	Cu-TiO_2 hybrid nanocomposite-based n-Octadecane PCM (HOP)	**NA**	**NA**	**Yes**	**Yes**	**Yes**	**Yes**	**NA**	**Yes**	**NA**
	Cu-TiO_2 HN based n-Octadecane PCM embedded cement mortar cube specimens (HOPC)	**NA**	**NA**	**NA**	**NA**	**Yes**	**Yes**	**NA**	**NA**	**Yes**

PCM	Preparation	PSA	FESEM	FTIR	DSC	Thermal conductivity	TGA	Thermal cycling	Freezing and Melting time	Compression Testing
n-Octadecane PCM	Nanoencapsulated n-Octadecane PCM (NP)	**Yes**	**Yes**	**Yes**	**Yes**	**Yes**	**Yes**	**Yes**	**NA**	**NA**
	Nanoencapsulated n-Octadecane PCM embedded cement mortar (NPeCM)	**NA**	**NA**	**NA**	**NA**	**Yes**	**Yes**	**NA**	**NA**	**Yes**
	Cu-TiO_2 hybrid nanocomposites adsorbed nanoencapsulated n-Octadecane PCM (HNNP)	**Yes**	**Yes**	**Yes**	**Yes**	**Yes**	**Yes**	**Yes**	**NA**	**NA**
	Cu-TiO_2 hybrid nanocomposites adsorbed nanoencapsulated n-Octadecane PCM embedded cement mortar (HNNPeCM)	**NA**	**NA**	**NA**	**NA**	**Yes**	**Yes**	**Yes**	**NA**	**Yes**
Cryogenic conditioning	Reference cement mortar	**NA**	**Yes**	**NA**	**NA**	**NA**	**NA**	**NA**	**NA**	**Yes**
	HNNPeCM-10 cube specimens	**NA**	**Yes**	**NA**	**NA**	**NA**	**NA**	**NA**	**NA**	**Yes**

Table 8. Strategy for water cured and cryogenic conditioning of reference cement mortar and HNNPeCM specimens.

S. No.	Sample Type	Details	Average compressive strength of water cured specimens (MPa)		Average compressive strength of Cryo-conditioned specimens			Average compressive strength of Cryo-conditioned specimens followed by 28 days water curing (MPa)		
			7 days	28 days	24 hrs.	12 hrs.	6 hrs.	24 hrs.	12 hrs.	6 hrs.
1	**Reference Cement Mortar**	The plain cement mortar without PCM capsules.	**Yes**	**Yes**	NA	NA	NA	NA	NA	NA
2		Cryo-conditioned plain cement mortar cured with liquid nitrogen with different curing rates.	NA	NA	**Yes**	**Yes**	**Yes**	NA	NA	NA
3		Cryo-conditioned plain cement mortar cured with liquid nitrogen with different curing rates followed by water curing.	NA	NA	NA	NA	NA	**Yes**	**Yes**	**Yes**
4	**HNNPeCM**	Optimized proportion of HNNP capsules impregnated cement mortar cube samples.	**Yes**	**Yes**	NA	NA	NA	NA	NA	NA
5		Optimized proportion of HNNP capsules impregnated cement mortar cube samples mortar cured with liquid nitrogen with different curing rates.	NA	NA	**Yes**	**Yes**	**Yes**	NA	NA	NA
6		Optimized proportion of HNNP capsules impregnated cement mortar cube samples mortar cured with liquid nitrogen with different curing rates followed by water curing.	NA	NA	NA	NA	NA	**Yes**	**Yes**	**Yes**

CHAPTER - 4

MATERIALS AND METHODS

This chapter emphasizes material details, synthesis procedure of HN, microencapsulated 1-Dodecanol PCM (MDP), nanoencapsulated 1-Dodecanol PCM (NDP), nanoencapsulated n-Octadecane PCM (NP) and Cu-TiO_2 hybrid nanocomposites adsorbed nanoencapsulated PCM (HNNP). This chapter also describes the procedure adopted for the direct impregnation of pure PCM and the prepared encapsulated PCM embedded in the cement mortar for cube specimen preparations.

4.1. Materials

The list of materials presented in Table 4 were used for the synthesis of Cu-TiO_2 hybrid nanocomposites, microencapsulated PCM, nanoencapsulated PCM, and the encapsulated PCM embedded cement mortar cube specimens.

Table 9. Details of the materials.

S. No.	Material name (Formula)	CAS no.	Manufacturers	Purpose
1	1-Dodecanol PCM ($C_{12}H_{26}O$)	112-53-8	Loba chemie	PCM
2	Polyvinylpyrrolidone $(C_6H_9NO)_x$	9003-39-8	SRL	Stabilizing agent for nano particle synthesis
3	Titanium dioxide (TiO_2)	13463-67-7	Loba chemie	Used as precursor for hybrid nanoparticle synthesis`
4	Cupric nitrate ($Cu(NO_3)_2$)	10031-43-3	Loba chemie	Used as precursor for hybrid nanoparticle synthesis`
5	Sodium borohydride ($NaBH_4$)	16940-66-2	SD Fine-Chem Limited.	Used as reducing agent for the preparation of hybrid nanoparticle synthesis`

S. No.	Material name (Formula)	CAS no.	Manufacturers	Purpose
6	Ascorbic acid ($C_6H_8O_6$)	50-81-7	Sigma Aldrich	Used as reducing agent for the preparation of hybrid nanoparticle synthesis`
7	Ethanol (C_2H_5OH)	64-17-5	Alpha Chemika	Used as solvent along with TiO2.
8	Superplasticizer (Masterglenium Sky 8233)	-------	BASF, India	Used as admixture along with cement mortar sample preparation to enhance the workability.
9	Melamine ($C_3H_6N_6$)	108-78-1	Finar Limited	Used as shell material for encapsulating the PCM
10	Formaldehyde (H_2CO)	50-00-0	Loba Chemie	Used as shell material for encapsulating the PCM.
11	Span 60 ($C_{24}H_{46}O_6$)	1138-41-6	SRL chemicals	Used as an emulsifier for the preparation of oil-in-water (O/W).
12	Tween 20 ($C_{58}H_{114}O_{26}$)	9005-64-5	SRL chemicals	Used as an emulsifier for the preparation of oil-in-water (O/W).
13	Ammonium chloride (NH_4Cl)	12125-02-9	SD Fine-Chem Limited.	Used as nucleating agent during the synthesis process of PCM encapsulation.
14	Sodium hydroxide (NaOH)	1310-73-2	SD Fine-Chem Limited.	Used as pH buffer
15	De-ionized double distilled water	-------	Millipore distiller	Used as solvent for reactions.
16	n-Octadecane $CH_3(CH_2)_{16}CH_3$)	593-45-3	Sigma Aldrich	Used as PCM

S. No.	Material name (Formula)	CAS no.	Manufacturers	Purpose
17	Span 80 ($C_{24}H_{46}O_6$)	1338-43-8	SRL chemicals	Used as an emulsifier for the preparation of oil-in-water (O/W) during the process of encapsulation.
18	Tween 80 ($C_{64}H_{124}O_{26}$)	9005-65-6	SRL chemicals	Used as an emulsifier for the preparation of oil-in-water (O/W) during the process of encapsulation.

4.2. Synthesis of Cu-TiO_2 hybrid nanocomposites (HN)

5 g of titanium dioxide (referred to as precursor 1) were combined with 30 ml of ethanol; subsequently, the resulting solution as shown in Fig. 15 (a) underwent 15 mins sonication process. Meanwhile, cupric nitrate (referred to as precursor 2) was dissolved in 30 ml of Double Distilled Water (DDW) as shown in Fig. 15 (b). This solution was subjected to continuous stirring at a rate of 350 rpm while maintaining a temperature of 50 °C.

Following this, the titanium dioxide solution was amalgamated with the cupric nitrate solution and subjected to 15 minutes of stirring. Simultaneously, 0.5 g of Polyvinylpyrrolidone (serving as a stabilizing agent) was dissolved in 30 ml of distilled water at room temperature. Once the Polyvinylpyrrolidone (PVP) powder was entirely dissolved in the water, the resulting solution was added drop by drop to the precursor solution.

Distinct solutions were prepared separately by dissolving 0.1 g of sodium borohydride (strong reducing agent) and 0.5 g of ascorbic acid (weak reducing agent) in 30 ml of distilled water. The sodium borohydride solution, acting as the strong reducing agent, was then gradually introduced drop by drop into the primary solution, succeeded by the addition of the ascorbic acid solution. Notably, during the incorporation of the reducing agents, observable

shifts in color transpired, transitioning from a light blue hue to a pale brown color as shown in Fig. 15 (c). The titration process persevered until a discernible change in coloration became apparent.

Subsequent to the procedure, decanting was performed when necessary, and washing with acetone on three times. The resultant hybrid nanoparticles were subsequently subjected to filtration through a dual-layer filter paper as shown in Fig. 15 (d). Following filtration as shown in Fig. 15 (e), the particles were dried before being collected for further analysis or applications.

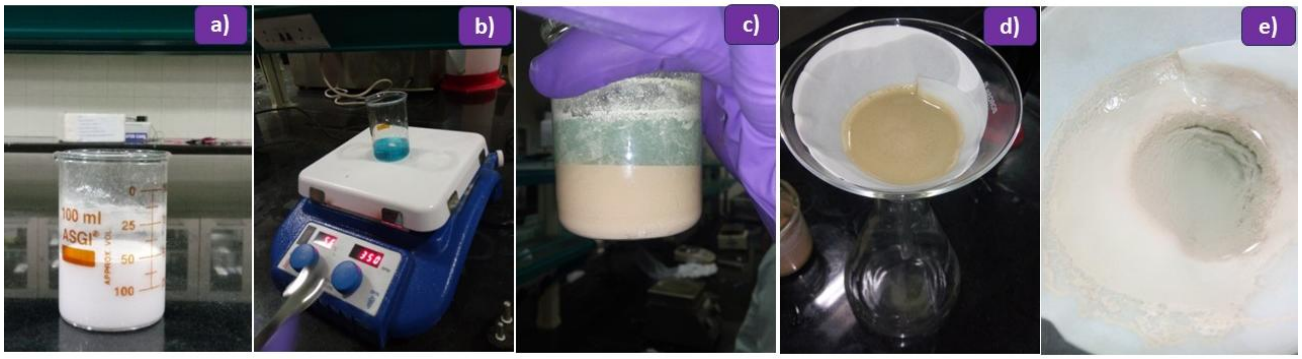

Fig. 15. Synthesis of HN. a) Titania solution. b) Cupric nitrate solution. c) Copper-titania colloidal solution. d) Filtering process. e) Drying process.

4.3. Preparation of Cu-TiO_2 hybrid nanocomposites based 1-Dodecanol PCM (HDP)

Cu-TiO_2 hybrid nanocomposite (HN) particles, synthesized during the present research work, were dispersed into the pure PCM using proportions varying between 0.02% and 0.1% by weight of PCM as shown in Fig 16. For stable and homogenous preparation of HN based PCM sample, probe sonicator was used, the samples were kept undisturbed for 1 day to study the settlement of the particles.

Fig. 16. Pure 1-Dodecanol PCM and HDP samples.

4.4. Preparation of Cu-TiO_2 hybrid nanocomposites based 1-Dodecanol PCM embedded Cement Mortar (HDPC)

The graphical representation of the HDPC is depicted in Fig. 17, illustrating the synthesis procedure of HN, which is followed by dispersing the as-prepared HN in the 1-Dodecanol PCM. Subsequently, the HDP was incorporated into the cement mortar for the preparation of cube specimens. More comprehensive details regarding this process can be found in the subsequent sections.

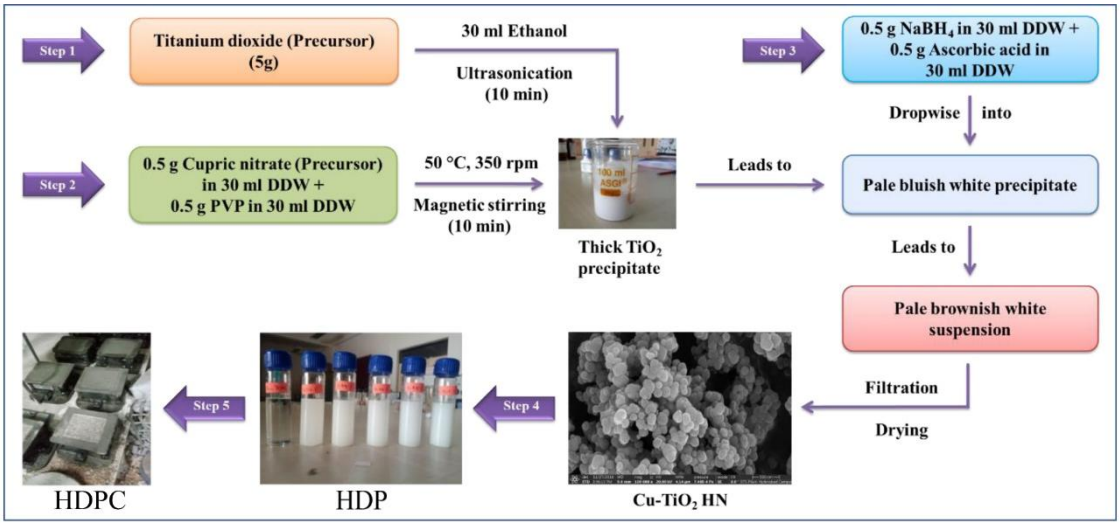

Fig. 17. Schematic representation for preparation of HDPC.

As it can be observed from Table 7 that the chosen cement has passed all the tests and hence is being used for making the HDPC and the reference mortar specimens. For the preparation of HDPC, measured quantities of the pure PCM with HN particles, varying between 2% and 10% by weight of cement, were being tried and an optimum of 6% was arrived at by the authors during in-house investigations.

The trial range for pure PCM was decided based on earlier studies **[30, 105, 106]**. The optimized quantity of 6% of pure PCM with HN particles (HDP) was thoroughly pre dry mixed with fresh cement, thus ensuring the uniform dispersion of HN in the mixture. The uniform dispersion of HN in the mixture is expected to tap full TES potential of HDP. Standard cement to fine aggregate ratio of 1:4 was considered for making the mortar specimens.

In the next stage, the prepared cement, with varying proportions of pure PCM dispersed with HN particles, was mixed with measured quantities of fine aggregates (river sand) and water. With a view to enhance the workability, 0.7% by weight of cement of High Range Water Reducing (HRWR) super plasticizer is being added to the measured quantity of water.

Freshly mixed HDPC, after placing inside the cube with the standard 70.6 mm sides, is vibrated for 2 mins with a dedicated mortar vibrator, vibrating at the specified speed of 12000±400 vibrations/minutes. A minimum of 3 cube specimens were cast to represent each attempted combination of HN particles and the pure PCM, to verify the reproducibility of the results. Then, the cube specimens with moulds were left at temperature of 27 °C and 90% relative humidity for 24 hrs. The cube specimens were then separated from the moulds, kept in still water for a total period of 28 days as shown in Fig. 18.

The specimens were removed from the water were immediately tested for compressive strength on a standard servo hydraulic closed loop feedback strain controlled 2000 kN compression testing machine. A standard rate of loading of 350 kg/cm^2/minute was applied during the testing process. For each combination three specimens were prepared for

reproducibility. The design proportions of all the ingredients of HDPC are summarized and presented in Table 8 for reference.

Fig. 18. HDPC preparation and curing process.

4.5. Synthesis of Microencapsulated 1-Dodecanol PCM (MDP)

A facile in-situ polymerization process was followed for the synthesis of the microencapsulated PCM, wherein 1-Dodecanol PCM was encapsulated with MF shell material. Several trials have been carried out for encapsulating the PCM. It was noticed from the trials that, by altering the proportion of cross-linking agent, the formation of the microcapsules was affected **[107]**. Moreover, the reaction under acidic conditions was much favoring for the formation of the microcapsules **[108]**.

Although, a complete control on the occurrence of agglomeration/coalescence could not be achieved, however, by reducing the copolymer percentage, fine tuning the Hydrophilic–Lipophilic Balance (HLB) scale of surfactant molecules, adjusting the pH value of reaction have led to a good control on the formation of the MDP **[109-112]**.

Based on the above observations, the reaction was fine-tuned as follows: Tween 20 and span 60 of equal quantities were used as surfactants for the O/W preparation. 50 ml of

1-Dodecanol PCM was added to the above mixture and stirred in the range of 8000 rpm to 8500 rpm using a high-speed shear mixer.

The pH value for O/W emulsion was in the range of 5-6. Whereas, for the preparation of the shell precursor, 10 g of melamine (precursor) was added into 100 ml DDW followed by the addition of 30 ml formaldehyde (another precursor) solution into it. The whole reaction was carried out at 700 rpm and 70 °C using a magnetic stirrer with hot plate. During this reaction, the NaOH solution was added to maintain the pH value in the range of 10-11, and the reaction was continued until a thick white colloidal solution turns into a transparent colourless solution. Finally, for encapsulation, the prepolymer was added drop by drop to the O/W emulsion very slowly.

To accelerate the above reaction, aliquot quantity of ammonium chloride aqueous solution was mixed **[113]**. Apart from accelerating the reaction, it also helps in removing residual formaldehyde as shown in the equation (2). During this process, it was ensured that the final solution pH had not exceeded the value of 7. Fig. 19 depicts the graphical representation of MDP synthesis.

$$4NH_4Cl + 6CH_2O \longrightarrow (CH_2)_6N_4 + 6H_2O + 4HCl \text{ ----- (2)}$$

The mixture is then stirred using a magnetic stirrer at 1500 rpm for 3 to 4 hours until sedimentation begins, and the solid particles start settling at the bottom. Later, the supernatant was decanted, and the whitish powder was collected. This powder was then cleaned twice with acetone and the final encapsulated PCM was obtained.

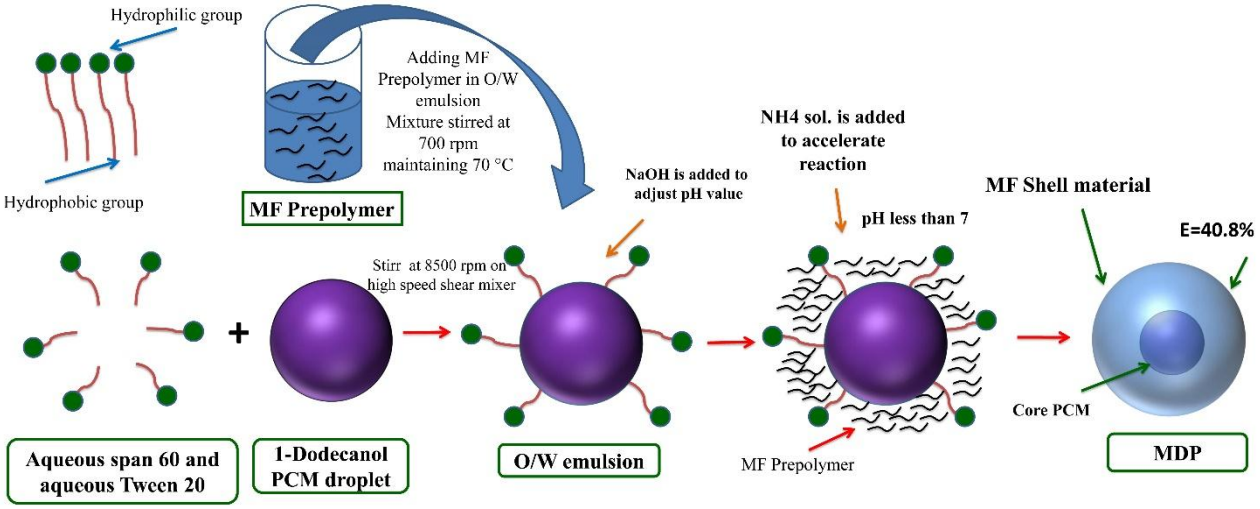

Fig. 19. Graphical representation of MDP synthesis procedure.

4.6. Synthesis of nanoencapsulated 1-Dodecanol PCM (NDP)

For the synthesis of nanoencapsulated PCM (NP) Tween 80 and Span 80 which were used as surfactant added to the water and stirred for 20 mins as shown in Fig. 20 (a) and (b), further n-Octadecane PCM was added to the solution and stirred for 10 minutes 5 (c). Later, for stable oil in water emulsion preparation, the solution was sonicated using a probe sonicator for 15 mins as shown in Fig. 20 (d). Whereas, for the shell precursor preparation, 20 g of melamine powder (shell precursor) was added slowly into 100 ml DDW, in due course, 40 ml formaldehyde (shell precursor) was added as shown in Fig. 20 (e). The hot plate magnetic stirrer was set to 75 °C and speed of 350 rpm. The pH regulator NaOH is added to the shell precursor solution to maintain the pH value in the range of 8-10. The whole reaction is continued stirring until a transparent colourless solution appears 20 (e). Further, the prepolymer was added drop by drop slowly to the Oil in Water emulsion to maintain the stirrer speed at 300 rpm. In the due, ammonium chloride aqueous solution was added to the whole reaction to remove out any unreacted formaldehyde as show in the eq. (2). **[113]**. Maintaining the pH value of not more than 7, the whole reaction should be stirred continuously at a speed of 300 rpm for 3 hrs. The resultant capsules were cooled to room temperature subsequently washed with acetone for 3 times to remove un-encapsulated PCM

if any and impurities as shown in Fig. 20 (c). Finally, the solution is filtered and dried in an oven to maintain a temperature of 60 °C for 1 day as shown in Fig. 20 (g). The capsules are in the form of white powder as shown in Fig. 20 (h), which is used for further characterization and preparation of cube specimens.

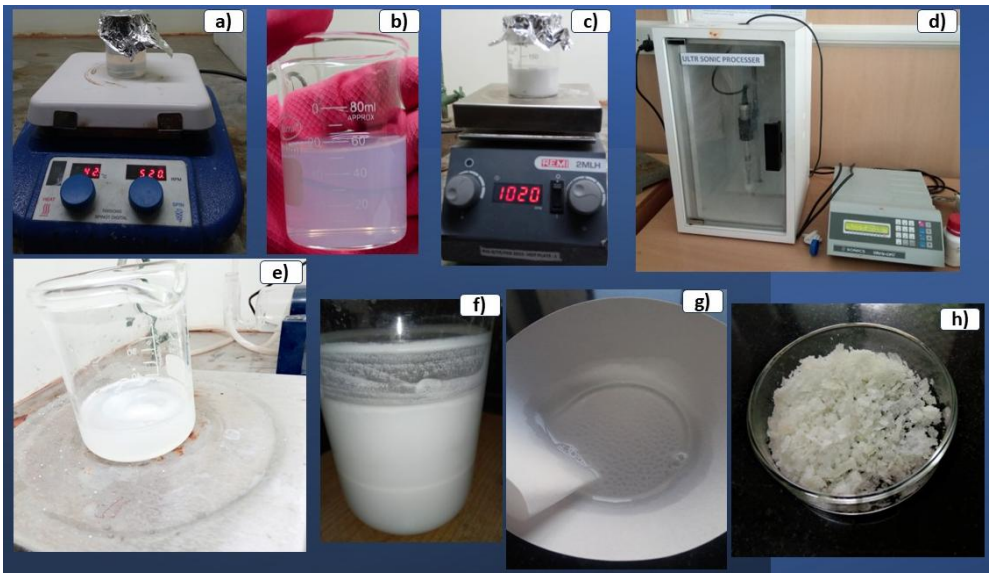

Fig. 20. Synthesis procedure of NDP. a) - c) O/W emulsion preparation. d) O/W emulsion preparation using probe sonicator. (e) Shell material preparation (f) Final solution. (g) Filtering process (h) Final dried nanocapsules in powder form.

4.7. Synthesis of Cu-TiO2 hybrid nanocomposite-based n-Octadecane PCM (HOP)

Cu-TiO_2 hybrid nanocomposite (HN) particles, synthesized during the current study, were dispersed into the pure PCM using the proportions varying between 0.02% and 0.1% by weight of PCM as shown in Fig. 21. For stable and homogenous preparation of HOP samples, probe sonicator was used, the samples were kept undisturbed for 1 day to study the settlement of the particles.

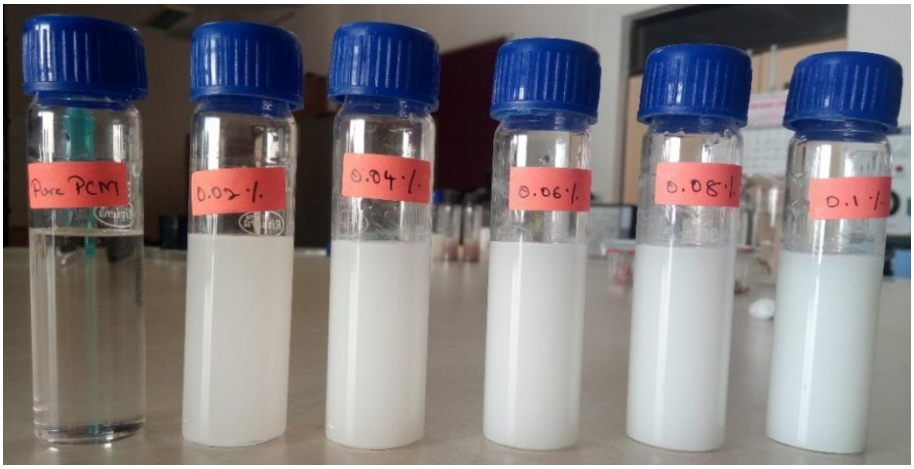

Fig. 21. Cu-TiO_2 Hybrid nanocomposite-based n-Octadecane PCM (HOP).

4.8. Preparation of Cu-TiO_2 HN based n-Octadecane PCM embedded cement mortar cube specimens (HOPC)

Cu-TiO2 hybrid nanocomposites were dispersed in the n-Octadecane PCM with the proportion ranging from 0.02 to 0.1% by weight of PCM with the incremental step of 0.02%. The prepared HN based n-Octadecane PCM samples were characterized to study thermo-physical properties such as thermal conductivity, chemical compatibility, freezing and melting time. Further, the prepared HN based n-Octadecane PCM samples were embedded in the cement mortar as shown in Fig. 22 to study the leakage issues, energy storage capability, thermal conductivity, compressive strength.

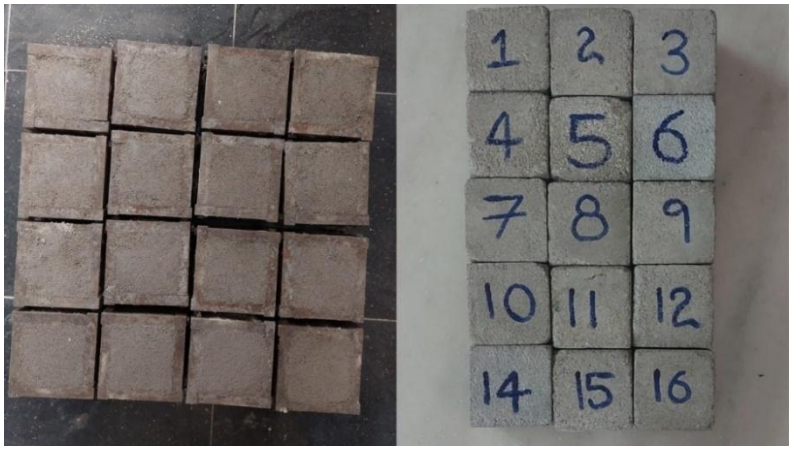

Fig. 22. Cu-TiO_2 HN based n-Octadecane PCM embedded cement mortar cube specimens.

4.9. Synthesis of nanoencapsulated n-Octadecane PCM (NP)

For the preparation of nano encapsulated PCM, Tween 80 and Span 80 nonionic surfactants were used for oil-in-water emulsions. To get the ideal Hydrophilic-Lipophilic Balance (HLB) values for emulsification, the mixing ratios were computed using eq. (3) **[114]**. The O/W ratio plays a vital role in developing capsules, keeping this in view; different trials were performed with varying oil-to-water ratios. The optimized proportions of Tween 80 and Span 80 were added to the DDW, and the mixture was stirred at 300 rpm, maintaining a temperature of 70 °C. Later, PCM was added drop by drop to the mixture slowly, and further the mixture was sonicated with a frequency of 20,000 Hz, and amplitude of 40% for a stable O/W emulsion as shown in Fig. 23 (a). During the synthesis process, it is important to maintain the temperature of the O/W emulsion at a higher level than melting point of PCM. As pH plays a vital role in affecting the size and morphology of the capsule, in this regard, citric acid was added to the O/W emulsion to regulate the pH value to 4.

Formation, smoothness, and dispersion of the capsules are significantly affected by the formaldehyde to melamine ratio. A single molecule of melamine has the potential to react with six molecules of formaldehyde. Thus, the reaction rate and degree of polymerization were both enhanced by high formaldehyde to melamine molar ratio, favouring the precipitation of resin capsules. Considering shell material precursor preparation, melamine to formaldehyde ratio is 1:4 **[115]**. Different trials of experiments were carried out varying the melamine to formaldehyde ratio and temperatures during shell material precursor preparation and the optimized proportions were considered for the present work. Melamine powder of 30 gm was dissolved in 100 ml of DDW; later 120 ml of formaldehyde was added to the mixture. The temperature during shell material precursor preparation should be maintained at 80 °C while stirring at 350 rpm as shown in Fig. 23 (b). The pH value of prepolymer should be regulated to 11 by adding NaOH solution, and the mixture continued for stirring; slowly the mixture changes its color from thick white colloidal solution to transparent colorless

solution. The reaction is stopped, and the shell material precursor is added drop by drop slowly to the O/W emulsion, the mixture is stirred at speed of 700 rpm maintaining temperature of 70 °C. An aliquot quantity of ammonium chloride aqueous solution was mixed to accelerate the aforesaid reaction. As demonstrated in the eq. (2), it not only accelerates the reaction but also aids in the removal of unreacted formaldehyde **[116]**. The whole reaction is continued stirring for 3 hrs which yields Nano capsules, the final solution shown in Fig. 23 (c) is further filtered, and the capsules are washed with acetone twice to collect finally the encapsulated PCM as shown in Fig. 23 (d).

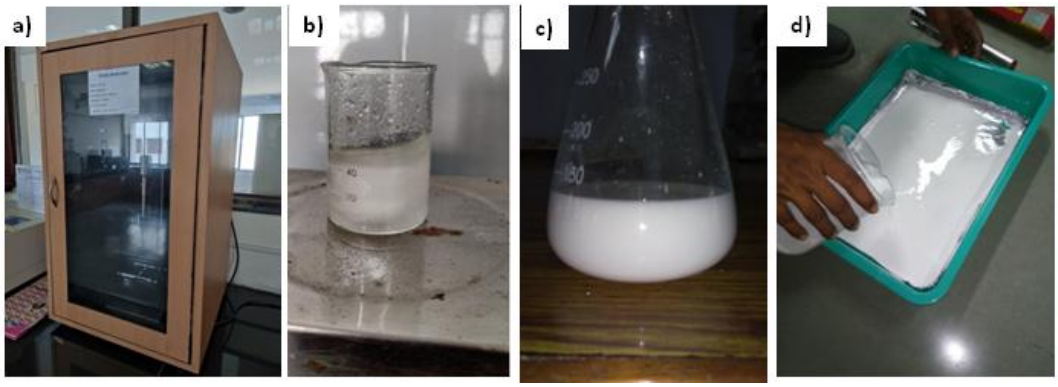

Fig. 23. Synthesis procedure of NP a) Oil in Water emulsion preparation using probe sonicator b) Shell material; c) Final Solution; d) Drying process of nanocapsules.

4.10. Synthesis of Cu-TiO_2 hybrid nanocomposites adsorbed nanoencapsulated n-Octadecane PCM (HNNP)

The as-prepared HN were adsorbed on the nanoencapsulated PCM. Fig. 24 depicts the principle behind the synthesis of nanoencapsulated PCM and the HN adsorption of the nanoencapsulated PCM (NP).

Various trials of experimentation were carried out adsorbing Cu-TiO_2 hybrid nanocomposites at different stages such as O/W emulsion phase, shell material phase etc. However, it was noticed that, by adding the Cu-TiO_2 hybrid nanocomposites colloidal solution either in O/W emulsion or along with the shell material precursor solution, the formation of nano encapsulated PCM (NP) is affected. In this context, the colloidal solution

was added separately to the final combination. The Cu-TiO_2 hybrid nanocomposites in dry powder condition are dispersed in DDW and sonicated for 15 minutes to deagglomerate.

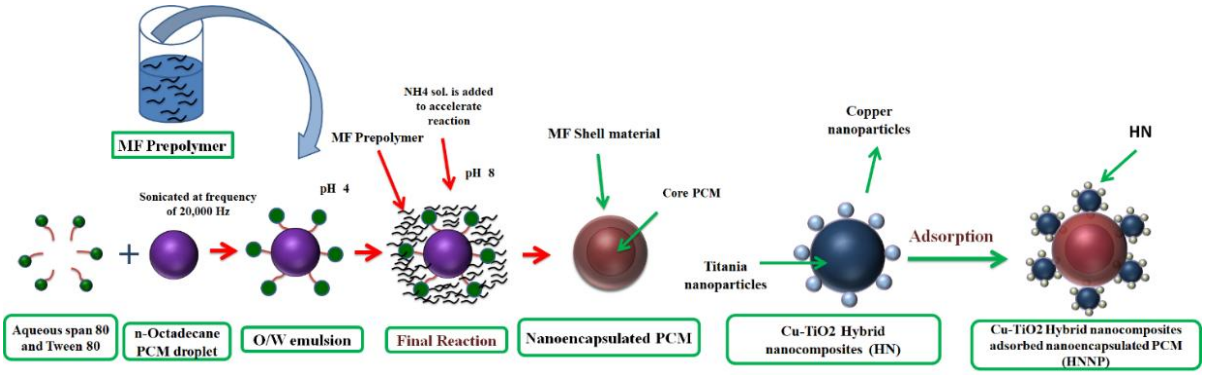

Fig. 24. Graphical representation of NP and HNNP synthesis procedure.

Later, the Cu-TiO_2 hybrid nanocomposites solution is added slowly to the solution which contains the nano capsules. The mixture is stirred very slowly on a magnetic stirrer at room temperature, in view of fact that the higher stirring speeds and higher temperatures will reduce the tendency of adsorption. The stirring is continued for 3 hours, further the capsules are filtered, and washed twice with acetone. Graphical representation regarding synthesis of Cu-TiO_2 hybrid nanocomposites adsorbed nanocapsules was presented in Fig. 25.

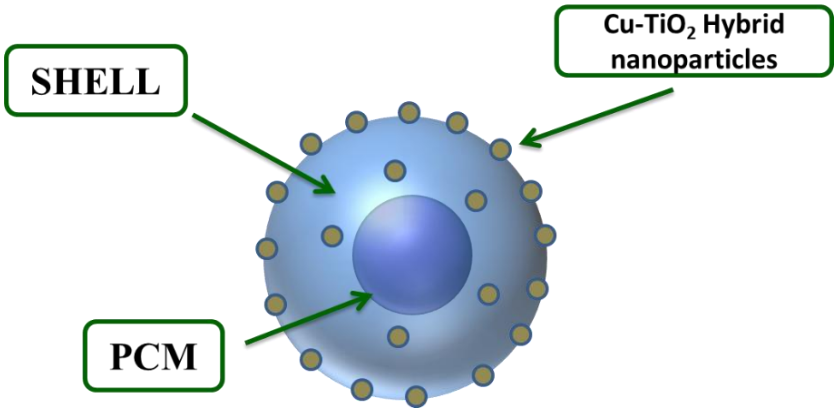

Fig. 25. Graphical representation of Cu-TiO_2 hybrid nanocomposites adsorbed nanoencapsulated n-Octadecane PCM (HNNP)

$$HLB_{mixture} = [(HLB_{Tween\ 80} * Tween\ 80\%) + (HLB_{Span\ 80} * Span\ 80\%)] \text{ -------- (3)}$$

$$HLB_{Tween\ 80} = 15,\ HLB_{Span\ 80} = 4.3$$

4.11. Challenges encountered during synthesis

1. Type of Emulsifiers and the Oil to Water (O/W) ratios plays a crucial role in the formation of PCM droplet which confirms the size of the capsules. Stirring speed of O/W emulsion also deciding factor for capsule size. After sonicating the O/W emulsion, it is important to avoid higher stirring speeds which affect the PCM droplet. While the pH value of shell material plays a vital role in the surface morphology of encapsulated PCM.
2. Methods like controlling the stirring rate, reactant concentrations, and polymerization temperature are used to influence size, but consistently applying these methods to produce nanoparticles within a narrow size range can be difficult.
3. Surfactants or stabilizers are often required to maintain stability and prevent aggregation. However, choosing the right surfactant that does not interfere with the PCM's thermal properties or the polymerization process is challenging.
4. Precisely controlling reaction conditions to modulate the polymerization rate without compromising the quality and functionality of the PCM is complex.

4.12. Preparation of pure PCM, NP and HNNP embedded cement mortar cube specimens

For the preparation of cube specimens, cement, fine aggregate, water, super plasticizer was used, and to accommodate thermal energy storage, additives such as pure PCM, NP and HNNP capsules were dispersed.

4.12.1. Mix Design for Cube specimen preparations

Two distinct types of capsules, namely NP and HNNP, were dispersed within the cement mortar matrix across a range of 3% to 15%, incrementing in 3% intervals relative to the cement weight. A lower limit of 3% was selected due to its substantial impact on thermal properties, as indicated in reference **[59]**. The cube specimens depicted in Fig. 26, were

crafted with dimensions of 70.6 mm, involving the dispersion of capsules within the cement mortar. The codes designated for these cube specimens are enumerated in Table 13.

Past literature underscores the correlation between the strength gain of cement mortar cubes and the duration of curing. In alignment with this, the cube specimens prepared underwent curing for durations of 7 days and 28 days in water **[59]**. To ensure precision and reproducibility, a minimum of 3 cube specimens were cast to represent each unique combination of NP and HNNP within the cement mortar. Table 14 outlines the allocation of separate codes to cube specimens based on their corresponding curing periods.

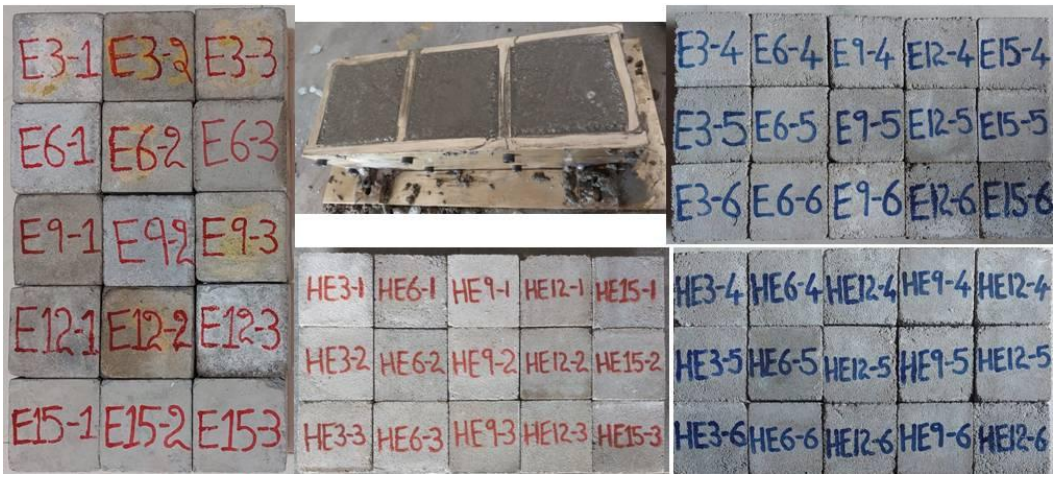

Fig. 26. NPeCM and HNNPeCM cube specimen preparation.

Subsequent to mixture preparation, the material was placed into the cube molds and subjected to vibration at a controlled speed of 12,000 vibrations/min. This step was undertaken to eliminate entrapped air pockets from the cube specimens, resulting in reduced porosity, heightened density, and increased compressive strength.

4.13. Cryogenic treatment

Cryogenic temperatures are acknowledged as one of the most extreme environments for utilizing concrete, exerting a substantial influence on various aspects of concrete performance, including its mechanical properties, freeze-thaw resistance, and overall durability. Cement-based materials exhibit markedly distinct characteristics at cryogenic

temperatures compared to ambient conditions. Liquid nitrogen, known for its extreme coldness with a boiling point of approximately -196 °C, at standard atmospheric pressure, is the preferred choice for cryogenic treatment.

4.13.1. Need for cryogenic conditioning of cement mortar

Cryogenic conditioning profoundly impacts the strength of concrete and regular practice for a few applications. The strength acquired during cement hydration is a pivotal factor, signifying the gradual enhancement of mechanical strength in cement mortar as it undergoes the hydration process. During the initial stages of cement hydration process, which transpire within the first few hours after mixing, there is a rapid dissolution of cement particles, and during this phase, the admixture does not yet possess significant mechanical strength. Subsequently, early strength gain occurs in the ensuing days to weeks, as the cement mortar progressively strengthens and begins to exhibit load-bearing capacity. Although the rate of strength gain decelerates significantly after the initial few months, concrete continues to fortify over an extended period. A wide range of investigations were carried out and also proven technique treating the concrete with cryogenic liquid. However, there are very limited studies reporting the cryogenic treatment of cement mortar.

4.13.2. Cryogenic conditioning of reference cement mortar and HNNPeCM

In the present study, an experiment involving the cryogenic conditioning of cement mortar using liquid nitrogen was carried out. Generally, the 28 days curing period is considered for the cement mortar for the appreciable strength gain. The investigations were carried out to study the impact of cryogenic conditioning of the reference cement mortar and HNNPeCM-10 cube specimens using liquid nitrogen with different curing periods such as 6 hrs, 12 hrs, and. 24 hrs as shown in Fig 27 (a). Fig. 27 (b) illustrates a close-up view of the cement mortar cube specimen after undergoing cryogenic treatment. Two different approaches for cryogenic conditioning were carried out as presented in Table 15. The first approach was the casted

cubes specimens were conditioned with liquid nitrogen for 6 hrs., 12 hrs., and 24 hrs., followed by the compression strength testing, the second approach was the cryogenically conditioned cube specimens were cured in the water for the 28 days. The cement mortar cube specimens as shown in the Fig. 28 (a) & (b) were further subjected to cryogenic conditioning and examined to assess their compressive strength using compression testing machine as shown in the Fig. 28 (c), providing valuable insights into the strength enhancement achieved through varying cryo-conditioned rates.

Fig. 27. Cryogenic conditioning of cube specimens

Fig. 28. a) Cryo-conditioned cement mortar cube specimens b) Cryo-conditioned HNNP based cement mortar cube specimens c) compression testing of Cryo-conditioned specimens.

CHAPTER - 5

RESULTS AND DISCUSSIONS

The present study involved a comprehensive thermal and structural investigations of HN based PCM. The test results encompassed a wide range of critical aspects, including the surface morphology, crystal structure, chemical stability, phase transitions, thermal energy storage capacity, thermal stability, thermal conductivity, and compressive strength of the novel HNNP and HNNPeCM.

These results highlight the importance of incorporating HN based PCM into cement mortar. This strategic integration serves towards enhancing the thermal properties of the material while ensuring the adequacy of structural integrity of the HN based PCM incorporated into the cement mortar. This underscores the potential significance of this innovative approach in the realm of sustainable construction materials.

5.1. Results of HN and HDP

5.1.1. Morphology of hybrid nanocomposite (HN)

The surface morphology of the Cu-TiO_2 HN being characterized through the FESEM has clearly showed (Fig. 29) the formation of the hybrid nanocomposite particles. The HN particles were nearly spherical in shape, and the adsorption of the tiny copper nanoparticles on the surface of the titania nanoparticles can be clearly visualized through the microscopic image. Similar results were reported in terms of the formation and nucleation of copper nanoparticles over the surface of the titania nanoparticles **[117, 118]**.

The copper nanoparticles present on the surface of the titania nanoparticles acts as extended heat transfer surfaces, with better heat transfer during phase transition process **[119]**. Furthermore, as depicted in Fig. 29. inset, the EDX spectra strongly supported the

formation of the HN and the strong peaks confirmed the presence of highly crystalline copper and titania nanoparticles.

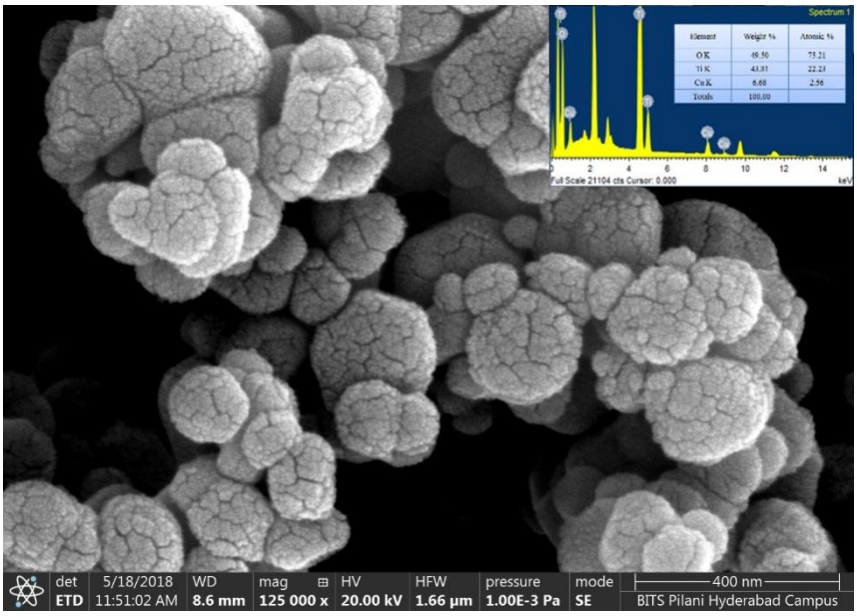

Fig. 29. FESEM and EDX of HN.

5.1.2. Crystal structure and chemical stability of the HDP

The results related to the XRD peaks at 2θ angle confirmed the formation of the copper-titania HN particles in terms of their intense and sharp Bragg reflections exhibited as shown in Fig. 30. The anatase phases of the titania nanoparticles were clearly observed which were attributed to the scattering occurred at interplanar spacing. On the other hand, the formation of the highly crystalline copper nanoparticles on the surface of the titania nanoparticles with prevailing (111) Face Centered Cubic (FCC) structure was also verified from the XRD results.

It is noteworthy that, the weight proportions of the HN has played a vital role in terms of building nucleation sites for reducing copper ions to be adsorbed on the surface of TiO_2 nanoparticles. The XRD results obtained for the HN were in good agreement with the JCPDS File No. 21-1272 for titania and 04-0836 for copper nanoparticles respectively **[120, 121]**

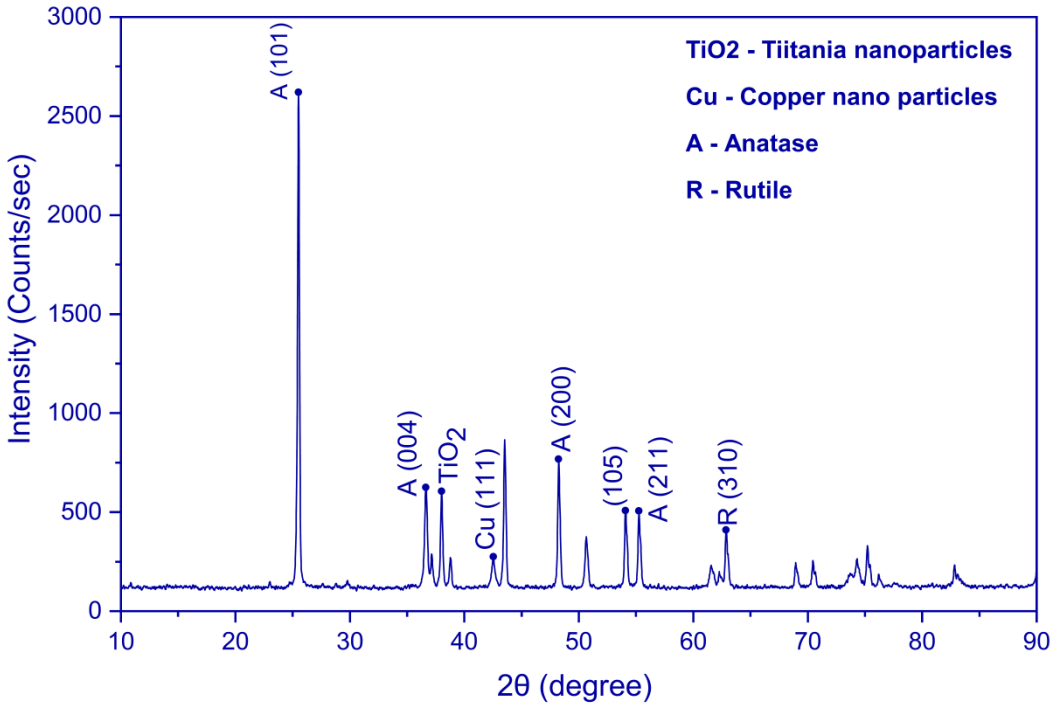

Fig. 30. XRD pattern of HN.

The Fourier transform infrared (FTIR) spectra measured for the pure PCM and HDP are depicted in Fig. 31. The test results infer that, a strong and broad band was observed at 3359.4 cm^{-1} which was ascribed to the stretching frequency of the characteristic alcohol group (C-H) of the PCM. Similarly, the absorption bands obtained at 2926.5 cm^{-1} and 2857.2 cm^{-1} were assigned to the alkane (C-H) functional groups of the pure PCM **[122]**. The vibrational peaks observed at 1460 cm^{-1} and 1057 cm^{-1} were attributed to the C-H stretching vibration of the methylene/methyl group and C-OH stretching vibration, respectively.

Interestingly, the vibrational peaks induced in the HDP were typical with the same functional group as that of the pure PCM. The marginal shifts observed in the wavenumbers of HDP were due to the physical blending and some capillary/surface tension forces between the HN and the pure PCM during the preparation of HDP. In short, the FTIR results clearly justified that, there was no chemical interaction between the pure PCM and the HN particles owing to the chemical stability of the HDP on a long run.

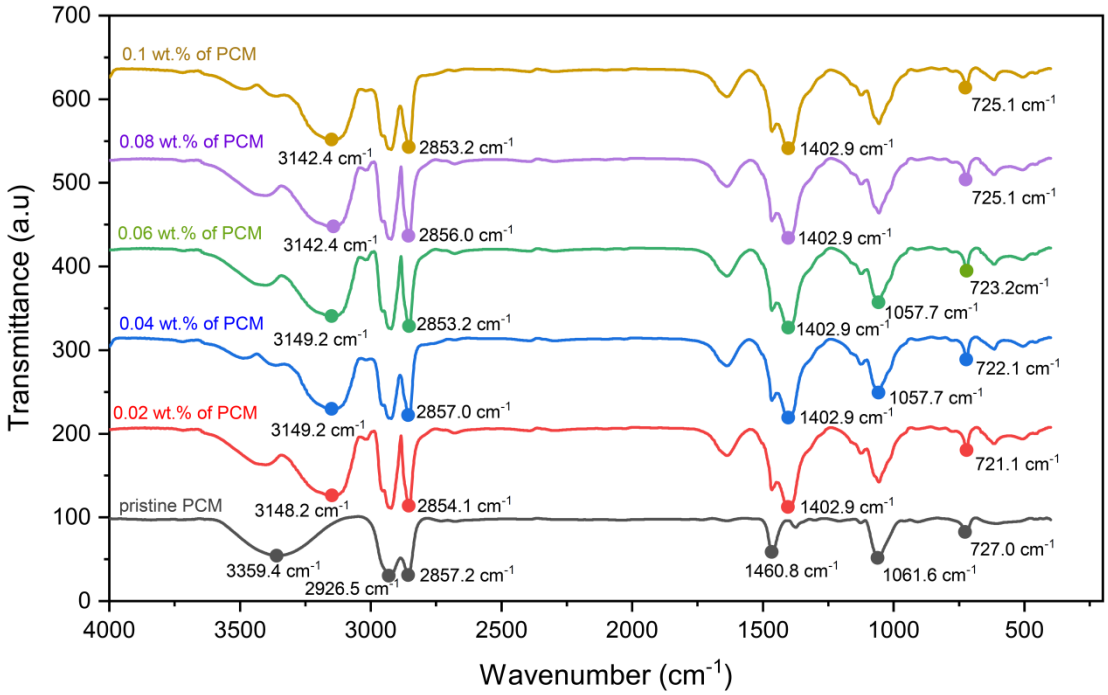

Fig. 31. FTIR spectra of the pure PCM and HDP.

5.1.3. Phase change characteristics of pure PCM and HDP

The DSC measurement results reveal that, the pure PCM and the HDP has exhibited near-congruent freezing and melting processes with the required phase transition temperatures and good latent heat capacities. The onset temperatures measured during the freezing process were consistent around 21 °C for both the pure PCM and the HDP. Likewise, during the melting process, the onset temperatures were recorded to be closer to 22 °C.

It is evident from the results presented in Fig. 32. that, with the increased dispersion of the HN into the pure PCM, still the differences in the onset phase transition temperatures were marginal and the latent heat enthalpies were also unaltered to a greater extent. The average values of enthalpy of latent heat for the HDP during freezing and melting were 190.03 J/g and 195.03 J/g, respectively. These values are in good agreement with the enthalpy values of the pure PCM.

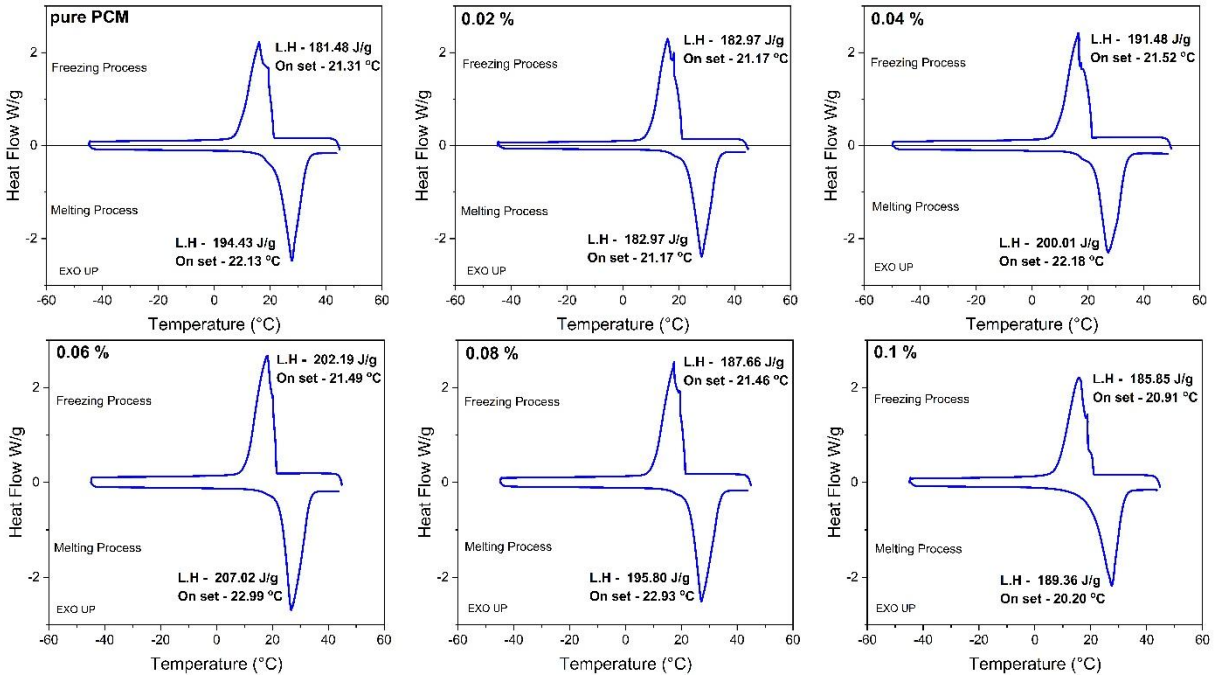

Fig. 32. DSC graphs of pure PCM and HDP

However, the variations observed in the latent heat values with regard to the loading of the HN were due to the physical interaction of the nanoparticles with the pure PCM, increased mass proportion and any dissipation effects due to viscosity of the HDP **[123, 94]**. Furthermore, the near-congruent phase transition effects and the relatively good latent heat enthalpies of the HDP can be attributed largely due to the incorporation of the highly crystalline and thermally conductive HN particles into the pure PCM.

The HN particles aided the process of heat transfer within the PCM matrix layers, which then paved way for achieving effective nucleation kinetics leading to the near-congruent freezing and melting characteristics of the HDP. The minor peaks being observed in the pure and the HDP can be ascribed to the supercooling effect of the pure PCM, but it was quite marginal and with 0.06% of HN in the PCM, the supercooling effect was eliminated (Fig. 32). The HN particles served as efficient nucleation sites within the PCM layers and promoted the heterogeneous nucleation due to freezing point depression. The results are in justification with the following reference **[124]**.

The thermally conductive HN enabled for achieving faster freezing of the HDP thereby; the effect of supercooling was minimized to a greater extent. Thus, the DSC results justified the usefulness of embedding the HN particles and due to which the HDP showed good heat storage (freezing) and discharge (melting) characteristics without any induced high concentration defects in the PCM. The results are in justification with the following reference**s [125, 27]**.

5.1.4. Heat storage and release properties

The Thermal Energy Storage (TES) experimental setup schematic shown in Fig. 33 was utilized to investigate the time taken for freezing and melting process of pure PCM and the HDP samples as shown in Fig. 33. The test samples shown in Fig. 34 (a), immersed in water, were gradually cooled to 15°C, while the cooled samples at 15°C were progressively heated to 30°C. Thermocouples were employed to record the temperature changes for each sample as shown in Fig. 34 (b). These recorded temperatures were then utilized to develop the cooling and freezing graph, as depicted in Fig. 35. The data acquired from these experiments were analysed, and the resulting findings were comprehensively presented in Table 19.

The findings clearly indicate that the pure PCM initiates its freezing and melting processes within a span of 9.5 mins. The complete freezing and melting of the pure PCM are accomplished within 25 and 28 mins, respectively. With the incorporation of HN into the PCM, both the commencement and completion times for freezing and melting processes were significantly reduced. Specifically, through maximum dispersion of HN at a concentration of 0.1%, the freezing and melting processes were remarkably expedited, occurring within approximately 15.83 and 34.4 minutes, respectively. Notably, the highest dispersion of HN at 0.1% led to a significant enhancement of 33.6% in freezing time and 14.28% in melting time.

The intrinsic Brownian motion, interaction of phonons, high surface-to-volume ratio, and surface modifications of the HN have collectively contributed to the attainment of enhanced thermal conductivity, accelerated solidification (crystallization), minimized degree of supercooling, and augmented heat energy transfer within the HDP. To be precise, the outcomes of the experiments unequivocally validate that HDP, exhibiting efficient and improved thermal properties, hold substantial promise as a viable contender for addressing the energy redistribution needs in specialized cooling and thermal energy storage applications.

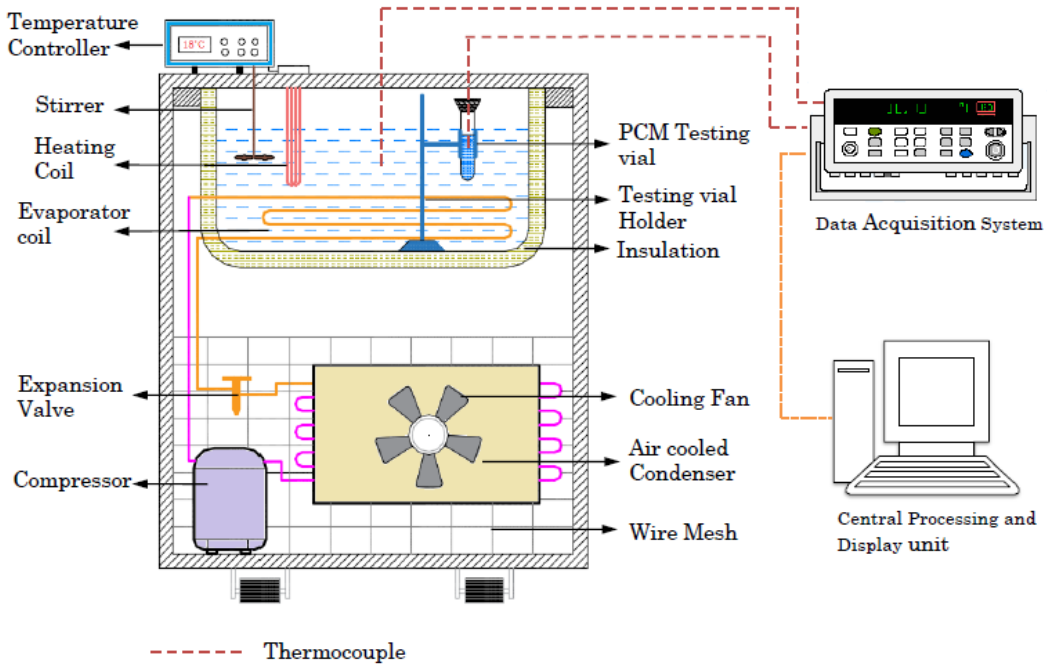

Fig. 33. Thermal energy storage setup

Fig. 34. a) HDP samples b) Testing the samples using TES setup.

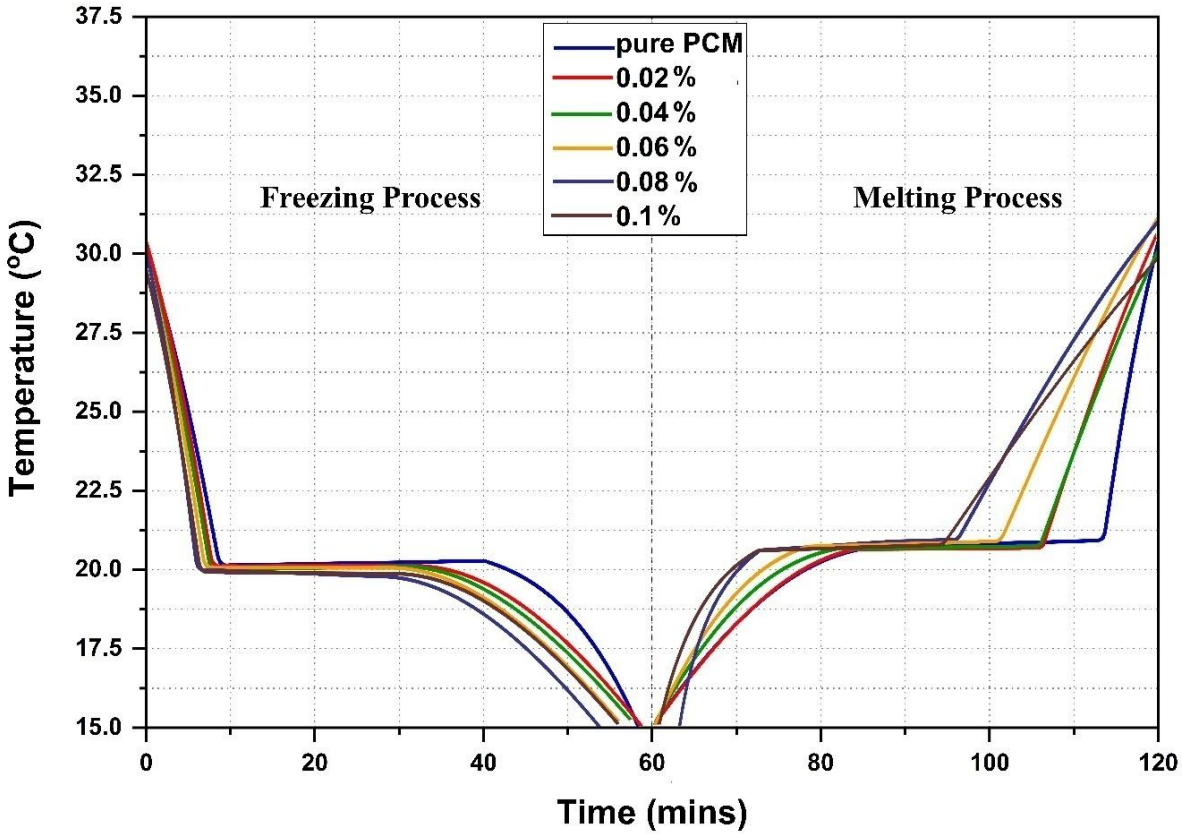

Fig. 35. Freezing and melting curves of pure PCM and HDP samples.

Table 10. Heat storage and release characteristics of pure PCM and HDP

Process	Parameters	HN based 1-Dodecanol PCM					
		Pure PCM	**0.02%**	**0.04%**	**0.06%**	**0.08%**	**0.1%**
Freezing	**Commencement (min)**	10.2	8.3	7.7	7.1	6.8	6.5
	Completion (min)	39.2	36.2	34.4	31.1	29.8	27.8
	Process duration (min)	29	27.9	26.7	24	23	21.3
	Enhancement %	----	18.6	24.5	30.3	33.3	36.2
Melting	**Commencement (min)**	92.1	83.6	80.8	76.6	73.4	71.7
	Completion (min)	118.2	105.3	101.2	96.4	92.4	89.9
	Process duration (min)	26.1	21.7	20.4	19.8	19.0	18.2
	Enhancement %	-	9.2	12.2	16.8	20.3	22.1

5.1.5. Thermogravimetric analysis

The thermal stability of the pure PCM and the HDP was determined using the TGA and the results are illustrated in Fig. 36. The test results infer that, the pure PCM and the HDP showed a single step dominant mass loss with an onset decomposition temperature of 100.4 °C. The pure PCM was thermally stable up to 100 ºC and beyond which the decomposition has started, and the process was completed at 190.11 ºC. Likewise, the HDP was thermally stable up to 100.4 °C, but the end points of the HDP being decomposed has shown some variation with respect to the mass concentration of the HN. With the dispersion of HN in pure

PCM, there was no much effect on the start of decomposition temperature but a slight shift in the end of the decomposition temperature was observed as shown in Fig. 36.

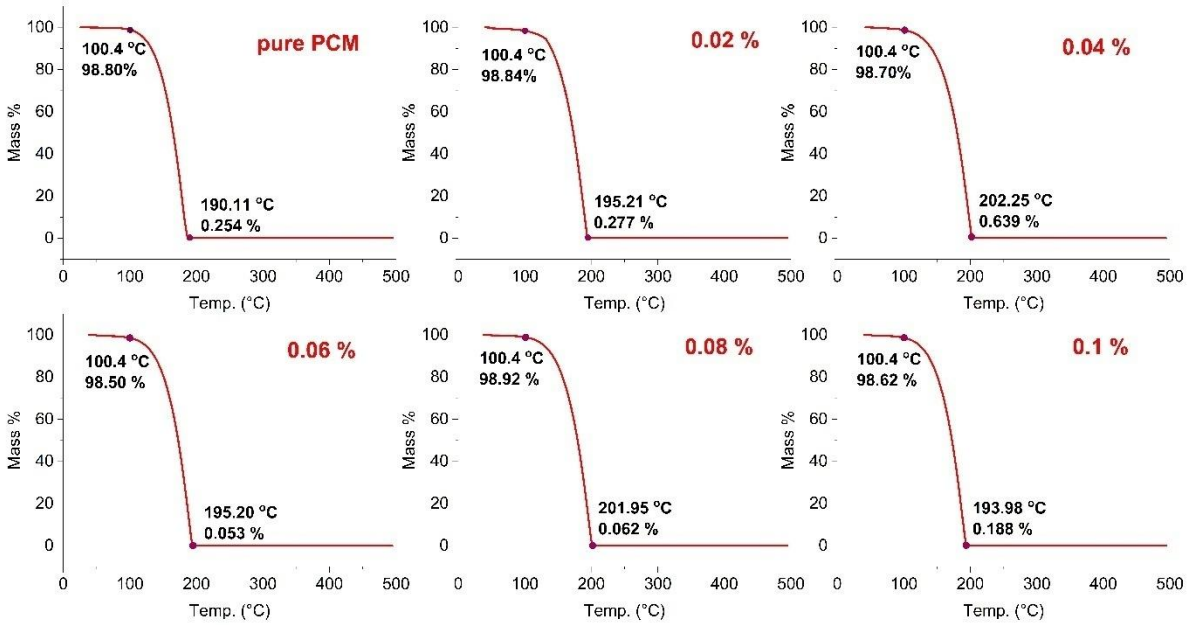

Fig. 36. TGA curves of pure PCM and HDP.

The TGA results showed that, the incorporation of the HN into the pure PCM paved way for a marginal improvement at the end-set temperature, however, for this 1-dodeconal PCM, the effect of HN on thermal stability was not appreciable. On the other hand, both the pure PCM and the HDP, they were thermally stable up to 100.4 °C, which was reasonably higher from the viewpoint of the intended passive TES application in buildings.

5.1.6. Thermal conductivity of pure PCM and HDP samples

The effective thermal conductivity of the pure PCM and the HDP were measured, and the results are depicted in Fig. 37. With the increased percentage of HN in the pure PCM, the thermal conductivity of the HDP has increased linearly to the maximum value of 0.1926 W/m K at 0.08% of the PCM, which is equivalent to 5.53% improvement in thermal conductivity of the HDP. The effect of improved thermal conductivity was mainly due to the surface morphology, phonon interaction, and the clustering of the HN particles **[126, 127]**.

The thermal conductivity enhancement was mainly because of buildup of closely packed thermal network by the HN in the pure PCM. Also, the copper nanoparticles adsorbed on the titania nanoparticles, which mimicked as fin like structures helped in achieving better heat transfer through the layers of the pure PCM thereby; augmented the heterogeneous nucleation, swift heat storage and release characteristics of the HDP.

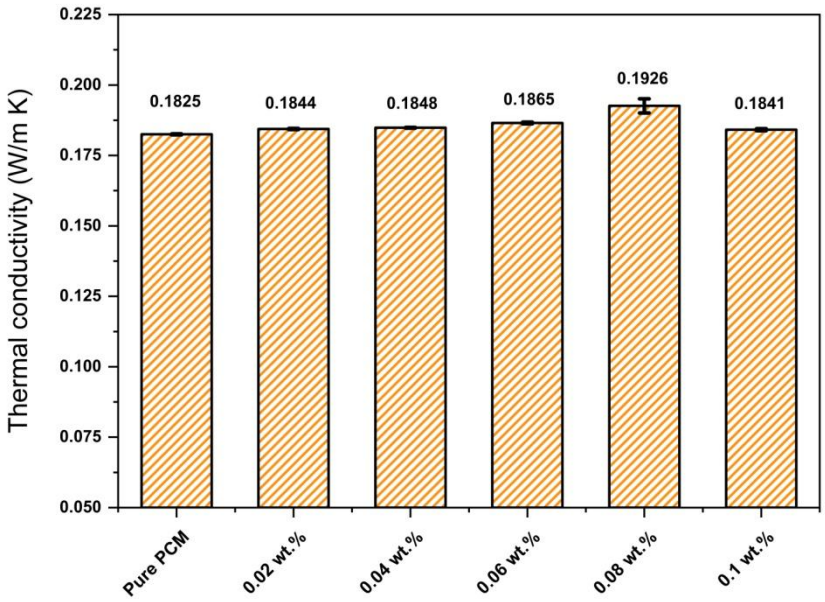

Fig. 37. Thermal conductivity of pure PCM and HDP.

The reduction in the value of thermal conductivity observed at 0.1% of HDP could be anticipated due to a possible settlement of some HN particles thereby; giving way to remaining HN particles to conduct the heat through the pure PCM. Due to the low mass proportions of the HN infused into the pure PCM, the thermal conductivity enhancement of HDP was observed to be minimal, however, any value of improvement in thermal conductivity would be beneficial for the PCM for storage and discharge of thermal energy.

5.1.7. Compressive strength of HDPC

Average values of compressive strengths of 28-day cured specimens for all the combinations are presented graphically through Fig. 38. Also a few selected photographs of the cube specimens are presented through Fig. 39 for reference.

It has been reported **[29, 128, 31]** that the addition of PCM in cement mortar has always shown the trend of drop in compressive strengths as the PCM, in the presence of water, due to the excessive lubricating effect induced to the mortar.

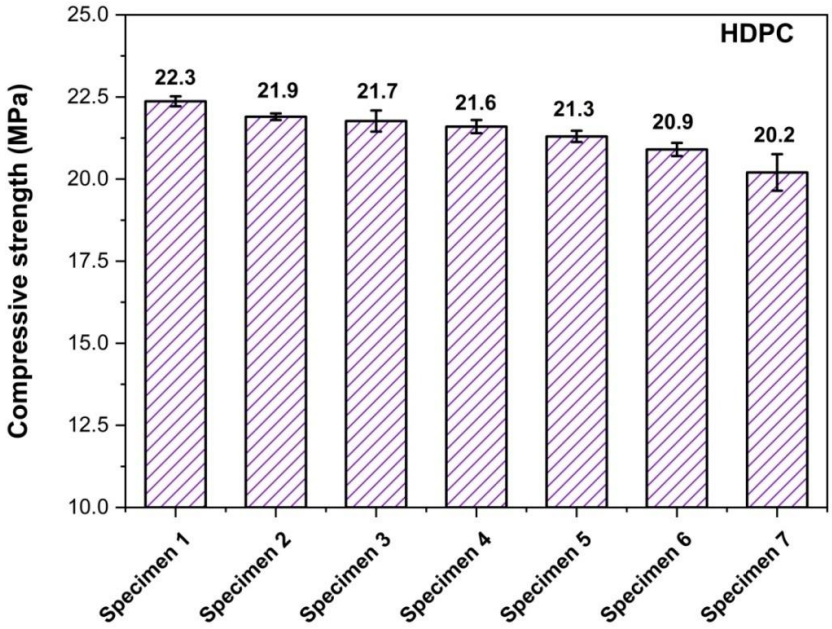

Fig. 38. 28-day compressive strength of HDPC specimens.

Fig. 39. Pictures showing the cube specimens during preparation, curing and post testing stages.

The results obtained during the present studies also confirm similar trend of drop in 28 days compressive strengths (22.3 MPa, recorded for specimen 1 with zero HDPC and 20.2 MPa, recorded for specimen 7 with 6% HDPC having 0.1% HN particles) with incremental proportion of HDPC in the mortar. The relative drop in strengths from specimen 2 to specimen 7, with uniform pure PCM inclusion of 6% and incremental HN particle ranging from 0.02% to 0.1%, was observed to be 1.7 MPa, which is quite marginal.

5.1.8. Summary

In the present work, the effects of dispersion of the HN particles into the pure PCM and in turn the incorporation of the HDP into the cement mortar for achieving enhanced thermal properties and TES capabilities were experimentally investigated. The test results clearly suggest that the HN dispersion in the PCM has really favoured in enhancing the thermal conductivity, this resulted in reducing the commencement of freezing and melting process, besides the time taken for freezing and melting process were reduced by 36.2% and 22.1% respectively.

However, it was noticed that the 1-Dodecanol PCM was leaking out from the cement mortar cube specimens during curing in water, besides the compressive strength was also reduced.

Despite the numerous benefits associated with HDP direct incorporation in cement mortar, the leakage of 1-Dodecanol PCM diminishes its energy storage capacity. This leakage issue stems from the constraint on increasing PCM percentage due to the direct impregnation method, subsequently leading to a reduction in the compressive strength of the cement mortar. Additionally, organic PCM are flammable in nature. From the application standpoint, it becomes evident that the direct impregnation technique of PCM might not be conducive and viable towards achieving optimal energy storage capabilities. In light of this, PCM

encapsulation emerges as the most viable alternative technique, effectively addressing the aforementioned challenges arising from PCM direct impregnation.

A comprehensive exploration of the synthesis process for encapsulating 1-Dodecanol organic PCM was presented in the preceding chapter. The subsequent section delves into the discussion of the characterization outcomes pertaining to MDP.

5.2. Microencapsulated 1-Dodecanol PCM (MDP)

5.2.1. Morphology of the MDP

FESEM with EDS detector was used to study the surface morphology of the as-synthesized microcapsules. The FESEM images as shown in Fig. 40 (a) depicts that, the microcapsules were spherical in shape with slight roughness on their surface being spotted. The formation of the MDP capsules mainly relied on the interfacial tension between the PCM, polymer and the surfactant. From Fig. 40 (b) and (c), it is observed that the microcapsules exhibited agglomeration or coalescence behaviour, which might have led to the slight increase in the size of the oil droplets/particles supported by the incremental inclusion/adjoining shell material **[129, 130]**.

The EDAX results of the MDP shown in Fig. 40 (d) revealed that, the weight percentage of carbon, nitrogen, and oxygen was observed to be 39.42%, 50.49%, and 10.09%, respectively. The existence of nitrogen in the capsule can be attributed to the amine (shell material) and the presence of the oxygen and carbon corresponds to the organic material (1-Dodecanol PCM). Hence, the EDAX confirmed the formation of the melamine formaldehyde shell which has effectively encapsulated the 1-Dodecanol PCM core.

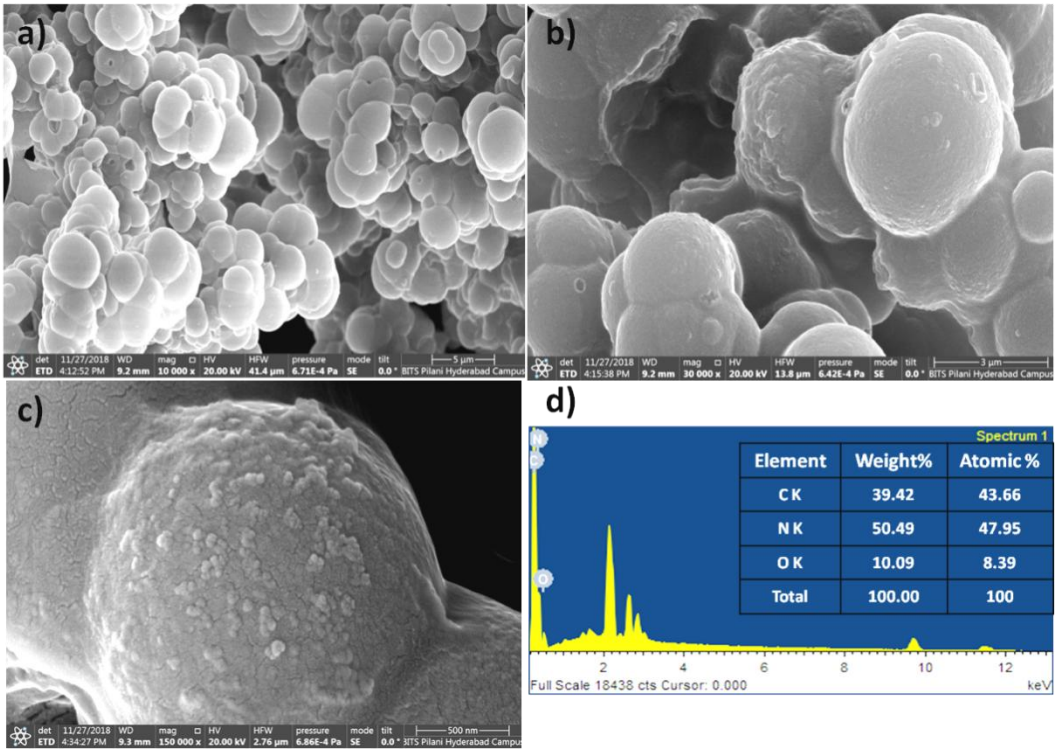

Fig. 40. FESEM images of MDP a) Microcapsules b) Agglomeration of microcapsules c) Coalescence of the microcapsule d) EDAX spectrum of the MDP.

5.2.2. Particle size distribution of the MDP

The size of the microcapsules varied from less than 60 nm to nearly 980 nm as illustrated in Fig. 41. The average capsule diameter for the first and second peaks was 119.6 nm and 549.8 nm with an intensity of 67.9% and 32.1%, respectively.

The Z-average size of the microcapsules diameter for both the peaks was determined to be 490.2 nm. This in turn well supported the formation of the micro/nano sized MDP through the facile synthesis carried out in this study. Furthermore, the surface energy was expected to increase as the radius of curvature between two adjoining particles was decreased as evident from Fig. 40 (b) and by virtue of the reduced size of the particles **[131]**.

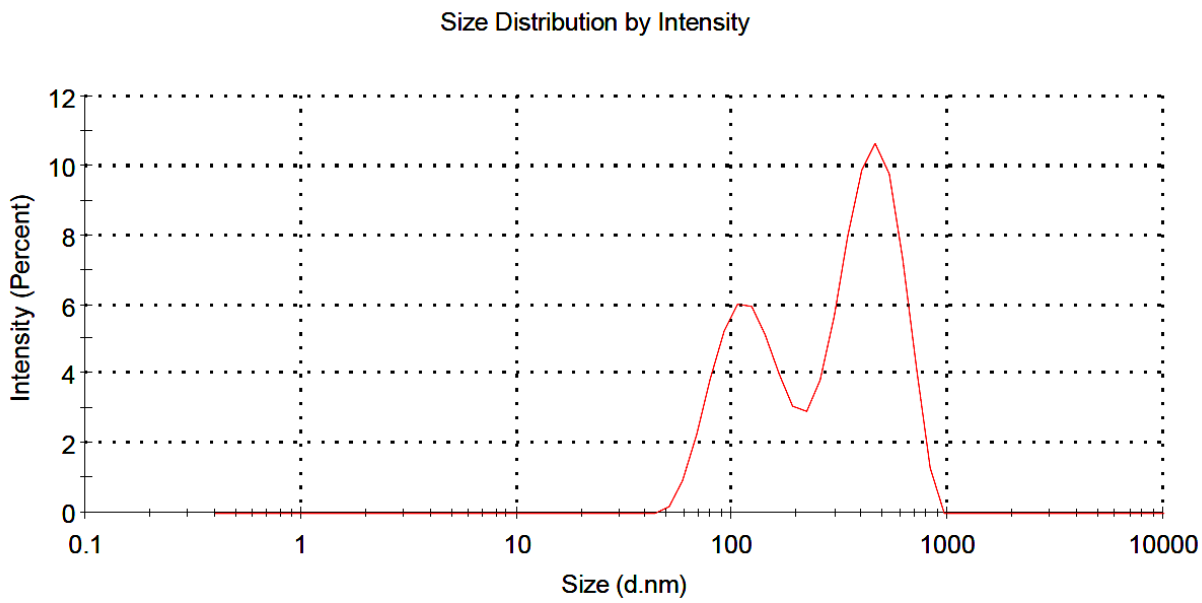

Fig. 41. Particle size distribution of the MDP.

5.2.3. Crystal structure of the MDP

The XRD pattern of the MDP is presented in Fig. 42, wherein a broad and a large peak was induced at 21.24° which signified that the material is largely amorphous in nature. The reason behind this could be due to some disordered molecular structure of the MDP, which could have resulted in the change in the lattice parameter.

The reason behind the absence of highly crystalline structure was either due to physical interaction of the PCM with the shell material **[132]**, or because of the less number of incident electrons being diffracted from that particular lattice direction of the MDP.

Besides, the grain size of the powder MDP sample could have also contributed towards the low peak intensity and non-high crystalline ability of the microcapsules. However, the amorphous structure of the MDP was expected to possess huge internal energy, and the microcapsules being synthesized were in powder form, they exhibited good dispersing capability as well **[133-135]**. Furthermore, the low peak intensity also characterized the shell

stability and resistance towards cracking, but at the penalty of reduction in the encapsulation properties **[136, 137]**.

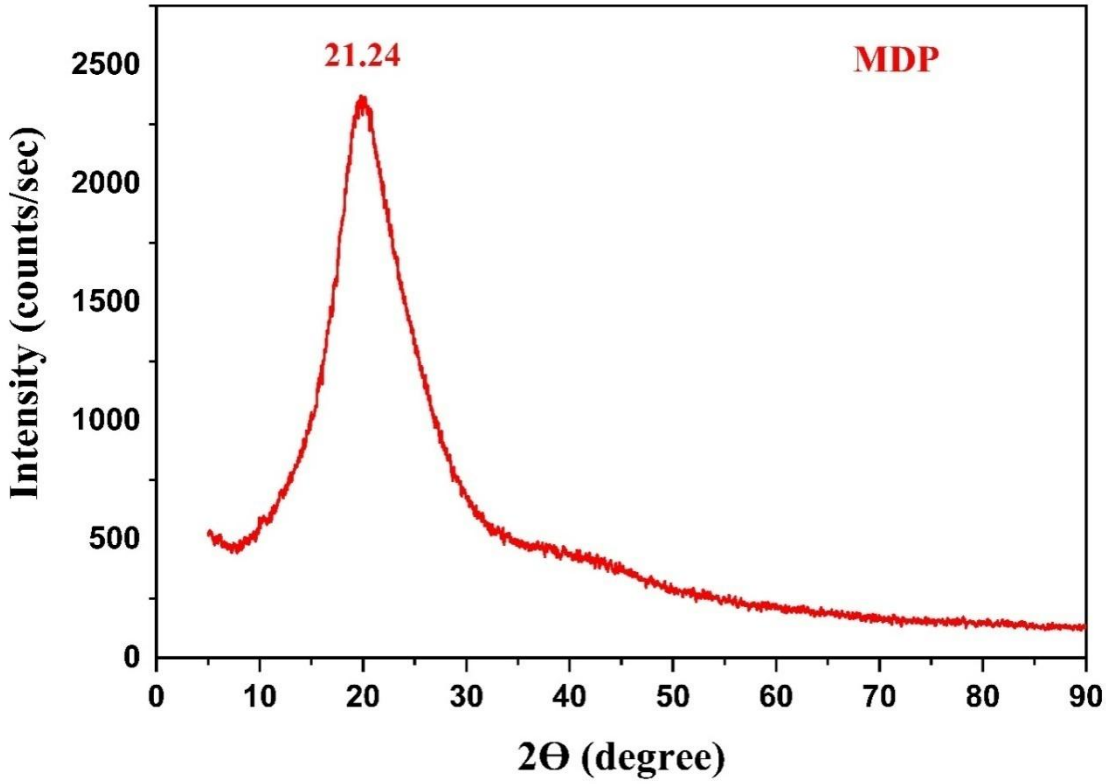

Fig. 42. XRD pattern of the MDP.

5.2.4. FTIR Analysis of MDP

The FTIR spectrum of the 1-Dodecanol PCM as shown in the Fig. 43 demonstrated that, the peak at 3359 cm^{-1} which is strong and very broad was characterized to the stretching frequency of the O-H group. The peak at 2926 cm^{-1} and 2857 cm^{-1}were belonged to the C-H stretching vibration of the aliphatic chain.

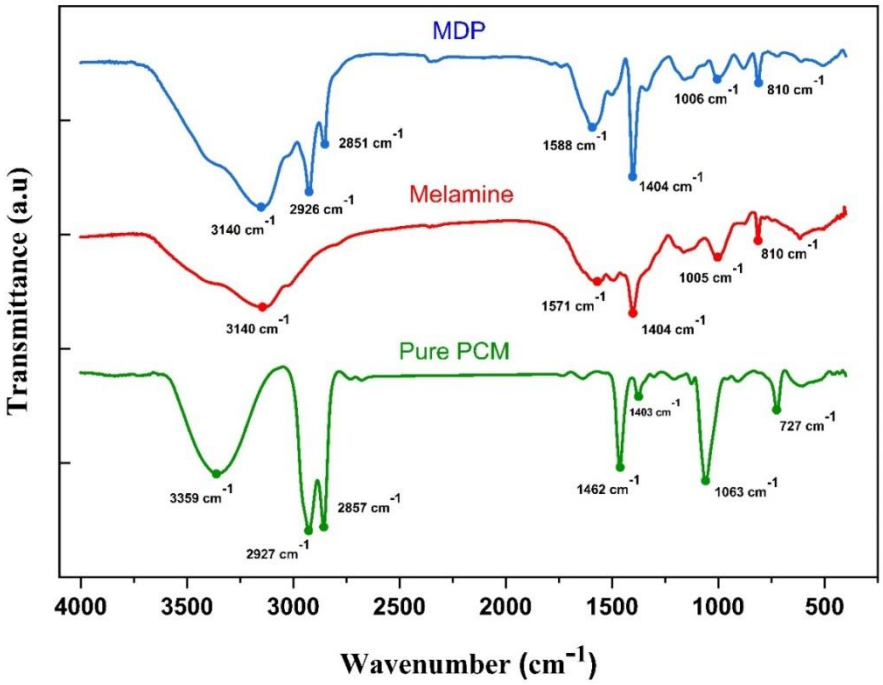

Fig. 43. FTIR spectra of the PCM, MF shell and the MDP.

Table 11. Summary of FTIR results of pure PCM, melamine and MDP.

Wavenumbers (cm^{-1})				**Assignment**	
1-Dodecanol PCM	**Melamine**	**MDP**	**MDP after thermal cycling**	**Vibration**	**Functional group**
3359	---	---	---	Stretching	O-H or N-H
---	3140	3140	3141	Stretching	N-H
2927	---	2926	2924	Stretching	C-H
2857	---	2851	2849	Stretching	C-H
---	1566	1594	1590	Bending	N-H
1462	---	---	---	Bending	C-H
1406	1404	1404	1410	Bending	N-O
1063	1005	1005	1002	Stretching	C-O
---	810	810	810	Out of plane deformation	Triazine
727	---	---	---	Rocking vibration	$-CH_2-$

The IR peaks at 1460 cm^{-1} and 1063 cm^{-1} correspond to the medium bending vibration of methylene/methyl and C-O stretching of primary alcohol functional group, respectively. The peak at 727 cm^{-1} was ascribed to in-plane rocking vibration of methylene group. The FTIR spectrum of the melamine showed a peak at 3140 cm^{-1}, which pertains to the N-H bending vibration of the amine group.

The strong peak at 1558 cm^{-1} was associated to the in-plane bending vibration of the N-H bonds. The peak at 810 cm^{-1} resembled to the stretching vibration of the triazine rings **[138-140]**. The results obtained from the FTIR test are summarized in Table 20 for ready reference.

The FTIR spectrum of the MDP contains the corresponding peaks of both the PCM and the melamine-formaldehyde shell, wherein no sign of shifts in the absorptions peaks was found. This clearly signified that there is no chemical interaction between core and shell material and also confirms the effective encapsulation of the PCM into the melamine-formaldehyde shell material.

5.2.5. Phase change and latent heat of the MDP

The phase change behaviour of the pure PCM and the MDP was studied using the DSC and the results obtained are depicted in Fig. 44 and summarized in Table 21. The results infer that, the pure 1-Dodecanol PCM exhibited a single peak congruent phase transformation during the cooling and melting processes. Interestingly, during the freezing process the pure PCM has directly transformed from the isotropic liquid phase to triclinic phase.

However, the MDP behaved differently during its phase transformation with the existence of dual peaks in the course of cooling process, whereas the MDP revealed a single peak during the melting process, which was quite similar to that of the pure PCM. The dual peaks

(α-rotator phase) and (β-triclinic phase) of the MDP were induced at an onset temperature of 20.78 °C and 14.21 °C, respectively.

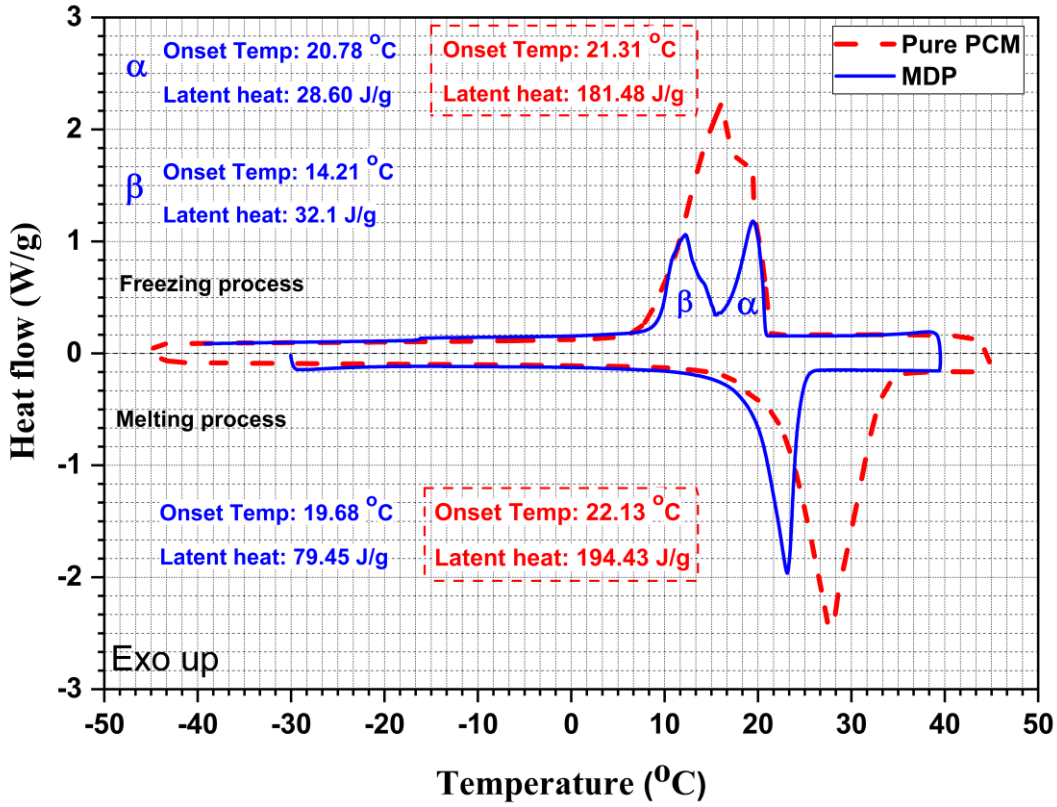

Fig. 44. DSC graphs of pure PCM and MDP

Table 12. Thermal properties of pure PCM and MDP.

Sample Type	Melting temperature T_m (°C)	Latent heat of melting ΔH_m (kJ/kg)	Freezing temperature T_f (°C)	Latent heat of freezing ΔH_f (kJ/kg)	k (W/m K)
1-Dodecanol PCM	22.13	194.43	21.31	181.48	0.186
Melamine/1-Dodecanol MDP	19.68	79.45	α = 20.78 β = 14.21	60.70	0.172
MDP after 200 thermal cycles	19.01	75.41	α = 20.41 β = 13.88	56.95	0.171

Sample Type	Melting temperature T_m (°C)	Latent heat of melting ΔH_m (kJ/kg)	Freezing temperature T_f (°C)	Latent heat of freezing ΔH_f (kJ/kg)	k (W/m K)
MDP after 500 thermal cycles	19.71	70.48	α = 20.21 β = 14.88	52.77	-
MDP after 1000 thermal cycles	19.24	68.79	α = 20.01 β = 14.23	49.06	-

The reasons behind the existence of the dual crystallization peak include (a) 1-Dodecanol PCM been confined in to a closed shell (MDP), (b) with the decreasing temperature of the MDP, the core PCM inside the shell has transited in to two stages from heterogeneously nucleated liquid phase to the rotator phase (α) and the rotator phase to the triclinic phase (β) at temperatures of 20.78 °C and 14.21 °C, respectively.

From the DSC results obtained (Fig. 44), the proportion of the latent heat of crystallization due to the α and β peaks was estimated to be 47.2% and 52.9% at 20.78 °C and 14.21 °C, respectively. With respect to the long axis, the rotator phase (α) exhibited a lack of molecular rotational degree of freedom and with weakly ordered crystallite phases **[141]**.

On the other hand, the degree of super cooling (which is the difference between the onset temperatures of melting and cooling processes) was also a major factor which influenced the nucleation kinetics of the PCM present inside the shell material.

The degree of super cooling for the pure PCM was computed to be 0.82 °C, whereas, for the MDP, there was a slight increase in the super cooling degree of 1.1 °C. With the increased value of super cooling, the phase change may occur over a wide range of

temperature, which may affect the nucleation of the ice crystals of the PCM during the freezing/crystallization process.

Also, the supercooling increases with lack of nucleation sites present inside the shell, and which generally occurs due to the reduced capsule size. However, the supercooling degree for the MDP was imperceptible when compared to the pure PCM, and hence the MDP exhibited good phase change behaviour **[132, 50, 142]**.

Furthermore, the thermal energy storage of the pure PCM and the MDP was evaluated based on three key parameters, namely, encapsulation ratio (R), encapsulation efficiency (EE) and thermal energy storage capability/capability (ε). The respective values are summarized in Table 22 for ready reference.

The encapsulation ratio (R) of MDP was estimated to be 40.9% using Eq. (4). It is worth noting that the encapsulation ratio describes the effective encapsulation of 1-Dodecanol PCM in MF shell material, while the loading content is considered as the total weight percent of PCM in the shell. However, only with encapsulation ratio, the thermal storage capacity of the PCM present in the shell cannot be decided.

Thus, the encapsulation efficiency (EE) of the MDP was considered as given in Eq. (5), and it was estimated to be 37.3% by the enthalpies involved in both of the melting and freezing processes. This is in turn preferred as a more suitable parameter for the evaluation the working efficiency of the PCM in MF shell, when compared to that of the encapsulation ratio. However, depending upon the application, the ratio of the core-to-shell can be varied, which may in turn influence on the latent heat enthalpies of the microencapsulated PCMs **[112]**.

In this regard, the thermal energy storage capability (ε) of the 1-Dodecanol PCM present inside the MF shell material was determined using the Eq. (6), wherein, the MDP exhibited a

high thermal storage capability (ε) of 91.2%. This indicated that, almost all the encapsulated 1-Dodecanol PCM could effectively store and release the energy through phase transformation. Eq. (5,) Eq. (6) Eq. (7) were referred from the references **[143-145]**.

$$R = \frac{\Delta H_{m,\ MDP}}{\Delta H_{m,\ PCM}} \times 100 \quad \text{----- (4)}$$

$$EE = \frac{\Delta H_{m,\ MDP} + \Delta H_{c,\ MDP}}{\Delta H_{m,PCM} + \Delta H_{c,PCM}} \times 100\% \quad \text{----- (5)}$$

$$\varepsilon = \frac{\Delta Hm,\ MDP + \Delta Hc,\ MDP}{\frac{R}{\Delta Hm,PCM + \Delta Hc,PCM}} \times 100\% \quad \text{----- (6)}$$

where, $\Delta H_{m,\ PCM}$ and $\Delta H_{c,\ PCM}$ are the latent heat of melting and freezing of pure PCM and $\Delta H_{m,\ MDP}$ and $\Delta H_{c,\ MDP}$ are the latent heat of melting and freezing of MDP, respectively.

Table 13. Thermal energy storage capability of pure PCM and MDP

Sample Type	**Latent heat of melting ΔH_m (kJ/kg)**	**Latent heat of freezing ΔH_f (kJ/kg)**	**Encapsulation ratio (R) (%)**	**Encapsulation efficiency (EE) (%)**	**Thermal storage capacity (ε) (%)**
1-Dodecanol PCM	194.43	181.48	-	-	-
Melamine/1-Dodecanol MDP	79.45	60.7	40.8	37.3	91.2
MDP after 200 thermal cycles	75.41	56.95	38.8	35.2	90.7
MDP after 500 thermal cycles	70.48	52.77	36.2	33.0	91.3
MDP after 1000 thermal cycles	68.79	49.06	35.3	31.6	89.5

The reasons behind the reduced latent heat of the MDP could be ascribed to the presence of solid-to-liquid and solid-to-solid phase transition behaviour of the pure PCM inside the shell material. In addition, the less content of the PCM availability inside the shell material could also be attributed to the reduced latent heat enthalpy **[146]**. The key parametric comparison of the synthesized MDP with the existing microencapsulated PCMs from the literature is presented in Table 23.

From Table 23, it is noteworthy that, the major thermal properties of the as-synthesized MDP were in good agreement with the similar kinds of encapsulated PCM. Thus, the DSC results suggest that the synthesized MDP in this study has exhibited good phase transition characteristics, appreciable latent heat potential and high thermal energy storage capacity.

5.2.6. Thermal stability of the MDP

Thermal stability of the pure PCM and the MDP was determined using TGA and the results are presented in Fig. 45. Based on the tangential method, the test results reveal that, the single step mass loss/degradation of the pure PCM commenced at 102.98 °C and the decomposition of the PCM was completed at 187.47 °C with mass loss of 99.67%, leaving

Table 14. Thermal properties of PCM (Literature)

Author	**PCM/Shell**	**Shell material**	**Encapsulation ratio (R) (%)**	**Encapsulation efficiency (EE) (%)**	**Thermal storage capacity(ε) (%)**	**Thermal cycling test (number of cycles)**
Zhang et al. **[147]**	n-Dodecanol	Melamine formaldehyde	79.61	50.21	75.6	No
Su et al.	Dodecanol	Methanol	91.2	68.4	141.5	No

[148]		modified Melamine formaldehyde				
Huang et al. **[149]**	Paraffin	Urea formaldehyde	-	32.7	-	No
Wu et al. **[112]**	n-Dodecanol	Melamine urea formaldehyde	63.11	63.65	99.15	No
Huang et al. **[138]**	n-Dodecanol	Melamine formaldehyde	52.4	54.1	101.7	Yes (50)
Wang et al. **[150]**	Methyl laurate	Polyurethene	83.3	83.9	99.35	Yes (30)
Present study	1-Dodecanol	Melamine formaldehyde	40.9	37.3	91.2	Yes (200)

the residual contents behind in the crucible. The decomposition of the MDP resulted in two steps: (a) during the first step decomposition there was a mass loss, which was mostly ascribed to the loss of water vapor and other molecular ingredients on the surface of the microcapsules.

When the temperature was further increased, cracking of the MF shell material was noticed and as a consequence of which, the PCM inside the shell material was exposed to the elevated temperature and it began to decompose at 132.82 °C. To substantiate this observation, the inset of Fig. 45 clearly shows the FESEM image of the cracked microcapsules after complete decomposition of the PCM.

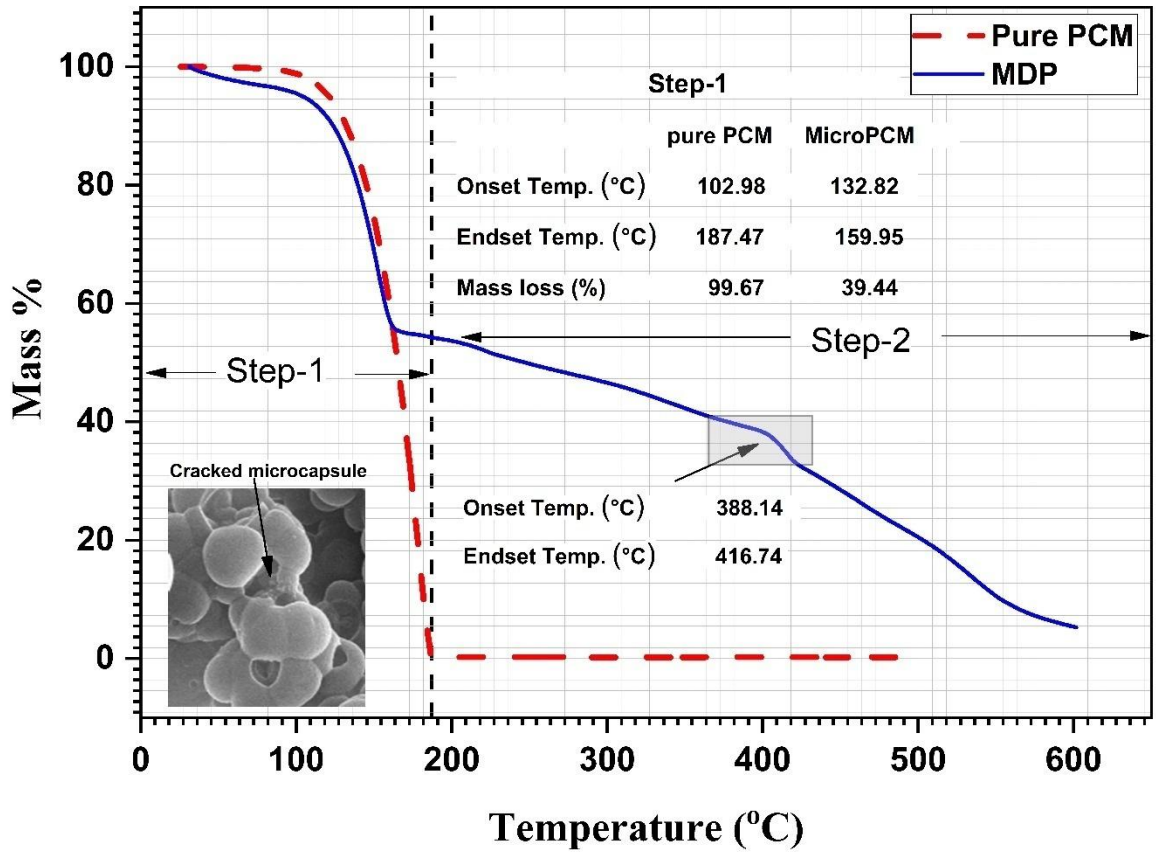

Fig. 45. TGA graphs of pure PCM and the MDP

The PCM in the shell was completely decomposed at 159.95 °C with mass loss of 39.44%. The second step decomposition commenced at around 190 °C which was related to the loss of the shell material (MF) and there was a sudden mass loss observed in the temperature range of 388.14 °C to 416.74 °C and the decomposition continued till 600 °C **[151]**.

It is obvious from the TGA results that, the MDP possessed excellent thermal stability in the sense that, the decomposition temperature of which was very high when compared to the operating temperature range of the PCM (22 °C to 26 °C) for low temperature TES applications.

5.2.7 Thermal conductivity of the MDP

The thermal conductivity of the pure PCM and the MDP were measured to be 0.186 W/m K and 0.172 W/m K, respectively. The test report in Table 21 suggests that the thermal

conductivity of the MDP was slightly lower than that of the pure PCM. This marginal reduction could be due to the presence of the outer MF polymeric shell material, which eventually possess a very low thermal conductivity **[152]**.

On one side, this low thermal conductivity was much favourable in terms of enabling the MDP to serve as a good thermal insulating material. On the other side, due to low thermal conductivity, the melting and freezing behaviour of the PCM inside the shell would have been slightly affected due to the insulating nature of the shell material towards the heat flow. This could have also influenced in the reduction of latent heat enthalpy of the MDP. Nevertheless, the MDP has established excellent thermal stability and good heat insulation ability.

5.2.8. Thermal cycling test of the MDP

Thermal cycling test was conducted to study the reliability and phase change behaviour of the MDP, wherein, the MDP was subjected to 200, 500 and 1000 cycles of heating and cooling from 10 °C to 60 °C and vice versa, respectively. The thermal cycling results being obtained for the MDP is shown in Fig. 46.

The result demonstrates that, after 200 thermal cycles, the onset temperatures of α and β phases of the MDP during the freezing process were slightly shifted to a lower temperature **[108]**. The drop in the onset temperatures of α and β phases during the freezing process was identified to be 0.37 °C and 0.33 °C. Likewise, the onset melting temperature after thermal cycling was observed to marginally drop by 0.67 °C, when compared to the MDP before thermal cycling test.

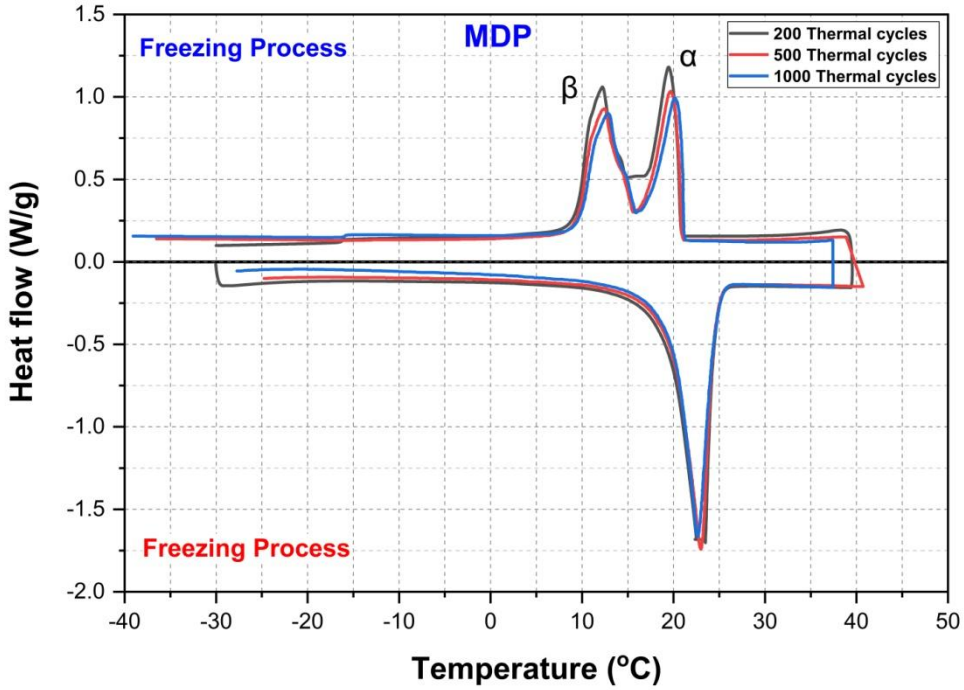

Fig. 46. DSC graph of MDP after thermal cycling

It is interesting to note that, based on Eq. (7), the thermal energy storage capacity of the MDP after the thermal cycling test was accounted to be 90.7% (Table 22). Besides, the latent heat during melting and freezing were reduced by 3.75 kJ/kg and 4.04 kJ/kg, respectively, and the reduction in the latent heat was very marginal. That is, the reduction in the latent heat potentials of 5.1% (melting) and 6.2% (freezing) of the MDP after 200 thermal cycles can be reasoned to its slight diminution of energy storage capability against the repeated thermal cycling **[153]**.

To further substantiate the thermal reliability of the MDP, the thermal reliability index (R_{rel}) was considered **[150]**, which is given by equation (7),

$$(R)_{rel} = \frac{(\text{Encpasulation efficiency})_{\text{After } thermal\ cycling}}{(\text{Encpasulation efficiency})_{\text{Before } thermal\ cycling}} \times 100\% \quad \text{----- (7)}$$

Table 15. Thermal energy storage capability of pure PCM and MDP

Sample Type	Latent heat of melting ΔH_m (kJ/kg)	Latent heat of freezing ΔH_f (kJ/kg)	Encapsulation efficiency (EE) (%)	Thermal reliability index (R_{rel}) (%)
1-Dodecanol PCM	194.43	181.48	-----	------
Melamine/1-Dodecanol MDP	79.45	60.7	37.3	100
MDP after 200 thermal cycles	75.41	56.95	35.2	94.4
MDP after 500 thermal cycles	70.48	52.77	33.0	88.4
MDP after 1000 thermal cycles	68.79	49.06	31.6	84.7

Thus, from Table 24 it can be clearly observed that, the thermal reliability index of the synthesized MDP after completion of 200 successful thermal cycles was estimated to be 94.4%. This revealed the good thermal reliability of the MDP and its feasibility for low temperature TES applications.

It was also noticed that there was no leakage of the 1-Dodecanol PCM from the microcapsules even after 200 thermal cycling. Hence, the thermal cycling results strongly confirmed the reliability of the MDP on a long term basis without any leakage of the PCM.

As observed from Fig. 47, the chemical stability of the MDP before and after the thermal cycling was excellent in the sense that, there was no change in the position and the chemical/surface structure of the functional groups even after 200 thermal cycles **[154, 150]**. In total, based on the aforementioned results, it is obvious that the as-synthesized MDP capsules have exhibited enhanced properties for them to be considered as potential candidate for low temperature TES applications **[155]**.

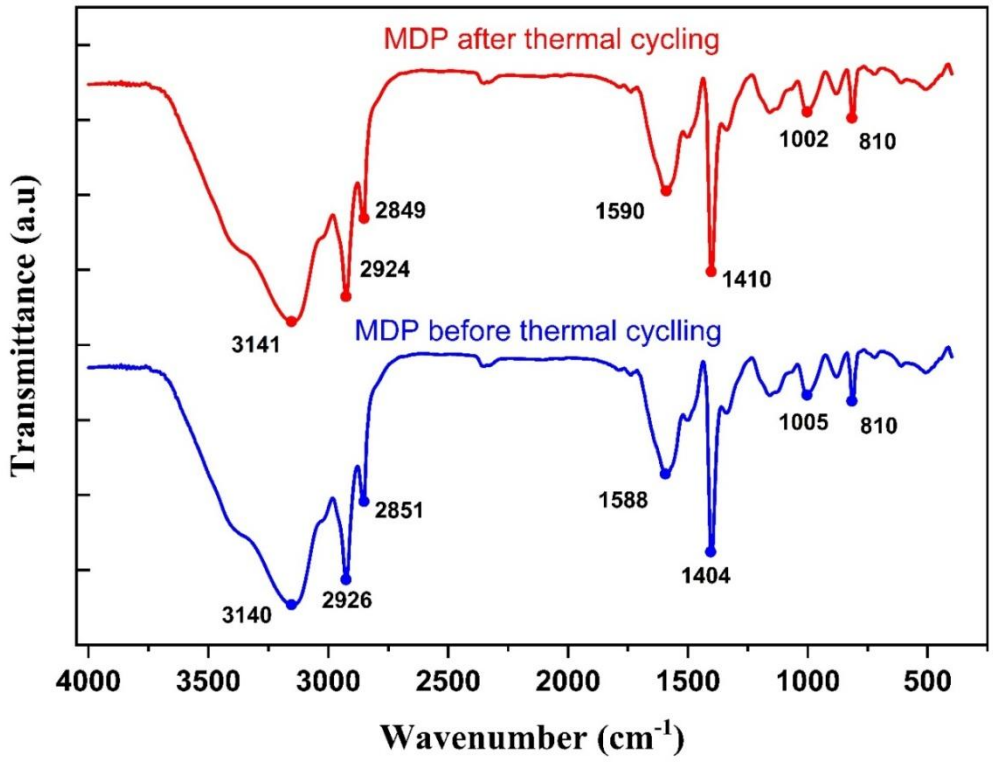

Fig. 47. FTIR spectra of MDP before and after thermal cycling

5.2.9 Summary from the synthesis of MDP

In this work, a new microencapsulated organic PCM (MDP) comprising of 1-Dodecanol as the PCM and melamine formaldehyde as the shell material was successfully synthesized through a facile in-situ polymerization process. The experimental characterization of the as-synthesized MDP suggested good thermo-physical properties, the MDP exhibited good thermal reliability even till 200 thermal cycling's. However, the freezing process took place in two stages such as α and β phases which commences at 20.78 °C and 14.21 °C respectively. The current research work aims to develop enhanced PCM based plastering material intended for internal plastering of buildings. When the MDP based mortar is incorporated as internal plastering for an air-conditioned room, it becomes evident that the crystallization temperature of the MDP deviates from the designated operating conditions of

22 °C to 26 °C. In an effort to tackle this concern, an endeavour was undertaken to encapsulate the PCM at the nano level.

5.3. Results and Discussions of Nanoencapsulated 1-Dodecanol PCM (NDP)

5.3.1. Surface Morphology of Nanoencapsulated 1-Dodecanol PCM (NDP)

FESEM was employed to analyze the surface morphology of the capsules. As illustrated in Fig. 48, the capsules exhibit a distinct spherical shape. It is noteworthy that the capsules display agglomeration tendencies as shown in Fig. 48. This occurrence might be attributed to an excessive PCM content that remained unencapsulated. Alternatively, the agglomeration could be linked to the proportion of emulsifier concerning the aqueous fraction in the Oil in Water preparation (O/W).

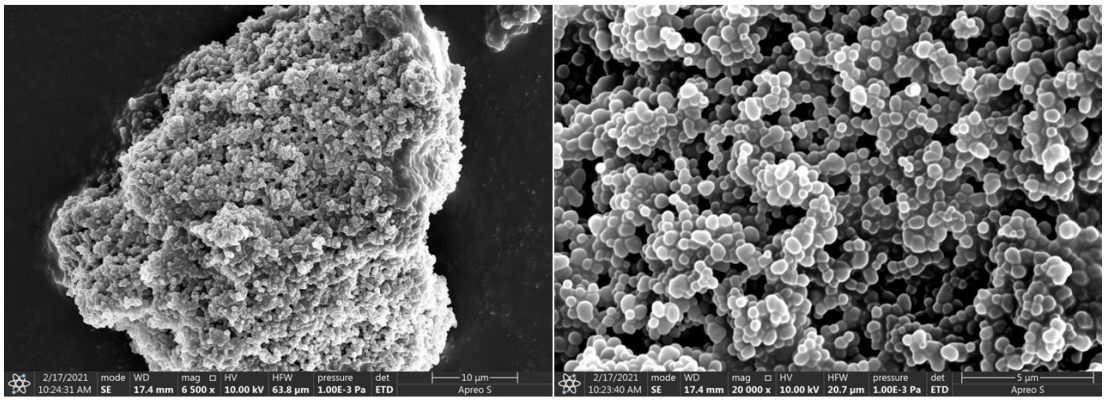

Fig. 48. FESEM Images of NDP

5.3.2. Phase change characteristics of nanoencapsulated 1-Dodecanol PCM (NDP)

It is very crucial to study the phase change characteristics of nanoencapsulated PCM. The phase change behaviour of the nanoencapsulated PCM (NDP) closely resembled that of MDP, exhibiting dual freezing peaks-namely, the (α-rotator phase) and the (β-triclinic phase). Nonetheless, minor deviations were observed in the phase transition temperatures as shown in Fig. 49. The assessment of capsule phase change behaviour spanned temperatures from -40 °C to 40 °C. Within this range, the core PCM in the shell material initiated its freezing at a

specific temperature of 19.01 °C, indicative of the α phase, accompanied by a latent heat of 55.80 kJ/kg. Similarly, the onset of the β phase occurred at 13.77 °C, with an identical latent heat value of 37.21 kJ/kg. Notably, the nanoencapsulated PCM exhibited a melting latent heat of 101.10 kJ/kg, and the core PCM embarked on its melting process at 20.11 °C, presented in Table 25.

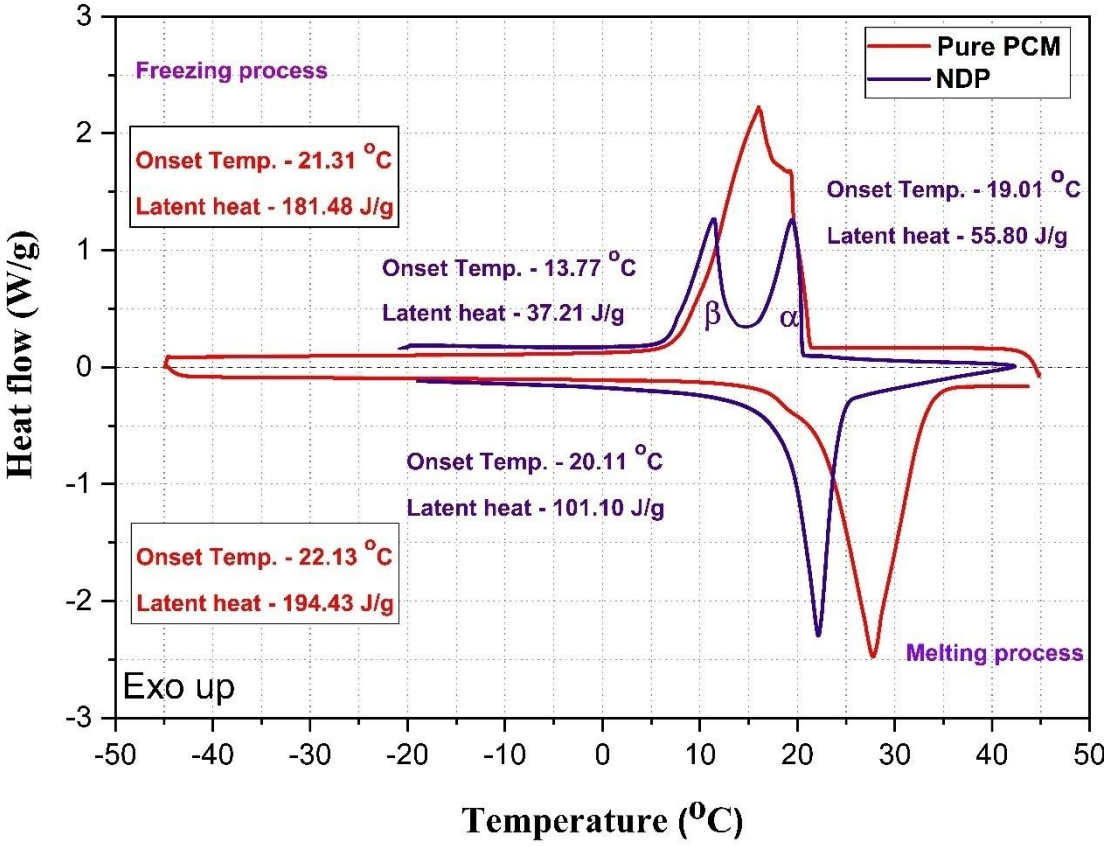

Fig. 49. Phase change characteristics of pure 1-Dodecanol PCM and NDP

The encapsulation ratio (R) of the NDP was calculated 51.9% as shown in Table 26. It's important to emphasize that this ratio elucidates the efficient incorporation of 1-Dodecanol PCM within the MF shell material. In contrast, the encapsulation efficiency (EE) of the nanoencapsulated PCM, as defined in Eq. (5), was determined at 51.6%. This estimation was grounded in the enthalpies inherent to both the melting and freezing processes, making it a

more fitting parameter for evaluating the operational efficacy of the PCM within the MF shell.

Table 16. Thermal properties of pure 1-Dodecanol PCM and NDP

Sample Type	**Melting temperature T_m (°C)**	**Latent heat of melting ΔH_m (kJ/kg)**	**Freezing temperature T_f (°C)**	**Latent heat of freezing ΔH_f (kJ/kg)**	**k (W/m K)**
1-Dodecanol PCM	22.13	194.43	21.31	181.48	0.186
Melamine/1-Dodecanol NDP	20.11	101.10	$T_f(\alpha) = 19.01$ $T_f(\beta) = 13.77$	$\alpha = 55.80$ $\beta = 37.21$	0.164

Notably, contingent upon the application, the core-to-shell ratio can be adjusted, thereby exerting an impact on the latent heat of the NDP. In this context, the thermal energy storage capability (ε) of the 1-Dodecanol PCM residing within the MF shell material was computed via Eq. (6), revealing a significant thermal storage capacity (ε) of 99.4% for the nanoencapsulated PCM. This observation underscores that nearly all the encapsulated 1-Dodecanol PCM could effectively store and release the energy through the process of phase transformation.

Table 17. Thermal energy storage capability of pure 1-Dodecanol PCM and NDP.

Sample Type	Latent heat of melting ΔH_m (kJ/kg)	Latent heat of freezing ΔH_f (kJ/kg)	Encapsulation ratio (R) (%)	Encapsulation efficiency (EE) (%)	Thermal storage capacity (ε) (%)
1-Dodecanol PCM	194.43	181.48	-	-	-
Melamine/1-Dodecanol NDP	101.01	54.38	51.9	51.6	99.4

5.3.3. Summary from the synthesis of NDP

It is evident from the characterization results that the modifications in surfactant and the Oil to Water ratios (O/W), resulted in the size reduction. The DSC results suggest that the freezing process of Nano PCM is similar to that of MDP which took place in two stages. The changes in the synthesis procedure also enhanced the encapsulation ratio from 37.3% to 51.9%. However, it's important to note that the phase change temperatures of both microencapsulated 1-Dodecanol PCM (MDP) and nanoencapsulated 1-Dodecanol PCM (NDP) falls beyond the operational parameters of end applications, which range from 22 °C to 26 °C. Given this context, the adoption of n-Octadecane PCM was deemed necessary to achieve the desired objectives.

5.4. Cu-TiO_2 hybrid nanocomposites-based n-Octadecane PCM embedded cement mortar (HOPC)

5.4.1. Chemical stability

The Fourier transform infrared (FTIR) spectra, as depicted in Fig. 50 were obtained for both pure n-Octadecane PCM and the HOP. In Fig. 50, the test results for n-Octadecane PCM reveal several significant IR peaks. Specifically, the peaks at 2921 cm^{-1} and 2847 cm^{-1} are attributed to the C-H stretching vibration of the aliphatic chain. Additionally, the peak at 1469 cm^{-1} corresponds to the bending vib1ration of the methylene/methyl group, while the peak at 727 cm^{-1} signifies the in-plane rocking vibration of the CH2 group **[37, 156, 157]**. Importantly, it is evident that the FTIR results for the HN-based PCM exhibit IR peaks comparable to those of the pure PCM, with no discernible additional peaks. This observation confirms the chemical stability between HN and the n-Octadecane PCM.

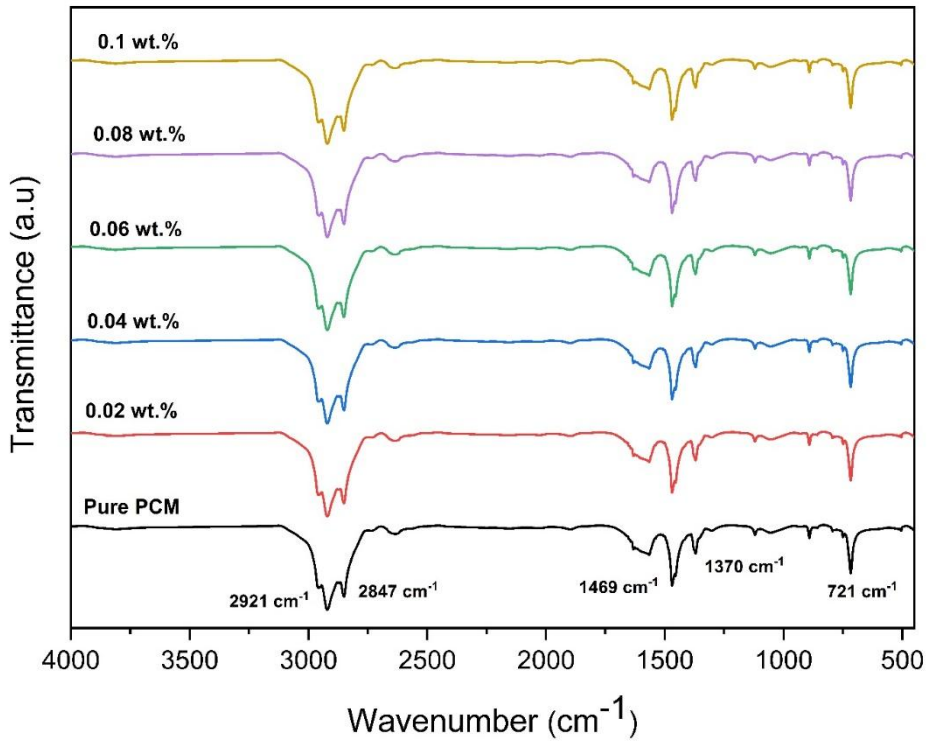

Fig. 50. FTIR spectra of the pure PCM and HOP

5.4.2. Phase change characteristics of pure PCM and HOP

The pure PCM and HN-based PCM samples were examined to explore their phase change characteristics. These findings significantly enrich our understanding of how the incorporation of HN impacts these characteristics. The test results suggest that the pure PCM commences its freezing and melting process in a single step at a temperature of 23.17 °C and 24.90 °C thereby absorbing and releasing the latent heat of 204.91 J/g and 203.18 J/g respectively as shown in the Fig. 51 **[158]**. The pure PCM both the base and HN enhanced PCMs exhibited a single peak, signifying a clear solid-liquid phase transition, devoid of any indications of secondary solid-solid peaks. These attributes confer significant advantages to PCMs, enhancing their ability to efficiently store and release heat throughout freezing and melting cycles. Besides, the HN dispersed in the n-Octadecane PCM varies in the proportion ranging from 0.02 to 0.1% by weight of PCM with the increment of 0.02%. The DSC results, as detailed in Table 27, suggest a significant phenomenon: the solid-liquid phase transition of

the base PCM occurred at a temperature below its designated melting point. Additionally, there was a minor reduction in the freezing temperature, resulting in the PCM exhibiting a relatively modest super cooling effect. A similar trend was observed for the HN-based PCMs, where the incorporation of HN in varying proportions, ranging from 0.02% to 0.1%, led to reductions in both freezing and melting points. From the results, it is evident that the degree of super cooling for HN based PCM decreased as the mass of HN increased, signifying that the introduction of HN into the n-Octadecane PCM induced heterogeneous nucleation, effectively promoting the phase-change process at the expense of depressing the freezing point. Conversely, the minor shifts in latent heat observed during the freezing (crystallization) of the base n-Octadecane PCM, in comparison to its melting (fusion), offer a comprehensive insight into its phase-change and heat storage capability. Interestingly, while the latent heat values for freezing and melting in HN based PCMs exhibited a marginal decrease, they remained nearly identical to those of the base PCM. This underscores the profound impact of the incorporated HN, specifically its surface adsorption and nucleation effects, on the latent heat capacities of the PCM.

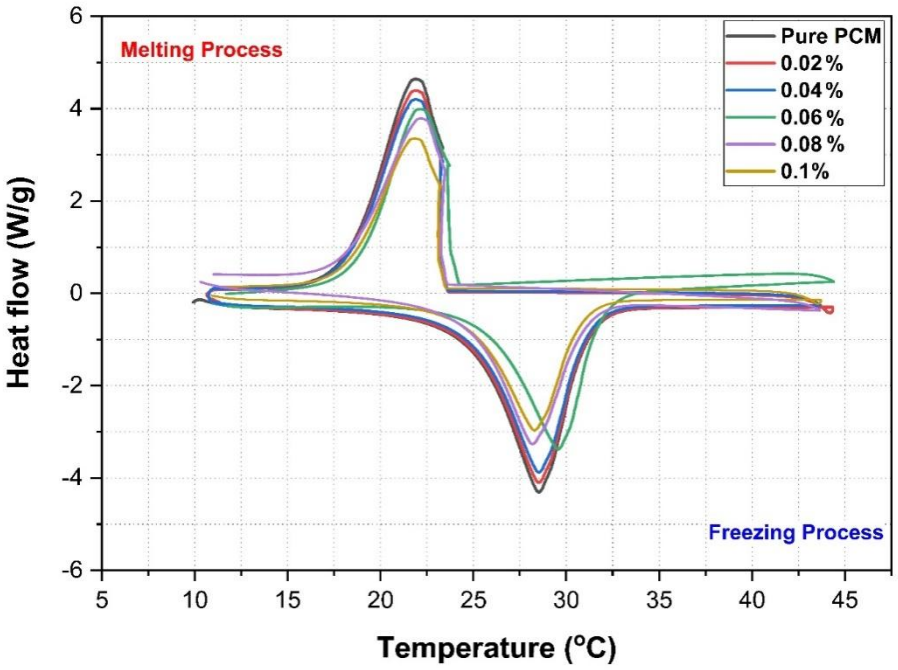

Fig. 51. Phase change characteristics of pure PCM and HOP

Table 18. Thermal properties of pure n-Octadecane PCM and HOP

Sample Type	Freezing Point (°C)	Melting Point (°C)	Latent heat of crystallization (kJ/kg)	Latent heat of fusion (kJ/kg)	Thermal conductivity (W/m K)
Pure PCM	23.17	24.90	204.91	203.18	0.195
0.02%	23.10	24.62	200.17	200.01	0.257
0.04%	23.01	24.40	196.76	195.41	0.291
0.06%	22.89	24.87	190.17	189.07	0.314
0.08%	22.70	23.81	183.36	182.22	0.396
0.1%	22.54	23.47	181.66	178.71	0.437

5.4.3. Heat storage and release characteristics of n-Octadecane pure PCM and HOP

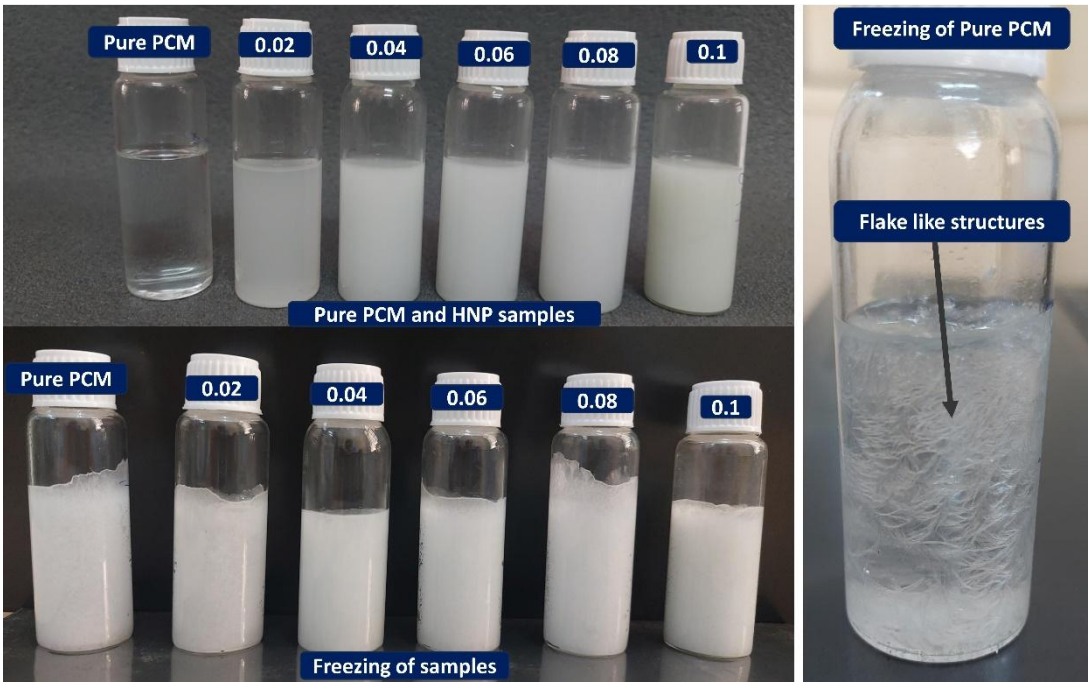

Fig. 52. Pure PCM and HOP samples

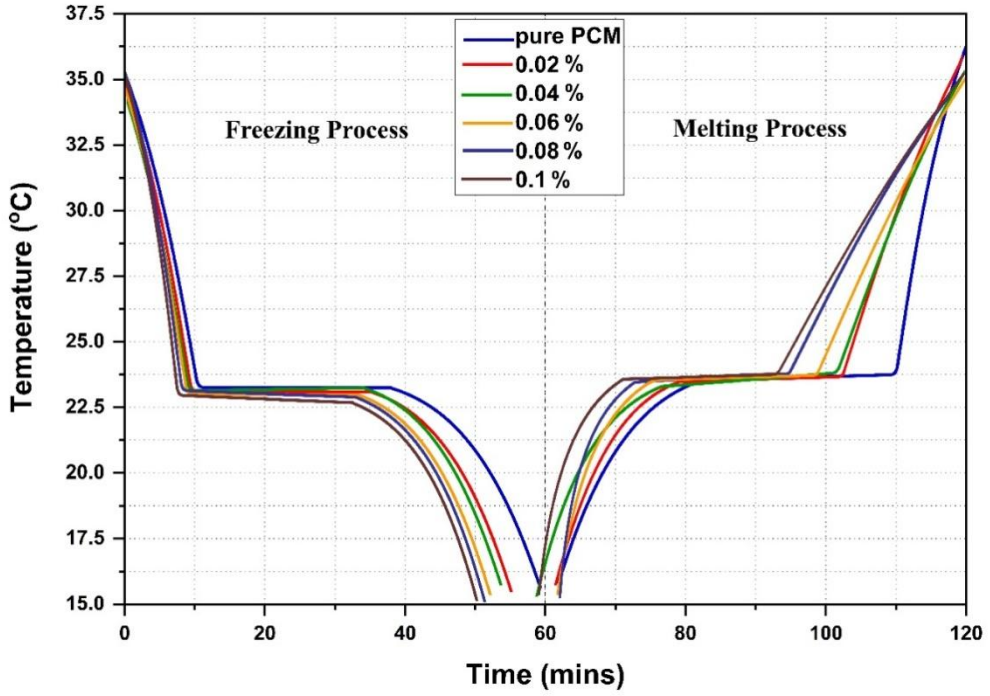

Fig. 53. Freezing and melting process of pure PCM and HOP samples

Table 19. Heat storage and release characteristics of pure n-Octadecane PCM and HOP

Process	Parameters	HN based n-Octadecane PCM					
		Pure	**0.02%**	**0.04%**	**0.06%**	**0.08%**	**0.1%**
Freezing	**Commencement (min)**	11.4	9.1	8.4	7.8	7.5	6.9
	Completion (min)	41.2	34.4	33.6	32.8	30.9	28.9
	Complete process duration (min)	29.8	25.3	25.2	24.4	23.1	22
	Enhancement %	----	20.1	26.3	31.5	34.2	39.4
Melting	**Commencement (min)**	83.4	79.2	77.4	73.5	71.0	65.3
	Completion (min)	111.6	103.2	100.7	96.1	91.3	84.7
	Complete process duration (min)	28.2	24	23.3	22.6	20.3	19.4
	Enhancement %	-	5.03	7.1	11.8	14.8	21.7

The cooling and heating curves of HOP samples as shown in Fig. 52 were tested depicting the heat storage and release capabilities of the HOPC are presented in Fig. 53. Detailed experimental observations were recorded at each time step throughout the test sequences, and the corresponding measurement results are comprehensively summarized in Table 28. Essentially, the thermal energy storage and release processes unfolded through a fundamental 3 stage progression during the freezing and melting of both pure and HOP samples. As depicted in Fig. 53, these three stages, delineating heat energy storage and release, are self-explanatory. According to the test results presented in Table 28, it can be depicted that, in comparison to the pure PCM, the time required for the complete phase transition of HOP was reduced. The experimental results infer that, the time taken for the pure PCM to commence the freezing process (that is to form the first ice crystal at onset temperature) and the time for complete solidification were recorded to be 11.4 min and 41.2 min, respectively. The pure PCM completed the freezing process in 29.8 mins. Due to HN inclusions in the n-Octadecane PCM with the proportions of 0.02%, 0.04%, 0.06%, 0.08% and 0.1%, the time taken for freezing process was enhanced by 20.1%, 26.3%, 31.5%, 34.2% and 39.4% respectively.

On the contrary, the pure PCM required approximately 28.2 minutes to complete the melting process, and these consistent findings were observed in the context of freezing process enhancement as well. The start time and duration of the melting process were significantly reduced. The addition of HN inclusions to the PCM in varying proportions, namely 0.02%, 0.04%, 0.06%, 0.08%, and 0.1%, led to substantial reductions in melting times by 5.03%, 7.1%, 11.8%, 14.8%, and 21.7%, respectively. This improvement can be attributed to enhanced thermal conductivity, effective promotion of heterogeneous nucleation, physical adsorption capabilities, surface modification, and the high surface-to-volume ratio of the HN, all of which have made significant contributions to the enhanced thermal storage capability and heat transfer characteristics of the HOP **[159-161]**.

5.4.4. Thermogravimetric analysis

The thermal stability of both the pure PCM and the HOP was assessed through TGA analysis, and the findings are presented in Fig. 54. The results indicate that both the pure PCM and the HOP exhibited a single-step mass loss, commencing at an onset decomposition temperature of 142 °C. The pure PCM demonstrated thermal stability up to 142 °C, after which decomposition commenced, ultimately completing at 242 °C. Remarkably, as the percentage of HN added to the PCM increased, the decomposition temperature also showed an upward trend. At the maximum dispersion of 0.1% HN in the PCM, the onset decomposition temperature increased by 55 °C compared to that of the pure PCM. In summary, the dispersion of HN in the PCM markedly enhanced its thermal stability. The Onset temperature and the mass (%) were presented in the Table 29.

Table 20. Thermal decomposition of pure n-Octadecane PCM and HOP

Sample Type	**Onset decomposition temperature (°C)**	**Mass (%)**
pure PCM	142	97
0.02%	179	95
0.04%	184	93
0.06%	189	92
0.08%	190	90
0.1%	197	92

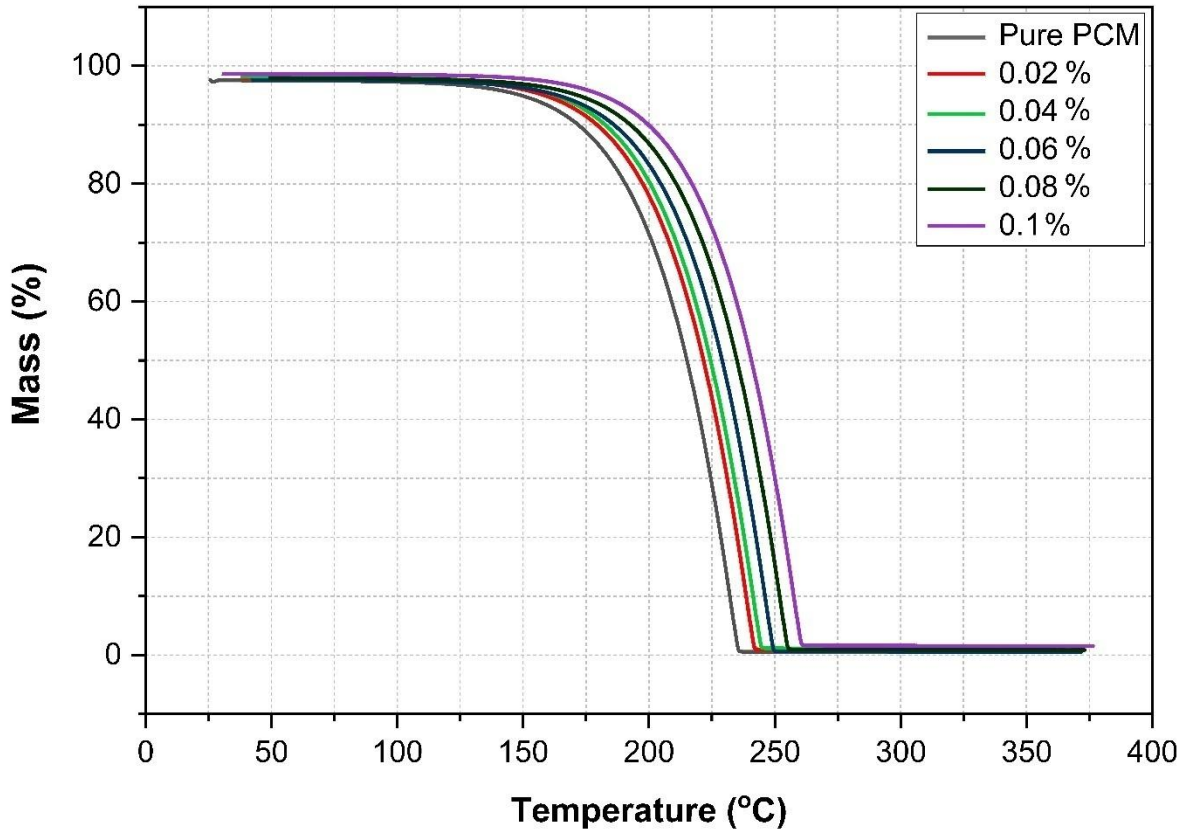

Fig. 54. TGA curves of pure PCM and HOP

5.4.5. Thermal conductivity of pure PCM and HOP samples

The effective thermal conductivity of both the pure PCM and the HOP was measured, and the outcomes are graphically represented in Fig. 55. From the Table 27 it is evident that with the increased proportion of HN in the pure PCM, the thermal conductivity of the HOP exhibited a consistent linear ascent, progressing from 0.195 W/m K to its peak value of 0.437 W/m K at a concentration of 0.1% within the PCM. This noteworthy increase, enhanced to 124.10% improvement, can be chiefly attributed to several factors: the surface morphology, phonon interaction, and the clustering of HN particles **[93, 161, 127]**. The enhancement in thermal conductivity primarily resulted from the formation of a densely interconnected thermal network by the HN within the pure PCM. Additionally, the presence of copper nanoparticles adsorbed onto the titania nanoparticles, resembling fin like structures, facilitated more efficient heat transfer through the layers of the pure PCM. This, in turn,

augmented the heterogeneous nucleation process and accelerated the heat storage and release characteristics of the HOP.

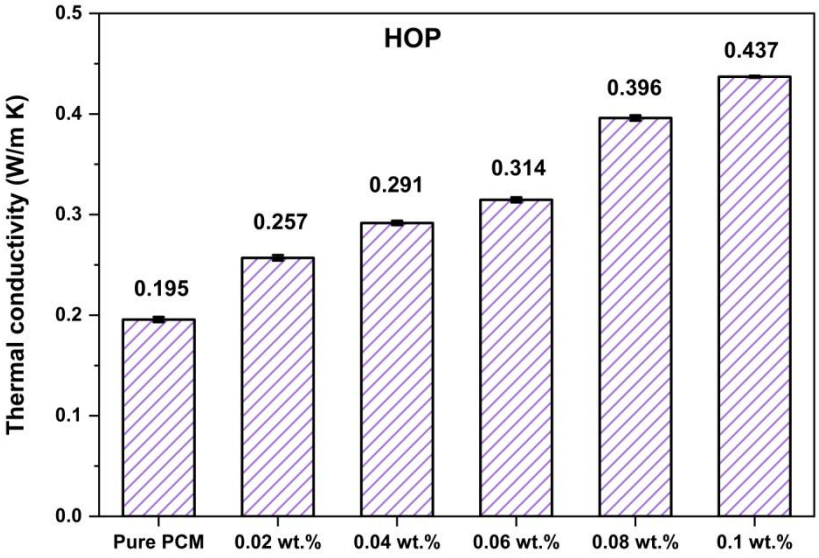

Fig. 55. Thermal conductivity of pure PCM and HOP samples

5.4.6. Thermal conductivity of HOPC cube specimens

The thermal conductivity analyzer was employed to investigate the thermal properties of the prepared cube specimens. As depicted in Fig. 56, the results indicate that the reference cement mortar exhibits excellent thermal conductivity. However, the introduction of an optimized 6% of n-Octadecane pure PCM into the cement mortar led to a significant 33.5% reduction in thermal conductivity. Moreover, a consistent 6% of PCM was maintained in the cement mortar, ranging from specimen 3 to specimen 7, while the HN inclusions increased from 0.02% to 0.1%. Notably, the decrease in thermal conductivity due to PCM inclusions in the cement mortar was likely enhanced by the incorporation of HN inclusions.

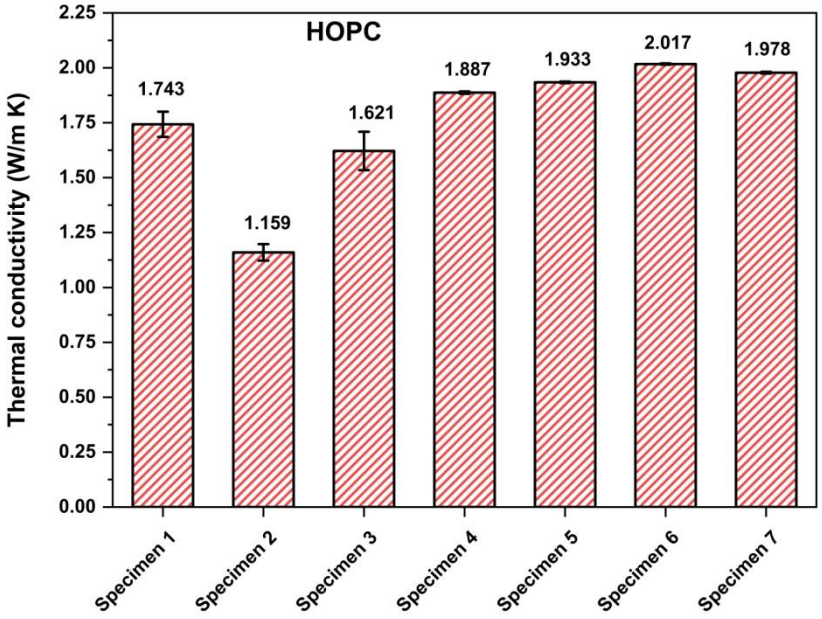

Fig. 56. Thermal conductivity of HOPC cube specimens

5.4.7. Compressive strength of HOPC cube specimens

Fig. 57 illustrates the compressive strength results for cube specimens. Specimen 1, representing the reference cement mortar, exhibited an appreciable compressive strength of 45.06 MPa. Nevertheless, in the case of specimen 2, where PCM (6% by weight of cement) was directly incorporated into the cement mortar, a substantial and sudden decline in compressive strength was observed. This decline can be attributed to the presence of PCM and the lubricating effect induced by water within the mortar, as elaborated in references **[29, 31, 128]**.

Specimens 3 to 7, in contrast, represent PCM-incorporated cement mortar with different levels of HN inclusion, spanning from 0.02% to 0.1% by weight of PCM. The test results indicate that the addition of HN had a minimal effect on the compressive strength of the cube specimens. Within this range, the compressive strength remained consistently stable, with only a slight decrease observed, transitioning from 21.14 MPa to 19.58 MPa as the HN content in the optimized PCM (6%) increased from 0.02% to 0.1%.

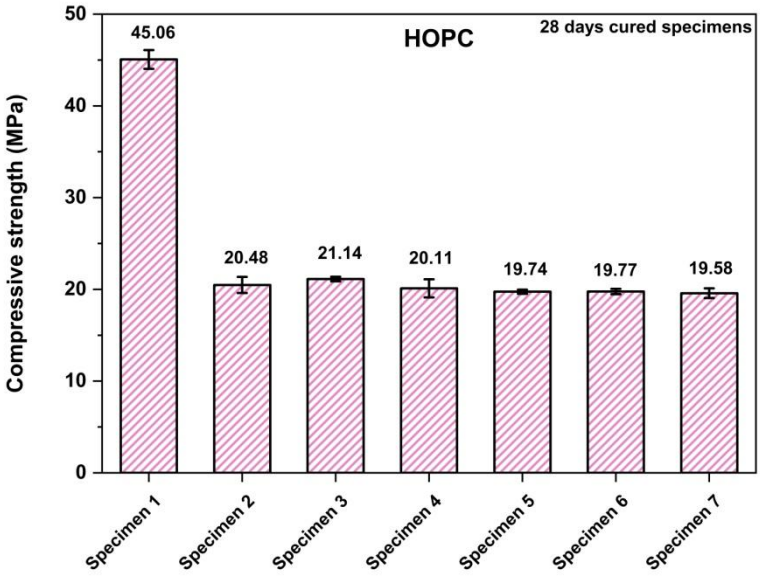

Fig. 57. 28-day compressive strength of HOPC specimens

5.4.8. Summary

In this current study, experimental investigations were carried out to examine the impact of dispersing HN particles within pure n-Octadecane PCM and subsequently incorporating HOP into cement mortar. The research unequivocally demonstrates an improvement in both thermal conductivity and thermal stability attributed to the inclusion of HN. This enhancement was directly proportional to the increased percentage of HN in the PCM. Furthermore, the presence of HN inclusions significantly accelerated both the onset and completion times of the freezing and melting processes in n-Octadecane PCM. However, the leakage issues were noticed due to direct impregnation of pure PCM and HOP in the cement mortar. As previously discussed, PCM encapsulation represents a superior method for mitigating leakage concerns in cement mortar. Among these approaches, nanoencapsulation stands out as a highly promising solution to enhance PCM efficiency, as it facilitates a significant increase in the specific surface area, thereby leading to improved thermal conductivity. In light of this, the subsequent section delves into the characterization of the n-Octadecane PCM encapsulated at nano size.

5.5. Nanoencapsulated n-Octadecane PCM (NP) and Cu-TiO_2 HN adsorbed nanoencapsulated PCM (HNNP)

5.5.1. Surface morphology of HN, NP and HNNP

FESEM was used to study the surface morphology and the elemental composition of HN, NP and HNNP. The FESEM images shown in Fig. 58 depict the formation of the hybrid nanocomposites. The HN particles were almost spherical in shape and the Fig. 58 (a) and (b) images depict the adsorption of the tiny copper nanoparticles onto the surface of the titania nanoparticles. The tiny copper nanoparticles on the surface of the titania nanoparticles resembled extended heat transfer surfaces, which are useful for attaining improved heat transfer during phase transition **[158]**. In addition, as shown in the Fig. 58 (d), EDAX analysis also confirms the presence of Titania, Oxide and Copper elements. The EDAX spectra significantly indicated the existence of highly crystalline copper and titania nanoparticles.

The encapsulated PCM was tested to study the surface morphology of nanoencapsulated PCM before HN adsorption. The FESEM results as shown in the Fig. 59 (a), (b) and (c) depicts that the capsules are spherical in nature and there was absence of the cracked capsules. The clear observation of capsules shows the rough surface morphology and besides, it is evident from the Fig. 59 (c) that the presence of spots which are in nano size all over the capsules. The size of the capsules are ranging from 50 nm to 450 nm as evident from particle size analysis, generally the reduced size of the capsules tends to agglomerate, nevertheless the FESEM images exhibited monodisperse NP capsules with an absence of agglomeration, this is due to the fact that the high temperature causes a quick reaction rate, which produces resins with a high degree of polymerization in a short time, which leads to reduce the tendency of agglomeration of smaller size capsules due to rapid formation of resin. EDAX analysis was performed to study the elemental composition of the capsules. The result shown

in the Fig. 59 (d), exhibits the presence of Carbon, Oxygen and Nitrogen with the weight proportion of 36.38%, 45.68% and 17.94% respectively. Fig. 60 (a) to (d) corresponds to the FESEM images of HNNP; and it is evident from the FESEM images that the HN was adsorbed on the nanoencapsulated PCM. The HNNP capsules are monodisperse with no agglomerations, and the settlement of Cu-TiO_2 hybrid nanocomposites were not coated randomly nor settled throughout the capsule, rather they coated with a perfect network like a structure. The amino groups in the MF resin based nano capsules played a vital role in the adsorption of HN on the nanoencapsulated PCM. The development of higher active sites during the adsorption process might have been significantly influenced by the protonation of the amine group. As a result, more Cu-TiO_2 hybrid nanocomposites (HN) are bound to functionally active surfaces on the nanoencapsulated MF resin shell. Considering the above, the core PCM was encapsulated with melamine shell material over which Cu-TiO_2 hybrid nanocomposites were adsorbed with perfect network like structure. EDAX results shown in

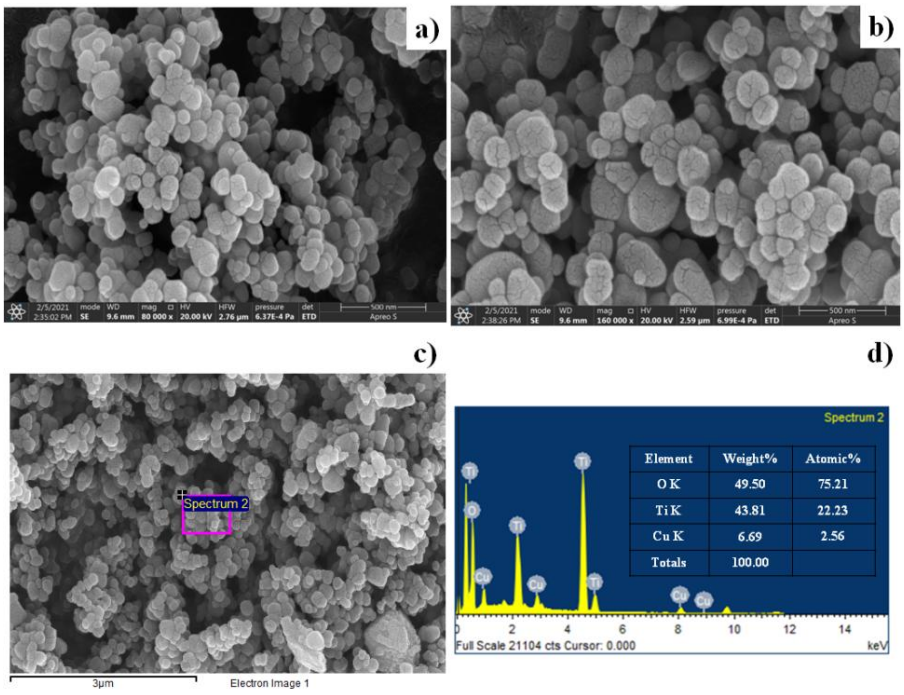

Fig. 58. (a) - (c) FESEM of HN and (d) EDAX results of HN

Fig. 61 also confirms the presence of Copper, Titania and Oxygen with weight percentage of 0.84, 26.79 and 11.73 respectively, which attributes to Cu-TiO_2 hybrid nanocomposites. Besides, the elemental composition of Carbon, Nitrogen and Oxygen in the EDAX report with the weight percentage of 35.92, 24.72 and 11.73 ensures the presence of n-Octadecane PCM and Melamine shell material.

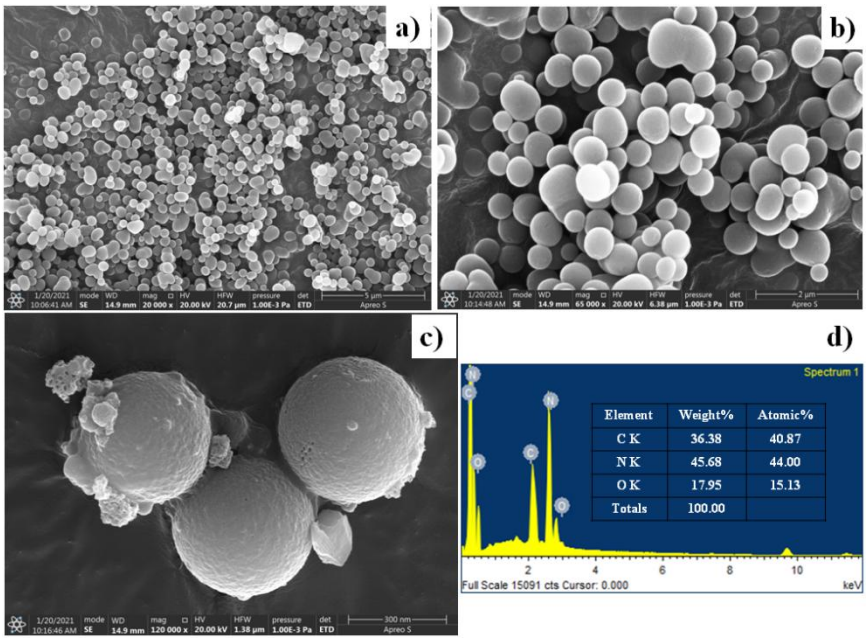

Fig. 59. (a) - (c) FESEM results of NP and (d) EDAX Results of NP

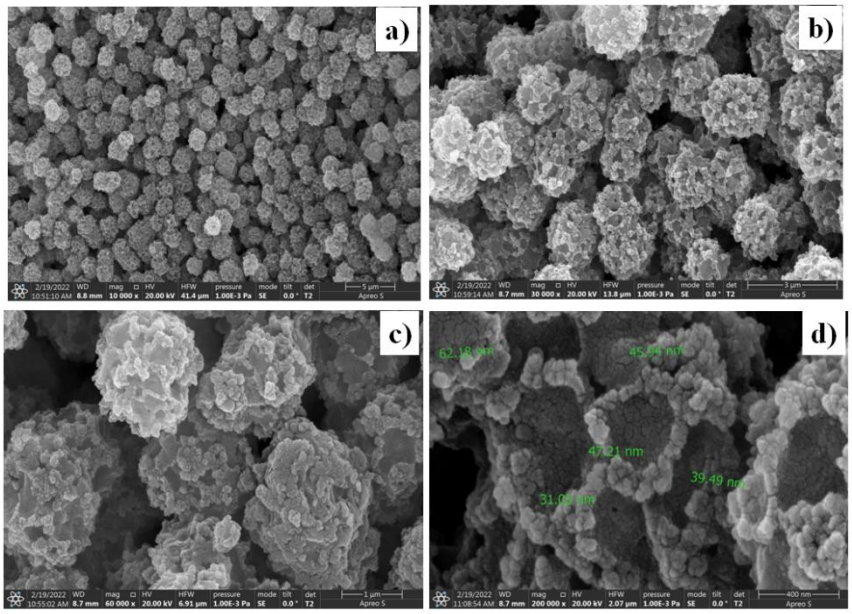

Fig. 60. (a) - (d) FESEM results of HNNP

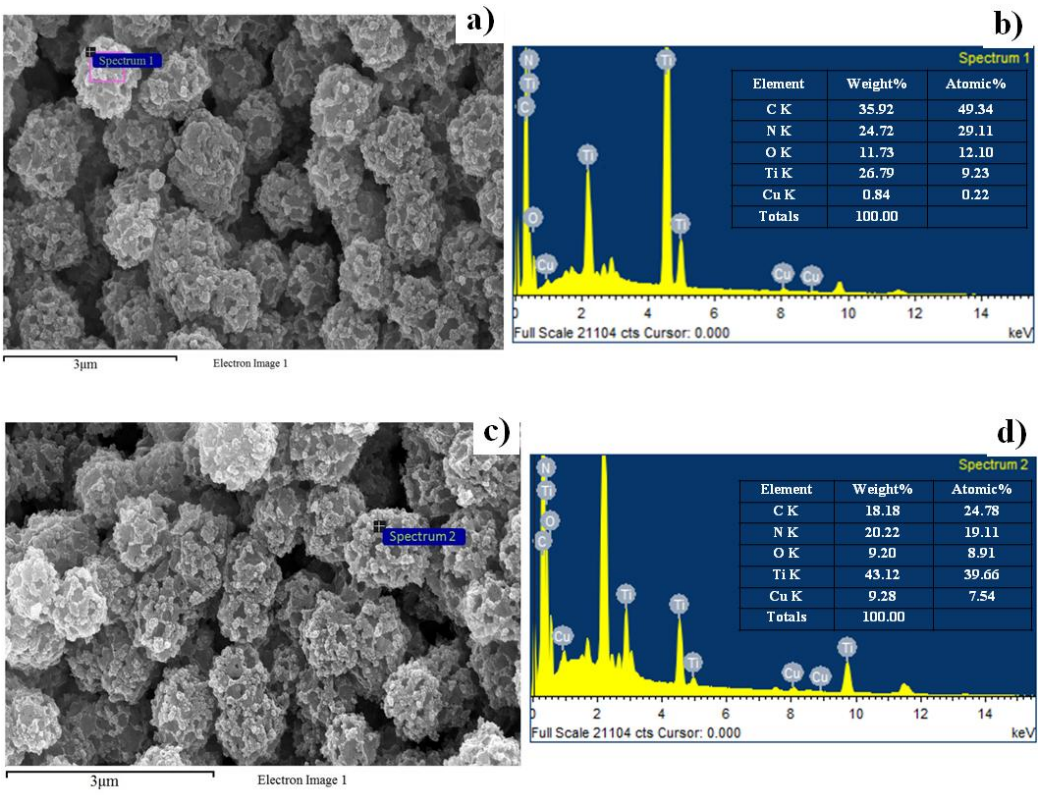

Fig. 61. (a) - (d) EDAX results of HNNP

5.5.2. Crystallinity of the HNNP

Cu-TiO_2 hybrid nanocomposites (HN) displayed an intense and sharp bragg reflection at 2Θ angle, as measured by XRD. The scattering at interplanar spacing clearly correlates to Titania nanoparticles, as seen in the Fig. 62. In addition, the highly crystalline copper nanoparticles adsorbing on Titania's surface exhibit a face-centered cubic shape (111). The XRD results of copper nano which were adsorbed over Titania nanoparticles are consistent with JCPDS (Joint Committee on Powder Diffraction Standards) file no. 04-0836 and 21-1272 respectively. XRD analysis was carried out to study the crystallinity of HNNP; the peaks induced at 2Θ angle exactly matches with the XRD results of Cu-TiO_2 hybrid nanocomposites. This confirms the adsorption of HN on the capsules **[38, 41]**.

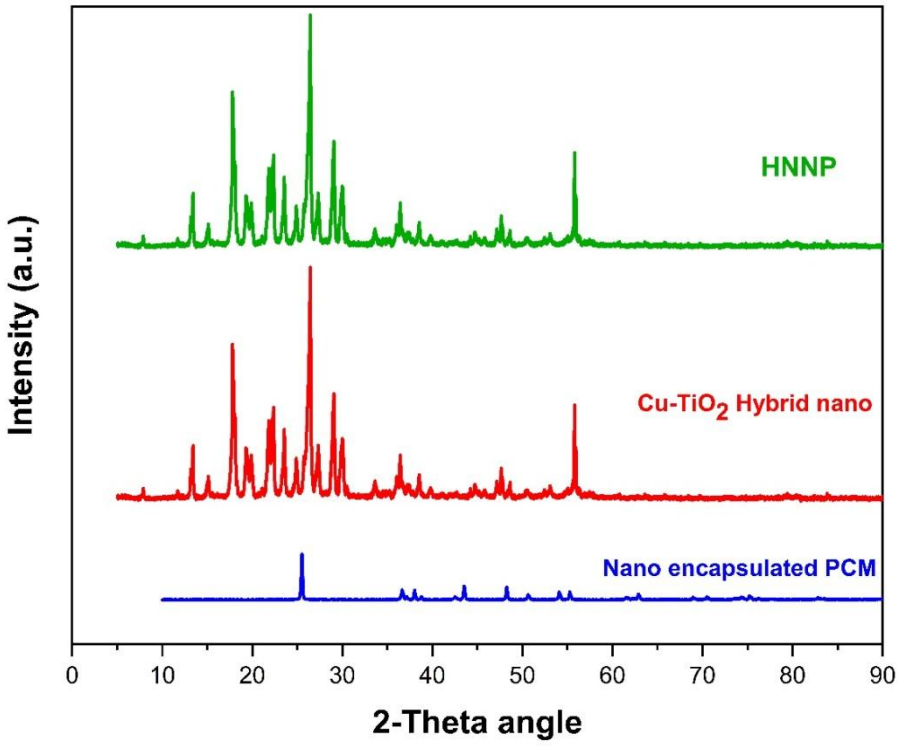

Fig. 62. XRD pattern of HN, NP and HNNP

5.5.3. Particle size analysis

Dynamic Light Scattering (DLS) was used to study the particle size distribution of HN, NP, and HNNP. The particle size influences the thermo-physical properties. Table 30 presents a brief literature survey on capsule size and their encapsulation efficiency of various nanoencapsulated PCM. Fig. 63 (a) shows the results pertaining to Cu-TiO_2 hybrid nanocomposites; it is evident from the results that the particles were in the range from approximately 30 nm to 200 nm with an average diameter of particle size of 68.14 nm. From the results it is clear that a single peak was evolved which suggests that the particles are monodisperse with the absence of multiple size particles. Besides, the size distribution of NP was ranging from approximately 50 nm to 450 nm with an average diameter of the capsule as 120.5 nm, the capsules are monodisperse as shown in the Fig. 63 (b).

Table 21. Literature on particle size of nanoencapsulated PCM

PCM	Shell Material	Particle Size (nm)	Encapsulation Efficiency (%)	References
n-Octadecane	Methyl methacrylate	300-500	52.9	**37**
n-tetradecane	Polystyrene	60-486	89	**57**
Paraffin	Methyl methacrylate	200-400	52.95	**41**
n-Octadecane	Polystyrene	50-200	53.5	**52**
n-Octadecane	Polymethyl methacrylate	60-360	89.5	**58**
n-Dotriacontane	Polystyrene	80-400	61.2	**57**
n-Octadecane	Styrene methyl methacrylate	63-129	45	**52**
n-Nonadecane	Polystyrene	200-300	55.9	**162**
n-Nonadecane	Poly (styrene-co-methacrylic acid)	180-280	54	**36**
Paraffin Wax	Melamine-Formaldehyde	260-450	75.58	**163**
n-Octadecane	Styrene methyl methacrylate	50-200	40	**164**
n-Octadecane	Melamine Formaldehyde	50-450	71.9	**Present study**

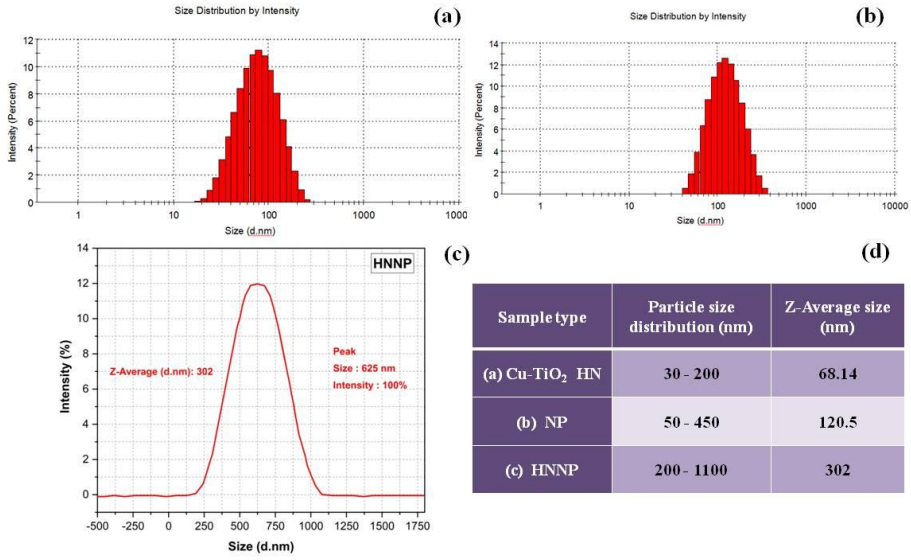

Fig. 63. Particle size distribution of a) HN b) NP c) HNNP and d) Average particle size

The HNNP capsules were tested to study the particle size distribution. Fig. 63 (c) suggests that there was a single peak evolved and the particle size was distributed over a wide range from approximately 200 nm to 1100 nm with an average diameter of 302 nm. Considering the maximum size of HNNP, there would have a two-step adsorption of HN for a few capsules. This is also in line with FESEM results. Table 30 presents the capsule size of nanoencapsulated PCM.

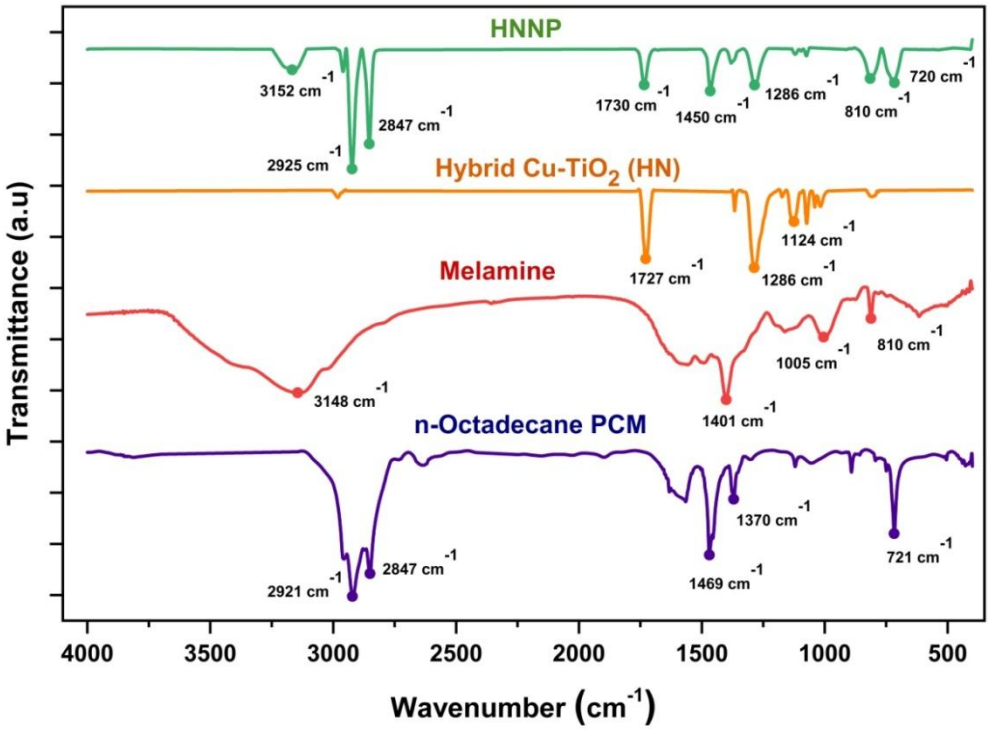

Fig. 64. FTIR spectra of pure PCM, Melamine, HN and HNNP

5.5.4. Chemical structure and chemical stability

The FTIR records the changes in the spectral bands between transmittance (%) and wavenumber (cm^{-1}) **[165]**. The FTIR analysis was carried out for the pure PCM, melamine, HN, and the HNNP to study the chemical compatibility between them, the results are presented in the Table 31. From the test results of n-Octadecane PCM as shown in the Fig. 64, the IR peaks evolved at 2921 cm^{-1} and 2847 cm^{-1} belongs to the C-H stretching vibration of the aliphatic chain. The peak at 1469 cm^{-1} corresponds to the bending vibration of

methylene/methyl group. The peak at 727 cm^{-1} corresponds to in-plane rocking vibration of CH_2 group **[37, 156, 157]**.

The FTIR spectrum of melamine from Fig. 64 shows a peak at 3140 cm^{-1} belongs to N-H bending vibration of the amide group. The strong peak at 1558 cm^{-1} associated to the in-plane bending vibration of N-H bonds. The peak at 810 cm^{-1} belongs to the stretching vibration of the triazine rings **[166, 167, 168]**.

Table 22. Summary of FTIR results of pure PCM, melamine, NP and HNNP

Wavenumbers (cm^{-1})					**Assignment**	
n-Octadecane PCM	Melamine	HN nanocomposites	HNNP	HNNP after thermal cycling	Vibration	Functional group
-----	3148	-----	3152	3141	Stretching	N-H
2921	----	-----	2925	2924	Stretching	C-H
2851	----	-----	2847	2849	Stretching	C-H
-----	----	1727	1730	-----	------	-----
1469	---	-----	1450	----	Bending	C-H
-----	1401	-----	------	1410	Bending	N-O
1370	-----	-----	------	-----	-----	-----
-----	-----	1286	1286	-----	-----	-----
-----	-----	1124	-----	-----	-----	-----
-----	1005	-----	-----	1002	Stretching	C-O
-----	810	-----	810	810	Out of plane deformation	Triazine
727	-----	-----	720	-----	Rocking vibration	$-CH_2-$

The FTIR results of HNNP shows the IR peaks of Pure PCM, melamine, and HN. There was no much deviation was observed in the IR peaks induced at particular wave number which suggest that there was no chemical reaction between n-Octadecane PCM, shell materials and hybrid nanocomposites and also probably the PCM encapsulated in melamine formaldehyde shell material with HN adsorption on the capsule, However, DSC and TGA results are also equally important for further justification.

5.5.5. Phase change characteristics of pure PCM, NP and HNNP

To study the phase change characteristics of pure PCM, NP and HNNP, a DSC instrument was used. The phase change characteristics results summary was presented in Table 32. The pure PCM commences its freezing and melting process in a single step at a temperature of 23.17 °C and 24.90 °C thereby absorbing and releasing the latent heat of 204.91 J/g and 203.18 J/g respectively as shown in the Fig. 65 **[114]**. Besides, the PCM encapsulated using melamine shell material at the nano level doesn't alter much in terms of freezing and melting temperatures. The nanoencapsulated PCM (NP) exhibited good phase change characteristics as shown in the Fig. 65. The core PCM inside the nanocapsules freezes and melts at 25.06 °C and 26.12 °C, their latent heats are 159.73 J/g and 156.89 J/g respectively. Furthermore, due to the adsorption of hybrid nanocomposites on the NP, the HNNP exhibited very good phase change characteristics in terms of freezing and melting process in a single stage with good encapsulation ratio and encapsulation efficiency. The HNNP behaved similarly to that of pure PCM with no major changes in their phase change temperature. As shown in the Fig. 66, the HNNP freezes and melts at temperature of 23.78 °C and 25.77 °C with the latent heat of 146.71 J/g and 144.46 J/g respectively**.** The freezing and melting of HNNP took place over a narrow range of temperatures when compared with pure PCM and NP; this is due to the fact that the hybrid Cu-TiO_2 nanocomposites (HN) on the capsule would have enhanced the thermal conductivity which in turn accelerated the heat

transfer characteristics. The latent heat of HNNP is less in comparison with NP; this is due to the presence of additional hybrid nanocomposites adsorbed on the capsule. Inspite of encapsulation, the phase change process of NP and HNNP took place in a single step with no major changes in freezing and melting temperatures. The NP and HNNP behaved similar to that of pure PCM, this clearly suggests the absence of chemical reaction between PCM, Cu-TiO_2 and Melamine shell material.

Encapsulation Ratio (R), Encapsulation Efficiency (EE), and Thermal Energy Storage capacity (ε) are the important factors for evaluating the thermal energy storage capability of NP and HNNP **[144, 169, 170]**.

The encapsulation ratio illustrates the degree to which n-octadecane PCM is effectively encapsulated within the Melamine Formaldehyde shell material, whereas the loading content is considered as the overall weight percentage of the PCM contained within the shell. Eq. (8) was used to calculate the encapsulation ratio for the NP and HNNP capsules, the results are presented in the Table 33. The encapsulation ratio calculated for the NP and HNNP were 77.2% and 71% respectively, nevertheless, only with the encapsulation ratio, the thermal storage capability of the PCM contained in the shell cannot be decided.

Hence, the encapsulation efficiency (EE) of the NP and HNNP were calculated using the enthalpies involved in both the freezing and melting process. Considering Eq. (9) the encapsulation efficiency calculated for NP and HNNP are 77.5% and 71.3% respectively. Encapsulation efficiency is a more appropriate parameter than the encapsulation ratio for evaluating the PCM energy storage and release capability in a Melamine Formaldehyde shell. The latent heat of encapsulated PCM latent, however, may be affected by alteration of core-to-shell ratio, which in turn depends on the application.

Using the Eq. (10), the thermal energy storage capacity (ε) of the n-Octadecane PCM enclosed within the shell material was determined, and the NP and HNNP demonstrated a 100% thermal energy storage capacity (ε). This indicated that all of the encapsulated n-Octadecane PCM could store and release energy efficiently during phase transformation **[108]**.

$$R = \frac{\Delta H_{m,\ NP}}{\Delta H_{m,\ PCM}} \times 100 \quad \text{----- (8)}$$

$$EE = \frac{\Delta H_{m,NP} + \Delta H_{c,NP}}{\Delta H_{m,PCM} + \Delta H_{c,PCM}} \times 100\% \quad \text{----- (9)}$$

$$\varepsilon = \frac{\frac{\Delta Hm,NP + \Delta Hc,NP}{R}}{\Delta Hm,PCM + \Delta Hc,PCM} \times 100\% \quad \text{----- (10)}$$

where, $\Delta H_{m\ PCM}$, $\Delta H_{c\ PCM}$, $\Delta H_{m,\ NP}$ and $\Delta H_{c,\ NP}$, and $\Delta H_{m,\ HNNP}$, $\Delta H_{c,\ HNNP}$ are the latent heat of melting and freezing of pure PCM, nanoencapsulated PCM and hybrid nanocomposites adsorbed nanoencapsulated PCM respectively. The same above eq. (8), (9) and (10) were used to calculate encapsulation ratio, encapsulation efficiency and thermal energy storage capability of HNNP.

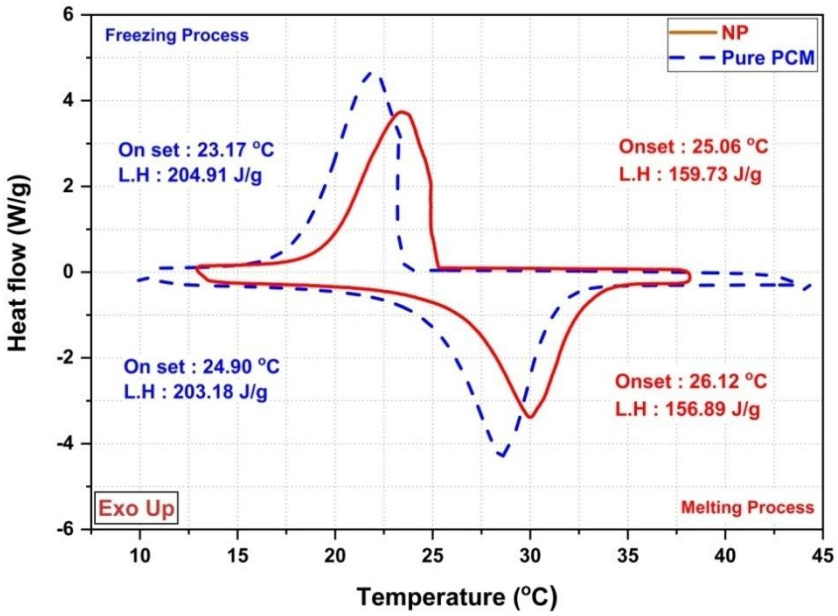

Fig. 65. Phase change characteristics of pure PCM, and NP

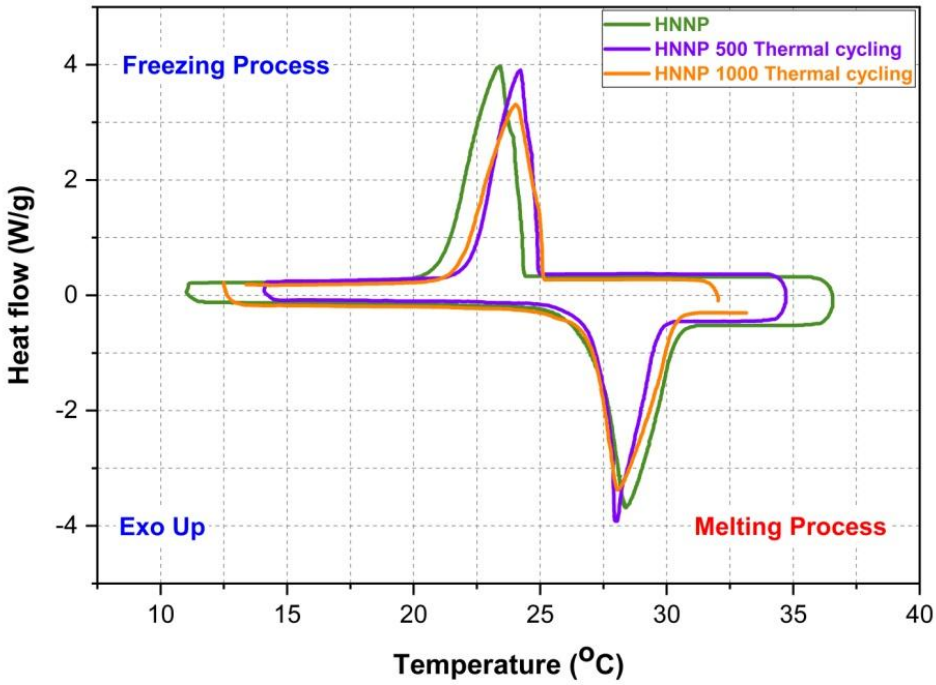

Fig. 66. Phase change characteristics of HNNP and thermal cycling of HNNP

Table 23. Thermal properties of pure PCM, NP and HNNP

Sample Type	Freezing temperature T_f (°C)	Melting temperature T_m (°C)	Latent heat of freezing ΔH_f (kJ/kg)	Latent heat of melting ΔH_m (kJ/kg)	k (W/m K)
n-Octadecane PCM	23.17	24.90	204.91	203.18	0.195
NP	25.06	26.12	159.73	156.89	0.121
HNNP	24.02	25.77	146.71	144.46	0.287
HNNP after 500 thermal cycles	24.42	26.01	133.11	136.21	0.285
HNNP after 1000 thermal cycles	24.77	25.62	121.92	127.84	0.262

Table 24. Thermal energy storage capability of pure PCM, NP, and HNNP.

Sample Type	Latent heat of freezing ΔH_f (kJ/kg)	Latent heat of melting ΔH_m (kJ/kg)	Encapsulation ratio (R) (%)	Encapsulation efficiency (EE) (%)	Thermal storage capacity (ε) (%)
Pure PCM	204.91	203.18	---	---	---
NP	159.73	156.89	77.2	77.5	100
HNNP	146.71	144.46	71	71.3	100
HNNP 500 cycles	133.11	136.21	67	65.9	98.5
HNNP 1000 cycles	121.92	127.84	62.9	61.2	97.3

5.5.6. Thermal stability of pure PCM, NP and HNNP

Examining thermal stability is essential for determining the maximum temperature in its application to prevent PCM decomposition. The details of onset and end set decomposition temperatures of pure PCM, NP, and HNNP are presented in the Table 34. The TGA curve of pure PCM as shown in the Fig. 67 depicts that the decomposition of pure PCM took place in a single step commences around 142 °C and the PCM completely decompose at 242 °C. In contrast, NP and HNNP behaved differently, and their degradation occurred in two stages. With the increased temperature of NP and HNNP capsules, there was a mass loss at a temperature of approximately 50 °C. The mass loss at 50 °C is due to water vapour and other molecular ingredients on the capsule's surface, and not the PCM. This is fact, as the PCM decomposition temperature took place at 142 °C; hence there is no possibility of PCM decomposition below 142 °C. As the temperature continues to increase, the core PCM in the capsule experiences a rise in pressure this tend to crack the shell of the capsule. This tendency causes the core PCM to degrade through the cracked shell at around 161 °C as shown in the Fig. 67. The first stage of decomposition completes around 210 °C, and 75.64%

of the core PCM from the shell material has decomposed in stage 1. Whereas on the other hand, the core PCM of HNNP capsules have commenced degradation at 184 °C, and around 259 °C, and the core PCM inside the HNNP capsules completely decomposes, resulting in a mass loss of 72.18%. The mass loss of the core PCM from NP capsules and HNNP capsules are in-line with the encapsulation ratio. With further increase in temperature, the second step of degradation begins which corresponds to the loss of copolymer shell material. Based on the above data, encapsulating the PCM using melamine formaldehyde shell material has enhanced the thermal stability by 19 °C than the pure PCM. Besides, the HNNP exhibited excellent thermal stability, delaying the commencement of decomposition by 23 °C and 42 °C than nanoencapsulated PCM and the pure PCM respectively. The Cu-TiO_2 hybrid nanocomposites adsorbed on the capsule performed a crucial impact in enhancing the thermal stability of the novel HNNP capsules. The HNNP and NP are proposed for use in cooling applications in buildings with operating temperatures between 21 °C and 26 °C. However, the onset decomposition temperatures of both NP and HNNP are higher than the operating temperatures.

Table 25. Thermal stability of pure PCM, NP and HNNP

Sample type	First step			Second step		
	Onset Temp. (°C)	End set Temp. (°C)	Mass Loss (%)	Onset Temp. (°C)	End set Temp. (°C)	Mass Loss (%)
Pure PCM	142	242	97	142	----	---
NP	161	210	75.64	234	284	12.47
HNNP	184	259	72.18	310	490	20.17
HNNP (500 Thermal cycling)	182	253	70.11	288	470	24.41
HNNP (1000 Thermal cycling)	177	240	66.79	271	450	21.58

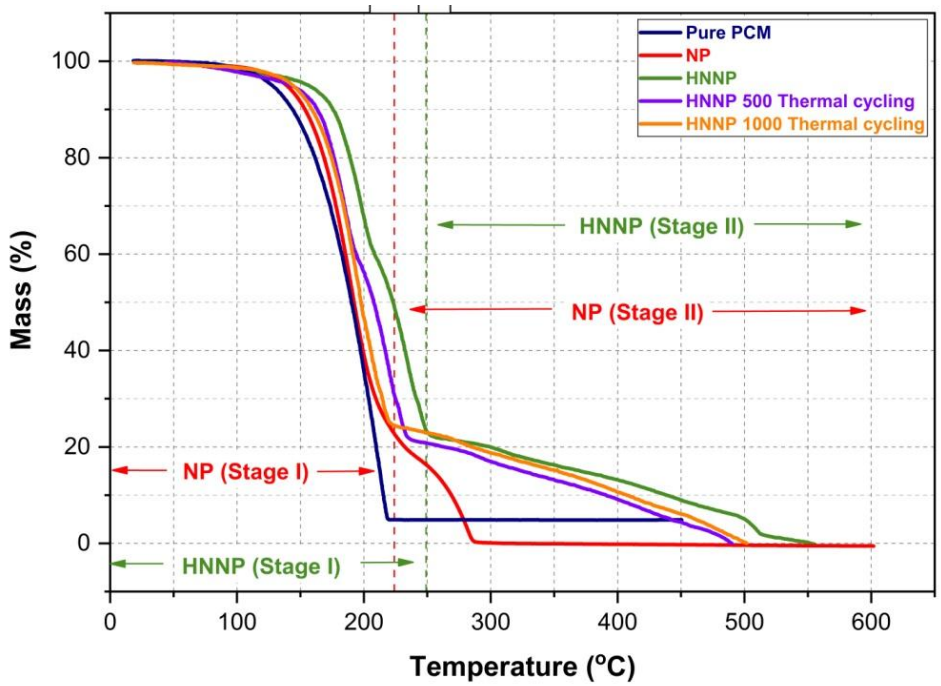

Fig. 67. Thermal decomposition of pure PCM, NP, HNNP before and after thermal cycling

5.5.7. Thermal conductivity of pure PCM, NP and HNNP

The thermal conductivity of pure PCM, NP, and the novel HNNP capsules was measured using a thermal conductivity analyzer. As shown in Fig. 68, the thermal conductivity of pure n-Octadecane PCM is 0.195 W/m K **[18, 171].** The thermal conductivity of NP and HNNP is 0.121 W/m K and 0.287 W/m K respectively. The thermal conductivity of nanoencapsulated PCM is in line with the literature presented in Table 35. The n-octadecane PCM when encapsulated using polymer-based melamine shell material, tends to reduce thermal conductivity**.** The percentage drop in thermal conductivity of NP was 37.94% compared with pure PCM.

The thermal conductivity of nanoencapsulated n-octadecane PCM using melamine as a shell material was very poor, due to this, the applications of melamine as a shell material was limited.

The adsorption of Cu-TiO_2 hybrid nanocomposites has greatly enhanced thermal conductivity of 47.17% and 137.19% over pure PCM and nanoencapsulated PCM respectively. The hybrid

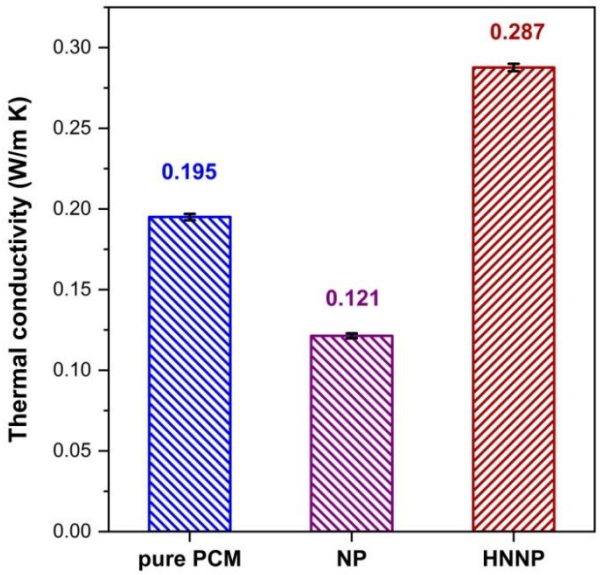

Fig. 68. Thermal conductivity of pure PCM, NP and HNNP

Table 26. Comparison of thermal conductivity of encapsulated PCM using melamine/urea formaldehyde shell material with literature.

PCM	Shell Material	Thermal conductivity (W/m K)	References
Paraffin	Melamine formaldehyde	0.12	**171**
n-hexadecane	Silver/Urea formaldehyde	0.0663	**172**
n-Octadecane	Silver/Urea formaldehyde	0.0695	
Dodecanoic acid	Melamine formaldehyde	0.134	**173**
n-Octadecane	poly(melamine-formaldehyde)/silicon carbide	0.20	**174**
Paraffin	Modified H-SiC Melamine formaldehyde	0.1739	**77**
n-Octadecane	Melamine formaldehyde (HNNP)	0.287	**Present study**

nanocomposites possess metallic (Cu) nanoparticles resembles fin like extended surface settled on slightly larger metal oxide (TiO_2) nanoparticles, is the reason behind enhancement of thermal conductivity of HNNP. The enhanced thermal conductivity of HNNP capsule surely enhances increased heat transfer capability from the cementitious material when used in buildings thereby increasing more number of phase change cycles per day.

5.5.8. Thermal Reliability of HNNP

The main intention of a performing thermal cycling test is to study the reliability of the material. Besides, PCMs would degrade over time if exposed to external environments without sufficient shielding. Similarly, when PCM is subjected to higher thermal cycles, its thermo-physical characteristics may change. Thermal cycling test is essential for ensuring the long-term behaviour of a thermal energy storage unit.

HNNP exhibited good thermal behaviour in terms of phase change characteristics, thermal stability, and thermal conductivity, keeping in view; thermal cycling test of HNNP was carried out. The HNNP was subjected to 500 and 1000 thermal cycles, and the capsules were examined to study their phase change characteristics, thermal conductivity, and thermal stability. The sample was heated and cooled over a temperature range of 10 °C to 50 °C. The phase change temperature and latent heat of HNNP subjected to thermal cycling are shown in the Table 32. As shown in Fig. 66**,** there was not much deviation in the phase change temperature of HNNP subjected to 500 and 1000 thermal cycling. The encapsulation ratio of HNNP subjected to 500 and 1000 accelerated thermal cycling's resulted in 67% and 61.9%, respectively as shown in Table 33. The thermal conductivity of HNNP capsules was slightly reduced when exposed to thermal cycles of 500 and 1000. The results presented in Table 33, suggest that there was negligible variation in thermal conductivity of HNNP before and after thermal cycling. Besides, The HNNP exhibited very thermal stability when subjected to 500 and 1000 thermal cycles. Fig. 67 depicts that there was a slight drop in the on-set

decomposition temperature of HNNP subjected to thermal cycling. The result depicts that mass loss of PCM from the HNNP capsules after subjected to 500 and 1000 thermal cycles was 70.11% and 66.79%, respectively. Considering the above test results, The HNNP subjected to thermal cycling exhibited very good reliability.

5.5.9. Distribution of capsules in the cement mortar

To study the distribution and the condition of capsules (NP and HNNP) in the cement mortar, FESEM instrument was used. Sample in the form of slices were extracted from the NPeCM-10 and HNNPeCM-10 28 days cured cube specimens, respectively. Fig. 69 and 70 clearly shows the NP and HNNP capsules distributed in the cement mortar respectively, the capsules are in good condition without any damage or crack formation. However, there is porous structure formed due to dispersion of capsules in the cement mortar evident from Fig. 69 and 70.

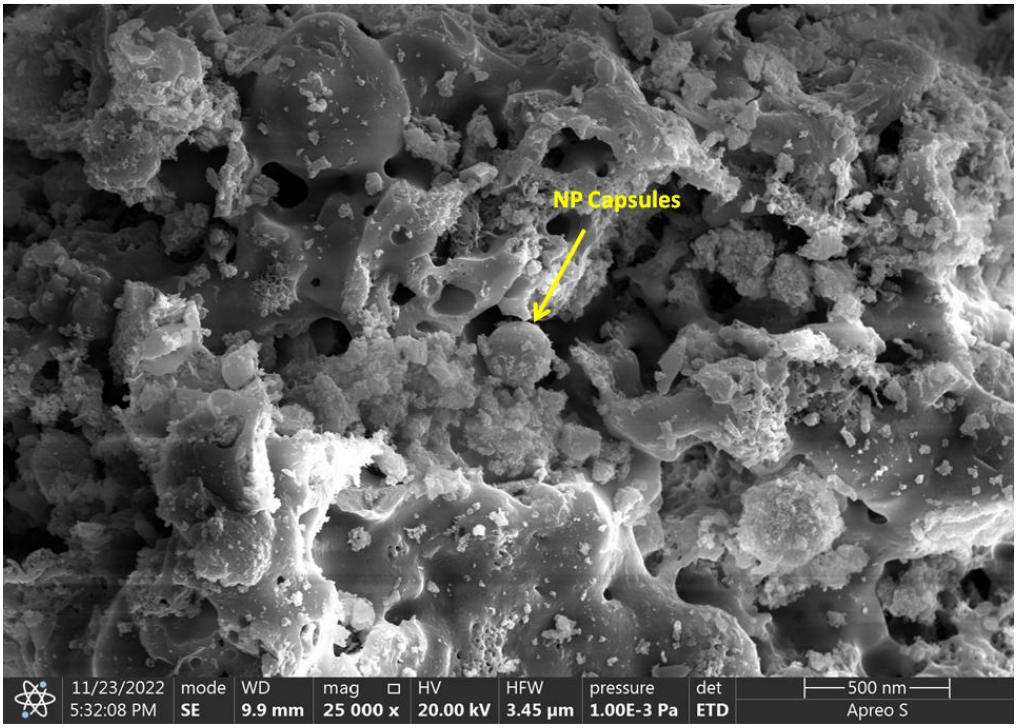

Fig. 69. FESEM results of NPeCM-10 sample (28 days curing period)

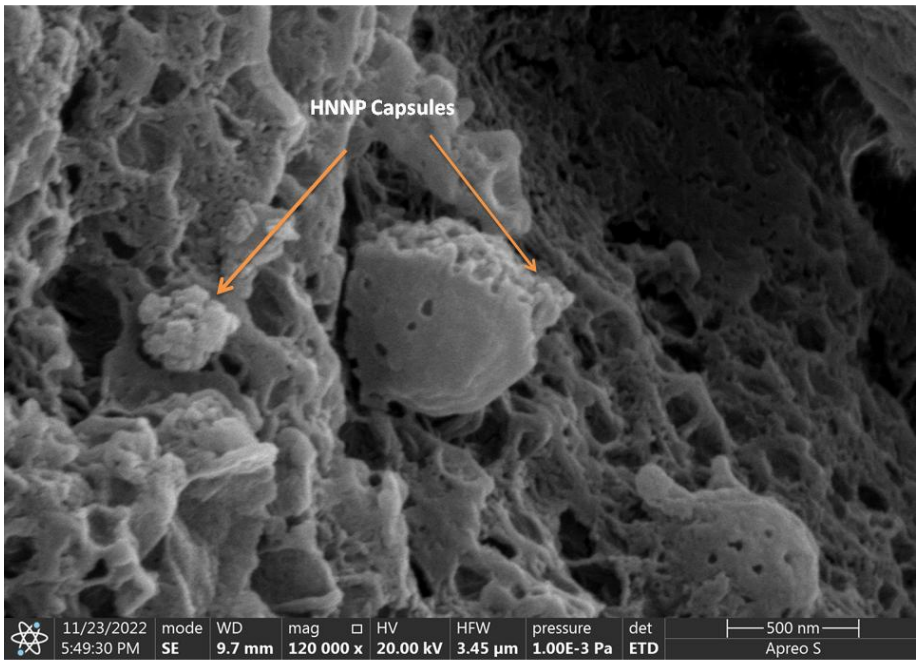

Fig. 70. FESEM results of HNNPeCM-10 sample (28 days curing period)

5.5.10. Density of the cube specimen

The cube specimens with dimension of 70.6 mm were prepared by dispersing the capsules (NP and HNNP) in the cement mortar as shown in the Fig. 22. It is crucial to study the density of cube specimens to get clarity on the compressive strength and thermal conductivity. The results shown in the Fig. 71 reveals that the density of the cube specimen decreases with increased percentage of capsules (NP and HNNP) embedded in the cement mortar.

This is due to fact that, with the increased percentage of low-density NP and HNNP capsules in the cement mortar, there is a possibility of fine aggregate replaced with PCM capsules which results in the reduced density compared with plain cement mortar. Moreover, NP and HNNP capsule dispersion in the cement mortar have led to the formation of porosity as evident from the Fig. 69 and 70. Generally, air void formation leads to the porosity in the cement mortar, may also be the reason for less dense microstructure of NPeCM and HNNPeCM cube samples **[64]**.

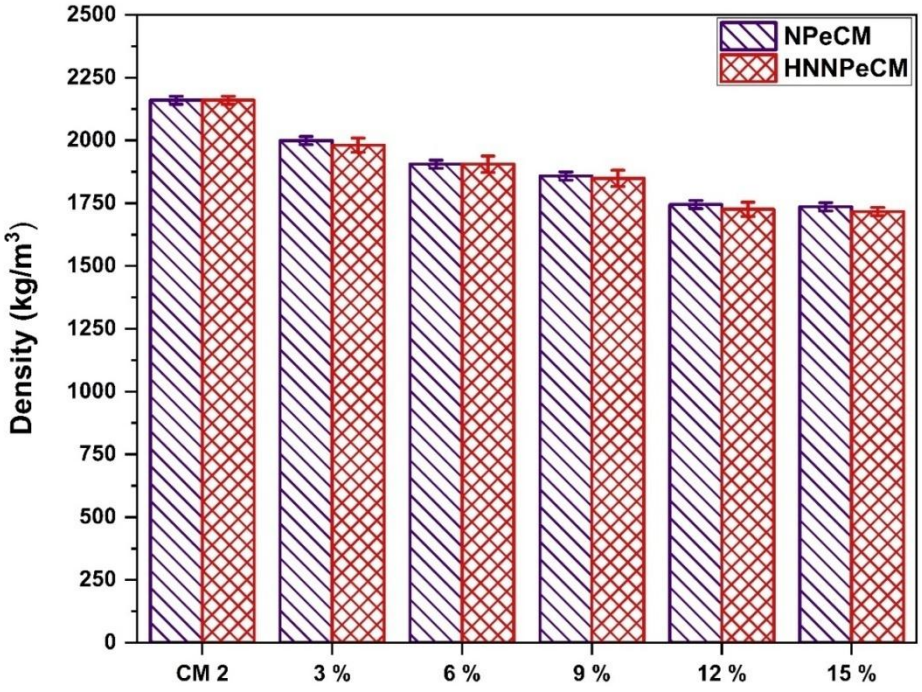

Fig. 71. Density of NPeCM and HNNPeCM 28 days cured specimens.

The percentage reduction in the density of NPeCM-6, NPeCM-7, NPeCM-8, NPeCM-9, and NPeCM-10 are 6.58%, 11.8%, 13.1%, 18.4%, and 19.7% respectively than plain cement mortar. Besides, the cube specimens of HNNPeCM-6, HNNPeCM-7, HNNPeCM-8, HNNPeC-9, and HNNPeCM-10 also exhibited reduced density in the percentage of 7.9, 10.5, 11.8, 14.4 and 17.1 respectively compared with reference cement mortar (CM-2).

5.5.11. Thermal conductivity of NPeCM and HNNPeCM cube specimens

The thermal conductivity study of cube specimens is very crucial; the tests were carried out at a temperature of 28 °C. The thermal conductivity results of NPeCM and HNNPeCM cube specimens cured for 28 days was summarized and presented in the Table 36. The thermal conductivity of reference cement mortar (CM-2) cube specimen is 1.746 W/m K; however with increased percentage of NP capsules, dispersed throughout the cement mortar, thermal conductivity was reduced as shown in the Fig. 72. The percentage drop in thermal conductivity of cube specimens NPeCM-6, NPeCM-7, NPeCM-8, NPeCM-9, and NPeCM-10 were 12.86%, 12.71%, 24.74%, 26.17% and 25.48% respectively. The main reason behind

reduction in thermal conductivity is due to polymer-based shell material whose thermal conductivity is poor as presented in the Fig. 68 **[64, 60]**.

Besides, HNNP capsules embedded in the cement mortar exhibited very good thermal conductivity as shown in the Fig. 72. The enhancement in the thermal conductivity of cube specimens HNNPeCM-6, HNNPeCM-7, HNNPeCM-8, HNNPeCM-9, HNNPeCM-10 are 3.02%, 5.57%, 8.22%, 12.18%, 13.14% respectively in comparison with reference cement mortar (CM 2). 51.50% of enhancement was achieved by HNNPeCM-10 cube specimen over NPeCM-10 cube specimen as shown in the Fig. 73. Cu-TiO_2 hybrid nanocomposites adsorbed on the capsules have really favoured enhancing the thermal conductivity of cement mortar cube specimens **[175].** This will for ensure enhances the heat transfer from the surrounding to the core PCM and vice versa, thereby the core PCM inside the capsule can undergo more number of phase change cycles per day.

Table 27. Thermal conductivity of NPeCM and HNNPeCM specimens cured for 28 days

Sample Type	**Proportions (% by weight of cement)**	**Thermal conductivity (W/m K)**			
		Trial 1	**Trial 2**	**Trial 3**	**Average Value**
CM 2	cement mortar	1.746	1.731	1.752	1.743
NPeCM 6	3%	1.521	1.501	1.53	1.517333
NPeCM 7	6%	1.488	1.503	1.475	1.488667
NPeCM 8	9%	1.314	1.299	1.333	1.315333
NPeCM 9	12%	1.289	1.271	1.254	1.271333
NPeCM 10	15%	1.231	1.202	1.211	1.214667
HNNPeCM 6	3%	1.788	1.768	1.839	1.798333
HNNPeCM 7	6%	1.811	1.829	1.799	1.813
HNNPeCM 8	9%	1.839	1.798	1.842	1.826333
HNNPeCM 9	12%	1.829	1.844	1.789	1.820667
HNNPeCM 10	15%	1.811	1.827	1.883	1.840333

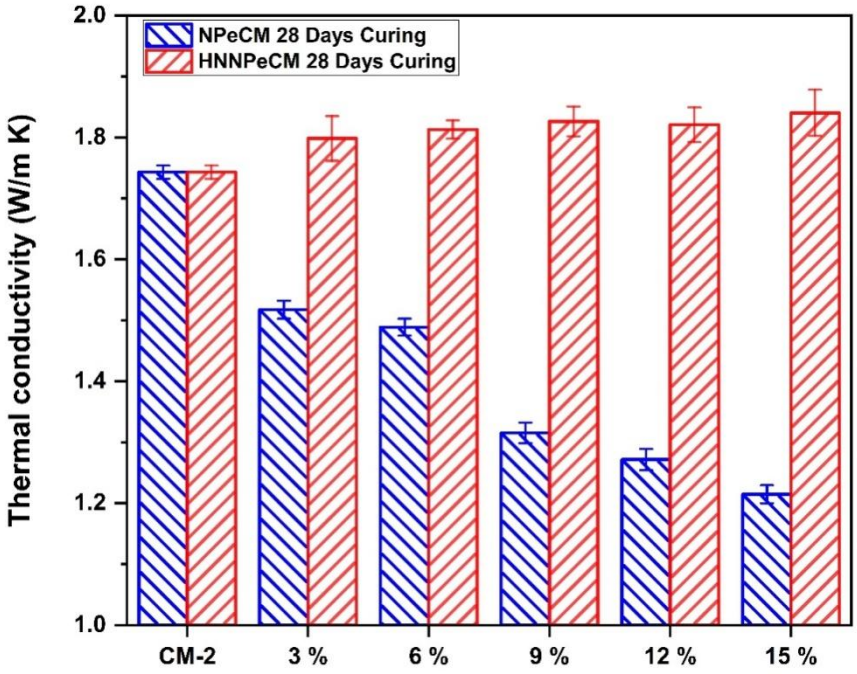

Fig. 72. Thermal conductivity of reference cement mortar (CM 2), NPeCM and HNNPeCM samples cured for 28 days

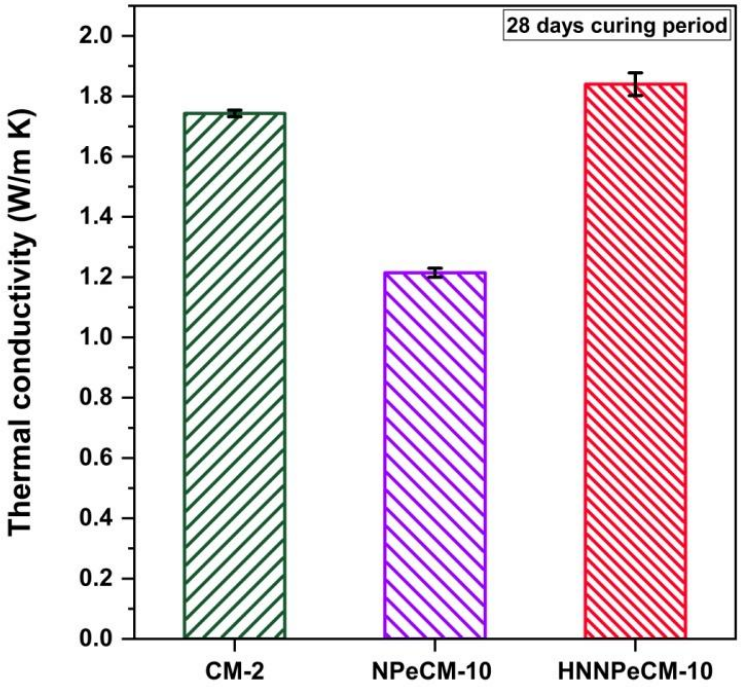

Fig. 73. Thermal conductivity of CM-2, NPeCM-10 and HNNPeCM-10 specimens cured for 28 days

5.5.12. Compressive strength of NPeCM and HNNPeCM

The cube specimens prepared with NP and HNNP capsule inclusions in the cement mortar were cured in water for 7 days and 28 days in the laboratory at a temperature of 28 °C. The main intention behind different curing periods is to study the rate of compressive strength gain. Further, the cured cube specimens were tested to study the compressive strength. Table 37 exhibits the compressive strength results of NPeCM and HNNPeCM cured for 7 days and 28 days, respectively. The average compressive strength of reference cement mortar specimens cured for 7 and 28 days are 31.06 MPa and 45.06 MPa, respectively.

The compressive strength was enhanced to 45.07% for 28 days curing period of reference cement mortar compared with 7 days curing period. Besides, with the increased percentage of NP in cement mortar, the compressive strength of the cube specimen was reduced, as shown in Fig. 74. There was a similar trend in the reduction of compressive strength of the cube specimens for both 7 days and 28 days curing periods. The percentage reduction in compressive strength of 7 days and 28 days cured NPeCM-5 and NPeCM-10 cube specimens (15% by weight of NP in cement mortar) are 42.59% and 39.28%, respectively, compared with reference cement mortar. The compressive test of the cube specimens were carried with HNNP inclusions in the cement mortar and the results are plotted as shown in the Fig. 74. The results suggest that with the increased percentage of HNNP capsules in the cement mortar, the compressive strength for both 7 days and 28 days cured specimens were reduced. When the HNNP capsules occupied 15%, the percentage reduction in the compressive strength of 7 days and 28 days cured specimen cubes are 53.54% and 45.27% respectively compared with reference cement mortar.

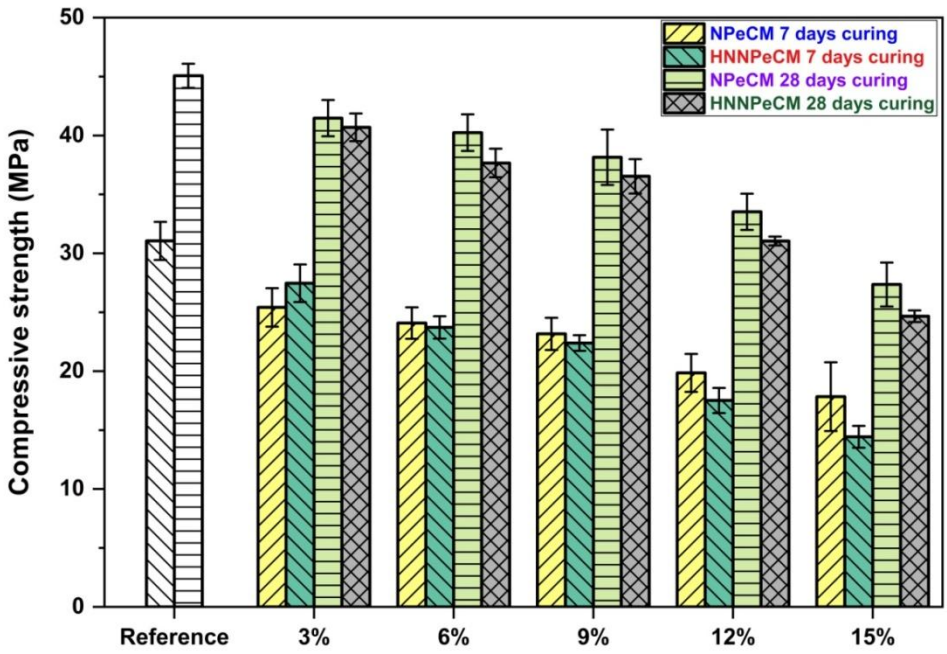

Fig. 74. Compressive strength of reference cement mortar, NPeCM and HNNPeCM specimens 7 days and 28 days curing period

Considering 7 days and 28 days curing period of both NPeCM and HNNPeCM samples, the compressive strength of 7 days curing period was less compared with 28 days curing samples this is due to fact that cement hydration plays a vital role gaining the compressive strength of the samples. 7 days of curing period is not sufficient to completely remove the heat evolved during curing of the samples, could be the reason for reduced compressive strength when compared with 28 days. The trend in the drop of compressive strength of 7 days and 28 days cured samples are in the line with the literature survey. Besides, there was a drop in compressive strength of both NPeCM and HNNPeCM cube specimens. The main reason behind this is due to dispersion of capsules (NP and HNNP) in the cement mortar, which leads to the porous structure as evident from the FESEM images of Fig. 69 and 70 **[161]**.

Table 28. Compressive strength of NPeCM and HNNPeCM specimens cured for 7 days and 28 days.

Sample Type	Proportions (by weight of cement)	Compressive strength (MPa)			
		Trial 1	Trial 2	Trial 3	Average Value
CM 1 (7 days)	cement mortar	29.22	31.7	32.26	31.06
CM 2 (28 days)	cement mortar	44.21	44.78	46.2	45.06333
NPeCM 1	3%	24.88	24.12	27.25	25.41667
NPeCM 2	6%	22.58	24.55	25.12	24.08333
NPeCM 3	9%	24.12	23.79	21.59	23.16667
NPeCM 4	12%	21.45	18.24	19.87	19.85333
NPeCM 5	15%	21.01	17.21	15.28	17.83333
NPeCM 6	3%	42.78	41.87	39.78	41.47667
NPeCM 7	6%	41.25	41.01	38.45	40.23667
NPeCM 8	9%	36.25	40.78	37.44	38.15667
NPeCM 9	12%	35.15	32.09	33.33	33.52333
NPeCM 10	15%	26.75	29.45	25.88	27.36
HNNPeCM 1	3%	27.12	26.08	29.21	27.47
HNNPeCM 2	6%	22.91	23.49	24.76	23.72
HNNPeCM 3	9%	22.14	23.15	21.89	22.39333
HNNPeCM 4	12%	18.69	17.25	16.61	17.51667
HNNPeCM 5	15%	14.49	15.33	13.48	14.43333
HNNPeCM 6	3%	39.58	40.58	41.91	40.69
HNNPeCM 7	6%	37.44	38.97	36.58	37.66333
HNNPeCM 8	9%	36.25	38.11	35.25	36.53667
HNNPeCM 9	12%	31.48	30.89	30.78	31.05
HNNPeCM 10	15%	24.12	25.09	24.78	24.66333

The larger size and surface morphology of HNNP capsule would be the reason for increased porosity which leads to further drop in compressive strength, this is the reason for more drop in compressive strength of HNNPeCM when compared with NPeCM for both 7 days and 28 days curing period samples **[59, 60, 175]**. The desired compressive strength of cement mortar used as plastering material for residential buildings, according to the Indian Standards (IS) code of practice 2250:1981 is around 7.5 MPa to 10 MPa for external plastering and 7.5 MPa for internal plastering. Keeping in view the above compressive strength, the maximum inclusion of HNNP capsules (15%) in the cement mortar for 7 days and 28 days yields the compressive strength of 14.66 MPa and 24.66 MPa respectively. The resulted compressive strength is more than the desired and can be used as plastering material for cooling applications in buildings.

5.5.13. Summary

As reported, extensive research has been conducted to enhance the novel Cu-TiO_2 hybrid nanocomposites adsorbed nanoencapsulated PCM (HNNP). Within the nanoencapsulated (NP) capsules, the core n-Octadecane PCM resides, freezing and melting at precise temperatures of 25.06 °C and 26.01 °C, respectively. During the phase transitions, the core PCM absorbs a substantial latent heat of 159.73 J/g and 156.89 J/g, respectively. It becomes evident from these results that the phase change characteristics of the nanoencapsulated n-Octadecane PCM align with the designed operating temperature range (22 °C to 26 °C).

Despite the commendable thermal properties of NP capsules, they fall short in terms of thermal conductivity, leading to a reduction in the number of phase change cycles per day. To tackle this challenge, HN particles were introduced onto the shell of the nanoencapsulated PCM (HNNP). The overarching objective of this work is to develop a thermally efficient PCM-based cement mortar with enhanced energy utilization efficiency. This achievement

was made possible by augmenting the thermo-physical properties of the polymer-based melamine formaldehyde shell material through the adsorption of Cu-TiO_2 hybrid nanocomposites over nanoencapsulated PCM.

Limited literature exists on the augmentation of the thermo-physical properties of polymer-based melamine shell material through nanoparticle adsorption. The incorporation of HN onto the nanoencapsulated PCM (HNNP) led to a remarkable 47.17% improvement in thermal conductivity compared to pure PCM, and an even more impressive 137.19% improvement compared to nanoencapsulated PCM. Furthermore, HNNP capsules exhibited outstanding thermal stability, with an onset decomposition temperature increased by 42 °C and 23 °C compared to pure PCM and nanoencapsulated PCM, respectively.

Cement mortar cube specimens embedded with NP and HNNP capsules were subjected to curing in water for 7 days and 28 days. Based on the aforementioned findings, the novel HNNPeCM demonstrated exceptional thermal conductivity and compressive strength. Notably, the highest percentage of HNNP embedded in the cement mortar (HNNPeCM-10) showcased an enhanced thermal conductivity of 1.84 W/m K. Moreover, its compressive strength reached a notable 24.66 MPa, positioning it on the higher end and rendering it suitable for plastering material applications.

The HNNP capsules, when integrated into cement mortar at a weight proportion of 15%, exhibited the ability to undergo freezing and melting within the human comfort temperature range. This makes them ideally suited for use as internal plastering material in buildings, particularly in hot climatic conditions where cooling requirements are paramount.

5.6. Cryogenic conditioning

Curing is a key process for cement-based materials achieving good compressive strength. Keeping in view, the cryogenic conditioning was carried out for the reference cement mortar

samples and HNNPeCM (15% of HNNP) samples. These specimens were subjected to liquid nitrogen cooling with varying rates, as described in section 4.12.2. Subsequently, the microstructural properties, crystalline structure, and compressive strength of CM 2 and HNNPeCM-10 cube specimens conditioned at cryogenic temperatures were examined. The outcomes of the tests are elaborated on in the sections following, providing clear and comprehensive observations based on the test results.

5.6.1. Microstructural behaviour of cryogenic conditioning of cube samples

Curing conditions influence the hydration degree and porosity directly, which leads to the changes in the compressive strength. The degree of hydration and porosity of cement mortar is also affected by temperature. Keeping in view the importance of curing of cement mortar, an attempt was made conditioning the reference cement mortar and the optimised HNNP based cube specimens using liquid nitrogen following the different strategies.

Numerous studies have been conducted to elucidate the intricate relationship between the strength and microstructural properties of cement mortar, notably its pore structure, which is deemed to exert a substantial influence on compressive strength. Keeping in view, FESEM instrument was employed to examine alterations in the microstructural behaviour of cryo-conditioned HNNPeCM-10 samples, aiming to evaluate their influence on relevant engineering properties for containment.

The test results indicate that, when compared to the microstructural images of untreated cryogenic samples of HNNPeCM-10, a major difference was observed in the cryo conditioned HNNPeCM-10 samples. The microstructure of cryo conditioned HNNPeCM-10 samples exhibited increased porous structure as shown in Fig. 75 a) & b). Given that the cryo-conditioned HNNPeCM-10 samples were structured in the mould prior to cryo-

conditioned, this likely accounts for the absence of evidence regarding cracks and increased air void sizes observed in the images.

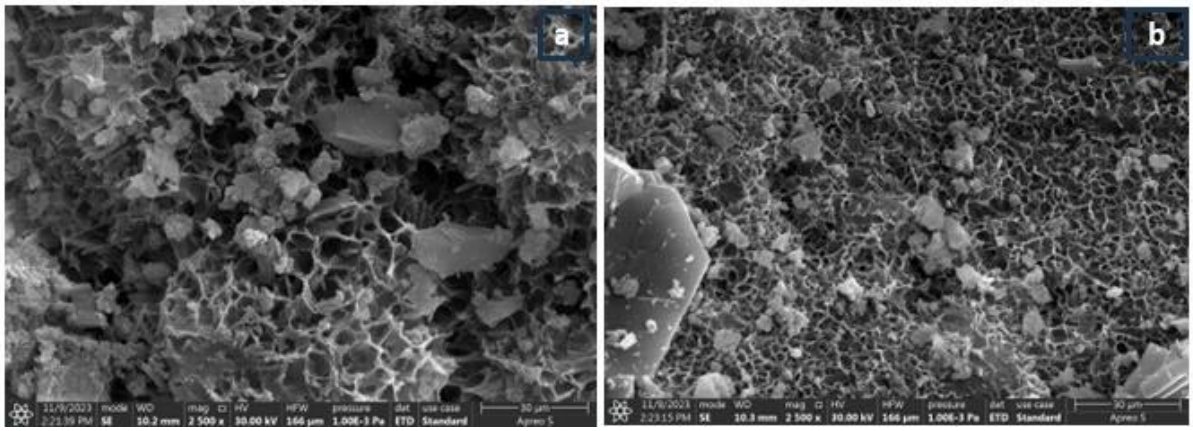

Fig. 75. a) 24 hrs cryogenic conditioning of cube specimens of HNNPeCM-10 b) 24 hrs cryogenic conditioning of cube specimens of HNNPeCM-10 followed by water curing

5.6.2. Compressive strength of Cryo-conditioned cube specimens

As previously discussed, reference cement mortar and HNNPeCM-10 cube specimens were cryogenically conditioned at varying curing rates to investigate compressive strength. The summarized results are presented in Table 38, revealing that the average compressive strength of reference cement mortar and HNNP-based cubes conditioned with liquid nitrogen for 6 hrs., 12 hrs., and 24 hrs. are 16.25 MPa, 17.33 MPa, 20.73 MPa, and 7.14 MPa, 8.72 MPa, 15.73 MPa, respectively.

The data indicates a consistent increase in compressive strength with prolonged cryogenic conditioning, although it remains lower than specimens cured in water for 28 days. Notably, the 24 hrs cryo-conditioned HNNPeCM-10 specimens exhibit superior compressive strength compared to those water cured for 7 days.

Furthermore, an attempt was made exploring a hybrid approach, processing reference cement mortar and HNNPeCM-10 samples with liquid nitrogen followed by 28 days of water curing. The compressive strength results for Cryo-conditioning of 6 hrs., 12 hrs., and 24 hrs.

are 25.65 MPa, 26.14 MPa, 34.01 MPa, and 10.43 MPa, 14.58 MPa, 16.15 MPa, respectively. This strategy demonstrates enhanced compressive strength, although it still falls below the levels achieved with traditional 28 days of water curing.

The reduced compressive strength in cryo conditioning samples is attributed to increased porosity, as evidenced by FESEM images in Fig. 75 a) & b). The inverse relationship between compressive strength and porosity is evident-lower porosity results in stronger hardened cement mortar. The impact of cryogenic conditioning on porosity influences the overall physical characteristics, and properties of the cement mortar.

Despite satisfactory compressive strength in samples processed for 24 hrs, suitable for internal plastering in buildings, challenges in cryo conditioning and application persist. The compressive strength needs further improvement to surpass the values achieved with the 28 days curing period, making it recommendable for specialized applications.

Table 29. Compressive strength of cryogenic conditioning of reference cement mortar and HNNPeCM-10 specimens.

Sample Type	Details	Average compressive strength of water cured specimens (MPa)		Average compressive strength of cryo conditioned specimens			Average compressive strength of cryo conditioned specimens followed by 28 days water curing (MPa)		
		7 Days	28 Days	6 hrs.	12 hrs.	24 hrs.	6 hrs.	12 hrs.	24 hrs.
Reference Cement Mortar	The plain cement mortar without PCM capsules.	**31.06**	**45.06**	NA	NA	NA	NA	NA	NA
	Cryo conditioned plain cement mortar cured with liquid nitrogen with different curing rates.	NA	NA	**16.25**	**17.33**	**20.73**	NA	NA	NA
	Cryo conditioned plain cement mortar cured with liquid nitrogen with different curing rates followed by water curing.	NA	NA	NA	NA	NA	**25.65**	**26.14**	**34.01**
HNNPeCM-10	15% of HNNP capsules impregnated cement mortar cube samples.	**14.43**	**24.66**	NA	NA	NA	NA	NA	NA
	15% of HNNP capsules impregnated cement mortar cube samples mortar cured with liquid nitrogen with different curing rates.	NA	NA	**7.14**	**8.72**	**15.73**	NA	NA	NA
	15% of HNNP capsules impregnated cement mortar cube samples mortar cured with liquid nitrogen with different curing rates followed by water curing.	NA	NA	NA	NA	NA	**10.43**	**14.58**	**16.15**

Table 30. Result summary

PCM	Preparation	PSA (nm)	DSC Results	Freezing and Melting time (Mins.)	Onset Decomposition (°C)	Thermal cycling	Thermal conductivity (W/m K)	Compressive strength (MPa)
1-Dodecanol PCM	Pure PCM	---	T_f =21.31 °C $(L.H)_f$ = 181.48 J/g T_m =21.31 °C $(L.H)_m$ = 194.43 J/g	Freezing time (t_f) = 29 Melting time (t_m) = 26.1	102.9	---	0.1825	---
	Cu-TiO_2 hybrid nanocomposites based 1-Dodecanol PCM (HDP)	68.14	Max. dispersion T_f =20.91 °C $(L.H)_f$ = 185.85 J/g T_m =20.20 °C $(L.H)_m$ = 189.36 J/g	Freezing time (t_f) = 21.3 Melting time (t_m) = 18.2	101.7	---	0.192	-----
	Cu-TiO_2 hybrid nanocomposites based 1-Dodecanol PCM embedded Cement Mortar (HDPC)	---	---	---	---	---	---	Reference cement mortar = 22.3 HDPC= 20.2
	Microencapsulated 1-Dodecanol PCM (MDP)	490.2	T_F α = 20.78 β = 14.21 $(L.H)_M$ = 60.7 J/g T_M=19.68, $(L.H)_M$ = 79.45 J/g	---	132.8	After 200 thermal cycles α = 20.41 β = 13.88 $(L.H)_M$ = 56.95 J/g Tm=19.01, $(L.H)_M$ = 75.41 J/g	0.172	---
	Nanoencapsulated 1-Dodecanol PCM (NDP)	157.4	α = 19.01 β = 13.77 $(L.H)_M$ = 93.01 J/g T_M=20.11, $(L.H)_M$ = 101.10 J/g	---	---	---	0.173	---

PCM	Preparation	PSA (nm)	DSC Results	Freezing and Melting time (Mins.)	Onset Decomposition (°C)	Thermal cycling	Thermal conductivity (W/m K)	Compressive strength (MPa)
n-Octadecane PCM	Pure PCM	---	T_f =23.17 °C $(L.H)_f$ = 204.91 J/g T_m =24.62 °C $(L.H)_m$ = 203.18 J/g	Freezing time (t_f) = 29 Melting time (t_m) = 26.1	142	---	0.195	---
	Cu-TiO_2 hybrid nanocomposite-based n-Octadecane PCM (HOP) (Max. dispersion 0.1%)	---	T_f =22.54 °C $(L.H)_f$ = 181.66 J/g T_m =23.47 °C $(L.H)_m$ = 178.71 J/g	Freezing time (t_f) = 29.8 Melting time (t_m) = 28.2	197	---	0.437	---
	Cu-TiO_2 HN based n-Octadecane PCM embedded cement mortar cube specimens (HOPC).	---	---	---	---	---	For 0.6% of HN 2.017	Reference CM= 45.06 HOPC = 19.58
	nanoencapsulated n-Octadecane PCM (NP)	120.5	T_f =25.06 °C $(L.H)_f$ = 159.73 J/g T_m =26.12 °C $(L.H)_m$ = 156.89 J/g	NA	161	---	0.121	
	nanoencapsulated n-Octadecane PCM embedded cement mortar (NPeCM)	---	---	---	---	---	Reference CM= 1.743 NPeCM10= 1.214	Reference CM= 45.06 NPeCM10= 27.36
	Cu-TiO_2 hybrid nanocomposites adsorbed nanoencapsulated n-Octadecane PCM (HNNP)	302	T_f =24.02 °C $(L.H)_f$ = 146.71 J/g T_m =25.77 °C $(L.H)_m$ = 144.46 J/g	NA	184	1000 thermal cycles T_f =24.77 °C $(L.H)_f$ = 121.92 J/g T_m =25.62 °C $(L.H)_m$ = 127.84 J/g	---	---

PCM	Preparation	PSA (nm)	DSC Results	Freezing and Melting time (Mins.)	Onset Decomposition (°C)	Thermal cycling	Thermal conductivity (W/m K)	Compressive strength (MPa)
	Cu-TiO_2 hybrid nanocomposites adsorbed nanoencapsulated n-Octadecane PCM embedded cement mortar (HNNPeCM)	---	---	---	---	---	Reference CM= 1.743 HNNPeCM10= 1.840	Reference CM= 45.06 HNNPeCM10= 24.66

Table 31. Comparison between MDP, NDP, NP and HNNP

	MDP (Microencapsulated 1-Dodecanol PCM)	NDP (Nanoencapsulated 1-Dodecanol PCM)	NP (Nanoencapsulated n-Octadecane PCM)	HNNP (Cu-TiO2 Hybrid Nanoencapsulated n-Octadecane PCM)
Phase change characteristics	T_f (α) = 20.78 °C (β) = 14.21 °C T_m = 21.31 °C	T_f (α) = 19.01 °C (β) = 13.77 °C T_m = 20.11 °C	T_f = 25.06 °C T_m = 26.12	T_f = 24.02 °C T_m = 25.77 °C
Encapsulation ratio	40.9%	51.9%	77.2%	71%
Thermal stability	132.82 °C	--	161 °C	184 °C
Thermal conductivity	0.172 W/m K	0.164 W/m K	0.121 W/m K	0.287 W/m K

	MDP (Microencapsulated 1-Dodecanol PCM)	NDP (Nanoencapsulated 1-Dodecanol PCM)	NP (Nanoencapsulated n-Octadecane PCM)	HNNP (Cu-TiO2 Hybrid Nanoencapsulated n-Octadecane PCM)
Ease of synthesis	In-situ polymerization technique was used for the synthesis of MDP. For the preparation of oil in water (O/W) emulsion, homogenizer was used. In situ polymerization requires less complex instruments compared to other encapsulation techniques like interfacial polymerization or spray drying. This reduces the initial capital investment in equipment.	In-situ polymerization technique was used for the synthesis of MDP. For reducing the size of capsules, probe sonicator was used, however the synthesis time and procedure was common with respect to the synthesis of MDP.	In-situ polymerization technique was used for the synthesis of NP. The process of synthesis and the time consuming was similar compared to NDP, however the stirring speed, pH value and temperatures were modified to enhance encapsulation ratio.	The procedure followed for the synthesis of NP capsules was considered for the adsorption of Cu-TiO2 hybrid nanocomposites. This is an extension of NP synthesis procedure. For developing HNNP capsules, complex instruments were not necessary, however it is time consuming process.
Merits	This property ensures that the material can withstand temperatures much higher than its melting point without degrading. This stability is crucial in applications where the PCM might be exposed to high temperatures,		This higher encapsulation ratio is beneficial for applications where high energy storage density is required, such as in thermal regulation systems for buildings and textiles. The narrow temperature gap between freezing (25.06 °C) and melting (26.12 °C) points suggest that NP can quickly respond to slight temperature variations, making it suitable for	HNNP exhibits enhanced thermal conductivity facilitates faster heat transfer, making HNNP more suitable for applications. HNNP can withstand higher temperatures than NP (161°C). This property makes it ideal for high-temperature applications and environments. The phase change temperatures (freezing at 24.02°C and melting at 25.77°C) are very close, suggesting that HNNP can efficiently manage heat with minimal temperature

	MDP (Microencapsulated 1-Dodecanol PCM)	NDP (Nanoencapsulated 1-Dodecanol PCM)	NP (Nanoencapsulated n-Octadecane PCM)	HNNP (Cu-TiO2 Hybrid Nanoencapsulated n-Octadecane PCM)
			precise temperature control applications, such as in medical transport and storage where strict temperature maintenance is crucial. The ability to withstand temperatures significantly higher than its melting point without degrading makes NP ideal for high-temperature applications, including high heat industrial processes where durability and stability are necessary.	deviation, essential for maintaining precise temperature control. HNNP operates effectively within a specific temperature range. This narrow operational window can limit its application in environments where the ambient temperatures do not frequently correspond to the phase change temperatures, reducing its effectiveness and efficiency in broader applications.
Demerits	The MDP capsules have low encapsulation ratio. Keeping in view, the cost for the synthesis of MDP and the resulted encapsulation ratio may not be beneficial. Besides, the freezing process takes place over long range in two stages. The dual freezing stages might complicate the control systems required to effectively utilize	This can be a disadvantage in applications requiring fast heat dissipation, such as in high-performance electronics cooling, where quicker thermal response is necessary to prevent overheating. Nano encapsulation can also add complexity to the manufacturing process, possibly increasing the cost and technical challenges associated with producing and	Due to poor thermal conductivity, potentially limiting its effectiveness in applications where faster rate of heat transfer is essential. This could hinder its use in active cooling systems where quick dispersion of heat is necessary. Nanoencapsulation generally involves complex and potentially costly manufacturing processes. This	Adsorption of Copper- Titania hybrid nanocomposites on the encapsulated PCM increases the complexity and cost of producing HNNP. This could make the material less economically viable for widespread application, particularly in cost-sensitive markets.

	MDP (Microencapsulated 1-Dodecanol PCM)	NDP (Nanoencapsulated 1-Dodecanol PCM)	NP (Nanoencapsulated n-Octadecane PCM)	HNNP (Cu-TiO2 Hybrid Nanoencapsulated n-Octadecane PCM)
	the PCM. This could lead to increased costs and complexity in system design and operation. The low thermal conductivity (0.172 W/m·K) is a drawback in applications requiring quick thermal response. For instance, the MDP capsules incorporated in the cement in electronic cooling systems, a higher thermal conductivity would facilitate faster heat transfer, thus maintaining optimal operating temperatures more efficiently.	using NDP. The effective temperature range of NDP may limit its application to regions or environments where the ambient temperature commonly falls within or fluctuates around the phase change temperatures. This could restrict its market potential to specific geographic areas or seasonal uses.	could limit its accessibility and increase the cost for end-users, making widespread adoption challenging	
Applications	The phase change temperatures suggest the developed capsules viable for the applications such as Building Applications, Thermal Regulation in Data Centers, Cooling Vests for Workplace Comfort.	The phase change temperatures of NDP are similar to that of MDP, so the applications of MDP are applicable to NDP.	Due to narrow freezing and melting temperatures they are specifically used for human comfort temperatures such as interior side of walls in buildings, thermo comfort clothing, and Interior space of vehicle for passenger comfort.	Due to narrow freezing and melting temperatures they are specifically used for human comfort temperatures such as interior side of walls in buildings, thermo comfort clothing, and Interior space of vehicle for passenger comfort.

CHAPTER - 6

THERMAL ANALYSIS OF HNNP BASED CEMENT MORTAR

This chapter presents a comprehensive study of heat transfer analysis of Hybrid Nanocomposites Adsorbed Nanoencapsulated PCM (HNNP) based cement mortar, exploring its potential to enhance the thermal behaviour of building materials. This analysis aims to quantify the thermal behaviour of HNNP based cement mortar, including its thermal conductivity, heat capacity, and its ability to maintain thermal comfort within built environments. Through detailed experimental studies and comparative assessments, this chapter evaluates the effectiveness of HNNP in modifying the traditional characteristics of cement mortar, thereby contributing to more sustainable and energy-efficient building practices.

6.1. Experimental setup details

The schematic of experimental setup shown in the Fig. 76, composed of two primary chambers: the cold chamber and the hot chamber. The insulated test chamber is shown in Fig. 77 (a). The cold and hot chambers are configured to simulate the interior and exterior environments that the building materials would face in actual usage. The specimen is mounted between these two chambers as shown in Fig. 77 (b), allowing for precise manipulation and measurement of the temperature on both sides of the material. The setup has a flexibility to maintain the set hot chamber temperature of maximum 70 °C. The cold chamber has a flexibility to set cold chamber minimum temperature of 15 °C and maximum of 30 °C. The test setup has a capability to vary a minimum 1 °C; there is a controller which maintains the setup temperatures.

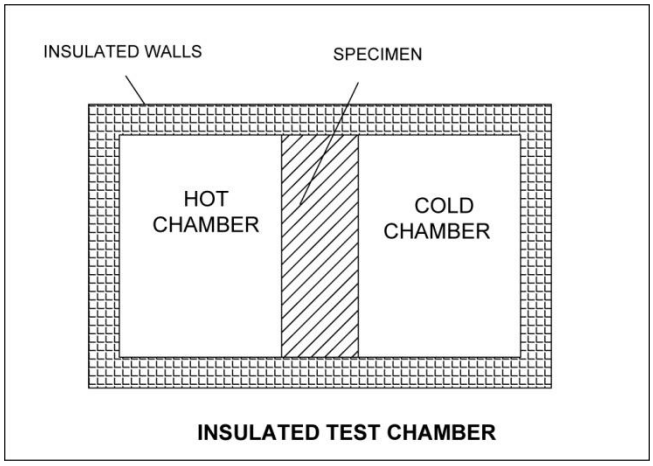

Fig. 76. Schematic of Insulated Test Chamber

The test setup is equipped with a precision temperature control system that is capable of varying the temperature by increments as small as 1°C. This fine control is achieved through an integrated controller, which actively monitors and adjusts the temperature within the setup to maintain the desired conditions. The controller ensures that the temperature settings are consistently upheld throughout the duration of the test, providing reliable and accurate data necessary for evaluating the thermal behaviour of the material being tested. This high degree of temperature control is crucial for conducting thermal tests under steady-state or dynamic conditions.

Fig. 77. a) Insulated test chamber b) slab positioned between the hot and cold chamber

6.2. Slab Preparation

For the purpose of this study, two distinct slabs were cast: a reference slab and a slab incorporating HNNPeCM-10. Given the constraints of the experimental setup, which can accommodate specimens measuring 1 feet X 1 feet, both slabs were constructed with a maximum thickness of 50 mm. It is important to note that this thickness does not represent typical wall constructions, where external walls generally range from 6 to 9 inches thick and internal walls approximately 4 inches thick.

In accordance with IS 2402: 1963 - Code of Practice, the thickness of plastering on walls is adjusted based on the application needs and local building standards. For external walls, plaster typically ranges from 12 to 20 millimeters to ensure robust protection against environmental elements and mechanical impacts. In contrast, internal plastering is usually thinner, ranging from 6 to 12 millimeters. This reduced thickness suffices for smooth finish applications and serves as an effective base for subsequent painting or decorative finishes.

The focus of this study is on internal plastering materials, maintaining a minimum plaster thickness of 6 mm. Although the slabs do not replicate the full scale of actual walls, the plastering applied mirrors the real-world application as per the standard code of practice, ensuring the study's relevance to practical scenarios. Fig. 78 in the accompanying documentation provides a schematic representation of the wall structure, illustrating the configuration and dimensions used in the experimental analysis**.**

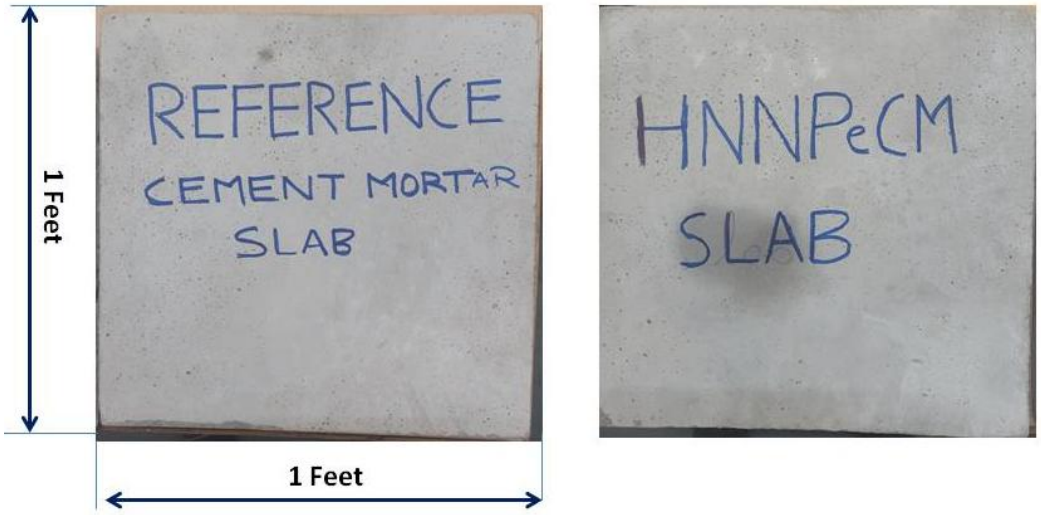

Fig. 78. Reference and HNNPeCM slab

6.3. Test Procedure

ASTM C1363 standard was followed for carrying out the experiments for the present investigation. The hot chamber was maintained with constant temperature of 42 °C, and cold chamber featuring an air conditioning system set at 22 °C. The test involves two types of cement mortar slabs, each measuring 1 feet by 1 feet with a thickness of 50 mm. Both slabs, one a reference cement mortar and the other HNNP-based cement mortar was subjected to a controlled comparison of their thermal behaviors. At the commencement of the experiment, both chambers reach and maintain their designated temperatures to ensure that any heat transfer observed is attributable solely to the material properties of the specimens and not external temperature fluctuations. Each slab is placed strategically in a groove located between the two chambers, exposing one face to the hot chamber and the other to the cold chamber. This setup creates a thermal gradient necessary for studying heat conduction through the materials.

J type thermocouples are used to record temperature variations across the slabs. This data collection is vital for analyzing how each material conducts heat from the hot side to the cold side. Before experimentation, the setup was calibrated following the procedures of

ASTM C1363 standards to ensure the accuracy of the measurements. The objective of this experimentation is to compare the thermal behaviour of the HNNP-based cement mortar slab against that of the reference slab. Key parameters of interest include the rate of temperature change, and the final equilibrium state. This comparison aims to ascertain the effectiveness of the HNNP additive in enhancing the cement mortar energy storage and release capabilities.

6.4. Observations from the experimentation

To study the behaviour of reference cement mortar and HNNPeCM-10 slabs were kept in between 42 °C and 22 °C. Due to temperature differences heat transfer takes place from hot chamber to cold chamber. Fig. 77 (b) exhibits the position of slab between the chambers and the thermocouples arrangement. The data recorded by the thermocouples were used to plot the graph considering Time (minutes) on X axis and Temperature (°C) on Y axis.

6.4.1. Heating process

The results presented in the Fig. 79 clearly depict that the reference cement mortar slab which is initially at 22 °C start raising its temperature. With respect to the time the gradual increase in temperature were noticed, nearly at 142 minutes the reference slab reached temperature from 22 °C to nearly 42 °C. However the HNNPeCM-10 slab behaved differently compared with the reference cement mortar slab. It is evident from the heating curve of HNNPeCM-10 slab that the time taken to reach 42 °C is 198 minutes. The time taken for HNNPeCM-10 slab to reach 42 °C is more than the reference slab. The peak temperatures of HNNPeCM-10 have delayed by 56 mins compared with the reference cement mortar slab. It is noticed that for HNNPeCM-10 slab the temperature rise nearly at 24 °C is delayed compared with the reference cement mortar slab. This is due to fact that the HNNP capsules incorporated in the cement mortar slab freezes and melts at 24.02 °C and 25.77 °C respectively. The HNNP capsules in the cement mortar slab start phase transforming due to

heat wave from hot chamber side. The delay in temperature rise noticed for HNNPeCM-10 approximately from 22 °C to 25 °C was due to fact that the heat wave from hot chamber is been absorbed by the HNNP capsules. The temperature was not exactly constant however the temperature gradient was very low compared with reference cement mortar slab. Due to this reason, the peak temperatures HNNPeCM-10 slab were delayed by 52 minutes compared with reference cement mortar slab. And on other side, by the time the reference cement mortar slab reaches 42 °C, the HNNPeCM-10 slab temperature is lower and the differences achieved was 3.12 °C.

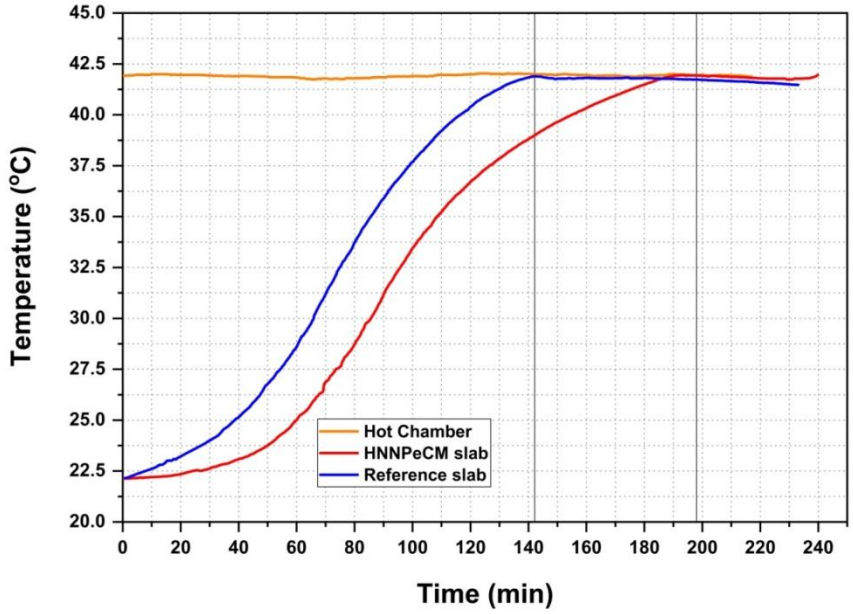

Fig. 79. Heating process of Reference cement mortar and HNNPeCM-10 slab specimen.

6.4.2. Cooling process

The cooling curves of reference cement mortar slab and HNNPeCM-10 slab were presented in the Fig. 80. The reference cement mortar slab and the HNNPeCM-10 which were initially at 42 °C were subjected to the cold chamber temperature of 22 °C. Due to this there was significant temperature drop noticed at initial stage for HNNPeCM-10 slab

compared with the reference cement mortar slab. Until 25 °C, the temperature drop for HNNPeCM-10 slab was more compared with the reference cement mortar slab. However closure to 25 °C, the HNNPeCM-10 slab experienced low temperature gradient than the reference cement mortar slab this is due to fact that the HNNP capsules commence its freezing thereby absorbing latent heat from the cold chamber. The time taken for the reference cement mortar and HNNPeCM-10 slabs to attain steady state temperature of 22 °C is 109 mins and 198 °C. The temperature differences noticed for reference cement mortar and HNNPeCM-10 was 3.42 °C. Due to freezing of HNNP capsules nearly around 25 °C, the delay in attaining the steady state cold chamber temperature is 89 min.

The results obtained from the experimental analysis clearly demonstrate that the HNNPeCM-10 slab outperforms the reference cement mortar slab in thermal performance. Specifically, the HNNPeCM-10 slab exhibited a good capability in delaying the peak temperatures within the testing environment. This attribute is crucial for enhancing thermal inertia and stability in built environments, potentially contributing to reduced cooling loads and increased energy efficiency.

Moreover, a noteworthy temperature difference of 3.12 °C was achieved between the HNNPeCM-10 slab and the reference slab during heating. This significant differential underscores the effectiveness of the HNNPeCM-10 material in maintaining cool internal conditions compared to traditional cement mortar. Such behaviour indicates the potential of HNNPeCM-10 plaster in improving indoor thermal comfort. These findings validate the enhanced thermodynamic properties of the HNNPeCM-10 material, making it a promising alternative for future construction applications where thermal management is a priority.

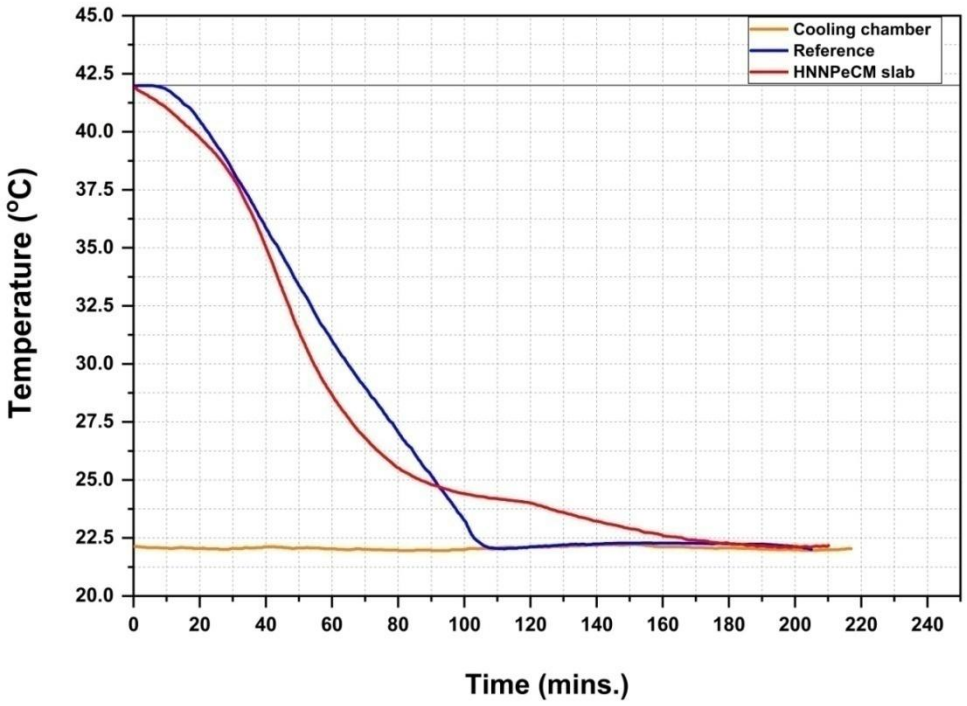

Fig. 80. Cooling process of Reference cement mortar slab and HNNPeCM slab

CHAPTER - 7

CONCLUSIONS AND RECOMMENDATIONS

The primary objective of this research work is to develop thermally efficient encapsulated PCM-based cement mortar, aiming to enhance energy utilization efficiency for cooling applications. To accomplish the research goals, two organic PCM varieties, namely 1-Dodecanol PCM and n-Octadecane PCM, were chosen based on their phase change characteristics. Although organic PCMs exhibit favourable properties, they are hindered by their poor thermal conductivity. To address this limitation, the as-prepared Cu-TiO_2 hybrid nanocomposites were dispersed into both 1-Dodecanol PCM and n-Octadecane PCM. Furthermore, the pure PCM and HN based PCM when directly integrated into cement mortar, it became apparent that PCM leakage was an issue. To tackle this challenge, both the PCMs were encapsulated at nano size using In-situ polymerization technique. Recognizing the advantages of using melamine in construction materials, it was decided to use melamine formaldehyde as the shell for encapsulating the PCM. Despite its numerous benefits, melamine formaldehyde suffers from poor thermal conductivity. To overcome this drawback, the as-prepared Cu-TiO_2 hybrid nanocomposites to the encapsulated PCM shell.

To establish an effective thermal energy storage system within the cementitious material, both NP (prior to HN adsorption) and the novel HNNP were embedded in the cement mortar in varying proportions, ranging from 3% to 15% by weight of cement. Besides, the compressive strength gain of the cement mortar is closely connected with the curing period; the investigations were carried out after curing the cube specimens for 7 days and 28 days. Summary of the comprehensive results was presented in Table 39. In conclusion, the following key findings were drawn from this research endeavour.

7.1. Conclusions

1. The Hybrid nanocomposites were synthesized using Sol-Gel chemical process. The main intention behind developing HN is to enhance the thermo-physical properties of 1-Dodecanol and n-Octadecane PCM.
2. The FESEM and EDAX results suggest that the HN particles were quasi-spherical and highly crystalline in nature. The formation of the tiny copper nanoparticles over the surface of the titania nanoparticles were clearly visible from the FESEM image, thus confirming the efficacy of the synthesis process.
3. The XRD results verified the formation of the copper-titania hybrid nanoparticles through their combined presence in terms of their sharp peaks being observed at the required 2θ angle, which were attributed to their high crystalline nature with enhanced surface characteristics.
4. FTIR results confirmed the chemical stability/compatibility between the HN and the PCM and the dispersion of the HN in the PCM was purely by physical amalgamation.
5. The DSC results infer that, on an average, the pure 1-Dodecanol PCM freezes and melts at a temperature of 21.31 °C and 22.13 °C and their latent heats are 190.03 J/g and 195.03 J/g, respectively. These values along with the phase change temperature of the HDP were found to be appreciable with respect to the pure PCM.
6. Thermal conductivity of the HDP was found to be improved by 5.53% with 0.08% increased mass proportion of the HN in the pure PCM. The HN dispersion in the PCM favoured in reducing the commencement time of the freezing process and the process completion time was also reduced by 39.4% and 22.1% respectively. it was noticed that few nanoparticles were settled for the HN proportion of 0.1%.
7. The optimized proportion of pure PCM and HDP were directly impregnated in the cement mortar and further the prepared cube samples were cured in the water for 28 days.

8. It was noticed that during the curing period the PCM was leaking from the cube specimens. This results in reduced PCM percentage in the cement mortar which further leads to the reduction in energy storage capability. Besides, due to PCM direct impregnation, the compressive strength was reduced. Due to this reason, the 1-Dodecanol PCM was encapsulated using melamine formaldehyde shell material.
9. In-situ polymerization technique was followed for the synthesis of encapsulating 1-Dodecanol PCM. Tween 20 and span 60 were used for the preparation of Oil in Water Emulsion. It is evident from the DSC results that the crystallization temperature of the MDP and NDP deviates from the designated operating conditions of 22 °C to 26 °C.
10. The same synthesis and investigative procedures were replicated with n-Octadecane PCM. The maximum HN inclusions in the n-Octadecane PCM enhanced the freezing and melting times by 39.4% and 21.7% respectively.
11. At the maximum dispersion of HN in the n-Octadecane PCM, the thermal conductivity was increased from 0.195 W/m K to 0.437 W/m K, the enhancement was nearly 124.10% compared with the pure PCM.
12. n-Octadecane PCM was encapsulated using melamine formaldehyde shell material. The surfactants were modified; Tween 80 and span 80 were selected for the preparations of O/W emulsion. To achieve the encapsulated PCM in nano size with enhanced encapsulation ratio. Different trials were carried out varying the O/W. The synthesis procedure yields the capsules with an average size of 120.5 nm.
13. The nanoencapsulated PCM (NP) exhibited good phase change characteristics, the core PCM inside the nanocapsules freezes and melts at 25.06 °C and 26.12 °C respectively. The encapsulation ratio was 77.2%.
14. The shell of the nanocapsules favoured enhancing the thermal stability; the onset decomposition temperature of NP was delayed by 19 °C compared with pure PCM.

Besides, the thermal conductivity of pure n-Octadecane PCM was reported 0.195 W/m K, and due to polymer-based melamine formaldehyde shell material it was dropped to 0.121 W/m K.

15. The reduced thermal conductivity of nanoencapsulated PCM (NP) will result in reduced phase change cycles when used in the cement mortar used as internal plastering. To overcome this issue, Cu-TiO_2 HN was adsorbed on the shell of nanoencapsulated PCM.
16. The HN adsorption on the NP capsules favoured in enhancing the thermal conductivity, the enhancement was 47.17% and 137.19% over pure n-Octadecane PCM and nanoencapsulated PCM (NP) respectively.
17. The developed HNNP capsules exhibited excellent thermal stability, the onset decomposition temperature was increased by 23 °C and 42 °C than the pure n-Octadecane PCM and the nano encapsulated PCM respectively. The mass loss of HNNP capsules was approximately 72%, this is in-line with the encapsulation ratio.
18. The HNNP capsules exhibited excellent thermal reliability; the encapsulation ratio was 67% and 61.9% when subjected to 500 and 1000 accelerated thermal cycles respectively.
19. The thermal conductivity of NPeCM cube specimens was reduced in comparison with reference mortar; this is mainly due to polymer-based shell material. Contrarily, the thermal conductivity of HNNPeCM cube specimens was increased. The thermal conductivity enhancement of HNNPeCM-10 over reference cement mortar and NPeCM-10 was 13.14% and 51.50% respectively.
20. With the increased percentage of NP and HNNP capsules dispersed in the cement mortar, there was a proportionate drop in the density and compressive strength of cube specimens compared with reference cement mortar.
21. The compressive strength of NPeCM-10 and HNNPeCM-10 cube specimens (15%) are 27.36 MPa and 24.66 MPa, Inspite of the reduction in compressive strength of cube

specimens due to maximum dispersion of NP and HNNP capsules, the compressive strength achieved is acceptable for plastering material.

22. Curing is a key process for cement-based materials achieving good compressive strength. Keeping in view, the cryogenic conditioning was carried out for the reference cement mortar and HNNPeCM-10 (15% of HNNP) samples.
23. These specimens were subjected to liquid nitrogen cooling with varying rates of 6 hrs., 12 hrs., and 24 hrs. followed by testing the samples. Furthermore, an attempt was made exploring a hybrid approach, processing reference cement mortar and HNNPeCM-10 samples with liquid nitrogen followed by 28 days of water curing.
24. The test results indicate that, when compared to the micro-structural images of untreated cryogenic samples of HNNPeCM-10, a major difference was observed in the cryo-conditioned HNNPeCM-10 samples. The microstructure of cryo-conditioned HNNPeCM-10 samples exhibited increased porous structure. The cryo-conditioned HNNPeCM-10 samples were structured in the mould prior to cryo-conditioned, this likely accounts for the absence of evidence regarding cracks.
25. The result indicates a consistent increase in compressive strength with prolonged cryogenic conditioning, although it remains lower than specimens cured in water for 28 days. Notably, the 24 hrs cryo conditioned HNNPeCM-10 specimens exhibit superior compressive strength compared to those treated for 7 days.
26. The reduced compressive strength in cryo-conditioning samples is attributed to increased porosity. Despite satisfactory compressive strength in samples processed for 24 hrs, suitable for internal plastering in buildings, challenges in cryo processing and application persist. The compressive strength needs further improvement to surpass the values achieved with the 28 days curing period, making it recommendable for specialized applications.

27. Heat transfer analysis was carried out to evaluate the behaviour of reference mortar and an HNNP-based mortar. The investigation conforms to ASTM C1363 standards, using an "Insulated Test Chamber" where the hot chamber is held constant at 42°C and the cold chamber at 22°C.
28. The results suggest that the peak temperatures of the HNNPeCM-10 slab during heating process were delayed by 52 minutes relative to the reference cement mortar slab, indicating enhanced thermal resistance. Moreover, when the reference slab reached 42°C, the HNNPeCM-10 slab maintained a significantly lower temperature, exhibiting a notable difference of 3.12°C.
29. This demonstrates the improved thermal behaviour of the HNNPeCM-10 slab. This significant differential underscores the effectiveness of the HNNPeCM-10 material in maintaining cool internal conditions compared to traditional cement mortar. Such behaviour indicates the potential of HNNPeCM-10 plaster in improving indoor thermal comfort.

7.2. Specific contributions

Based on the above findings and facts, the Novel HNNP capsules exhibit the remarkable capability to undergo freezing and melting within the range of human comfort temperatures (22 °C to 26 °C). This distinctive feature renders them exceptionally well-suited for integration into the internal plastering materials for air conditioning room in the building, addressing the cooling requirements in hot climatic conditions. Moreover, HNNP proves to be highly compatible for incorporation into cement mortar, seamlessly enhancing cooling applications within structures without compromising structural stability. This not only makes it an optimal choice but also contributes to increased energy utilization efficiency in buildings.

7.3. Potential Commercialization Paths for HNNP in Building Applications

The market entry of HNNP capsules for cooling applications in buildings faces practical barriers, but these can be addressed with targeted strategies:

1. High Initial Costs

Barrier: The initial cost of encapsulated PCM products is often higher than conventional cooling materials, which cannot be deter potential buyers.

Overcoming Strategy: Highlighting the long-term savings in energy costs and the potential for reduced HVAC system load can make a compelling case. Additionally, seeking subsidies or incentives for energy-efficient technologies can help lower the upfront cost for end-users.

2. Technical and Performance Uncertainties

Barrier: Concerns about the long-term stability, effectiveness under varying climatic conditions, and integration into existing building designs can act as barriers.

Overcoming Strategy: Conducting and publishing extensive performance testing and research demonstrating the reliability and effectiveness of PCMs in different climates and buildings can address these concerns. Offering warranties and technical support can also reassure potential users.

3. Lack of Awareness

Barrier: There's a general lack of awareness among the end users about the benefits of PCMs in building cooling applications.

Overcoming Strategy: Education and marketing efforts focused on the energy savings, comfort improvements, and sustainability benefits of PCMs can increase adoption. Providing case studies, pilot projects, and training sessions for industry professionals can also boost awareness and acceptance.

4. Regulatory and Building Code Challenges

Barrier: Existing building codes and regulations may not account for innovative materials like PCMs, complicating their adoption.

Overcoming Strategy: Working with regulatory bodies to update building codes and standards to include PCMs and their benefits. This may involve demonstrating the safety, environmental, and energy efficiency benefits of PCMs to regulatory agencies.

5. Integration with Building Materials and Systems

Barrier: Integrating PCMs into existing building materials and systems requires technical know-how, which can be a barrier for adoption by construction and building industry professionals.

Overcoming Strategy: Developing easy-to-use PCM products that can be readily incorporated into existing building designs and materials. Collaboration with manufacturers of building materials to create integrated solutions that are plug-and-play can also facilitate adoption.

6. Perception and Trust

Barrier: Doubts regarding new technologies can be a significant market entry barrier.
Overcoming Strategy: Offering transparent, third-party validated data on PCM performance and engaging in pilot projects that allow potential customers to witness the benefits firsthand can help build trust. Testimonials and endorsements from credible industry leaders can also change perceptions.

Overcoming the Barriers

To successfully overcome these barriers, a multi-faceted approach that includes technological advancements, market education, strategic partnerships, and advocacy for regulatory change is essential. Collaboration across the industry to establish standards and

best practices for the use of PCMs in cooling applications can also pave the way for broader adoption.

7.4. Practical Challenges of Implementing Cryogenically Conditioned Plastering Materials in Real-Time Building Applications

For the current study an attempt was made cryo-conditioning the HNNP-based cement mortar (HNNPeCM-10) to improve its compressive strength, in addition to enhance its thermal properties. The expectation from this work was a significant increase in compressive strength, potentially allowing for a higher proportion of HNNP in the cement mortar. This adjustment is anticipated to enhance the mortar thermal energy storage capacity.

Handling and Storage: Maintaining cryogenic temperatures for a building material like plaster requires specialized equipment and storage facilities, which would significantly increase costs and complexity.

Application: Once conditioned, the material must be quickly applied and allowed to return to ambient temperatures before hydration (in the case of cement) or setting occurs. This rapid temperature change could result in unpredictable behavior such as rapid setting or reduced workability.

While cryogenic conditioning of plastering materials is an interesting concept, it faces significant challenges that currently make it impractical for widespread use in construction. The cost, equipment requirements, and potential risks to material performance outweigh the theoretical benefits, making it a less viable option compared to more traditional methods and technologies in building construction.

Keeping in view the above results, the cryo-conditioning of HNNP-based cement mortar used as internal plastering may not be advantage due to difficulty in handling

cryogenic liquid (Liquid Nitrogen), further more studies are required to recommend for specialized industrial applications.

7.5. Future Scope of Work

The novel HNNP proved to absorb, store, and release energy in the range of human comfort temperature, which best suits its use in building for cooling applications. There is a scope to evaluate the performance of the developed HNNP by incorporating in the traditional building construction materials. The focus will be on utilizing prototype constructions as experimental platforms to comprehensively investigate the behavior of the developed Cu-TiO_2 hybrid nanocomposite adsorbed Nano-encapsulated PCM (HNNP) under realistic climatic conditions. This approach will provide invaluable insights into the material performance in actual environmental scenarios, enabling us to refine its properties and optimize its suitability for practical applications. By subjecting these prototypes to varying climatic conditions, expect to elucidate the material thermal dynamics, structural integrity, and overall efficacy in regulating indoor temperatures and energy consumption. This future work will not only contribute to advancing our understanding of innovative construction materials but also pave the way for their widespread adoption in sustainable building practices.

Life Cycle Assessment (LCA), often referred to as LCA, stands as a pivotal approach for conducting a thorough investigation into the environmental impacts of any product or system. It serves as a crucial tool in evaluating the environmental implications of Phase Change Materials (PCMs) when applied in building contexts. The goal is to strike a balance between the positive environmental contributions during the operational phase of PCMs and the negative environmental consequences throughout their entire life cycle.

The innovative HNNP-embedded cement mortar, designed for cooling applications within buildings, offers a fertile ground for conducting Life Cycle Inventory Analysis (LCI). A comprehensive examination of factors such as cost, material performance, and environmental sustainability is imperative.

This comprehensive approach not only aids readers, designers, manufacturers, and customers in gaining a broad understanding of the environmental implications but also ensures informed decision-making in the realm of sustainable building materials.

REFERENCES

[1] IEA. World energy outlook, International Energy Agency (2022).

[2] EIA. International energy outlook, Energy Information Administration (2022).

[3] M. Santamouris, K. Vasilakopoulou, Present and future energy consumption of buildings: Challenges and opportunities towards decarbonisation, e-Prime - Advances in Electrical Engineering, Electronics and Energy 1 (2021) 100002.

[4] R. Parameshwaran, S. Kalaiselvam, S. Harikrishnan, A. Elayaperumal, Sustainable thermal energy storage technologies for buildings: A review, Renewable and Sustainable Energy Reviews 16 (2012) 2394– 2433.

[5] Yi Xiao, Huan Huang, Xin Meng Qian, Lan Yue Zhang, Bo Wen, Can new type urbanization reduce urban building carbon emissions, New evidence from China, Sustainable Cities and Society 90 (2023) 104410.

[6] Eric Ohene, Albert P.C. Chan, Amos Darko, Review of global research advances towards net-zero emissions buildings, Energy and Buildings 266 (2022) 112142.

[7] Radwan A. Almasri, M.S. Alshitawi, Electricity consumption indicators and energy efficiency in residential buildings in GCC countries: Extensive review, Energy and Buildings 255 (2022) 111664.

[8] Allan Takudzwa Muzhanje, M.A. Hassan, Hamdy Hassan, Phase change material based thermal energy storage applications for air conditioning: Review, Applied Thermal Engineering 214 (2022) 118832.

[9] Mostafavi, Mohammad Tahsildoost, ZahraSadat Zomorodian, Energy efficiency and carbon emission in high-rise buildings: A review (2005-2020), Building and Environment 206 (2021) 108329.

[10] Swellam W. Sharshir, Abanob Joseph, Marwan Elsharkawy, Mohamed A. Hamada, A.W. Kandeal, Mohamed R. Elkadeem, Amrit Kumar Thakur, Yanbao Ma, Moustapha Eid

Moustapha, Maher Rashad, Muslum Arici, Thermal energy storage using phase change materials in building applications: A review of the recent development, Energy and Buildings 285 (2023) 112908.

[11] Lidia Navarro, Alvaro de Gracia, Shane Colclough, Maria Browne, Sarah J. McCormack, Philip Griffiths, Luisa F. Cabeza, Thermal energy storage in building integrated thermal systems: A review. Part 1. active storage systems, Renewable Energy 88 (2016) 526-547.

[12] Johan Heier, Chris Bales, Viktoria Martin, Combining thermal energy storage with buildings – a review, Renewable and Sustainable Energy Reviews 42 (2015) 1305-1325.

[13] Fenil Desai, Sunku Prasad Jenne, P. Muthukumar, Muhammad Mustafizur Rahman, Thermochemical energy storage system for cooling and process heating applications: A review, Energy Conversion and Management 229 (2021) 113617.

[14] Chengbin Zhang, Yongping Chen, Liangyu Wu, Mingheng Shi, Thermal response of brick wall filled with phase change materials (PCM) under fluctuating outdoor temperatures, Energy and Buildings 43 (2011) 3514-3520.

[15] Ayman G. Anter, Ahmed A. Sultan, A.A. Hegazi, M.A. El Bouz, Thermal performance and energy saving using phase change materials (PCM) integrated in building walls, Journal of Energy Storage 67 (2023) 107568.

[16] X. Huang, X. Chen, A. Li, D. Atinafu, H. Gao, W. Dong, G.e. Wang, Shape-stabilized phase change materials based on porous supports for thermal energy storage applications, Chemical Engineering Journal 356 (2019) 641–661.

[17] Chaowei Huang, Qiuting Li, Yubin Yang, Sheng Wei, Rong Ji, Qingfeng Zhang, Yucao Zhu, Huanzhi Zhang, Fen Xu, Lixian Sun, Yongpeng Xia, A novel bifunctional microencapsulated phase change material loaded with ZnO for thermal energy storage and light–thermal energy conversion, Sustainable Energy Fuels 4 (2020) 5203-5214.

[18] G.H. Zhang a, S.A.F. Bon b, C.Y. Zhao, Synthesis, characterization and thermal properties of novel nanoencapsulated phase change materials for thermal energy storage, Solar Energy 86 (2012) 1149–1154.

[19] Amirah Abdul Ghani, Saidatul Shima Jamari & Sumaiya Zainal Abidin, Waste materials as the potential phase change material substitute in thermal energy storage system: a review, Chemical Engineering Communications 208 (2020) 687-707.

[20] Suhanyaa S. Magendran, Fahad Saleem Ahmed Khan, N.M. Mubarak, Mahesh Vaka, Rashmi Walvekar, Mohammad Khalid, E.C. Abdullah, Sabzoi Nizamuddin, Rama Rao Karri, Synthesis of organic phase change materials (PCM) for energy storage applications: A review, Nano-Structures & Nano-Objects 20 (2019) 100399.

[21] Liu Yang, Jia-nan Huang, Fengjiao Zhou, Thermophysical properties and applications of nano-enhanced PCMs: An update review, Energy Conversion and Management 214 (2020) 112876.

[22] Roberta Ansuini, Roberto Larghetti, Alberto Giretti, Massimo Lemma, Radiant floors integrated with PCM for indoor temperature control, Energy and Buildings 43 (2011) 3019-3026.

[23] M. Alizadeh, S.M. Sadrameli, Indoor thermal comfort assessment using PCM based storage system integrated with ceiling fan ventilation: Experimental design and response surface approach, Energy and Buildings 243 (2021) 110981.

[24] Mohammad Kheradmand, Miguel Azenha, Jose L.B. de Aguiar, Konrad J. Krakowiak, Thermal behavior of cement based plastering mortar containing hybrid microencapsulated phase change materials, Energy and Buildings 84 (2014) 526-536.

[25] W. He, C. Yu, J. Yang, B. Yu, Z. Hu, D. Shen, X. Liu, M. Qin, H. Chen, Experimental study on the performance of a novel RC-PCM-wall, Energy and Buildings 199 (2019) 297–310.

[26] Yongcai Huang, Alex Stonehouse, Chamil Abeykoon, Encapsulation methods for phase change materials – A critical review, International Journal of Heat and Mass Transfer 200 (2023) 123458.

[27] Pushpendra Kumar Singh Rathore, Shailendra Kumar Shukla, Enhanced thermophysical properties of organic PCM through shape stabilization for thermal energy storage in buildings: A state of the art review, Energy and Buildings 236 (2021) 110799.

[28] Sandra Cunha, Pedro Leite, Jose Aguiar, Characterization of innovative mortars with direct incorporation of phase change materials, Journal of Energy Storage 30 (2020) 101439.

[29] M. Kheradmand, R. Vicente, M. Azenha, J.L.B. de Aguiar, Influence of the incorporation of phase change materials on temperature development in mortar at early ages: Experiments and numerical simulation, Constrcton and Buildng Materals 225 (2019) 1036–1051.

[30] Sandra Cunha, Marine Lima, Jose B. Aguiar, Influence of adding phase change materials on the physical and mechanical properties of cement mortars, Construction and Building Materials 127 (2016) 1–10.

[31] S.Y. Kong, Z.H. See, C.L. Lee, X. Yang, L.S. Wong, T.S. Goh, Thermal and mechanical properties of mortar incorporated with paraffin/palm oil fuel ash composite, Journal of Building Engineering 26 (2019) 100923.

[32] Khaireldin Faraj, Mahmoud Khaled, Jalal Faraj, Farouk Hachem, Khaled Chahine, Cathy Castelain, Short recent summary review on evolving phase change material encapsulation techniques for building applications, Energy Reports 8 (2022) 1245-1260.

[33] Muhammad Imran Khan, Faisal Asfand, Sami G. Al-Ghamdi, Progress in research and development of phase change materials for thermal energy storage in concentrated solar power, Applied Thermal Engineering 219 (2023) 119546.

[34] Felipe Rodriguez-Cumplido, Elizabeth Pabon-Gelves, Farid Chejne-Jana, Recent developments in the synthesis of microencapsulated and nanoencapsulated phase change materials, Journal of Energy Storage 24 (2019) 100821.

[35] Xiaolin Qiu, Wei Li, Guolin Song, Xiaodong Chu, Guoyi Tang, Microencapsulated n-octadecane with different methylmethacrylate-based copolymer shells as phase change materials for thermal energy storage, Energy 46 (2012) 188-199.

[36] Ali Karaipekli, Taner Erdogan, Semahat Barlak, The stability and thermophysical properties of a thermal fluid containing surface-functionalized nanoencapsulated PCM, Thermochimica Acta 682 (2019) 178406. 36

[37] Yutang Fang, Shengyan Kuang, Xuenong Gao, Zhengguo Zhang, Preparation and characterization of novel nanoencapsulated phase change materials, Energy Conversion and Management 49 (2008) 3704–3707.

[38] Yutang Fang, Huimin Yu, Weijun Wan, Xuenong Gao, Zhengguo Zhang, Preparation and thermal performance of polystyrene/n-tetradecane composite nanoencapsulated cold energy storage phase change materials, Energy Conversion and Management 76 (2013) 430–436.

[39] Ahmet Sarı, Cemil Alkan, Alper Bicer, Ays Altuntas, Cahit Bilgin, Micro/nanoencapsulated n-nonadecane with poly (methyl methacrylate) shell for thermal energy storage, Energy Conversion and Management 86 (2014) 614–621.

[40] Mohammad Rezvanpour, Mahdi Hasanzadeh, Danial Azizi, Alireza Rezvanpour, Mohammad Alizadeh, Synthesis and characterization of micro-nanoencapsulated n-eicosane with PMMA shell as novel phase change materials for thermal energy storage, Materials Chemistry and Physics 215 (2018) 299–304.

[41] Jian Shi, Xiaolin Wu, Rong Sun, Boyuan Ban, Jingwei Li, Jian Chen, Nano-encapsulated phase change materials prepared by one-step interfacial polymerization for thermal energy storage, Materials Chemistry and Physics 231 (2019) 244–251.

[42] Behrouz Mohammadi, Fardin Seyyed Najafi, Heydar Ranjbar, Jalal Mohammadi, Mohsen Zakaryazadeh, Nanoencapsulation of butyl palmitate in polystyrene-co-methyl methacrylate shell for thermal energy storage application, Energy and Buildings 118 (2016) 99–105.

[43] Shenjie Han, Shaoyi Lyu, Siqun Wang, Feng Fu, High-intensity ultrasound assisted manufacturing of melamine-ureaformaldehyde/paraffin nanocapsules, Colloids and Surfaces A 568 (2019) 75–83.

[44] Xiaosheng Du, Yuanlai Fang, Xu Cheng, Zongliang Du, Mi Zhou, Haibo Wang, Fabrication and Characterization of Flame-Retardant Nanoencapsulated n-Octadecane with Melamine−Formaldehyde Shell for Thermal Energy Storage, ACS Sustainable Chemical Engineering 6 (2018) 15541−15549.

[45] M Karthikeyan, T Ramachandran, OL Shanmuga Sundaram, Nanoencapsulated phase change materials based on polyethylene glycol for creating thermoregulating cotton, Journal of Industrial Textiles 44 (2014) 130–146.

[46] Ming Guang Li, Yang Zhang, Yu Han Xu, Dong Zhang, Effect of different amounts of surfactant on characteristics of nanoencapsulated phase-change materials, Polymer Bulletin 67 (2011) 541–552.

[47] Hairong Li, Ming Jiang, Qi Li, Denian Li, Jing Huang, Waping Hu, Lijie Dong, Haian Xie, Chuanxi Xiong, Facile Preparation and Thermal Performances of Hexadecanol/Crosslinked Polystyrene Core/Shell Nanocapsules as Phase Change Material, Polymer composites 35 (2014) 2154-2158.

[48] Xiaofeng Niu, Qing Xu, Yi Zhang, Yue Zhang, Yufeng Yan, Tao Liu, Fabrication and Properties of Micro-Nanoencapsulated Phase Change Materials for Internally-Cooled Liquid Desiccant Dehumidification, Nanomaterials 96 (2017).

[49] Suqing Tan, Albert P. C. Chan, Pei Li, Nanoencapsulation of Organic Phase Change Material in Water via Coacervation Using Amphoteric Copolymer, Industrial & Engineering Chemistry Research 58 (2019) 21080−21088.

[50] Xiaofen Tang, Wei Li, Haifeng Shi, Xuechen Wang, Jianping Wang, Xingxiang Zhang, Fabrication, characterization, and supercooling suppression of nanoencapsulated n-octadecane with methyl methacrylate–octadecyl methacrylate copolymer shell, Colloid and Polymer Science 291 (2013) 1705–1712.

[51] Ahmet Sarı, Cemil Alkan, Alper Bicer, Thermal energy storage characteristics of micro-nanoencapsulated heneicosane and octacosane with poly (methylmethacrylate) shell, Journal of microencapsulation 33 (2016) 221-8.

[52] K. Tumirah, M.Z. Hussein, Z. Zulkarnain, R. Rafeadah, Nano-encapsulated organic phase change material based on copolymer nanocomposites for thermal energy storage, Energy 66 (2014) 881-890.

[53] Monica Fuensanta, Umaporn Paiphansiri, María Dolores Romero-Sánchez, Celia Guillem, Angel M. Lopez-Buendía, Katharina Land fester, Thermal properties of a novel nanoencapsulated phase change material for thermal energy storage, Thermochimica Acta 565 (2013) 95-101.

[54] Xiaofen Tang, Wei Li, Xingxiang Zhang, Haifeng Shi, Fabrication and characterization of microencapsulated phase change material with low supercooling for thermal energy storage, Energy 68 (2014) 160-166.

[55] Xiaolin Qiu, Guolin Song, Xiaodong Chu, Xuezhu Li, Guoyi Tang, Preparation, thermal properties and thermal reliabilities of microencapsulated n-octadecane with acrylic-based polymer shells for thermal energy storage, Thermochimica Acta 551 (2013) 136– 144.

[56] Ahmet Sarı, Cemil Alkan, Derya Kahraman Doguscu, Alper Bicer, Micro/nano-encapsulated n-heptadecane with polystyrene shell for latent heat thermal energy storage, Solar Energy Materials & Solar Cells 126 (2014) 42–50.

[57] Yutang Fang, Xin Liu, Xianghui Liang, Hong Liu, Xuenong Gao, Zhengguo Zhang, Ultrasonic synthesis and characterization of polystyrene/n-dotriacontane composite nanoencapsulated phase change material for thermal energy storage, Applied Energy 132 (2014) 551-556.

[58] Annabelle Joulin, Laurent Zalewski, Stéphane Lassue, Hassane Naji, Experimental investigation of thermal characteristics of a mortar with or without a micro-encapsulated phase change material, Applied Thermal Engineering 66 (2014) 171-180.

[59] Zakaria Ilyes Djamai, Ferdinando Salvatore, Amir Si Larbi, Gaochuang Cai, Mohamed El Mankibi, Multiphysics analysis of effects of encapsulated phase change materials (PCMs) in cement mortars, Cement and Concrete Research 119 (2019) 51–63.

[60] Amitha Jayalath, Rackel San Nicolas, Massoud Sofi, Robert Shanks, Tuan Ngo, Lu Aye, Priyan Mendis, Properties of cementitious mortar and concrete containing micro-encapsulated phase change materials, Construction and Building Materials 120 (2016) 408–417.

[61] Sandra Cunha, José B. Aguiar, António Tadeu, Thermal performance and cost analysis of mortars made with PCM and different binders, Construction and Building Materials 122 (2016) 637–648.

[62] K.J. Kontoleon, M. Stefanidou, S. Saboor, D. Mazzeo, A. Karaoulis, D. Zegginis, D. Kraniotis, Defensive behaviour of building envelopes in terms of mechanical and thermal responsiveness by incorporating PCMs in cement mortar layers, Sustainable Energy Technologies and Assessments 47 (2021) 101349.

[63] Rogiros Illampas, Ioannis Rigopoulos, Ioannis Ioannou, Influence of microencapsulated Phase Change Materials (PCMs) on the properties of polymer modified cementitious repair mortar, Journal of Building Engineering 40 (2021) 102328.

[64] Laia Haurie, Susana Serrano, Montserrat Bosch, Ana I. Fernande, Luisa F. Cabeza, Single layer mortars with microencapsulated PCM: Study of physical and thermal properties, and fire behaviour, Energy and Buildings 111 (2016) 393–400.

[65] Dong Ho Yoo, In Kyu Jeon, Byeong Hun Woo, Hong Gi Kim, Performance of energy storage system containing cement mortar and PCM/ epoxy/SiC composite fine aggregate, Applied Thermal Engineering 198 (2021) 117445.

[66] Zeyad Amin Al-Absi, Mohd Isa Mohd Hafizal, Mazran Ismail, Hanizam Awang, Abdullah Al-Shwaiter, Properties of PCM-based composites developed for the exterior finishes of building walls, Case Studies in Construction Materials 16 (2022) 00960.

[67] A. Vaz Sa, R. M. S. F. Almeida, H. Sousa, J. M. P. Q. Delgado, Numerical Analysis of the Energy Improvement of Plastering Mortars with Phase Change Materials, Advances in Materials Science and Engineering (2014) 582536.

[68] Frederic Kuznik, Joseph Virgone, Experimental assessment of a phase change material for wall building use, Applied Energy 86 (2009) 2038-2046.

[69] Xiaoqin Sun, Yuan Zhang, Kun Xie, Mario A. Medina, A parametric study on the thermal response of a building wall with a phase change material (PCM) layer for passive space cooling, Journal of Energy Storage 47 (2022) 103548.

[70] E. Meng, H. Yu, B. Zhou, Study of the thermal behavior of the composite phase change material (PCM) room in summer and winter, Applied Thermal Engineering 26 (2017) 212-225.

[71] Andrea Frazzica, Vincenza Brancato, Valeria Palomba, Davide La Rosa, Francesco Grungo, Luigi Calabrese, Edoardo Proverbio, Thermal performance of hybrid cement mortar-PCMs for warm climates application, Solar Energy Materials and Solar Cells 193 (2019) 270–280.

[72] Z.A. Al-Absi, M.I.M. Hafizal, M. Ismail, Experimental study on the thermal performance of PCM-based panels developed for exterior finishes of building walls, Journal of Building Engineering 52 (2022) 104379.

[73] Mustapha Salihia, Maryam El Fitia, Yasser Harmenc, Younes Chhitia, Ahmed Chebaka, Fatima Ezzahrae M'Hamdi Alaouia, Mounia Achake, Fouad Bentissg, Charafeddine Jamah, Evaluation of global energy performance of building walls integrating PCM: Numerical study in semi-arid climate in Morocco, Case Studies in Construction Materials 16 (2022) 00979.

[74] Mohammad Kheradmand, Miguel Azenha, Jose L.B. de Aguiar, Joao Castro-Gomes, Experimental and numerical studies of hybrid PCM embedded in plastering mortar for enhanced thermal behaviour of buildings, Energy 94 (2016) 250-261.

[75] W. Su, J. Darkwa, G. Kokogiannakis, Numerical thermal evaluation of laminated binary microencapsulated phase change material drywall systems, Building Simulation 13 (2020) 89–98.

[76] M. Saffari, A. de Gracia, C. Fernandez, L.F. Cabeza, Simulation-based optimization of PCM melting temperature to improve the energy performance in buildings, Applied Energy 202 (2017) 420–434.

[77] K.O. Lee, M.A. Medina, X.Q. Sun, On the use of plug-and-play walls (PPW) for evaluating thermal enhancement technologies for building enclosures: evaluation of a thin phase change material (PCM) layer, Energy and Buildings 86 (2015) 86–92.

[78] M.A. Izquierdo-Barrientos, J.F. Belmonte, D. Rodríguez-Sánchez, A.E. Molina, J.A. Almendros-Ibáñez, A numerical study of external building walls containing phase change materials (PCM), Applied Thermal Engineering 47 (2012) 73-85.

[79] Xiaonan Wang, Wengui Li, Zhiyu Luo, Kejin Wang, Surendra P. Shah, A critical review on phase change materials (PCM) for sustainable and energy efficient building: Design, characteristic, performance and application, Energy and Buildings 260 (2022) 111923.

[80] Ana Vaz Sa, Miguel Azenha, Hipólito de Sousa, António Samagaio, Thermal enhancement of plastering mortars with Phase Change Materials: Experimental and numerical approach, Energy and Buildings 49 (2012) 16–27.

[81] Qudama Al-Yasiri, Marta Szabo, Experimental study of PCM-enhanced building envelope towards energy-saving and decarbonisation in a severe hot climate, Energy & Buildings 279 (2023) 112680

[82] P.K.S. Rathore, S.K. Shukla, An experimental evaluation of thermal behavior of the building envelope using macroencapsulated PCM for energy savings, Renew. Energy. 149 (2020) 1300–1313, https://doi.org/10.1016/j. renene.2019.10.130.

[83] S. Y. Wu, H. Wang, S. Xiao, D. S. Zhu, An investigation of melting/freezing characteristics of nanoparticle-enhanced phase change materials, Journal of Thermal Analysis Calorimetry 110 (2012) 1127–1131.

[84] P. Samiyammal, Veeresh Fuskele, S.K. Fakruddin Babavali, Nawaz Mohammed Khan, Mohd Shoukhatulla Ansari, D.T. Sakhare, Experimental investigations on thermal conductivity and thermal stability of the PCM using Nano-MgO, Materials Today proceedings, 69 (2022) 759-763.

[85] Kalaiselvam, Parameshwaran, Harikrishnan, Analytical and experimental investigations of nanoparticles embedded phase change materials for cooling application in modern buildings, Renewable Energy 39 (2012) 375-387.

[86] Ma Z, Lin W, Sohel MI. Nano-enhanced phase change materials for improved building performance. Renewable and Sustainable Energy Reviews 58 (2016) 125668.

[87] Abdulateef AM, Abdulateef J, Al-Abidi AA, Sopian K, Mat S, Mahdi MS. A combination of fins-nanoparticle for enhancing the discharging of phase-change material used for liquid desiccant air conditioning unit, Journal of Energy Storage, 24 (2019) 100784.

[88] J. L. Zeng, Z. Cao, D. W. Yang, L. X. Sun, L. Zhang, Thermal conductivity enhancement of Ag nanowires on an organic phase change material, Journal of Thermal Analysis Calorimetry 101 (2010) 385–389.

[89] C.J. Ho, J.Y. Gao, Preparation and thermophysical properties of nanoparticle-in-paraffin emulsion as phase change material, International Communications in Heat and Mass Transfer 36 (2009) 467–470.

[90] Soni V, Kumar A, Jain V, Performance evaluation of nano-enhanced phase change materials during discharge stage in waste heat recovery, Renewable and Energy 127 (2018) 587–601.

[91] Li C, et al. Stearic acid/expanded graphite as a composite phase change thermal energy storage material for tankless solar water heater, Sustainable Cities & Society 44 (2019) 458–464.

[92] Elbahjaoui R, El Qarnia H, El Ganaoui M. Solidification heat transfer characteristics of nanoparticle-enhanced phase change material inside rectangular slabs, Energy Procedia 139 (2017) 590–5.

[93] R. Parameshwaran, P. Dhamodharan, S. Kalaiselvam, Study on thermal storage properties of hybrid nanocomposite-dibasic ester as phase change material, Thermochimica Acta 573 (2013) 106– 120.

[94] R. Parameshwaran, R. Jayavel, S. Kalaiselvam, Study on thermal properties of organic ester phase-change material embedded with silver nanoparticles, Journal of Thermal Analysis and Calorimetry 114 (2013) 845–858.

[95] Wang J, Xie H, Xin Z, Li Y, Chen L. Enhancing thermal conductivity of Palmitic acid-based phase change materials with carbon nanotubes as fillers, Solar Energy 84 (2010) 339–344.

[96] Harikrishnan S, Kalaiselvam S. Preparation and thermal characteristics of CuO–oleic acid nanofluids as a phase change material. Thermochim Acta. 533 (2012) 46–55. 93

[97] G. V. N. Trivedi, R. Parameshwaran, Cryogenic conditioning of microencapsulated phase change material for thermal energy storage, Scientific Reports 10 (2020) 18353.

[98] Zhonghua Chen, Jianchuan Wang, FeiYu, Zhengguo Zhang, Xuenong Gao, Preparation and properties of graphene oxide-modified Poly(melamine-formaldehyde) microcapsules containing phase change materials n-Dodecanol for thermal energy storage, Journal of Materials Chemistry A, Journal of Material Chemistry 3 (2015) 11624-11630.

[99] Hongzhi Cui, Wenyu Liao, Xuming Mi, TommyY. Lo, Dazhu Chen, Study on functional and mechanical properties of cement mortar with graphite-modified microencapsulated phase-change materials, Energy and Buildings, 105 (2015) 273-284.

[100] Zhang B, Li S, Fei X, Zhao H, Lou X, Enhanced mechanical properties and thermal conductivity of paraffin microcapsules shelled by hydrophobic-silicon carbide modified melamine-formaldehyde resin, Colloids and Surfaces A: Physicochemical and Engineering Aspects 603 (2020) 125219.

[101] Song Qingwen, Li Yi, Xing Jianwei, Hu J.Y, Marcus Yuen, Thermal stability of composite phase change material microcapsules incorporated with silver nano-particles, Polymer 48 (2007) 3317-3323.

[102] Weiwei Cui, Yongpeng Xia, Huanzhi Zhang, Fen Xu, Yongjin Zou, Cuili Xiang, Hailiang Chu, Shujun Qiu, Lixian Sun, Microencapsulation of phase change materials with carbon nanotubes reinforced shell for enhancement of thermal conductivity, IOP Conf. Series: Materials Science and Engineering 182 (2017) 012-015.

[103] Sumit Parvate, Jitendra Singh, Prakhar Dixit, Jagadeeswara Reddy Vennapusa, Tushar Kanti Maiti, and Sujay Chattopadhyay, Titanium Dioxide Nanoparticle-Decorated Polymer Microcapsules Enclosing Phase Change Material for Thermal Energy Storage and Photocatalysis, ACS Applied Polymer Materials 3 (2021) 1866−1879.

[104] Jinghang Wang, Xinyu Zhai, Zunrui Zhong, Xinwen Zhang, Hao Peng, Nanoencapsulated n-tetradecane phase change materials with melamine–urea–formaldehyde–TiO2 hybrid shell for cold energy storage, Colloids and Surfaces A Physicochemical and Engineering Aspects 636 (2021) 128162.

[105] M. Li, Z. Wu, J. Tan, Heat storage properties of the cement mortar incorporated with composite phase change material, Applied Energy 103 (2013) 393–399.

[106] Y. Liu, M. Xie, X. Gao, Y. Yang, Y. Sang, Experimental exploration of incorporating form-stable hydrate salt phase change materials into cement mortar for thermal energy storage, Applied Thermal Engineering 140 (2018) 112–119.

[107] M. Hawlader, M.S. Uddin, M.M. Khin, Microencapsulated PCM thermal-energy storage system, Applied Energy 74 (2003) 195–202.

[108] F. He, X. Wang, D. Wu, New approach for sol-gel synthesis of microencapsulated n-octadecane phase change material with silica wall using sodium silicate precursor, Energy 67 (2014) 223-233.

[109] J. Su, Z. Huang, L. Ren, High compact melamine-formaldehyde micro PCMs containing n-octadecane fabricated by a two-step coacervation method, Colloid and Polymer Science 285 (2007) 1581–1591.

[110] T. Nomura, J. Yoolerd, N. Sheng, H. Sakai, Y. Hasegawa, M. Haga, T. Akiyama, Al/Al2O3 core/shell microencapsulated phase change material for high temperature applications, Solar Energy Materials and Solar Cells 193 (2019) 281–286.

[111] A. Louise Tasker, J. Paul Hitchcock, L. He, E. Alice Baxter, S. Biggs, O. Jean Cayre, The effect of surfactant chain length on the morphology of poly (methyl methacrylate) microcapsules for fragrance oil encapsulation, Journal of Colloid and Interface Science 484 (2016) 10–16.

[112] N. Wu, L. Xu, C. Zhang, The influence of emulsifiers on preparation and properties of microencapsules of melamine–urea–formaldehyde resins with n-Dodecanol as phase-change material, Advances in Polymer Technology (2018) 1–7.

[113] Wei Li & Jianping Wang & Xuechen Wang & Shizhen Wu & Xing xiang Zhang, Effects of ammonium chloride and heat treatment on residual formaldehyde contents of melamine-formaldehyde microcapsules, Colloid and Polymer Science 285 (2007) 1691–1697.

[114] Yan Wang, Jianping Wang, Guanghua Nan, He Wang, Wei Li, Xingxiang Zhang, A novel method for the preparation of narrow-disperse nanoencapsulated phase change materials by phase inversion emulsification and suspension polymerization, Industrial & Engineering Chemistry Research 54 (2015) 9307–9313.

[115] H. Xia, Y. Zhang, S. Sun, Y.u. Fang, Ag-polymer composite microspheres with patterned surface structures, Colloid and Polymer Science 285 (2007) 1655–1663.

[116] Wei Li, Xing-Xiang Zhang, Xue-Chen Wang, Jian-Jin Niu, Preparation and characterization of microencapsulated phase change material with low remnant formaldehyde content, Materials Chemistry and Physics (2007) 437-442.

[117] N. Nino-Martínez, G.A. Martinez-Castañon, A. Aragon-Pina, F. Martinez-Gutierrez, J.R. Martinez-Mendoza, F. Ruiz, Characterization of silver nanoparticles synthesized on titanium dioxide fine particles, Nanotechnology 19 (6) (2008) 65711.

[118] S. Angkaew, P. Limsuwan, Preparation of silver-titanium dioxide core-shell (Ag@TiO2) nanoparticles: Effect of Ti-Ag mole ratio, Procedia Engineering 32 (2012) 649–655.

[119] D. Madhesh, R. Parameshwaran, S. Kalaiselvam, Experimental investigation on convective heat transfer and rheological characteristics of Cu–TiO2 hybrid nanofluids, Experimental Thermal and Fluid Science 52 (2014) 104–115.

[120] H. E. Swanson, E. Tatge Standard X-ray Diffraction Powder Patterns National Bureau of Standards (U.S.), Circular 539 (1953) 1-95.

[121] A. Khan, A. Rashid, R. Younas, R. Chong, A chemical reduction approach to the synthesis of copper nanoparticles, International Nano Letters 6 (1) (2016) 21–26.

[122] J. Coates, Interpretation of Infrared Spectra, A Practical Approach, Encyclopedia Analytical Chemistry (2006).

[123] G.H. Zhang, C.Y. Zhao, Thermal and rheological properties of microencapsulated phase change materials, Renewable Energy 36 (11) (2011) 2959–2966.

[124] S. Zhang, J. Y. Wu, C. T. Tse, J. Niu, Effective dispersion of multi-wall carbon nano-tubes in hexadecane through physiochemical modification and decrease of supercooling, Solar Energy Materials & Solar Cells 96 (2012) 124–130.

[125] C. Jiao, B. Ji, D. Fang, Preparation and properties of lauric acid–stearic acid/expanded perlite composite as phase change materials for thermal energy storage, Materials Letters 67 (1) (2012) 352–354.

[126] L. Colla, L. Fedele, S. Mancin, L. Danza, O. Manca, Nano-PCMs for enhanced energy storage and passive cooling applications, Applied Thermal Engineering 110 5 (2017) 584–589.

[127] J.W. Gao, R.T. Zheng, H. Ohtani, D.S. Zhu, G. Chen, Experimental investigationof heat conduction mechanisms in nanofluids. Clue on clustering, Nano Letters 9 (2009) 4128–4132.

[128] Cunha, J. Aguiar, F. Pacheco-Torgal, Effect of temperature on mortars with incorporation of phase change materials, Constr. Build. Mater. 98 (2015) 89–101.

[129] Maulidna, B. Wirjosentono, Tamrin, L. Marpaung, Microencapsulation of ginger-based essential oil (Zingiber cassumunar roxb) with chitosan and oil palm trunk waste fiber prepared by spray-drying method, Case Studies in Thermal Engineering 18 (2020) 100606.

[130] M. H. G. Gomes, L. E. Kurozawa, Improvement of the functional and antioxidant properties of rice protein by enzymatic hydrolysis for the microencapsulation of linseed oil, Journal of Food Engineering 267 (2020) 109761.

[131] M. F. Ashby, P. J. Ferreira, D. L. Schodek, Nanomaterials, Nanotechnologies and Design: An Introduction for Engineers and Architects, Butterworth-Heinemann, (2009) 193-194.

[132] X. Zhang, Y. Fan, X. Tao, K. Yick, Crystallization and prevention of supercooling of microencapsulated n-alkanes, Journal of Colloid and Interface Science 281 (2005) 299–306.

[133] Yu L. Amorphous pharmaceutical solids: preparation, characterization and stabilization. International Journal of Pharmaceutics 48 (2001) 27–42.

[134] H.T. Banu, S. Meenakshi, Synthesis of a novel quaternized form of melamine–formaldehyde resin for the removal of nitrate from water, Journal of Water Process Engineering 16 (2017) 81–89.

[135] X. Hu, Z. Huang, Y. Zhang, Preparation of CMC-modified melamine resin spherical nano-phase change energy storage materials, Carbohydrate Polymers 101 (2014) 83–88.

[136] Y. Chai, T. Zhao, X. Gao, J. Zhang, Low cracking ratio of paraffin microcapsules shelled by hydroxyl terminated polydimethylsiloxane modified melamine-formaldehyde resin, Colloids and Surfaces A: Physiochemical Engineering Aspects 538 (2018) 86–93.

[137] G.V.N.Trivedi, R.Parameshwaran, Microencapsulated phase change material suspensions for cool thermal energy storage, Materials Chemistry and Physics 242 (2020) 122519.

[138] R. Huang, W. Li, J. Wang and X. Zhang, Effects of oil-soluble etherified melamine formaldehyde prepolymers on in situ microencapsulation and macroencapsulation of n-Dodecanol, New Journal of Chemistry 41 (2017) 9424.

[139] C.J. Ho, P.C. Chang, W. M.Yan, M. Amani, Microencapsulated n-eicosane PCM suspensions: Thermophysical properties measurement and modeling, International Journal of Heat and Mass Transfer 125 (2018) 792–800.

[140] S. Wu, P. Zhang, Z. Xu, Y. Gao, Preparation of 1-Dodecanol Microcapsules 1 with Cellulose Nanofibers-Modified Melamine-Formaldehyde Resin as a Potential Phase Change Material, Materials Resaerch Express, 6 (2019) 125376.

[141] F. Cao, B. Yang, Supercooling suppression of microencapsulated phase change materials by optimizing shell composition and structure, Applied Energy 113 (2014) 1512–1518.

[142] S. Zhang, J. Niu, Experimental investigation of effects of supercooling on microencapsulated phase-change material (MPCM) slurry thermal storage capacities, Solar Energy Materials Solar Cells 94 (2010) 1038–1048.

[143] L. Geng, S. Wang, T. Wang, R. Luo, Facile Synthesis and Thermal Properties of Nanoencapsulated n-Dodecanol with SiO2 Shell as Shape-Formed Thermal Energy Storage Material, Energy Fuels 30 (2016) 6153−6160.

[144] B. Li, T. Liu, L. Hu, Y. Wang, L. Gao, Fabrication and Properties of Microencapsulated Paraffin@SiO2 Phase Change Composite for Thermal Energy Storage, ACS Sustainable Chem. Eng. 1 (2013) 374−380.

[145] S. Yu, X. Wang, D. Wu, Self-Assembly Synthesis of Microencapsulated n-Eicosane Phase-Change Materials with Crystalline-Phase-Controllable Calcium Carbonate Shell, Energy Fuels, 28 (2014) 3519−3529.

[146] Sarı, C. Alkan, A. Altıntas, Preparation, characterization and latent heat thermal energy storage properties of micro-nanoencapsulated fatty acids by polystyrene shell, Applied Thermal Engineering 73 (2014) 1158-1166.

[147] H. Zhang, W. Li, R. Huang, N. Wang, J. Wang, X.X. Zhang, Microstructure regulation of microencapsulated bio-based n-Dodecanol as phase change materials via in-situ polymerization, New Journal of Chemistry (2017) .

[148] Jun-Feng Su, Sheng-Bao Wang, Jian-Wei Zhou, Zhen Huang, Yun-Hui Zhao & Xiao-Yan Yuan & Yun-Yi Zhang & Jin-Bao Kou, Fabrication and interfacial morphologiesof methanol–melamine–formaldehyde (MMF) shell microPCMs/epoxy composites, Colloids and Polymer Science 289 (2011) 169–177.

[149] Z-H Huang, X. Yu, W. Li, S-X. Liu, Preparation of urea-formaldehyde paraffin microcapsules modified by carboxymethyl cellulose as a potential phase change material, Journal Forest Research (2015) 253-260.

[150] Z. Wang, W. Ma, D. Hu, Li Wu, Synthesis and characterization of microencapsulated methyl laurate with polyurethane shell materials via interfacial polymerization in Pickering emulsions, Colloids and Surfaces A Physiochemical and Engineering Aspects 600 (2020) 124958.

[151] X. Fei, H. Zhao, B. Zhang, L. Cao, M. Yu, J. Zhou, L. Yu, Microencapsulation mechanism and size control of fragrance microcapsules with melamine resin shell, Colloids and Surfaces A Physiochemical and Engineering Aspects 469 (2015) 300-306.

[152] M. Biron, Detailed accounts of thermoset resins for moulding and composite matrices, Thermosets and Composites:Technical Information for Plastics Users, Elsevier (2004) 183-327.

[153] M. George, A.K. Pandey, N.A. Rahim, V.V. Tyagi, S. Shahabuddin, R. Saidur, A novel polyaniline (PANI)/ paraffin wax nano composite phase change material: Superior

transition heat storage capacity, thermal conductivity and thermal reliability, Solar Energy 204 (2020) 448–458.

[154] M. Silakhori, M. S. Naghavi, H. S. C. Metselaar, T. M. I. Mahlia, H. Fauzi, M. Mehrali, Accelerated thermal cycling test of microencapsulated paraffin wax/polyaniline made by simple preparation method for solar thermal energy storage, Materials 6 (2013) 1608-1620.

[155] F. Yu, Z-H. Chen, X-R. Zeng, Preparation, characterization, and thermal properties of microPCMs containing n-Dodecanol by using different types of styrene-maleic anhydride as emulsifier, Colloid and Polymer Science 287 (2009) 549–560.

[156] Tumirah Khadiran, Mohd Zobir Hussein, Hashim Wan Syamsi, Zulkarnain Zainal, Rafeadah Rusli, Laboratory-Scale Studies on Smart Gypsum Composite Boards Incorporated with Nano-Encapsulated Organic Phase Change Material for Thermal Comfort Building Application, Journal of Materials in Civil Engineering 28 (2015) 04015137.

[157] Jiaji Cheng, Yue Zhou, Dan Ma, Shaoxiang Li, Feng Zhang, Yu Guan a, Wenjuan Qu, Yang Jin, Dong Wang, Preparation and characterization of carbon nanotube microcapsule phase change materials for improving thermal comfort level of buildings, Construction and Building Materials 244 (2020) 118388.

[158] Yan Wang, Jianping Wang, Guanghua Nan, He Wang, Wei Li, Xingxiang Zhang, A Novel Method for the Preparation of Narrow-Disperse Nanoencapsulated Phase Change Materials by Phase Inversion Emulsification and Suspension Polymerization, Industrial and Engineering Chemistry Research 54 (2015) 9307−9313.

[159] D. MacPhee, I. Dincer, A. Beyene, Numerical simulation and exergetic performance assessment of charging process in encapsulated ice thermal energystorage system, Energy 41 (2012) 491–498.

[160] L. Xia, P. Zhang, R. Z. Wang, Numerical heat transfer analysis of the packed bedlatent heat storage system based on an effective packed bed model, Energy 35 (2010) 2022–2032.

[161] Kim D, Kwon Y, Cho Y, Li C, Cheong S, Hwang Y, et al. Convective heat transfer characteristics of nanofluids under laminar and turbulent flow conditions, Current Applied Physics 9 (2009) 119–123.

[162] Xuezhen Wang, Lecheng Zhang, Yi-Hsien Yu, Lisi Jia, M. Sam Mannan, Ying Chen, Zheng dong Cheng, Nano-encapsulated PCM via Pickering Emulsification, Scientific Reports 5 (2015) 13357.

[163] Nan Zhang, Yanping Yuan, Synthesis and thermal properties of nanoencapsulation of paraffin as phase change material for latent heat thermal energy storage, Energy and Built Environment 1 (2020) 410–416.

[164] Hussain H. Alzoubi, Borhan Albiss, Shatha S. Abu sini, Performance of cementitious composites with nano PCMs and cellulose nano fibers, Construction and Building Materials 236 (2020) 117483.

[165] Rodrigo Polo-Mendoza, Gilberto Martinez-Arguelles, Lubinda F. Walubita, Fernando Moreno-Navarro, Filippo Giustozzi, Luis Fuentes, Tatiana Navarro-Donado, Ultraviolet ageing of bituminous materials: A comprehensive literature review from 2011 to 2022, Construction and Building Materials 350 (2022) 128889.

[166] G.V.N. Trivedi, R. Parameshwaran,Micro/nanoencapsulation of dimethyl adipate with melamine formaldehyde shell as phase change material slurries for cool thermal energy storage, Chemical Thermodynamics and Thermal Analysis 6 (2022) 100037.

[167] Junfeng Su, Lixin Wang, Li Ren, Fabrication and Thermal Properties of MicroPCMs: Used Melamine-Formaldehyde Resin as Shell Material, Journal of Applied Polymer Science 101 (2006) 1522–1528.

[168] Amol Tarachand Naikwadi, Asit B. Samui, Prakash A. Mahanwar, Melamine-formaldehyde microencapsulated n-Tetracosane phase change material for solar thermal energy storage in coating, Solar Energy Materials & Solar Cells 215 (2020) 110676.

[169] Taegu Do, Young Gun Ko, Youngsang Chun,Ung Su Choi, Encapsulation of Phase Change Material with Water-absorbable Shell for Thermal Energy Storage, ACS Sustainable Chemistry and Engineering 11 (2015) 2874–2881.

[170] Huanzhi Zhang, Xiaodong Wang, Dezhen Wu, Silica encapsulation of n-octadecane via sol–gel process: A novel microencapsulated phase-change material with enhanced thermal conductivity and performance, Journal of Colloid and Interface Science 343 (2010) 246–255.

[171] Virginija Skurkyte-Papieviene, Ausra Abraitiene, Audrone Sankauskaite, Vitalija Rubeziene, Julija Baltusnikaite-Guzaitiene, Enhancement of the Thermal Performance of the Paraffin-Based Microcapsules Intended for Textile Applications, Polymers 13 (2021) 1120.

[172] Nihal sarier, Emel onder, Gokcen ukuser, Silver Incorporated Microencapsulation of n-Hexadecane and n-Octadecane Appropriate for Dynamic Thermal Management in Textiles, Thermochimica Acta 613 (2015) 17-27.

[173] R. Naresh, R. Parameshwaran, V. Vinayaka Ram, Microcapsules of n-dodecanoic acid/melamine-formaldehyde with enhanced thermal energy storage capability for solar applications, Journal of Science: Advanced Materials and Devices 7 (2022) 100462.

[174] Xianfeng Wang, Chunhong Li, Tao Zhao, Fabrication and characterization of poly(melamine-formaldehyde)/silicon carbide hybrid microencapsulated phase change materials with enhanced thermal conductivity and light-heat performance, Solar Energy Materials and Solar Cells 183 (2018) 82-91.

[175] Rodrigo Alves Silva, Paulo de Castro Guetti, Mário Sergio da Luz, Francisco Rouxinol, Rogério Valentim Gelamo, Enhanced properties of cement mortars with multilayer graphene nanoparticles, Construction and Building Materials 149 (2017) 378–385.

APPENDIX 1

PRELIMINARY TESTS ON CEMENT AND SAND

A1. Introduction

The cement and the sand used for preparation and testing the cube specimens, necessary tests were carried out. The tests carried out on cement and sand were confirmed to IS code of practice mentioned below.

A1.1.Tests on fine aggregates

Grain size distribution plays a major role in selecting the fine aggregate for use in mortars. Sieve analysis was performed, and the results are presented in Table A1.1. IS 1542:1992 (reaffirmed in 2003) confirms the fine aggregate as passing the required gradation standards. In addition, 4 different tests were performed on the fine aggregates, as per IS 2386 (parts 1 to 8) standard specifications and the results are presented in Table A1.2. The results confirm the suitability of fine aggregate for mortars when compared with specified values in the relevant parts of IS 2386 code of practice.

Table A1.1. Results of sieve analysis on fine aggregates

S. No	IS Sieve Designation	Percent passing	Percent range allowed as per IS 1542:1992
1	10 mm	100	100
2	4.75 mm	98	95-100
3	2.3 mm	97.5	95-100
4	1.18 mm	94	90-100
5	600 µm	92	80-100
6	300 µm	37	20-65
7	150 µm	8	0-15

Table A1.2. Properties of fine aggregates

Property	Value
Fineness modulus	2.675
Sand specific gravity	2.43
Silt content	2.25%
Bulking of sand	18%

A1.2. Tests on cement

To establish the suitability of the cement as the binder in the mortar, relevant tests were conducted as per IS 4031 Part 5: 1988 and IS 12269: 2013 and the results are summarized in Table A1.3.

Table A1.3. Results of tests conducted on cement.

Property	Observed value	Standard value
Specific gravity	3.146	3.15
Initial setting time	42 min	Minimum of 30 min
Final setting time	480 min	Maximum of 600 min
Normal consistency	31.2%	----

The essential experiments were carried out in accordance with the standards to determine the suitability of the materials, namely fine aggregate and cement.

A1.3. Bulking of sand

"Bulking of sand" pertains to the expansion of sand's volume due to elevated moisture levels. This phenomenon occurs as a water film envelops the sand particles, compelling them to disperse from each other. Consequently, both the sand's volume and its moisture content experience augmentation. Analysis of the test outcomes, detailed in Table A1.5, revealed

calculated sand bulking of 19.35%. This value correlates with an approximate moisture content increase of 3%.

Table A1.4. Properties of fine aggregates

Property	Value
Fineness Modulus	2.52
Specific gravity	2.63
Bulking of sand	19.35%

A1.4. Tests for Water to cement ratio (W/C)

The main intention of performing Cement-Normal consistency test is to determine the amount of water by weight that should be added to cement, to form a paste of standard consistency. Eq. (A1.1) was used to calculate the normal consistency. The results from the experiment are shown in the Table A1.7.

Normal consistency of cement = (weight of water/weight of cement) * 100 ---- (A1.1)

Table A1.5. Normal consistency of cement.

S. No.	W/C ratio	Wt. of water (g)	Penetration of plunger (mm)
1.	29%	116 g	29 mm
2.	31%	124 g	20 mm
3.	33%	132 g	16 mm
4.	35%	140 g	10 mm
5.	36%	144 g	8 mm
6.	36.5%	146 g	6 mm

The design proportions of all the ingredients of HDPC are summarized and presented in Table A1.6 for reference.

Table A1.6. Proportions for mix design of reference and HDPC specimens

Specimen	Weight of cement (g)	Weight of fine aggregate (g)	Weight of water (g)	Weight of super plasticizer (g)	Weight of PCM (%)	Weight of HN (%)
1 (Reference)*	155.5	622.2	70	1.19	0	0.00
2 (with PCM)#	155.5	622.2	70	1.19	6	0.00
3 (HDPC)@	155.5	622.2	70	1.19	6	0.02
4 (HDPC)	155.5	622.2	70	1.19	6	0.04
5 (HDPC)	155.5	622.2	70	1.19	6	0.06
6 (HDPC)	155.5	622.2	70	1.19	6	0.08
7 (HDPC)	155.562	622.248	70.0029	1.19	6	0.1

*Refers to plain cement mortar specimen; #Refers to cement mortar with only PCM; @Refers to cement mortar incorporated with HDP.

Table A1.7. Assigned codes for the cube specimens.

Control Mix	**NPeCM**					**HNNPeCM**				
	3%	**6%**	**9%**	**12%**	**15%**	**3%**	**6%**	**9%**	**12%**	**15%**
C1	E3-1	E6-1	E9-1	E12-1	E15-1	HE3-1	HE6-1	HE9-1	HE12-1	HE15-1
C2	E3-2	E6-2	E9-2	E12-2	E15-2	HE3-2	HE6-2	HE9-2	HE12-2	HE15-2
C3	E3-3	E6-3	E9-3	E12-3	E15-3	HE3-3	HE6-3	HE9-3	HE12-3	HE15-3
C4	E3-4	E6-4	E9-4	E12-4	E15-4	HE3-4	HE6-4	HE9-4	HE12-4	HE15-4
C5	E3-5	E6-5	E9-5	E12-5	E15-5	HE3-5	HE6-5	HE9-5	HE12-5	HE15-5
C6	E3-6	E6-6	E9-6	E12-6	E15-6	HE3-6	HE6-6	HE9-6	HE12-6	HE15-6
C7	E3-7	E6-7	E9-7	E12-7	E15-7	HE3-7	HE6-7	HE9-7	HE12-7	HE15-7
C8	E3-8	E6-8	E9-8	E12-8	E15-8	HE3-8	HE6-8	HE9-8	HE12-8	HE15-8

Table A1.7 represents the coding for the various proportion of NP and HNNP embedded in the cement mortar cube specimens. Table A1.8 outlines the allocation of separate codes to cube specimens based on their corresponding curing periods.

Subsequent to mixture preparation, the material was placed into the cube molds and subjected to vibration at a controlled speed of 12,000 vibrations/min. This step was undertaken to eliminate entrapped air pockets from the cube specimens, resulting in reduced porosity, heightened density, and increased compressive strength.

Table A1.8. Assigned codes for the cube specimens based on the average values.

S. No.	PCM inclusions by weight of cement	NP embedded cement mortar		HNNP embedded cement mortar	
		7 Days	28 Days	7 Days	28 Days
1	0	CM 1	CM 2	CM 1	CM 2
2	3%	NPeCM-1	NPeCM-6	HNNPeCM-1	HNNPeCM-6
3	6%	NPeCM-2	NPeCM-7	HNNPeCM-2	HNNPeCM-7
4	9%	NPeCM-3	NPeCM-8	HNNPeCM-3	HNNPeCM-8
5	12%	NPeCM-4	NPeCM-9	HNNPeCM-4	HNNPeCM-9
6	15%	NPeCM-5	NPeCM-10	HNNPeCM-5	HNNPeCM-10

APPENDIX 2

ERROR ANALYSIS

A 2.1 Introduction

In the course of the experimental work, due diligence is given to account for both the experimental error and the uncertainty associated with the measured values. This entails a thorough consideration of errors stemming from human actions or instrumental inaccuracies throughout the experiment. Broadly speaking, measurement uncertainty is the numerical representation that signifies the reliability of measurement results. The errors arising in experimentation can be categorized into rough errors, random errors, and systematic errors, each serving as explanatory facets. During the experimentation, essential precautions were taken to minimize errors. Thermocouple junctions were employed to measure the temperature of various surfaces covered by insulation, thus mitigating the impact of atmospheric temperature on the readings. The instruments were calibrated based on the output results obtained. The calibration process included connecting all the used thermocouples to the logger. Temperature measurement errors stem from inaccuracies in the voltage output from the thermocouple. The maximum uncertainty in temperature measurement is contingent upon the precision of the instrument.

A 2.2 Uncertainty specifications

The origin of error hinges on the selection of both the sampling rate and the total integration time. Here, only the essential equations for delineating the uncertainty of the measured quantity are presented.

It is evident that, when examining a singular set of measurement data, the average mean (X) of the sample over time becomes discernible as the ratio of the sum of the individual data

to the total number of data points (N). In this particular context, the expression for the variance of $\widehat{\bar{X}}$ can be articulated as follows:

$$\text{Var}\,[\widehat{\bar{X}}] = \sigma^2\,[\widehat{\bar{X}}] \approx \frac{2T1\sigma\,x2}{T}$$

$\sigma^2\,[X]$: The variance of time averaged mean X

$\sigma_x^{\,2}$ = The variance of X

N: Number of sample in data

T_1 = Integral timescale

T = Total integration time

For multiple set of measurement data, the ensemble mean $[X_N]$ for N (different) set of measurement data can be defined as the proportion of the sum of the mean of the individual measurement data set to the number of sample in data (N). the variance of X_N for the evenly distributed and statically independent samples can be obtained by:

$$\text{Var}\,[\bar{X}_N] = \frac{\sigma\,x^2}{N}$$

In the context of an ergodic process, the assessment of a statistical quantity can be carried out through either ensemble averaging or time-mean averaging methods. Building upon the previously mentioned equations,

$$\text{Var}\,[\widehat{\bar{X}}_N] = \sigma^2\,[\widehat{\bar{X}}] = \sigma_x^{\,2} \approx \frac{2T1\,\sigma\,x^2}{T}$$

After simplification of the aforementioned equation

$$N \approx \frac{T}{2T1}$$

This equation reveals that, in a single time history record the N independent realizations can be treated as N consecutive independent samples. By separating the samples into two

integral time scales, I, the evaluated quantitates in terms of statically independent samples can be accomplished.

This equation unveils that within a single time history record, the N independent realizations can be considered as N consecutive independent samples. Through the segregation of these samples into two integral time scales, denoted as I, the computation of evaluated quantities in terms of statistically independent samples can be achieved.

The sample interval can be expressed as:

$$\Delta t = 2\ TI$$

This implies the determination of the optimal sampling interval for digital measurements. To acquire the optimal N number of measurement data, a single set of measurement data should be gathered at the sampling interval of Δt for a tool integration time of $N\Delta t$, when they are at their optimum. Sampling should then continue at a longer interval until the necessary N (optimal) number of samples is achieved. This approach allows for an extension of the total integration time without a significant increase in accuracy.

Likewise, sampling should be conducted at shorter intervals (below the optimal sampling interval) until the total integration time is achieved. Halting the measurement of the quantity before reaching the (optimal) total integration time, even if the optimal number of data points has been attained, would lead to increased uncertainty. This is because the sample under measurement would cease to be statistically independent at that point.

The normalized error can be defined by

$$\varepsilon\,[\widehat{\bar{X}}] = \frac{\sigma\,[\widehat{\bar{X}}]}{[\bar{\bar{X}}]} = \frac{1}{\sqrt{N}}\,\frac{\sigma\,x}{X}\,\left[\frac{2TI}{T}\right]^{1/2}\frac{\sigma\,x}{X}$$

The specification uncertainty with a probability of (1-α) can be expressed by,

$$1\text{-}Z_{\alpha/2}\,\varepsilon\,[\bar{\bar{X}}] < \frac{\hat{X}}{\bar{X}} < 1+ Z_{\alpha/2}\,\varepsilon\,[\bar{\bar{X}}\ \ [\bar{\bar{X}}]$$

Where ε [X] : The normalized error of X

$Z_{\alpha/2}$: Gaussian probability function

A 2.3 Error in measured and computed values

The parametric measurements related to temperature for PCM frrezing and melting temperatures were monitored using sensors equipped at the corresponding locations as depicted in experimental pic. The error analysis for the measurements obtained using the sensors utilized in the experiment was executed using the root mean square method and their range and error in Table A1.1

Table A2.1 Description of sensors utilized in the experiment with the range and error.

Parameters measured	**Sensor type**	**Range**	**Uncertainty error**
Temperature	J type thermocouple	0 °C to 100 °C	1.40
Latent heat, phase change temperatures	Differential scanning calorimetry	-170 to 600 0.01 to 500 K/min	1.5
Thermal conductivity analyzer	Thermal conductivity analyzer	Thermal conductivity: 0.03 to 200 W/m K; Measuring temperature range: -35 °C to 200 °C	2

BRIEF BIOGRAPHY OF THE STUDENT

G. Naveen Kumar is presently a research scholar at the Department of Mechanical Engineering, Birla Institute of Technology and Science, Pilani (BITS Pilani), Hyderabad Campus. He is currently working as Assistant Professor in CVR College of Engineering, Hyderabad for the past 10 years. He obtained his B-Tech in Mechanical Engineering from Swami Ramananda Tirtha Institute of Science and Technology, JNTUH, Nalgonda. Thereafter he obtained his M-Tech in Mechanical Engineering (with specialization in CAD/CAM) from Swami Ramananda Tirtha Institute of Science and Technology, JNTU-H, Nalgonda. His research interests include Nanomaterials, Thermal Energy Storage Systems and Sustainable Energy in Buildings.

BRIEF BIOGRAPHY OF THE SUPERVISOR

Prof. Parameshwaran Rajagopalan obtained his Ph.D. from Anna University, Madras, India and Post-Doc from University of Tokyo, Japan (JSPS Postdoctoral Researcher). Currently, he is working as an Associate Professor, in the Department of Mechanical Engineering, Birla Institute of Technology and Science, Pilani, Hyderabad Campus. He has 45 international journals, 32 international conference publications, 3 national conference publications, 2 books and 6 book chapters to his credit (so far). His research work focuses on Thermal Energy Storage Technologies, Nanomaterials and Nanoscale Heat Transport, Materials for Energy Efficient and Sustainable Buildings, Artificial Intelligence, Biomaterials and Composites. Currently, he has successfully completed 2 research projects funded by DST-SERB and has (one as a Principal investigator and one as a Co-principal investigator) two on-going sponsored projects from DSTSERB and CDRF as a Principal investigator. He is Associate Editor of Heliyon Energy, Heliyon Journal, Cell Press, Elsevier, 2023 and Energy Storage, Frontiers in Energy Research Journal, 2022. Also he is the editorial member of International Journal of Hydromechatronics, 2017, Trends in Renewable Energy Journal, 2021. Materials Science Research India, Current Indian Science Journal, 2021, International Journal, 2021. Further, he is serving as Guest Editor, Energies Journal, 2022 and Academic Editor, PLOS ONE Journal, 2021. He is professional member of International Solar Energy Society (ISES) and American Society of Thermal and Fluids Engineers (ASTFE), and life member of Indian Society of Applied Mechanics (IASM).

BRIEF BIOGRAPHY OF THE CO-SUPERVISOR

Prof. V. Vinayaka Ram completed his doctoral degree from the National Institute of Technology Warangal, located in the state of Telangana, India. Presently, he holds the position of Professor in the Department of Civil Engineering at Birla Institute of Technology and Science, Pilani, Hyderabad Campus. To date, he has been published in 43 international journals, 23 international conferences, 1 patent, 3 books, and 8 book chapters. His research focuses on bitumen rheology, aging and modified bitumens, high modulus asphalt pavements, stone matrix asphalt, pervious asphaltic concrete pavements, green building materials for building applications, thermal energy storage in building materials, energy efficient and sustainable building materials, nano and biomaterials and composites for building applications. Currently, he has completed four research projects funded by SOAR, ABS & TC, MoRT&H, and GOI (three as a Principal investigator and one as a Co-principal investigator), and he has four ongoing sponsored projects from DST-SERB-CRG and SPARKLE, ASCRIN, and CDRF (three as a Principal investigator and one as a Co-principal investigator). He currently holds the position of Editorial Board Member for the journal Green Building and Construction Economics, published by Universal Wiser Publisher. Additionally, he serves as a Guest Editor for a special publication titled "Special Issue: Advances in Thermal Energy Storage Systems for Buildings" in the journal Energies, published by MDPI. Additionally, he serves as a reviewer for esteemed international journals including Construction and Building Materials (Elsevier), ACI Materials Journal - American Concrete Institute, Renewable & Sustainable Energy Reviews (Elsevier), Journal of Environmental and Chemical Engineering (Elsevier), Journal of Traffic and Transportation Engineering - English edition (Elsevier), Sustainable Cities and Society (Elsevier), and Journal of Building Engineering (Elsevier). He holds positions as a member of the board of studies at esteemed universities and engineering colleges

in Telangana state, India. Specifically, he serves on the board for the undergraduate (UG) Civil Engineering programs at Jawaharlal Nehru Technological University (JNTU) Hyderabad, the postgraduate (PG) Transportation Engineering program at Jawaharlal Nehru Technological University (JNTU) College of Engineering, the UG Civil Engineering programs at Osmania University College of Engineering, Hyderabad, the UG Civil Engineering program at Vasavi College of Engineering (Autonomous), Ibrahim Bagh, Hyderabad, the UG and PG Civil Engineering programs at VNR Vignana Jyothi Institute of Technology (VNRVJIT), Hyderabad, and the UG and PG programs at CVR College of Engineering, Ibrahimpatnam, RR District and QIS College of Engineering & Technology, Vengamukkapalem, Ongole. He holds professional memberships in various esteemed organizations, including the Indian Roads Congress in New Delhi (LM - 23834), the Institute of Urban Transport in New Delhi (M-272), the Indian Society of Technical Education in New Delhi (LM 16518), the Indian Geotechnical Society's Local Chapter at NIT, Warangal, the Institution of Engineers (India) (M 133675-9), the Indian Concrete Institute (8942), the American Society of Thermal and Fluids Engineers (ASTFE) – 10420, and the International Solar Energy Society in Freiburg, Germany.

LIST OF PUBLICATIONS

SCI/SCIE Indexed Journals

1. **G. Naveen Kumar**, R. Parameshwaran, V. Vinayaka Ram, Thermal and structural properties of cement mortar embedded with hybrid nanocomposite-based phase change nanocapsules for building application, Construction and Building Materials 385 (2023) 131481.
2. **G. Naveen Kumar**, Bader Al-Aifan, R. Parameshwaran, V. Vinayaka Ram, Facile synthesis of microencapsulated 1-Dodecanol/melamine formaldehyde phase change material using in-situ polymerization for thermal energy storage, Colloids and Surfaces A: Physicochemical and Engineering Aspects 610 (2021) 125698.
3. R. Parameshwaran, **G. Naveen Kumar**, V. Vinayaka Ram, Experimental analysis of hybrid nanocomposite-phase change material embedded cement mortar for thermal energy storage, Journal of Building Engineering 30 (2020) 101297.

SCOPUS Indexed Journal

1. K.V.L.N. Raju, **G. Naveen Kumar**, V. Vinayaka Ram, R. Parameshwaran, Preparation, thermal and structural properties of n-octadecane/melamine formaldehyde nanocapsules embedded cement mortar for energy storage application in buildings, Materials Today: Proceedings 26 (2022) 1424-1431.

International Conference

1. **G. Naveen Kumar**, R. Parameshwaran, V. Vinayaka Ram, Development of hybrid nano based PCM embedded cement mortar for building cooling applications – an Experimental Investigation, Proceedings of International Conference on Nanotechnology: Ideas, Innovations & Initiatives-2017 (ICN:3I-2017), Energy & Nano. Elect._1058-ICN3I, pp. 345, December 06-08, 2017, IIT Roorkee, India.